Molecular genetic analysis of steroid hormone signalling in the zebrafish

By:

Jack Paveley

A thesis submitted in partial fulfilment of the requirements for the degree of
Doctor of Philosophy

The University of Sheffield
Faculty of Medicine, Dentistry and Health
Department of Oncology and Metabolism

March 2021

Acknowledgements

This thesis is the culmination of four years of challenging yet stimulating work that would not have been possible without the enduring support of many people around me.

Firstly, I would like to thank my supervisors Dr Nils Krone and Dr Vincent Cunliffe for their guidance and endless support. Thank you for giving me the opportunity to take this project forward. Under your supervision, I have acquired invaluable knowledge and skills that have helped me to improve as a scientist and as a person. Thank you both for your words of encouragement; you provided assurance when things were not going as planned.

This project was made all the more enjoyable by the great friends I made along the way. A heartful thanks to James, Nan, Helen, Dheemanth, Irina, Neil and Lara for your technical and moral support in the lab, and for your invaluable friendship. I am also very grateful to members of D18 lab, C10 lab and the Aquarium staff of the Bateson Centre, for their extremely helpful support and stimulating discussion contributing to this study. It certainly has been a more enjoyable journey with you all along for the ride.

Special thanks go to my parents and grandparents. I would not have been able to complete this huge task without your constant encouragement and immeasurable love. In addition, thank you to my friends in Sheffield, whom I now call my family.

A gigantic thank you to my wife-to-be, Katie; without her constant encouragement, emotional support and inexhaustible patience, the last four years of work, and the writing of this thesis, would not have been possible.

Finally, I am very grateful to the Medical Research Council for funding my PhD, and the additional support, training and mentoring the MRC DiMeN DTP (Discovery Medicine North Doctoral Training Partnerships) has provided.

Abstract

Corticosteroids and their cognate receptors play a pivotal role in a variety of biological processes, including hypothalamic-pituitary-adrenal (HPA) axis regulation, developmental processes, the inflammatory response and metabolism. Mineralocorticoid Receptor (MR) and Glucocorticoid Receptor (GR) signalling is essential for survival in mammals. As such, there are limitations to investigating the systemic biological functions of these receptors in mammalian model organisms. In the last decade, the zebrafish (*Danio rerio*) has become an established model organism for studies of the endocrine system and related biological processes.

This project aimed to enhance our understanding of corticosteroid receptor signalling in such processes and investigate the distinct and redundant roles of the MR and GR in zebrafish, as they are currently poorly defined. Initially, CRISPR-Cas9 genomic editing was used to produce zebrafish carrying mutations in the MR. The phenotype of one such new zebrafish line was characterised in depth to elucidate the role of the MR in hypothalamic-pituitary-interrenal (HPI) axis regulation. MR loss-of-function mutations resulted in a hyperactivated or de-repressed HPI axis state, resulting in elevated cortisol concentrations. Utilising novel MR mutant zebrafish and the established GR *s357* mutant zebrafish, and through multiple transcriptomic experiments, I have revealed novel systemic molecular impacts due to loss of MR or GR function, including an altered gene expression profile which strongly suggests a major role for GR in regulating mitochondrial functions in neurons, and a role for MR in regulating synaptic signalling. To investigate the level of active genomic compensation between MR and GR, I utilised a GR knock out mutant zebrafish line to generate double $MR^{46Del};GR^{sh543}$ mutant zebrafish and characterise their morphology at adult stages.

In parallel to this work, CRISPR-Cas9 genomic editing was used to produce zebrafish carrying a mutation in the steroidogenic enzyme *cyp17a2*. *Cyp17a2* was shown to be essential for glucocorticoid synthesis in zebrafish and a role for this enzyme in female spawning was also identified.

Together, this thesis has described molecular, genetic and phenotypic analysis of several zebrafish lines carrying targeted mutations in genes encoding essential components of steroid hormone signalling.

Table of Contents

Figure Index

Abbreviations

11KT – 11-ketotestosterone

aa – Amino acids

ACTH – adrenocorticotropic hormone

ANOVA – analysis of variance

bp – Base pairs

AVP - Arginine Vasopressin

cAMP – cyclic adenosine monophosphate

CRF – corticotropin-releasing factor

CRH – corticotropin-releasing hormone

CRISPR – clustered regularly interspaced short palindromic repeats

Cas - CRISPR-associated

CRISPR - Clustered Regularly Interspaced Short Palindromic Repeats

crRNA – crisprRNA

Ct – cycle threshold

Cyp - cytochrome p450

CYP11B1/2 - Cytochrome P450 Family 11 Subfamily B Member 1

Cyp11c1 - Cytochrome P450 Family 11 Subfamily C Member 1

CYP17A1/a2 - Cytochrome P450 Family 17 Subfamily A Member 1/2

Cyp19a1a/1b - Cytochrome P450 Family 19 Subfamily A Member 1a/1b

CYP21A2 - Cytochrome P450 Family 21 Subfamily A Member 2

DAVID - Database for annotation, visualization and integrated discovery

DBD – DNA binding domain

DEG - Differentially expressed gene

DHEA – Dehydroepiandrosterone

DNA - Deoxyribonucleic acid

DOC - 11-deoxycorticosterone

Dpf – days post fertilisation

DSB – Double strand break

ECM - Extracellular matrix

EtOH – ethanol

FC – fold change

FDR - False discovery rate

Fdx1 - Ferredoxin 1b

Fkbp5 - FK506-binding protein 5

GO - Gene ontology

GR – glucocorticoid receptor

GRE – Glucocorticoid response element

gRNA – CRSPR guide RNA

HDR – homologous DNA repair

HPA - Hypothalamic-pituitary-adrenal

Hpf - hours post fertilisation

HPG – Hypothalamic-pituitary-gondal

HPI - Hypothalamic-pituitary-interrenal

Hsd11b1/2 - Hydroxysteroid 11-Beta Dehydrogenase 1/2

Hsd17b1/3 - Hydroxysteroid 17-Beta Dehydrogenase 1/3

Hsd3b1/2 - – Hydroxy-Delta-5-Steroid Dehydrogenase, 3 Beta- And Steroid Delta-Isomerase 1

HSP – Heat shock protein

KEGG - Kyoto encyclopedia of genes and genomes

LBD - Ligand binding domain

LC-MS/MS - Liquid chromatography tandem mass spectrometry

MAPKs - mitogen-activated protein kinases

MC2R - melanocortin 2 receptor

MeOH – Methanol

MR – mineralocorticoid receptor

mtDNA - mitochondrial DNA

NHEJ – Non-homologous End Joining

NPO - hypothalamic nucleus preopticus

NTD - N-terminal domain

PAM - Protospacer adjacent motif

PCA - Principal component analysis

PCR - Polymerase chain reaction

PFA – Paraformaldehyde

PI3K - phosphoinositide 3-kinase

POMC - proopiomelanocortin

PVN - paraventricular nucleus

qPCR - Quantitative polymerase chain reaction

StAR - steroidogenic acute regulatory protein

TAE - Tris-Acetate-EDTA

TALEN - Transcription activator-like effector nucleases

TF RE - Transcription factor-specific response element

trRNA – trans-activating crRNA

VBA - Visual background adaptation

WISH – Whole mount in situ hybridisation

Chapter 1: Introduction

1.1 The zebrafish as a model organism

Zebrafish are an important model organism for experimental studies of many biological processes, including embryogenesis, organogenesis and various human diseases such as genetic, brain and immunological disorders (Goody et al., 2014; Kalueff et al., 2014; Lieschke and Currie, 2007; Ota and Kawahara, 2014; Shin and Fishman, 2002). Not only are developmental processes well conserved with mammalian counterparts, but the zebrafish has become an established model organism for studies of the endocrine system and related diseases (Löhr and Hammerschmidt, 2011; McGonnell and Fowkes, 2006; Schaaf et al., 2009; Schoonheim et al., 2010; Tokarz et al., 2013, 2015).

There are many practical benefits to using zebrafish as a model organism: adults are small (up to 5cm), and relatively cheaper and less labour-intensive to maintain than experimental mammals such as mice and rats. Zebrafish breed well under laboratory conditions and are able to produce hundreds of eggs per week that are externally fertilised. Additionally, zebrafish development is an advantage for developmental studies, as it is much faster than any mammal, resulting in most organs and glands having formed after 5 days post fertilization (dpf). Moreover, the optical clarity of the zebrafish embryo and larva enables imaging of gene and protein expression patterns in whole specimens, and live imaging of fluorescent reporter transgenes enables developmental and physiological processes to be observed in intact live organisms.

The *ex utero* development of zebrafish embryos and larval stages further offers opportunities for molecular and genetic manipulation of developmental processes by microinjection of DNA, mRNA or morpholinos (Schoonheim et al., 2010). The zebrafish genome, as described in the GRCz10 (Genome Reference Consortium Zebrafish Build 10) (http://www.ensembl.org/Danio_rerio/Info /Annotation), is essentially complete, with a total sequence length of 1.37Gb. Coupled with high fecundity and rapid development, zebrafish have become a valuable tool in modelling genetic disease (Lieschke and Currie, 2007).

Steroid hormones play important roles in regulating many biological and metabolic processes, including the stress response, the inflammatory response, glucose, protein and lipid metabolism, electrolyte homeostasis and gametogenesis and reproductive behaviour. In contrast to murine models, zebrafish synthesise the same principal glucocorticoid as humans, cortisol. Moreover, unlike

other teleosts, zebrafish only have one homolog of each cortisol-binding receptor, the glucocorticoid receptor (GR) and the mineralocorticoid receptor (MR) (Faught and Vijayan, 2018; Schaaf et al., 2008). However, the distinct and redundant roles of these receptors are unclear. As such, zebrafish are a unique model in which to study these well-conserved cortisol receptors and their roles in various biological and molecular processes. This chapter will describe the current literature concerning corticosteroid and sex steroid biosynthesis and known roles of corticosteroids and their respective receptors.

1.2 Genetic Manipulation With CRISPR/Cas9

CRISPR/Cas9 technology has been developed to efficiently and reliably target specific sequences of the genome in living cells. The function of CRISPR (Clustered Regularly Interspaced Short Palindromic Repeats) and CRISPR-associated (Cas) genes are vital in adaptive immunity in certain bacteria, enabling protective responses to bacteriophages and other mobile genetic elements (Blackburn et al., 2013). This bacterial immunity mechanism has been modified and adapted as a new tool for eukaryotic genome modification. There are three components required for the CRISPR nuclease to create targeted mutations in a defined DNA sequence: Cas9 nuclease, crRNA and trRNA (guideRNA). The Cas9 enzyme is responsible for the catalysing the double-strand break (DSB) within the DNA target sequence that is complementary to the guide RNA. DSBs can be repaired either through homology-directed repair (HDR) when a donor template is provided, or more commonly through Non-Homologous End Joining (NHEJ), resulting in insertions or deletions (indels) causing targeted locus disruption (Sander and Joung, 2014). Zebrafish have been widely used to create mutant lines using CRISPR/Cas9 as described previously, as zebrafish are genetically tractable, providing easy-to-use methods of administration due to their large 1-cell stage embryos that are readily manipulated by microinjection (Hwang et al., 2013).

1.3 Steroid hormone biosynthesis in zebrafish and other teleosts

Biosynthesis of steroid hormones and stress responses of zebrafish are known to be similar to those found in the mouse and in humans (McGonnell and Fowkes, 2006). Mammals, such as the mouse and the rat, are leading animal models to study the endocrine systems as they are biochemically and genetically similar to humans (Löhr and Hammerschmidt, 2011). However, in rodents, corticosterone is the principal glucocorticoid, whereas in both humans and zebrafish, cortisol is the predominant glucocorticoid with biological activity. The zebrafish endocrine system is also relatively well-conserved

with mammals, as both fish and humans respond to a stress stimulus through elevating systemic cortisol levels (Alsop and Vijayan, 2008). In zebrafish, steroid hormone biosynthesis occurs primarily in peripheral tissues such as the gonads, the interrenal gland and the brain (Tokarz et al., 2015). The interrenal gland is located in the head kidney of zebrafish and is functionally homologous to the mammalian adrenal gland (Chai et al., 2003). These major sites of steroidogenesis are regulated by the hypothalamus-pituitary-interrenal (HPI) axis, equivalent to the mammalian hypothalamus-pituitary-adrenal (HPA) axis, and the hypothalamus-pituitary-gondal (HPG) axis (Steenbergen et al., 2011). Steroid hormones regulate many essential biological processes, including metabolism, the immune response, the stress response and reproduction.

In teleosts, steroidogenesis occurs in specific cell-types; gonads are the primary site of sex steroid biosynthesis such as androgens, oestrogens and progestins, whereas peripheral tissues such as the interrenal are the main sources of glucocorticoids and mineralocorticoid production. However, steroidogenesis may occur in other organs such as the brain, liver, intestine and adipose tissue (Jiang et al., 1998; Rajakumar and Senthilkumaran, 2020; Tokarz et al., 2013, 2015).

Cholesterol is the common precursor of all classes of steroids that are synthesised *de novo* (Miller, 2013). Initially, the rate-limiting step of steroid hormone biosynthesis is the transport of cholesterol across the outer and inner membrane of mitochondria, facilitated by the steroidogenic acute regulatory protein (StAR) (Nematollahi et al., 2012). Initially, steroidogenesis is initiated by the conversion of cholesterol to pregnenolone by the Cytochrome p450 (Cyp) enzymes Cyp11a1 or Cyp11a2 in zebrafish (Parajes et al., 2013). Mitochondrial steroidogenic enzymes such as Cyps, which catalyse a multitude of reactions, require electron donors (Miller, 2005). Conversion of cholesterol to pregnenolone by Cyp11a1/Cyp11a2, requires the electron donating steroidogenic cofactor Fdx1b , as observed in androgen and glucocorticoid deficient adult $fdx1b^{-/-}$ and $cyp11a2^{-/-}$ mutant zebrafish (Griffin et al., 2016; Oakes et al., 2019). Next, pregnenolone may be converted to progesterone by the hydroxysteroid dehydrogenase (HSD) enzyme Hsd3b1 (Lin et al., 2015). This step is a branching point for steroid hormone synthesis. Precursors pregnenolone and progesterone are then either directed into the mineralocorticoid synthesis pathway, or they undergo 17α-hydroxylation by either Cyp17a1 or Cyp17a2 and are directed into glucocorticoid and sex steroid synthesis pathways (Pallan et al., 2015) (Figure 1.1). Recently, Cyp17a1 was shown to be essential for the production of sex steroids but not glucocorticoids (Zhai et al., 2018). The physiological role of Cyp17a2 in zebrafish is currently unknown but it is thought to be responsible for glucocorticoid synthesis.

At the 17α-hydroxylation branching point, precursors may be directed into the mineralocorticoid biosynthesis pathway, where pregnenolone is thought to be converted to 11-deoxycorticosterone (DOC) by Cyp21a2, followed by further hydroxylation by Cyp11c1 (homolog to mammalian CYP11B1) to produce corticosterone (Jiang et al., 1998). In mammals, the primary mineralocorticoid is aldosterone, essential for ion homeostasis and water retention (Rogerson and Fuller, 2000). However, it is currently unknown whether zebrafish can synthesise corticosterone or aldosterone as they are measured at negligible concentrations in adult wildtype zebrafish, with cortisol acting as the key ion-water balance regulator (Paveley et al., unpublished; Bern, 1967; Gilmour, 2005). In addition, the teleost homolog for the mammalian enzyme aldosterone synthase (CYP11B2), responsible for aldosterone synthesis, has not been identified (Bridgham et al., 2006).

After 17α-hydroxylation of pregnenolone and progesterone, these precursors can be directed into the glucocorticoid or sex steroid synthesis pathways (Figure 1.1). The glucocorticoid synthesis pathway is highly conserved between humans and zebrafish (Tokarz et al., 2015). First, 17α-hydroxyprogesterone is converted to 21-deoxycortisol by Cyp21a2 (Eachus et al., 2017). Followed by further conversion to the primary glucocorticoid, cortisol, by Cyp11c1 (Jiang et al., 1998). The catalytic activity of Cyp11c1 requires the electron donor Fdx1b, as loss of *cyp11c1* function in zebrafish results in similar phenotypes as *fdx1b*^{-/-} and *cyp11a2*^{-/-} zebrafish, including androgen and glucocorticoid deficiency (Li et al., 2020; Oakes et al., 2019, 2020; Zhang et al., 2020). Alternatively, 17α-hydroxylated precursors can enter the sex steroid biosynthetic pathway (Figure 1.1). 17α-hydroxypregnenolone can be converted to DHEA by Cyp17a1 and subsequently converted to androstenedione by either Hsd3b1 or Hsd3b2 (Lin et al., 2015; Pallan et al., 2014), whereas 17α-hydroxyprogesterone can be converted directly to androstenedione by Cyp17a1 (Pallan et al., 2014; Zhai et al., 2018). Unlike mammals, the principal androgen in fish is 11-ketotestosterone (11KT); sequential steroidogenic modifications start with Cyp11c1 converting androstenedione to 11β-hydroxyandrostenedione, conversion to 11-ketoandrostenedione thought to be performed by Hsd11b2, and finally production of the principal androgen 11KT by Hsd17b3 (Fernandes et al., 2007; Mindnich et al., 2004; Tokarz et al., 2015). Alternatively, 11KT hypothetically can be synthesised from androstenedione to testosterone by Hsd17b3, to 11β-hydroxytestosterone by Cyp11c1, and finally to 11KT by Hsd11b2. However, this pathway is unlikely due to very low physiological concentrations of 11β-hydroxytestosterone in fish (de Waal et al., 2008). Testosterone can also be converted to the principal oestrogen in fish, estradiol, by Hsd17b3. Or an alternative oestrogen synthesis pathway is from androstenedione to estrone by Cyp19a1a/Cyp19a1b, then estradiol by Hsd17b1 (Figure 1.1). Many of the steroidogenesis pathways

are highly conserved within vertebrates, and as such, zebrafish have a great potential to become a high-throughput model for translational endocrine research (Tokarz et al., 2013).
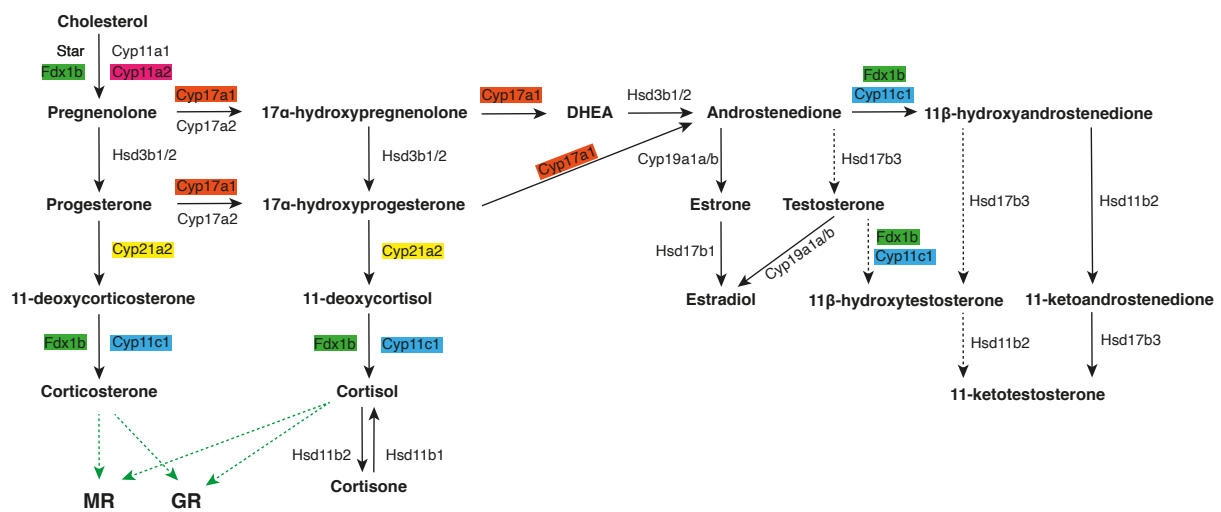
Figure 1.1. Schematic representation of the postulated pathway for steroid hormone biosynthesis in zebrafish. Steroid hormone biosynthetic pathways for mineralocorticoids, glucocorticoids and sex steroids in zebrafish. Coloured boxes highlight genes for which loss-of-function mutations exist. The minor androgen pathway is indicated by dashed arrows. Ligands of the mineralocorticoid receptor (MR) and glucocorticoid receptor (GR) are indicated by dashed green arrows.

1.4 Corticosteroid receptors and their structures

Corticosteroids are a class of steroid hormone that includes mineralocorticoids and glucocorticoids. These corticosteroids exert their systemic functions through their respective receptors, the MR and GR, through either genomic, or, non-genomic pathways (Lösel and Wehling, 2008).

The human protein MR is encoded by a single gene, *NR3C2*, located on chromosome 4. This gene consists of 9 exons, with a non-coding exon 1 and subsequent 8 exons translated to produce a 984 amino acids (aa) protein (Morrison et al., 1990). Similarly, its mammalian counterpart in mouse is located on chromosome 8 and also consists of 9 exons with only the final 8 translated to a 980aa MR protein (Kwak et al., 1993). Zebrafish *nr3c2* is located on chromosome 1 and consists of 9 exons, the last 8 of which encode a 970aa protein (Ensembl, 2016; Yates et al., 2020) In humans the single gene *NR3C2* is alternatively spliced, resulting in multiple mRNA and protein isoforms (Pascial-Le Tallec and Lombes, 2005), whereas in zebrafish, *nr3c2* encodes three protein coding transcripts, however two are flagged as incomplete coding sequences (Yates et al., 2020).

The GR in humans is translated from the single gene, *NR3C1,* on chromosome 5. This gene in humans, mice and zebrafish is comprised of 9 exons, 8 of which are protein coding (Kadmiel and Cidlowski, 2013). Once transcribed, alternative splicing, translation initiation and posttranslational modification result in multiple functional GR protein isoforms (Oakley and Cidlowski, 2013). In both rodents and zebrafish there are splice variants of a single GR gene; GRβ acts as a dominant-negative inhibitor of canonical isoform GRα (Schaaf et al., 2008). These splice variants are similar to those in humans, which also produce GRα and GRβ isoforms. Most other studied teleost fish have two GR-encoding genes, termed GR1 and GR2 (Greenwood et al., 2003), which are not equivalent to mammalian and zebrafish GRα and GRβ isoforms but were the result of a historical teleost gene duplication event (Bury et al., 2003; de Kloet, 2003; Stolte et al., 2006, 2008; Taylor et al., 2001).

Both the MR and GR are members of a nuclear hormone receptor superfamily, members of which are ligand-activated DNA-binding transcription factors. These nuclear steroid hormone receptors have a similar modular structural domain architecture. The N-terminal domain (NTD) contains the first transactivation domain, followed by a central DNA-binding domain (DBD) containing zinc finger motifs, a hinge region, and finally a ligand binding domain (LBD) at the C-terminus that also includes a second transactivation domain. A sequence comparison of human (h)MR and zebrafish (z)MR revealed a relatively high degree of conservation in the major functional domains despite diverging

450 million years ago (Pippal et al., 2011). The DBD region shared 95.6% identity and the LBD region shared 81.2% identity, although, the NTD only shared 37.5% and hinge regions only 18.5% identity (Pippal et al., 2011). Major domains can function independently, however there is also 'cross-talk' between domains that can influence the receptor's transcriptional activity (Rogerson and Fuller, 2003).
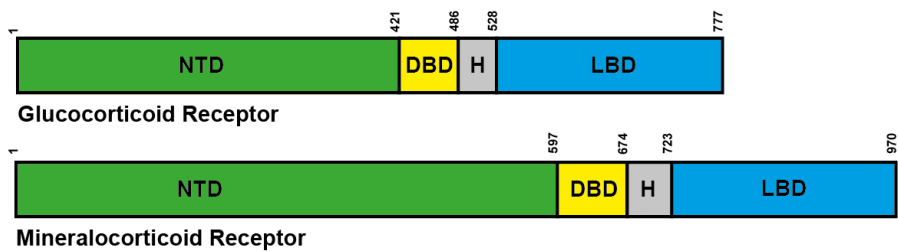
Figure 1.2. Representative figure of structure domains in zebrafish glucocorticoid and mineralocorticoid receptors. The N-terminal domain (NTD), DNA-binding domain (DBD), hinge region (H) and Ligand-binding domain (LBD) are labelled. Numbers indicate protein amino acid position.

1.5 Genomic and non-genomic corticosteroid signaling pathways

Steroid hormones are lipophilic compounds that can cross cell membranes and bind to their respective receptors in the cytoplasm. The MR and GR are classically seen as ligand-activated transcription factors, that when unbound to ligand are located in the cytoplasm, each in a multimeric protein complex with heat shock protein (HSP) 90, HSP70, and immunophilin FKBP51 (FK506-binding protein 51), which maintains the MR/GR in a conformation capable of binding to ligand (Binart et al., 1995; Binder, 2009; Bruner et al., 1997). Upon ligand binding, FKBP51 is replaced by FKBP52 which recruits dynein to translocate the ligand-bound corticosteroid receptor multiplex to the nucleus, where the MR/GR-HSP90 heterocomplex enters through the nuclear pore complex and then dissociates into its constituent parts (Binder, 2009). Genomic signaling may occur through at least three different mechanisms (Figure 1.3): i) directly - a ligand-bound receptor forms homo- or heterodimers, then the DBDs bind genomic DNA mineralocorticoid/glucocorticoid response elements (MREs/GREs) and regulate transcription of a downstream target gene; ii) tethering – a ligand-bound receptor interacts with other transcription factors to regulate transcription; iii) composite DNA binding - a ligand-bound receptor binds both MREs/GREs whilst also interacting with another transcription factor to regulate transcription (Oakley and Cidlowski, 2013). Interestingly, regulation of transcription may be in the form of activation or repression, dependent on target gene, neighbouring transcription factors and cell-type (Kadmiel and Cidlowski, 2013).

As well as genomic signaling, MR and GR may exert some functions in a non-genomic manner, characterised by rapid changes that occur too fast for genomic mechanisms to be responsible (Lösel and Wehling, 2003; Love et al., 2014; Wehling et al., 1991). Non-genomic mechanisms are suggested to act through membrane-bound corticosteroid receptors, or cytosolic interactions with kinases such as phosphoinositide 3-kinase (PI3K), and mitogen-activated protein kinases (MAPKs) (Oakley and Cidlowski, 2013). More recently, ligand-activated GRα has also been shown to translocate into mitochondria and regulate transcription of mitochondrial DNA (mtDNA) (Lapp et al., 2019).

Two antagonistic enzymes regulate the bioavailability of cortisol within the cell. 11β-hydroxysteroid dehydrogenase type 2 (HSD11B2) oxidises cortisol to cortisone, an inactive metabolite that is incapable of binding either GR or MR in the cytoplasm. Alternatively, 11β-hydroxysteroid dehydrogenase type 1 (HSD11B1) converts cortisone to cortisol (Oakley and Cidlowski, 2013). These enzymes regulate the sensitivity of glucocorticoid and mineralocorticoid activity in different cells or tissues.
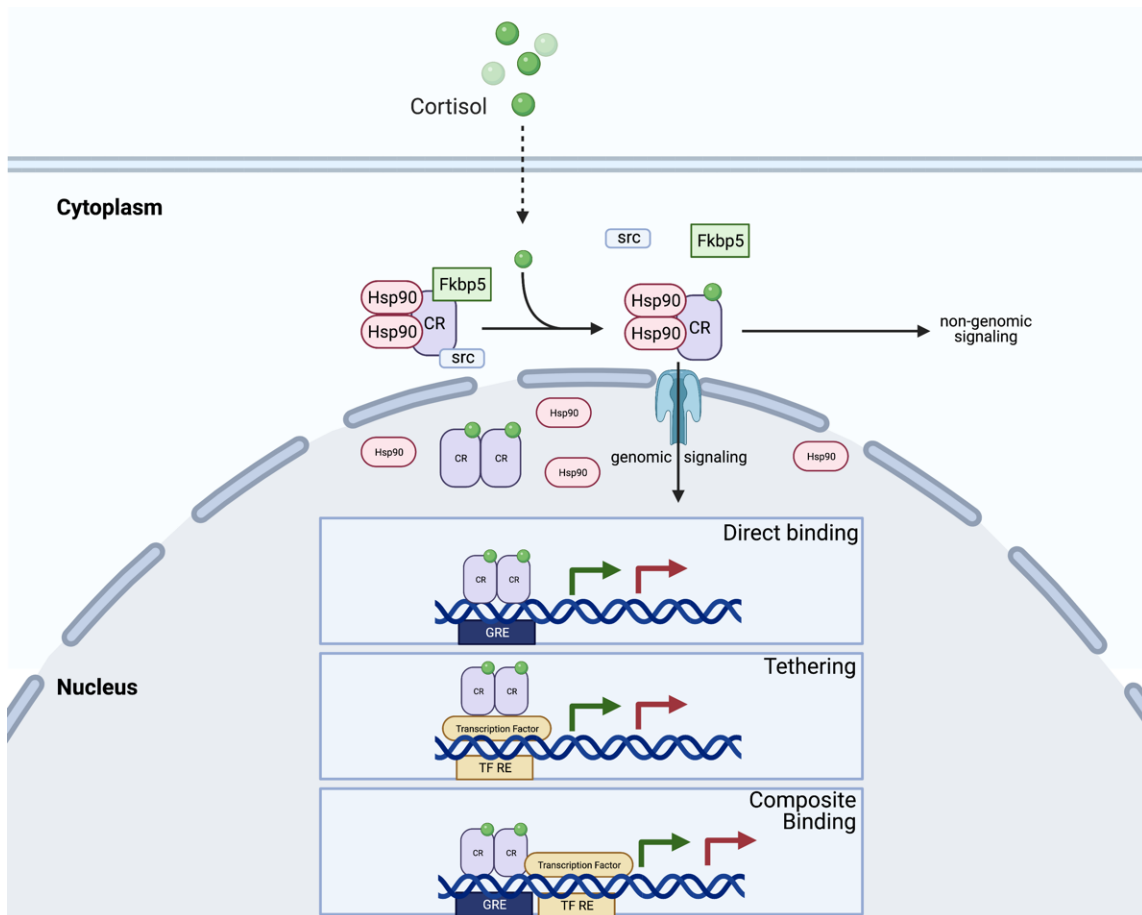
Figure 1.3. Representative figure of the canonical corticosteroid receptor signaling pathway. Cortisol enters the cell and binds corticosteroid receptor (CR), cytoplasmic CR undergoes a conformational change and disassociates from certain chaperone proteins. Cortisol-activated CR with heat shock protein (HSP) 90 translocate to the nucleus. CRs form homo- or heterodimers to regulate gene expression, either through enhancement or repression (green & red arrows). CRs may regulate transcription through direct binding of palindromic glucocorticoid response elements (GREs); tethering to another transcription factor which binds their own transcription factor-specific response element (TF RE) distant from a GRE; or composite binding to both a GRE and a neighbouring transcription factor.

1.6 Glucocorticoids and their roles in the stress response

Glucocorticoids (Gluco-cort-icoid) are named as such due to their key roles in glucose metabolism, their biosynthesis in the adrenal cortex and steroid nature. They exhibit a circadian rhythm and are biosynthesised in the adrenal gland of mammals and interrenal tissue of teleosts. The production of glucocorticoids is regulated in part by the HPI axis in teleosts and its mammalian counterpart, the HPA axis, both of which are fundamental for generating a stress response (Alsop and Vijayan, 2009; Faught and Vijayan, 2018; Griffiths et al., 2012; Tokarz et al., 2013).

Stress is a state of perturbed homeostasis (Chrousos, 2009), the physiological response to which involves activation of sympathetic-adrenal axis, resulting in release of catecholamines (adrenaline and noradrenaline), and activation of the HPA/HPI axis. Increased HPA/HPI axis activity leads to the release of the glucocorticoid, cortisol, from the adrenal gland (Charmandari et al., 2005; Joëls and Baram, 2009), and is well established that increased concentrations of blood cortisol are detectable immediately after stress in both fish and humans (Alsop and Vijayan, 2009a). Independent of the HPI, catecholamine release causes glucose mobilization, increased oxygen uptake via gills and enhanced oxygen transfer to tissues, to provide surplus energy to manage stressors (Ohr and Hammerschmidt, 2011). Homeostasis is subsequently restored through metabolic, behavioural and endocrine responses, controlled by the hypothalamus (Chrousos, 2009).

The stress response is well conserved between humans and zebrafish, and relies on activation of the HPI/HPA axis to coordinate adaptive physiological changes to resume homeostasis. In teleost fish, stress exposure is detected by sensory neurons, which relays this information to a sub-region of the hypothalamus termed the hypothalamic nucleus preopticus (NPO). The NPO response machinery is analogous to the mammalian neurons localised in the paraventricular nucleus (PVN) (Steenbergen et al., 2011). Activation of the NPO then triggers activation of the HPA/HPI axis cascade (Figure 1.4), initiated by the release of corticotrophin-releasing factor (CRF) and arginine vasopressin (AVP) from the endfeet of cells within the NPO. In teleosts, CRF and AVP is transported via neuronal projections known as the hypophyseal stalk into the anterior region of the pituitary gland, where it binds to its receptor in corticotropic cells (Steenbergen et al., 2011). This direct transport between the hypothalamus and pituitary gland does not occur in mammals, where CRF is transported to the pituitary indirectly via the blood circulation (Flik et al., 2006).

In both mammals and teleosts, binding of CRF to its receptor in the pituitary causes increased expression of pituitary-produced proopiomelanocortin (*POMC*) mRNA and increased post-

translational cleavage of the POMC, resulting in production of adrenocorticotropic hormone (ACTH). To note, two *pomc* genes have been identified in the zebrafish, named *pomca* and *pomcb* (Gonzalez-Nunez et al., 2003; Hansen et al., 2003). However, only *pomca* is associated with the HPI axis and it is the only one expressed in the pituitary gland; pomca is required for interrenal tissue development (Shi et al., 2020; Wagle et al., 2011). ACTH is secreted into the systemic circulation and targets the interrenal tissue in teleosts or adrenal cortex in mammals. Biosynthesis of the stress hormone cortisol is stimulated upon ACTH binding to the melanocortin 2 receptor (MC2R), expressed on steroidogenic cells (Steenbergen et al., 2011). After release, circulating cortisol acts on a multitude of tissues such as the liver, heart, vascular and the brain to exert metabolic and cardiovascular effects to support cognitive processes and an adaptive response (Alsop and Vijayan, 2008; Fietta and Fietta, 2007).

Importantly, glucocorticoids also regulate the HPI/A axis and their own biosynthesis through a negative feedback pathway (Figure 1.4). This is to prevent an exacerbated response to stress and return circulating glucocorticoid concentrations down to basal levels. This negative feedback loop is mediated through glucocorticoid binding GRs in both the hypothalamus and the pituitary, resulting in repression of CRH and ACTH biosynthesis (Alsop and Vijayan, 2008; Griffiths et al., 2012; Jones et al., 1977; Marchi et al., 2020). Other areas of the brain (i.e. amygdala, prefrontal cortex and hippocampus) may modulate the HPA axis through influence on neurons of the paraventricular nucleus (Spiga et al., 2014; Ulrich-Lai and Herman, 2009).

In addition to GR, MR may play an important role in feedback to the pituitary gland. It is suggested that due to the high affinity of MR for low cortisol concentrations, MR is responsible for ambient glucocorticoid signalling such as basal secretion in the circadian cycle (Dallman et al., 1989; de Kloet et al., 1998; Steenbergen et al., 2011). However, the extent to which GR and MR have distinct or redundant roles in the regulation of stress responses are still unclear in mammals and zebrafish.

During zebrafish development, larvae hatch from their protective shell, known as a chorion, between 48-72 hours post fertilisation (hpf) (Parichy et al., 2009). By this time, zebrafish larvae are expressing all components for a functioning HPI axis and *de novo* steroid biosynthesis. This includes CRF-synthesising neurons by 36hpf, corticotropic cells responsible for ACTH synthesis by 26hpf, and steroidogenic enzymes such as various hydroxylases and StAR by 28hpf. *De novo* cortisol synthesis starts at the approximate time of hatch ~48hpf, however it isn't until ~96hpf zebrafish are capable of initiating a stress response, such as elevated cortisol levels and GR-mediated gene regulation (Alsop and Vijayan, 2008; Nesan et al., 2012; Weger et al., 2018).
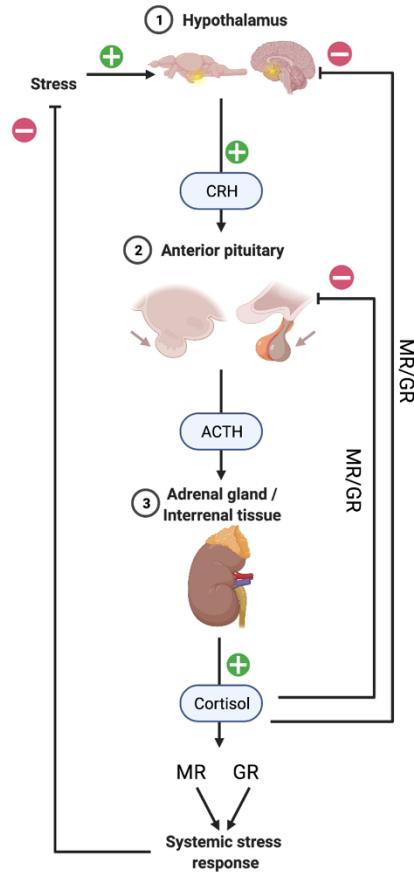
Figure 1.4. The HPA/I axis is well conserved in vertebrates. In response to stressful stimulus, hypothalamic neurons release corticotropin-releasing factor (CRF) and arginine vasopressin (AVP) which bind their respective receptors located at the anterior pituitary. POMC expression is increased and post-translational modification produces ACTH, which is subsequently released into the blood circulation. ACTH binds the melanocortin 2 receptor (MC2R) on the surface of steroidogenic cells located in the adrenal gland in mammals; interrenal in zebrafish, which stimulates corticosteroid biosynthesis leading to the stress hormone cortisol to be released into the circulation. The HPA/I has a negative feedback loop mediated through cortisol binding corticosteroid receptors such as the glucocorticoid and mineralocorticoid receptors in the hypothalamus and pituitary, resulting in suppression of CRF and ACTH production (adapted from Griffiths et al., 2012).

1.7 Systemic effects of glucocorticoid receptor signaling in zebrafish

Over the last 15 years, research into the physiological effects of glucocorticoid action mediated by the GR in zebrafish has revealed an extensive degree of evolutionary conservation between these processes in fish and mammals. Early studies of glucocorticoid receptor function using $GR^{-/-}$ mutant mice identified the importance of GR in essential physiological processes in organs such as the liver, brain, adrenal gland and HPA axis (Cole et al., 1995; Schmid et al., 1995). However, $GR^{-/-}$ mice die soon after birth, restricting the model's use to early development but not adulthood (Cole et al., 1995). Conditional mouse knockouts have been created, but they impose different limitations to investigating GR function, primarily a narrow-focused approach on a specific cell-type or organ which may limit a comprehensive understanding of systemic GR function (Tronche et al., 1999). However, zebrafish have provided an alternative model to study the physiological and pathological implications of glucocorticoid receptor dysfunction. Moreover, genetic mutants of GRs in zebrafish have become particularly valuable tools in the field (reviewed in Dinarello et al., 2020). Initial forward genetic screening of zebrafish mutants for sensory system defects identified a *gr* mutant line named s357 (Muto et al., 2005). Gr^{s357} mutants are homozygous-viable but homozygotes display a defective neuroendocrine response to a light background compared to gr^{wt} (wildtype) siblings, identified via the visual background adaptation (VBA) assay. The s357 allele harbours a point mutation resulting in a substitution of a well-conserved arginine with cysteine at aa position 443 in its DBD. Hence, this mutant's open reading frame is translated into a full-length GR protein, capable of ligand binding and translocation to the nucleus, but it lacks the DNA binding function (Griffiths et al., 2012). Gr^{s357} mutants exhibit hyperactivity of the HPI axis, due to the loss of the GR-mediated negative feedback loop, as seen by increased expression of HPI-associated genes such as *pomca* and *crh*, and elevated concentrations of the stress hormone cortisol (Griffiths et al., 2012; Ziv et al., 2013). A behavioural phenotype was also discovered. Gr^{s357} mutants displayed a decrease in exploratory behaviour and reduced habituation to stressful conditions (Ziv et al., 2013). Surprisingly, the antidepressant fluoxetine and anti-anxiety drug diazepam partially rescue these anxiety-like phenotypes (Ziv et al., 2013). Further phenotypic analysis of this mutant has revealed the importance of GR function in light adaptation in the retina and dopaminergic signaling (Muto et al., 2013), and also that adult GR^{s357} mutants display a profound increase in general locomotor and anxiety-related behaviours (Sireeni et al., 2020). Interestingly, GR is important, but not essential for exercise-enhanced growth of white skeletal muscle (Palstra et al., 2019) and glucocorticoid-induced attenuation of the inflammatory response such as neutrophil migration is signalled through the GR (Chatzopoulou et al., 2016). GR signaling is required for hematopoietic stem and progenitor cell formation (Kwan et al., 2016), for

toxicity-induced developmental defects, such as methylmercury-induced developmental neurotoxic effects (Spulber et al., 2018), and GR function is associated with ototoxicity (Hayward et al., 2019) and with plastic waste nanoparticle-induced disruption in glucose homoeostasis (Brun et al., 2019).

Recently, various novel GR knock out (KO) mutants have been generated through multiple technologies, including CRISPR/Cas9- and TALEN-mediated mutagenesis. These various GRKO mutants are viable and fertile, and have been used to study a variety of biological processes, including neuroendocrine signalling, immune responses, circadian rhythms, lipid metabolism, bone and cartilage development, and xenobiotic metabolism (Facchinello et al., 2017; Faught and Vijayan, 2018, 2019a, 2019b; Gans et al., 2020; Morbiato et al., 2019). One phenotype in common with all GRKO mutants is the existence of systemic elevated cortisol levels due to loss of the negative feedback loop on the HPI axis. Thus, a GRKO null line carrying the gr^{ia30} mutation exhibited increased expression of basal *crh* and *pomca* (Facchinello et al., 2017). One distinct difference between the gr^{ia30} and gr^{s357} mutant lines is their differential ability to elicit a response to an immune challenge. Inflammation-related gene expression was upregulated in WT control and gr^{s357} mutants after an immune challenge, which was restored following dexamethasone treatment, whereas gr^{ia30} mutants did not respond to the challenge or dexamethasone treatment (Facchinello et al., 2017).

The gr^{ia30} null line was used to identify the importance of GR function in circadian clock entrainment (Morbiato et al., 2019). The circadian clock is a physiological anticipation of the rhythmically changing environment, such as light/dark, food availability, and is regulated by evolutionarily conserved clock genes and zeitgebers (environmental synchronisers)(Morbiato et al., 2019). gr^{ia30} mutants were resistant to feeding entrainment in larvae and adults, and they exhibited both a decrease of clock gene *per2* (period 2) expression and loss of rhythmic expression of glucose and lipid metabolic genes (Morbiato et al., 2019). Together, these observations support previous findings in mammals, indicating a role for the GR and glucocorticoids in feeding synchronisation that is conserved between fish and mammals (Challet, 2019).

As outlined earlier, GR exerts its actions through a multitude of mechanisms, including both genomic and non-genomic mechanisms. Recently, a new GRKO mutant carrying the gr^{369} mutation revealed a member of the krüppel-like family of zinc finger transcription factors, *klf9*, to be a glucocorticoid-responsive, GR-specific, downstream target gene (Gans et al., 2020). This transcription factor was shown to be essential for the transcriptional induction of glucocorticoid-inducible pro-inflammatory genes (Gans et al., 2020), and had previously been identified as a GR target in other vertebrate models

(Bonett et al., 2009; Shewade et al., 2017; Spörl et al., 2012). Moreover, *klf9* has also been identified as a robustly glucocorticoid-induced transcription factor gene in the mammalian brain (Sander and Joung, 2014; Scobie et al., 2009), suggesting that this gene may perform additional biological functions to its pro-inflammatory role in the immune system.

1.8 Comparative analysis of the systemic effects of corticosteroids exerted through Glucocorticoid Receptor and Mineralocorticoid Receptor signaling in teleosts

To understand the different physiological roles of MR and GR in zebrafish, two novel mutants were generated by CRISPR-Cas9: a GRKO *gr^{ca401}*, and an MRKO *mr^{ca402}* (Faught and Vijayan, 2018a). This study established that both MR and GR are regulators of the stress response, with homozygous MRKO *mr^{ca402}* mutants exhibiting increased expression of HPI-genes *pomca* and *crh* and glucocorticoid-responsive gene *hsd11b2*, but no increase in cortisol concentrations. Furthermore, they discovered that homozygous GRKO *gr^{ca401}* mutants were unable to respond to an acute stress stimulus, whereas the response to stress in MRKO *mr^{ca402}* mutants was delayed. However, contrary to the results of Faught & Vijayan (2018a), new GRKO and MRKO mutant lines, that have been developed more recently, demonstrated a requirement for a functioning ACTH receptor *mc2r* and *gr* in generating a stress-induced locomotor-response, whereas *mr* was not required (Lee et al., 2019).

In addition to the stress response, immune response and the circadian clock, protein and lipid metabolism was studied individually in both *gr^{ca401}* mutants and *mr^{ca402}* mutants. Hypercortisolaemic *gr^{ca401}* mutants exhibited higher body mass due to an increase of lipid and protein content but not carbohydrate. This suggested that glucocorticoid signaling via GR is a growth suppressor in fish, predominantly through protein catabolism (Faught and Vijayan, 2019a, 2020). In this study, MR was shown to also have an important function in growth regulation, with activation of MR was required for glucocorticoid-induced protein catabolism. In addition, MR was important for protein synthesis, whereas GR played a larger role in protein and lipid catabolism (Faught and Vijayan, 2019a, 2020). Similarly, lipid metabolism was studied in both *gr^{ca401}* and *mr^{ca402}* mutants, which revealed an important role for MR in lipid accumulation and the biosynthesis of triglycerides, whereas GR is fundamental in lipid catabolism (Faught and Vijayan, 2019b).

There is an abundance of recent studies investigating the role of the GR in zebrafish, with a small number of very recent comparative studies of MR function. In mammals, the principal ligand of the MR is aldosterone, a key component in the regulation of sodium reabsorption in the kidney. This role

as an ion homeostasis regulator identified aldosterone and MR as major controllers of water retention, blood volume, and therefore blood pressure (Pearce et al., 2003). However, there are some critically important differences between teleosts and mammals, such as the environment they live in: teleosts are aquatic and mammals' terrestrial animals. Moreover, teleosts are unable to synthesise aldosterone and the main organ in fish responsible for the maintenance of hydromineral homeostasis is the gill, with contributions from the kidney and the intestine (Kiilerich et al., 2011). As such, it is understandable that zebrafish ion/water homeostasis mechanisms are distinct from those of mammals.

Cortisol has been suggested to be the key hormone in electrolyte homeostasis and water balance, that may be essential for seawater-freshwater adaption in fish (McCormick, 2001; McCormick and Bradshaw, 2006). Cortisol treatments upregulate saltwater adaptive electrolyte transport processes, such as increasing transcription of ion channels *NKAα1b*, *NKCC* and *CFTR* (Takahashi and Sakamoto, 2013), and cortisol treatment of the teleost intestine stimulates salt and water absorption to maintain water balance in salt water (Veillette et al., 1995). Similarly, cortisol treatment applied to the gills resulted in increased transcription of the ion channel *NKAα1a*, as well as increasing the surface area of chloride cells (indicative of ion uptake) (McCormick et al., 2008; Perry et al., 1992). The wealth of evidence establishing this important function of cortisol signalling in fish was further demonstrated to be via glucocorticoid-GR signaling, as RU486 (GR antagonist) treatment on the rainbow trout gill *in vitro*, demonstrating a reduction in cortisol-induced permeability changes, but not a complete inhibition (Kelly and Chasiotis, 2011). DOC, a ligand with high affinity for MR, was shown to change the expression of ionic transporters in the rainbow trout gill *in vitro* during hypo- and hyper-saline acclimation. However, *in vivo*, rainbow trout DOC concentrations did not significantly differ during acclimation to FW or SW (Kiilerich et al., 2011). These findings suggest that MR may act as a secondary receptor for cortisol, or that the balance of GR/MR expression is important for physiological responses in fish. Despite the essential cortisol-GR mechanism of ion homeostasis in teleosts, it is apparent that zebrafish GR mutants are competent in electrolyte homeostasis, as they do not suffer from oedema or dehydration. However, on a molecular level, this is unknown. As cortisol concentrations are elevated in GR mutants, this potentially highlights MR redundancy, or cortisol concentration compensation.

The first constitutive MR-KO homozygous viable mutant genetically engineered in teleost was one of a group of three TALEN-engineered medaka mutants (Sakamoto et al., 2016). The effect of the MR-KO mutation on osmoregulation was studied by measuring muscle water content after incubation in

different salinity environments. Sakamoto et al. (2016) showed the MR-KO medaka adapted to both freshwater (FW) and saltwater (SW, saline) similar to wildtype medaka, indicating that the MR was not required for osmoregulation in medaka. They did show MR was highly expressed in the eyes and brains of medaka, and MR-KO mutants exhibited abnormal responses to visual stimuli (Sakamoto et al., 2016). A second mutant line, a GR knockout mutation (GR-KO) was generated, which determined the importance in glucocorticoid-GR signalling in the bone repair process and osteoblast recruitment (Azetsu et al., 2019). Both MR-KO and GR-KO are viable, suggesting some potential redundancy of MR and GR functions. In zebrafish, the gr^{ia30} mutant line exhibited a four-fold increase of mr ($nr3c2$) expression in 5dpf larvae (Dinarello et al., 2020). Similarly, a significant increase of gr ($nr3c1$) expression was observed in the mr^{ia32} mutant line (Dinarello et al., 2020). In conclusion, distinct biological processes are attributed to both cortisol-GR and cortisol-MR signaling, although some functional redundancy may exist between the two proteins. A double mutant of $MR^{-/-}GR^{-/-}$ has not been reported, but it would be a desirable to create such a line to understand the biological phenotypes resulting from a complete loss of corticosteroid receptor function.

1.9 Alternative methods to studying steroid signaling in zebrafish

To investigate the roles of steroid hormones in zebrafish, genetic mutants targeting different steps of steroidogenesis have provided novel insights into the steroid biosynthetic pathway and complex biological processes regulated by steroid hormone signaling. As previously described, families of steroidogenic enzymes, their electron donor cofactors, and HSDs are responsible for the production of various steroid hormones (Figure 1.1). The first conversion step of steroid hormone biosynthesis in zebrafish requires the activities of Cyp11a2 and Fdx1b. $Fdx1b^{-/-}$ mutant larvae exhibited severe reduction in cortisol and androgen concentrations and typical glucocorticoid-deficient phenotypes, such as disrupted pigment adaptation during the VBA assay, similar to GR mutants (Griffin et al., 2016). Transcriptomic analysis of 5dpf $fdx1b^{-/-}$ mutant 5dpf larvae revealed a dysregulated oxidative stress phenotype, displaying a decrease in glutaminase transcript levels and a general increase in transcription of genes involved in glutathione metabolism, suggesting a phenotype of higher oxidative stress levels (Weger et al., 2018). Cortisol and androgen-deficient adult $fdx1b^{-/-}$ mutants display a feminised phenotype, such that males developed with predominantly female secondary sex characteristics and disorganised seminiferous tubules within the testis (Oakes et al., 2019). Together, the phenotypes of fdx1b mutants demonstrates the requirement for an electron donor to support 11β-hydroxylase activity. Fdx1b is also a cofactor for Cyp11c1, an essential enzyme in glucocorticoid synthesis, which catalyses the conversion of 11-deoxycortisol to cortisol, which is also necessary for

the conversion of androstenedione and testosterone to 11KT (Oakes et al., 2020). Cyp11a2-deficient zebrafish displayed a feminised adult male phenotype similar to that of *fdx1b* mutant males, and a similar steroid hormone profile, that includes both glucocorticoid and androgen deficiency (Li et al., 2020).

The p450 21-hydroxylase enzyme encoded by *cyp21a2* was previously demonstrated to be essential for cortisol biosynthesis in zebrafish (Eachus et al., 2017). Our group used transcription activator-like effector nucleases (TALENs) to introduce a 14-base pair deletion into the zebrafish *cyp21a2* gene, resulting in a frameshift and termination codon into the open reading frame which abolished *cyp21a2* function (Figure 8). This block in the steroidogenesis pathway caused a significant decrease in cortisol and significant accumulation of glucocorticoid precursors such as 21-deoxycortisol and 17-hydroxyprogesterone. However, the increase in glucocorticoid precursors did not rescue reduced *fkbp5* expression in *cyp21a2$^{-/-}$* mutants, suggesting *fkbp5* expression is mediated specifically through cortisol-GR signaling. Moreover, expression of the HPI axis marker gene *pomca* was found to be increased in homozygous mutants, illustrating an upregulation of the HPI stress axis (Eachus et al., 2017).

Cyp11c1, the zebrafish 11β-hydroxylase enzyme critical for glucocorticoid and 11KT biosynthesis has been mutated in two zebrafish lines (Oakes et al., 2020; Zheng et al., 2020). Similar phenotypes to adult *fdx1b* mutants were described, with feminisation of secondary sex characteristics, glucocorticoid and androgen deficiency, with disorganised testis histology and reduced sperm production. Interestingly, *cyp11c1*-deficiency also impaired female reproduction (Zhang et al., 2020). Female *cyp11c1$^{-/-}$* fish displayed defective natural mating behaviours and a reduction in egg spawning, but still produced mature eggs(Zhang et al., 2020)(Zhang et al., 2020)(Zhang et al., 2020)(Zhang et al., 2020)(Zhang et al., 2020)(Zhang et al., 2020). Cortisol treatment partially rescued this fertility phenotype, and together with reduced fertility rates of *gr^{ia30}* mutant fish, suggest a role for cortisol in zebrafish reproduction (Zhang et al., 2020).

One class of steroid hormone biosynthetic process, the mineralocorticoid pathway, has been neglected in many studies, most likely due to the lack of detectable aldosterone in zebrafish, and the fact that its principal osmoregulatory function in mammals is thought to be performed by cortisol instead. In mammals, CYP17A1 is responsible for two critical reactions of steroid biosynthesis: first, the 17α-hydroxylase activity responsible for the branching of precursors into either the mineralocorticoid pathway via pregnenolone and progesterone, and the glucocorticoid and sex

steroid pathways via 17α-hydroxyprogesterone and 17α-hydroxypregnenolone, followed by 17,20-lyase activity, which is specifically required for sex steroid production (Auchus et al., 2017) (Figure 1.1).

Zebrafish contain two 17α-hydroxylase coding genes, *cyp17a1* and *cyp17a2*, which are differentially expressed in certain tissues and perform distinct functions (Pallan et al., 2015). The Cyp17a2 enzyme is unable to perform 17,20 lyase activity even in the presence of b_5 and after an extended incubation time, whereas Cyp17a1 is a catalyst of both steroidogenic reactions (Pallan et al., 2015). Interestingly, in this study zebrafish Cyp17a2 was also discovered to be more active than Cyp17a1 in catalysing 17α-hydroxylation of both pregnenolone and progesterone. Previously it has been shown that *cyp17a1*-deficiency in a TALEN-generated mutant zebrafish line produced an all-male phenotype (Zhai et al., 2017). More recently, a novel CRISPR-generated *cyp17a1*-deficient zebrafish line was developed (Zhai et al., 2018). These *cyp17a1*-deficient fish were oestrogen- and androgen-deficient, but not cortisol-deficient. As previously described, *cyp17a1*-deficiency leads to an all-male phenotype with normal testis, spermatogenesis and normal male sexual secondary sex characteristics and sexual behaviour, implying that male development does not require testosterone or oestrogen (Zhai et al., 2018). Interestingly, the development of a juvenile ovary to a mature ovary was arrested. Here, the authors found that either testosterone or estradiol treatment from 18dpf resulted in ovarian differentiation to produce mature oocytes. As testosterone is the precursor to estradiol, it was suggested that estradiol is essential in ovarian differentiation, and that oestrogen-deficiency is the defining cause of the all-male *cyp17a1*-deficient fish (Zhai et al., 2018).

The *cyp17a1* and *cyp17a2* genes are differentially expressed in certain tissues of the tilapia, a fish within the teleost infraclass. *Cyp17a2* is expressed specifically in the head kidney, the location of the steroidogenic interrenal tissue, whereas both *cyp17a1* and *cyp17a2* are expressed in the ovary (granulosa and theca cells) and testis (interstitial cells) (Zhou et al., 2007). If Cyp17a1 is required for the correct synthesis of sex steroids but not for synthesis of cortisol, then this may suggest that the paralog *cyp17a2* is responsible for the 17α-hydroxylase activity that produces glucocorticoids. Furthermore, it is of interest to understand the molecular differences between the Cyp17a1 and Cyp17a2 paralogs that could account for their different biochemical properties.

1.10. Aims and objectives

Corticosteroids clearly play an important role in a variety of biological processes, including HPI axis regulation, developmental processes, the inflammatory response and metabolism. However, the specific and redundant roles of their nuclear hormone receptors, the MR and GR, are poorly defined.

This work aimed to enhance our understanding of corticosteroid receptor signaling in such processes. Initially, CRISPR-Cas9 genomic editing was used to produce zebrafish carrying mutations in the Mineralocorticoid Receptor. The phenotype of one such new zebrafish line was characterized in depth to elucidate the role of the MR in HPI axis regulation. Transcriptomic analysis of $MR^{-/-}$ 5dpf larvae was performed, to enable in-depth investigation of the biological and molecular processes regulated by the MR. In parallel, transcriptomic analysis of previously described gr^{s357} mutant 5dpf larvae was performed, and a comparative analysis of the two transcriptomic datasets was undertaken to identify those processes that are subject to shared and distinct regulation by MR and GR. To investigate the level of active genomic compensation between MR and GR, I also generated double $MR^{46Del};GR^{sh543}$ mutant zebrafish and characterised their morphology at adult stages.

In parallel to this work, CRISPR-Cas9 genomic editing was used to produce zebrafish carrying a mutation in the steroidogenic enzyme *cyp17a2*. Characterisation of this new zebrafish line was performed to test the hypothesis that *cyp17a2* is required for glucocorticoid synthesis and that a block preventing 17α-hydroxylase activity, but not 17,20-lyase activity, would cause precursors to flood the mineralocorticoid pathway.

Chapter 2. General Materials and Methods

2.1 Zebrafish husbandry and ethics

Adult zebrafish were maintained in a recirculating system (ZebTECTM, Tecniplast; Sheffield, UK) under a 14 hour light/ 10 hour dark photoperiod at 28.5°C. Embryos were obtained by natural spawning, incubated in E3 medium (5mmol/L NaCl, 0.17mmol/L KCl, 0.33mmol/L $CaCl_2$, 0.33mmol/L MgSO4) at 28.5°C and staged according to standard methods (Kimmel et al., 1995). Adult fish were kept in groups of the same genotype, with equal sex ratios, at comparable densities and in the same size of tank. Handling of fish was kept to a minimum in order to minimise stress and all fish were experimentally naive. All fish were humanely euthanized by administration of the anaesthetic tricaine mesylate (Pharmaq, Fordingbridge, Hampshire, UK) followed by a confirmation of death by secondary methods such as destruction of the brain by piercing of the skull with a needle or by a regulated procedure such as decapitation. All zebrafish procedures involving any experimental animals conformed to the institution's ethical requirements and UK Home Office regulations.

2.2 Breeding

Zebrafish breeding was conducted using two common methods: 'marbling' and pair mating (Westerfield, 2000). The pair mating technique was used to outcross mutant fish with wildtype fish. Both mutant and wildtype fish were sexed by conventional secondary characteristic sex differences. On the evening prior to breeding, a female and a male fish were transferred to a pairing tank, separated by a transparent divider. The next morning, soon after the initiation of the light cycle, the separating divider was removed facilitating mating. Released eggs fell through slots of the inner container and collected from the outer container. Or an inner container housing marbles was placed into an egg collecting outer container. This marble unit was placed into a single genotype tank of fish the night before and the next morning when the lights came on, spawning was initiated. Marble units were removed, and eggs collected.

2.3 Morphological Analysis

After fish were humanely euthanised, adult zebrafish body length and weight was measured and recorded. Fish were photographed intact under a dissecting microscope and organs subsequently dissected. Muscle, kidneys, gonads, livers and brains were collected for RNA extraction or whole bodies were snap frozen on dry ice and stored at -80°C for steroid extraction. Zebrafish larvae <5.2dpf

body length, Images were taken from above and body length was measured from the most anterior point (head) to the posterior tip of the tail.

2.4 Targeted genetic disruption of *nr3c2* and *cyp17a2* by CRISPR-Cas9 mutagenesis

To achieve genetic disruption of *nr3c2,* a double-stranded long oligonucleotide that included a guideRNA (gRNA) consisting of a tracrRNA backbone scaffold sequence with a T7 polymerase promoter sequence was designed, along with a custom crRNA targeting an 18-nucleotide sequence (bold, underlined), directly 3' to a protospacer adjacent motif (PAM) that targeted exon 3 of *nr3c2* (ENSDART00000172111.2). In general, it is preferable to target the start of the open reading frame to disrupt downstream domains, however *nr3c2* exon 2 contained conserved start codons (AUG) that may be able to generate shorter but functional isoforms (Oakley and Cidlowski, 2013). As such, the start of the DNA binding domain in exon 3 was targeted. To genetically disrupt *cyp17a2* (ENSDART00000076086.4), I targeted exon 1 with a custom 18-nucleotide target sequence directly next to a PAM site in the same gRNA scaffold sequence.

Nr3c2 gRNA sequence

5'
AAAAAAGCACCGACTCGGTGCCACTTTTTCAAGTTGATAACGGACTAGCCTTATTTCAACTTGCTATGCTGTTT
CCAGCATAGCTCTGAAAC**CGTAGTGGCATCCTGACG**CCTATAGTGAGTCGTATTACGC   3'

Cyp17a2 gRNA sequence

5'
AAAAAAGCACCGACTCGGTGCCACTTTTTCAAGTTGATAACGGACTAGCCTTATTTCAACTTGCTATGCTGTTT
CCAGCATAGCTCTGAAAC**CAACAGCGGCAGGCGCGG**CCTATAGTGAGTCGTATTACGC
3'

Double-stranded gRNA oligonucleotides were commercially synthesised (IDT, Coralville, Iowa, United States) and amplified by PCR with gRNA specific-primers (Table 1), 5x FIREPol PCR Mastermix (FIREpol, Solis Biodyne) and the following thermocycling conditions: 95°C, 1 minute; 40 cycles of 95°C, 15 seconds; 60°C, 30 seconds; 72°C, 20 seconds; followed by 72°C, 5 minutes. PCR products were visualised on a 3% agarose.

PCR-amplified double-stranded gRNA was extracted from the agarose gel as per manufacturer's instructions using the MinElute Gel Extraction Kit (Qiagen). 1µL of double stranded gRNA was transcribed to single strand guideRNA using Invitrogen™ Ambion™ MEGAshortscript™ T7 Transcription Kit. Transcribed gRNA was purified using an ethanol precipitation protocol: Transcription

product was diluted with 80µL of RNAase-free water, followed by the addition of 350µL 100% ethanol and 33µL of 10M Ammonium Acetate and incubated overnight at -80°C. On the following day the sample was centrifuged (30 minutes; 13000 rpm; 4°C). Supernatant was removed, pellet washed with 500µL of 70% ethanol and vortexed and centrifuged (10 minutes; 13000 rpm; 4°C). Supernatant was removed and pellet air-dried for 5 minutes at room temperature. Pellet was resuspended in 15µL of RNAase-free water and success of the transcription was determined through gel electrophoresis and quantified using a NanoDrop ND-1000 spectrophotmeter.

A 3µl solution containing 1µL gRNA (~2400ng), 1µL Cas9 enzyme (New England Biosciences, Massachusetts, US) and 1µL phenol red was prepared. Approximately 1nL of solution was microinjected into one-cell stage embryos as previously described (Hruscha et al., 2013). Post-injection, embryos were incubated in E3 medium at 28°C. The gRNA targeted a Cas9 cut-site that overlapped a target sequence for the restriction enzyme BsiYI, facilitating efficient screening for mutant alleles by restriction digest. 24hours post-injection, a random sample of injected embryos was selected, genomic DNA was extracted, and the CRISPR-targeted region was amplified by PCR using 5x FIREPol PCR Mastermix (FIREpol, Solis Biodyne) and mutagenesis target region primers (Table 1) and digested with BsiYI (NEB, Massachusetts, US) for 4 hours at 55°C. When novel mutations were identified by partial digestion of the PCR product by BsiYI, injected embryos (F0 generation) were raised to 10-12 weeks post-fertilisation and out-crossed to unrelated wildtype fish. The progeny of these out-crosses (F1 generation) were screened by PCR for mutations large enough to be visualised on a 1.8-2% agarose gel (a second band present indicating distinct allele). PCR products were TOPO-TA cloned into pCR 2.1-TOPO vector as per manufacturer's instructions (Thermo Fisher Scientific, California, United States). Plasmids were transformed into competent *E. coli* cells and plated out onto LB (*Luria bertani*) +100µg/ml ampicillin agar plates and incubated at 37°C overnight. Colony PCR was performed using FIREPol Mastermix and M13 primers and visualised on a 2% agarose gel.

Alleles distinct by size on an agarose gel were sent for in-house DNA sequencing on a 3730 DNA Analyser (Applied Biosystems, California, US). F_1 fish, heterozygous for wildtype and the identical mutant allele were incrossed to produce an F_2 generation carrying stable mutations in exon 3 of *nr3c2* or exon 1 of *cyp17a2* in heterozygotes and homozygotes.

2.5 Genotyping of *nr3c1*, *nr3c2* and *cyp17a2* mutants

Adult zebrafish were genotyped at 3 months of age. Fish were anaesthetised with Tricaine (1.53 mM Ethyl 3-aminobenzoate methanesulfonate salt, Sigma; 21 mM Tris, pH 7) diluted to 4.2%, a maximum of a third of the caudal fin was removed and stored in individual tanks for identification. Genomic DNA

was extracted from caudal fin tissue with the addition of 100µL 50 mM NaOH, boiled at 98°C for 10 minutes and cooled on ice for 5 minutes. Subsequently, 10µL of 1M Tris pH8 was added, then vortexed and centrifuged at 13,000 rpm for 5 minutes. Genomic DNA extractions were stored at -20°C. For zebrafish embryos and larvae, an individual was placed into a 200µL PCR tube, water or E3 media was extracted and genomic DNA extracted using the same method as adult caudal fins. The genomic DNA region of the mutagenesis target site was amplified using RT-PCR (reverse transcriptase-polymerase chain reaction). Region-specific primers were designed either side of the CRISPR-targeted area (Table 1). DNA was amplified in a 10µL reaction volume containing a 5x PCR MasterMix (FIREpol, Solis Biodyne) with the following thermocycling conditions: 95°C, 5minutes; 35 cycles of 94°C, 30 seconds; 58°C, 30 seconds; 72°C, 1 minute; followed by 72°C, 5 minutes. PCR products were visualised on a 2% agarose gel run at 150V for 40-45 minutes.

2.6 Steroid Hormone Measurements by Liquid Chromatography Tandem Mass Spectrometry

Zebrafish larvae aged 5dpf and adult zebrafish were humanely euthanised. 150 larvae were collected per sample, whilst adult zebrafish were collected individually; larval samples were collected in a silanized test and adult samples in bijous, which were and snap frozen on dry ice and stored at -80°C. Samples were transferred to liquid nitrogen for further freezing and subsequently fine grinded using a Mikro-Dismembrator S (Sartorius, Göttingen, Germany) and freeze dried. Samples were transported to our collaborators in S. Africa (Professor Storbeck, University of Stellenbosch) who performed Liquid Chromatography Tandem Mass Spectrometry (LC-MS/MS) to quantify steroid hormones.

Provided method:

Approximately 50mg of the dried samples were transferred to a 2ml microcentrifuge tube and resuspended in 900µl ultrapure deionised MilliQ water (Millipore, Burlington, Massachusetts, United States) and 100µl MilliQ water containing deuterated internal standard (15ng D4-cortisol, D8-17α-hydroxyprogesterone, D7- androstenedione and 1.5ng D2-testosterone). A small metal bead was added to each tube and the samples were subsequently homogenized using an Omni bead rupter 24 (Omni International, Inc., Kennesaw, Georgia, United States) for 1.5 minutes at 3.3m/s. Samples were then centrifuged for 5 minutes at 8000 x g. Supernatant was collected in a glass test tube and steroids were extracted twice using methyl tertiary-butyl ether (MTBE) (1:3). The pellet was resuspended in 1ml MilliQ water, homogenized again and extracted as described. All MTBE fractions for each sample were pooled and dried under a stream of nitrogen at 45°C. The dried samples were resuspended in 150µl 50% MeOH prior to analysis. Steroids were separated and quantified using an Acquity UPLC

System (Waters, Milford, Connecticut, United States) coupled to a Xevo TQ-S tandem mass spectrometer (Waters) as previously described (O'Reilly et al., 2017).

2.7 Sorting glucocorticoid-resistant/deficient homozygous mutants using the Visual Background Adaptation assay (VBA-assay).

Zebrafish larvae adapt to an illuminated environment by contracting their skin pigment cells resulting in a lighter phenotype. It has previously been shown that the gr^{s357} homozygous mutant larvae appear darker than gr^{wt} larvae in the VBA assay because the pigmented melanophore cells cannot concentrate their pigment granules away from the cell periphery as much as in wild-type larvae, likely due to the chronic persistence of Pomc-derived a-Melanocyte-Stimulating Hormone (a -MSH) (Muto et al., 2005). Larvae aged 4-5dpf, born from an in-cross of heterozygotes, were housed in dark conditions for 1 hour, followed by a 20-minute light exposure period. Larvae were subsequently sorted into two visual phenotypes: VBA+ (lightly pigmented wild-type or heterozygotes) and VBA- (darkly pigmented homozygotes). Subsequent genotyping identified that *nr3c2* mutants were VBA+ and *cyp17a2* and *GR*^{11Del} mutants were VBA-.

2.8 Quantification of larval and adult swimming behaviour

Zebrafish larval behaviour experiments with exposure to alternating light/dark conditions were conducted as previously described (Best et al., 2017). On the day of testing, zebrafish larvae were transferred individually into a well of a 48 multi-well plate in 500µL of E3 medium using a P1000 pipette and left to acclimate for 1 hour prior to testing. Analyses were performed in a temperature-controlled room (28.5 °C). Individuals of each genotype were randomly distributed across all wells. The locomotion of 5dpf larvae was video captured and quantified using the Zebrabox infrared camera setup and Zebralab behavioural tracking software (ViewPoint, Lyon, France). The light conditions alternated between light and dark periods every 5 minutes (300s). This 10 min cycle was repeated 6 times for a total of 60 min. The integration period for movement data was calculated and recorded every 30 sec. Total distance travelled was the sum of distance travelled during inactivity, small activity (3mm/s - 9mm/s) and large activity (>9mm/s).

For analysis of adult swimming behaviour, zebrafish were exposed to an open field test. Fish were individually placed into an opaque tank and a video recording of an individual fish's movements was tracked for a duration of 5 minutes, using the Zebralab software (Viewpoint, Lyon, France). Fish were regarded to exhibit fast swimming behaviour at speeds greater than 9cm/s.

2.9 Organ Dissection

Adult zebrafish were humanely euthanised and brain tissue was collected via dissection of the head. Firstly, the dorsal skull-plate and mandible were removed. Tissue not associated with the brain was subsequently removed. Optic nerves were severed, and the brain was lifted off the sphenoid bone plate, being careful to remove the olfactory bulbs from their skeletal sockets. The pituitary gland resides in a protective bone fossa situated in the sphenoid, which usually detaches during dissection. The pituitary was not removed and included during brain dissection.

2.10 Gene expression analysis by quantitative RT-PCR (qPCR)

To determine the expression of glucocorticoid-responsive, steroidogenic and HPI-related genes, mRNA expression analysis by quantitative RT-PCR (qPCR) was performed. Larvae were collected from incrossed $MR^{+/+}$ and $MR^{-/-}$ fish, or incrossed $GR^{+/-}$ and $cyp17a2^{+/-}$ adults. Larvae were pooled according to phenotype, ie. whether they were VBA+ or VBA-, and pools of 30 4dpf or 5dpf, 40 3dpf, 50 2dpf or 60 24hpf aged larvae and snap frozen on dry ice. Adult zebrafish were humanely euthanised, tissues of interest were then dissected and snap frozen on dry ice. Tissue was stored at -80°C overnight to denature potential inhibitors of RNA extraction and ribonucleases. Total RNA was extracted from pooled larvae or adult organs using Trizol (Ambion, Texas, United States). 1mg of total RNA from each sample was used for first strand cDNA synthesis using a Superscript III reaction kit (Thermo Fisher Scientific, California, United States) and 20mer oligo(dT) primers (IDT, Coralville, Iowa, United States). For the qPCR reaction, qPCR primers were taken from published studies or designed with multi-software approach, using Primer3 (Untergasser et al., 2012) and OligoAnalyser (IDT) and are listed in Table 1. The amplification specificity and efficiency of the qPCR primer pair were validated with accepted ranges between 90-110% efficiency with an R^2 value of >0.98.

To measure the relative gene expression, a 10mL qPCR reaction comprising of 5mL of GoTaq qPCR master mix (Promega, Madison, Wisconsin, United States), 1mL forward and reverse primers (1mM), 3mL H_2O and 1mL of 1:10 diluted cDNA was run on a 7900HT Fast Real-Time PCR System. Fold changes in gene expression are presented, with samples normalised using the elongation factor 1 alpha (*ef1a*) reference gene, with fold changes relative to age-matched wild-type controls or 24hpf timepoints.

2.11 Whole-mount *in situ* hybridisation of zebrafish larvae

2.11.1 Synthesis of DIG-labelled probe

DNA Plasmids, bacterial subcloning, plasmid extraction and preparation.

RNA probes for in situ hybridisation were made for the detection of antisense mRNA of genes of interest, with sense mRNA probes as controls. Plasmids containing DNA constructs were: *pomca*, Vincent Cunliffe lab, University of Sheffield. Plasmid DNA was suspended in dH_2O and stored long-term at -20°C. Plasmid DNA was subcloned into *E. coli* cells (DH5α competent cells, Invitrogen) with the addition of 1-20ng of DNA to 50mL of cells. Cells were incubated on ice for 30 minutes, heat-shocked for 30 seconds, incubated at 42°C in a water bath then placed on ice for 2 minutes. Subcloned cells were added to pre-warmed (37°C) SOC medium (Super Optimal Catabolite Medium, ThermoFisher Scientific) and incubated for 1 hour at 37°C at 200rpm. Approximately 100mL of subcloned cells were spread on pre-warmed selective LB and incubated at 37°C overnight. A single colony culture was taken and proliferated in LB broth as per standard molecular cloning methods (Green and Sambrook, 2012).Propagated plasmid was extracted from LB broth culture and purified using Midi-Prep Plasmid Extraction Kit (Qiagen). 5-10mg of plasmid DNA was linearised with the appropriate restriction enzyme and incubated. Linearised DNA was purified by adding an equal volume of phenol/chloroform/isoamyl alcohol (25:24:1, v/v; Invitrogen). The organic phase was extracted and precipitated with 1/10 volume 3M sodium acetate pH 5.2 and 2.5 volumes of ethanol (EtOH) at -20°C overnight. Precipitate was centrifuged and resuspended in DEPC-treated dH_2O and kept at -20°C for long-term storage.

Transcription reaction and probe purification

A 20mL *in vitro* transcription reaction containing: 1mg linearised DNA, 2mL RNA polymerase (NEB), 1mL RNase Inhibitor (NEB), 1X transcription buffer (NEB) and 1X DIG-labelling mix (Roche). The *in vitro* transcription reaction was gently mixed, briefly centrifuged and incubated for 2-5 hours at 37°C. Once successfully transcribed, 5 units of RNase-free DNase I enzyme was added and incubated for an additional 15minutes at 37°C. The RNA probe was precipitated with the addition of 2.5mL LiCl and 75mL EtOH at -80°C overnight. Solution was centrifuged at 13,000rpm for 30 minutes at 4°C. Pellet was washed with RNAase-free 70% EtOH and re-centrifuged for 20 minutes. Pellet was air-dried for 5 minutes at room temperature and resuspended in 50mL RNase-free water. RNA probe QA check was performed by gel electrophoresis on a 1% agarose gel to confirm the presence of a band the correct expected size. 50mL of deionised formamide was added and probe stored at -20°C for long-term storage.

2.11.2 Embryo harvesting and fixation

Larvae to be analysed by whole-mount *in situ* hybridisation were collected at 4dpf in 1.5mL Eppendorf tubes and anaesthetized using Tricaine Solution (MS-222, Sigma-Aldrich). Larvae were subsequently fixed in 1ml 4% PFA solution overnight at 4°C. The next day larvae were washed twice in PBST for 10 minutes and stored in 100% MeOH at -20°C.

2.11.3 Three-day whole-mount *in situ* hybridisation protocol

A standard three day *in situ* hybridisation protocol was followed, starting with rehydrating fixed zebrafish larvae that were stored in methanol, adding hybridised RNA-probe, adding appropriate antibody and finally inducing the chromogenic reaction for development of signal. All washes performed were with 1ml volume of appropriate solution and rocked gently unless otherwise specified.

Day 1: Fixed zebrafish larvae stored in methanol underwent re-hydration through methanol:PBS dilution series, washed in PTW (PBS 0.1% Tween 20) x 5, then incubated with 10mg/mL Proteinase K (Sigma) in PTW for 30 minutes. Larvae were then re-fixed for 20 minutes at room temperature. Fix was washed out through 5 x PTW washes and then larvae were incubated in 250mL hybridisation solution (50% Formamide, 5x SSC, 9.2 mM Citric acid, 0.1% Tween 20, 50µg/ml Heparin (Heparin sodium salt from porcine intestinal mucosa, Sigma), 0.5mg/ml tRNA (tRNA from baker's yeast, Sigma)) for 3 hours at 65-70°C to equilibrate. Larvae were hybridised in 250µL pre-heated hybridisation solution with 1:200 DIG-labelled RNA probe at 65-70°C overnight.

Day 2: RNA probe hybridisation solution was removed through a dilution series of pre-warmed SSC solutions at 65-70°C. Initially, 50**:**50 2xSSC: hybridisation solution (absent of Heparin and tRNA) for 20 minutes; 2xSSC for 20 minutes; 0.2xSSC for 1 hour x2. Next, larvae underwent a dilution series into PBT (PTW 2% sheep serum and 0.2% BSA) at room temperature: 50:50 0.2xSSC:PBT for 10 minutes; PBT for 10 minutes; then blocked for 3 hours in PBT. Larvae were incubated in PBT 1:2000 anti-DIG-AP (Roche) overnight at 4°C.

Day 3

The chromogenic antibody solution was removed from larvae through PTW washes for 20 minutes at room temperature x6. Larvae were equilibrated in staining buffer (100mM Tris pH 9.5, 50mM $MgCl_2$, 100mM NaCl, 0.1% Tween 20) for 10 minutes x 4 then transferred to a multi-well plate. Larvae were incubated in staining buffer including 3.5µL/ml BCIP (5-bromo-4-chloro-3'-indolyphosphate p-

toluidine salt, Roche) and 4.5µl/ml NBT (nitro blue tetrazolium chloride, Roche) until the dark signal developed. Once developed, chromogenic reaction was terminated by washing in PTW for 5 minutes x3. Larvae were fixed overnight at 4°C.

2.11.4 Image acquisition

Standard DIC images of whole-mount zebrafish larvae were captured using an Olympus BX60 and QCapture programme (QImaging). Larvae were transferred through a glycerol dilution series after *in situ* hybridization for imaging. Larvae were transferred onto microscope slides (Super Premium, VWR) in small wells that were created by layering 1-3 pieces of electrical tape with a central well cut out and mounted with a coverslip (22 x 22 mm # 1, VWR) for imaging.

2.12 RNA Sequencing

2.12.1 RNA Isolation

Thirty 5dpf zebrafish larvae were pooled into 1 sample, snap frozen on dry ice and stored at -80°C until RNA extraction. Individual 18-month old adult zebrafish brains were dissected with olfactory bulbs and stored at -80°C. Total RNA extraction was performed using the commercial RNAeasy Mini Kit (Qiagen) as per manufacturer's instructions. RNA integrity was evaluated on a 1% TAE agarose gel and the Agilent Bioanalyser (2100, Agilent Technologies, USA). RNA samples were sent to Technische Universität Dresden, Germany on dry ice by next-day-delivery (FedEx).

2.12.2 RNA library preparation and sequencing

RNA library preparation and sequencing were performed by the Deep Sequencing Facility at Technische Universität Dresden, Germany. mRNA isolation was achieved using the NEB Next poly(A) mRNA magnetic isolation module with approximately 300ng total RNA input. Libraries were produced using the NEBNext ultra II directional RNA library prep kit for Illumina (NEB, Ipswich, Massachusetts, United States). mRNA libraries were sequenced using a 75bp single-end method and performed on a NextSeq 500 sequencing system (Illumina, San Diego, California, United States) to a depth of approximately 30 million reads per sample.

2.12.3 mRNA sequencing data analysis

Raw data sequencing files (Fastq.gz) were produced by Technische Universität Dresden and were made available. RNA sequencing reads were trimmed using Trimmomatic v0.39 (ILLUMINACLIP:Trimmomatic-0.39/adapters/TruSeq3-SE.fa:2:30:10 LEADING:3 TRAILING:3 SLIDINGWINDOW:4:15 MINLEN:36) (Bolger et al., 2014), and rRNA sequence contaminants were removed using SortmeRNA v2.1 (Kopylova et al., 2012). Sequence reads were quality controlled using FastQC (Andrews, 2010). Individual quality control files were combined with MultiQC (Ewels et al., 2016). Quality processed sequence reads were aligned to the zebrafish genome (GRCz11) using STAR and number of reads per gene was quantified using STAR's --quantMode GeneCounts option.(Dobin et al., 2013). These steps were performed on the University of Sheffield's high-performance computing (HPC) cluster ShARC.

2.12.4 RNAseq differential expression analysis

Bioinformatic analysis was performed in RStudio (R v3.6.1). R package DESeq2 was used for differential expression analysis (Love et al., 2014). The DESeq2's 'result' function accepted FDR score input was 0.05, a more stringent threshold than the default 0.1. The threshold of significance was an adjusted p-value <0.05. PCA plots, heatmaps and graphs were created using the ggplot2 package in R. Schematic of RNAseq pathway displays workflow (Figure 2.1).

2.13 Statistical Methods

All statistical analyses were performed using GraphPad Prism 7 (GraphPad Software, San Diego, California, US). Data normality was evaluated using normality tests available: Shapiro-Wilk, D'Agostino-Pearson and Kolmogorov-Smirnov, and all other assumptions for any statistical test were carried out. Normally distributed data was analysed using unpaired *t*-tests or ANOVA. A Tukey Multiple Comparison test was used post-ANOVA to identify between which means a significant difference occurred. If data did not meet the required assumptions for any statistical test, outliers were identified using ROUT method, data transformations may have been applied, or non-parametric tests were performed.
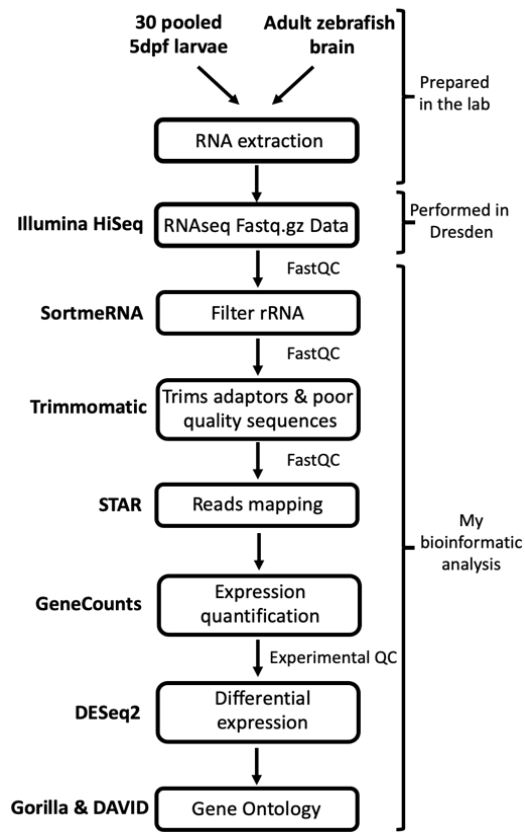
Figure 2.1. Schematic of RNAseq analysis pathway.

Table 2.1. Primer sequences for genotyping and RT-quantitative PCR

Gene	Forward	Reverse	Citation
CRISPR gRNA	AAAAAAGCACCGACTCGGTGCCAC	GCGTAATACGACTCACTATAG	Marchi et al., (2020)
cyp17a2 genotype	AGAGTGTGTGTTGCTCCAGG	CAACGCCCCAATTGTGAAAT	This thesis
ef1a	GTGGCTGGAGACAGCAAGA	AGAGATCTGACCAGGGTGGTT	This thesis
fkbp5	TTCCACACTCGTGTTCGAGA	ACGATCCCACCATCTTCTGT	Griffin et al., (2016)
GR genotype	CCAAACTTTCAGGCAGCAGT	TCCGCAAGTGAGAACTCCAT	Marchi et al., (2020)
hsd11b2	TGCTGCTGGCTGTACTTCAC	TGCATCCAACTTCTTTGCTG	Alsop and Vijayan (2008)
MR genotype	GACCATGAGAACACCTGCAC	TGAGTCTTACCTTCTACCGCTC	This thesis
pck1	TGACGTCCTGGAAGAACCA	GCGTACAGAAGCGGGAGTT	Griffin et al., (2016)
star	TTGAACAAGCTCTCCGGACC	TCACTGTATGTCTCCTCGGC	This thesis
tsc22d3	CGGAGGGGATGTAGTATCGG	CTCCACTTCCTCCCTGACTG	This thesis

Chapter 3.   Creation of mineralocorticoid receptor loss-of-function mutant zebrafish lines and phenotypic analysis of mutants at larval stages of development

3.1 Introduction

The mineralocorticoid receptor (MR) was originally recognised as the regulator of blood pressure in mammals, mediating the effects of its principal ligand, aldosterone, through regulation of renal electrolyte and fluid homeostasis (Funder, 2005). In mammals, the MR is essential for survival to adulthood as MR-null mutant mice die prematurely, approximately 1-2 weeks postnatally, from defective homeostatic control of renal electrolyte balance (Cole and Young, 2017). However, teleosts appear to lack the canonical mineralocorticoid, aldosterone, and their control of ion balance and osmoregulation are mediated by glucocorticoids through the glucocorticoid receptor (Cruz et al., 2013). The aldosterone precursor, corticosterone was measured at negligible concentrations in wild-type zebrafish (Oakes, Li, Cunliffe and Krone, unpublished), and with no aldosterone synthase homolog yet identified in teleosts, it has been suggested that zebrafish lack the ability to produce aldosterone (Bury and Sturm, 2007). Yet the MR is present in every major vertebrate clade, including all teleosts, indicating its physiological importance independently of a potential role in osmoregulation (Baker et al., 2013). The current view is that the aldosterone-activated MR evolved during the transition from salt water to land in response to dramatic osmoregulatory challenges encountered by pioneer species, which is supported by aldosterone first appearing as a detectable steroid in terrestrial tetrapods (Bridgham et al., 2006).

In addition to the kidneys, MR is expressed and functions in a variety of non-epithelial tissues, including the heart, adipose tissue, endothelial and immune cells; and the brain (Funder, 2017). In mammals and zebrafish, the MR can be activated not only by aldosterone, but also by glucocorticoids such as cortisol, and mineralocorticoid precursors such as corticosterone and 11-deoxycorticosterone at a similar concentrations of ligand (Baker and Katsu, 2017). In mammals, the importance of the MR and its various physiological ligands is highlighted by the co-expression of 11ß-hydroxysteroid dehydrogenase type 2 (HSD11B2) in mammalian epithelial cells where aldosterone-MR activation is essential (Edwards et al., 1988). At these locations, HSD11B2 converts endogenous cortisol to the inactive metabolite, cortisone, facilitating MR activation by aldosterone. By contrast, at locations of low HSD11B2 expression, such as the brain, glucocorticoids are the major ligands for the MR and regulate MR-specific functions such as its involvement stress recognition and regulation (Berger et al., 2006; Rozeboom et al., 2007).

Stress is a state of perturbed homeostasis (Chrousos, 2009), the physiological response to which involves the activation of the Hypothalamic-Pituitary-Adrenal (HPA) axis in mammals, or the Hypothalamic-Pituitary-Interrenal (HPI) axis in fish (Wendelaar Bonga, 1997). Recognition of a stress stimulus results in CRH release from the hypothalamus, binding of its receptor in the pituitary gland and then causing the consequent release of ACTH into the circulatory system. ACTH binds its receptor MC2R in the adrenal cortex in mammals, or analogous interrenal cells in fish, initiating synthesis of the stress hormone, cortisol (Charmandari et al., 2005). The role of corticosteroid receptors in fish, and specifically the regulation the HPI axis has primarily focused on the GR in fish (Alsop and Vijayan, 2009; Best and Vijayan, 2017; Facchinello et al., 2017; Griffiths et al., 2012; Marchi et al., 2020; Nesan et al., 2012; Pikulkaew et al., 2010; Wilson et al., 2013; Ziv et al., 2013). Previously, an MR-KO mutant medaka was reported, but the role of MR on the HPI axis functioning was not investigated (Sakamoto et al., 2016). Recently, an $MR^{-/-}$ mutant zebrafish line was developed, which exhibited increased HPI axis-related gene expression of *pomca* and *crh*, however no changes in cortisol concentration were observed between $MR^{-/-}$ mutants and wildtype controls (Faught and Vijayan, 2018). Under a stress stimulus $MR^{-/-}$ elicited a delayed stress response; resulting cortisol concentrations were sustained for longer than wildtype controls (Faught and Vijayan, 2018).

To investigate the function of the MR in teleosts, and to test the hypothesis that the conserved HPI axis is regulated by the MR, I generated an MR-deficient zebrafish line using CRISPR/Cas9 mutagenesis The use of zebrafish as a model is advantageous as this species has only one MR-encoding gene (*nr3c2*) and one GR-encoding gene (*nr3c1*), unlike other teleost species that have additional paralogs of GR (Alsop and Vijayan, 2008). My results indicate that the MR plays an important role in maintaining baseline HPI axis levels, and with the loss of MR function there is a de-repression of stress-related gene expression and increase in whole body cortisol concentrations.

3.2 Results

3.2.1 Expression of *GR* (*nr3c1*), *MR* (*nr3c2*), and the glucocorticoid-induced gene *hsd11b2* is significantly increased at time of hatching in wildtype zebrafish larvae.

During early zebrafish development, embryos are encased in a protective shell known as the chorion. The chorion is composed of mainly proteins and glycoproteins and provides a structure to house the perivitelline fluid that embryos develop in. This chorion functions to provide physical, chemical and ionic protection from the conditions of the external environment (Cotelli et al., 1988; Groot and

Alderdice, 1985). Zebrafish larvae hatch from their chorions between 48-72 hours post fertilisation (hpf) and are exposed for the first time to the external environment and are known to begin *de novo* cortisol synthesise cortisol *de novo* between ~48-72hpf, whereas HPI axis-induced cortisol synthesis commences at ~97hpf (Alsop and Vijayan, 2009).

To understand the expression dynamics of cortisol receptors and the glucocorticoid-induced gene *hsd11b2* during various intervals of early development, a *MR* and *GR* mRNA expression was measured by quantitative-PCR (qPCR). Pools of 60x 24hpf, 50x 48hpf, 40x 72hpf, 30x 96hpf and 30x 120hpf wildtype AB strain zebrafish larvae were snap frozen and RNA extracted. Target gene expression in each sample was normalised to the reference gene *ef1a*, and each organ-specific ΔCT expression relative to the target gene expression detected in 24hpf (Figure 3.1). Low expression of *MR*, *GR*, and *hsd11b2* was detected at 24hpf, suggesting maternal transcript deposition or early zygotic transcription of these genes. No significant difference was seen between stages 24hpf and 48hpf ($p > 0.9999$). However, a large significant increase was seen in *MR* ($p = 0.0381$), *GR* ($p = 0.0004$) and *hsd11b2* ($p < 0.0001$) mRNA expression at 72hpf in comparison to their expression levels at 48hpf. This corresponds with the previously identified *de novo* cortisol synthesis and HPI axis component gene expression timeframe (Alsop and Vijayan, 2009b). *MR* mRNA expression is significantly increased from 72hpf to 96hpf ($p = 0.0429$), whereas *GR* displays a non-significant increase ($p = 0.0559$), where it plateaus, and no significant difference is seen between 96hpf and 120hpf ages (*MR* $p = 0.9999$; *GR* $p = 0.9273$). After the great increase of *hsd11b2* mRNA expression between 48hpf and 72hpf, subsequent *hsd11b2* expression is significantly reduced between 72hpf and 96hpf ($p = 0.0005$). Similarly, no significant difference in *hsd11b2* expression was seen between 96hpf and 120hpf ($p = 0.0894$). This mRNA expression suggests that cortisol synthesis, the HPI axis and the *MR*, *GR* and *hsd11b2* play an important role at the hatching stage of development in zebrafish larvae.

3.2.2 - The mRNA expression of *GR* (*nr3c1*), *MR* (*nr3c2*), and the glucocorticoid-induced gene *hsd11b2* varies between organs of adult wildtype AB zebrafish.

In mammals, the *MR* is highly expressed in the renal epithelial cells of the kidney, alongside the glucocorticoid-induced, cortisol inactivating enzyme *hsd11b2;* this facilitates aldosterone-specific MR activation. In the brain, *MR* is expressed in certain regions with little to no *hsd11b2* expression, facilitating cortisol-mediated signaling (Edwards et al., 1988). To investigate the gene expression patterns of *MR* (*nr3c2*), *GR* (*nr3c1*) and *hsd11b2* in zebrafish organs, adult wildtype AB fish were humanely euthanised, organs harvested and snap frozen, and RNA extracted. Target gene expression

in each sample was normalised to the reference gene *ef1a*, and each organ's ΔCT expression relative to the target gene expression detected in the kidney. The expression of *MR* was significantly higher in the brain (p=0.0004), eyes (p=0.0001) and gill (p<0.0001) than the kidney; whereas there was no significant difference in expression seen in the gut, heart muscle or testes (Figure 3.2). A similar pattern was seen for *GR* expression, with significantly greater expression exhibited in the brain (p<0.0001) and eyes (p=0.0012); and a trend of increase expression exhibited in the gill, gut, muscle and testes that did not reach statistical significance in a one-way ANOVA Tukey's multiple comparison test (although the threshold for significance was reached using individual unpaired t-tests). By contrast, *hsd11b2* expression was significantly less in the brain compared to the kidney (p=0.0063); no other statistically significant difference was observed between the kidney and the gill, gut, muscle, eye or testes (Figure 3.2).
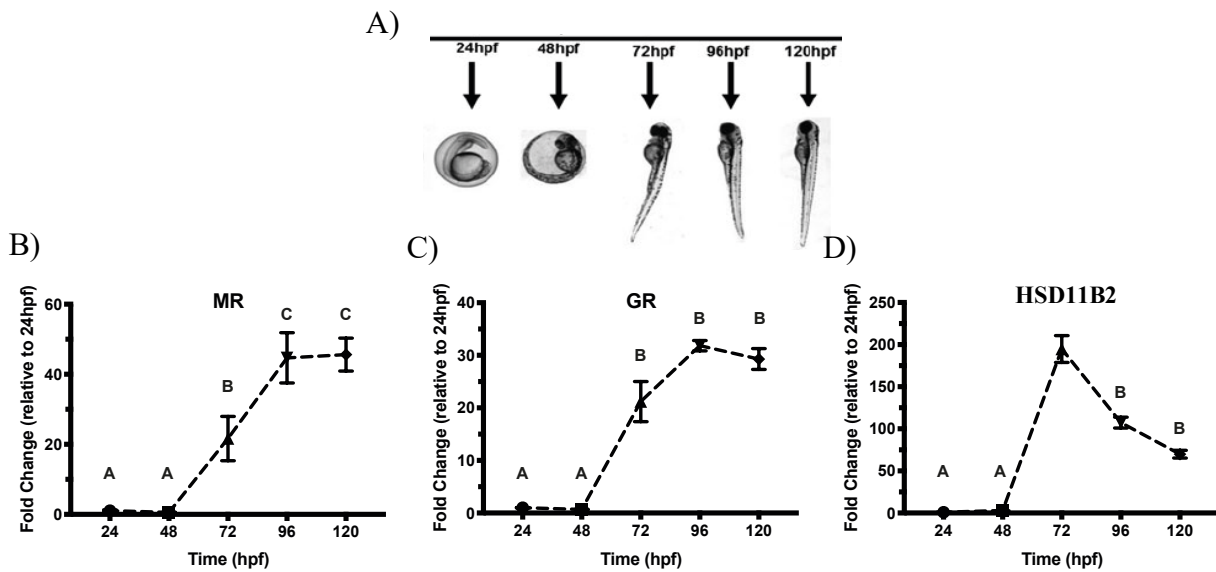
Figure 3.1. A time course of *MR* (*nr3c2*), *GR* (*nr3c1*) and *hsd11b2* mRNA expression dynamics throughout zebrafish larvae development. A) Image of zebrafish larval development between 24hpf and 120hpf (Adapted from: Oyarbide et al., 2012). B) For each sample, 60 24hpf, 50 48hpf, 40 72hpf and 30 96hpf and 30 120hpf wildtype AB zebrafish larvae were pooled, snap frozen, RNA extracted, and qPCR was employed to quantify mRNA expression of *MR*, *GR* and *hsd11b2*. Fold change for each timepoint is relative to 24hpf. There was no significant difference in *MR* expression between 24hpf and 48hpf, however a subsequent significant increase in *MR* expression was identified at 72hpf (48 vs 72: p=0.0381), and further significant increase at 96hpf (72 vs 96: p=0.0429), where expression plateaued and no difference was seen at 120hpf. C)Similarly, there was no significant difference in *GR* expression between 24hpf and 48hpf, however there was a subsequent significant increase at 72hpf (48 vs 72: p=0.0004), and a further trend displaying an increase at 96hpf (72 vs 96: p=0.056) and no difference at 120hpf. D) Likewise, *hsd11b2* expression did not significantly increase until 72hpf (48 vs 72: p=<0.0001), however expression was then significantly reduced at 96hpf (72 vs 96: p=0.0005) and no significant difference was seen at 120hpf. All data points are mean ±SEM (n = 15, each n is a pooled sample). Results analysed by one-way ANOVA and Tukey's multiple comparison test. Letters signify statistical significance between timepoints (A<B<C).
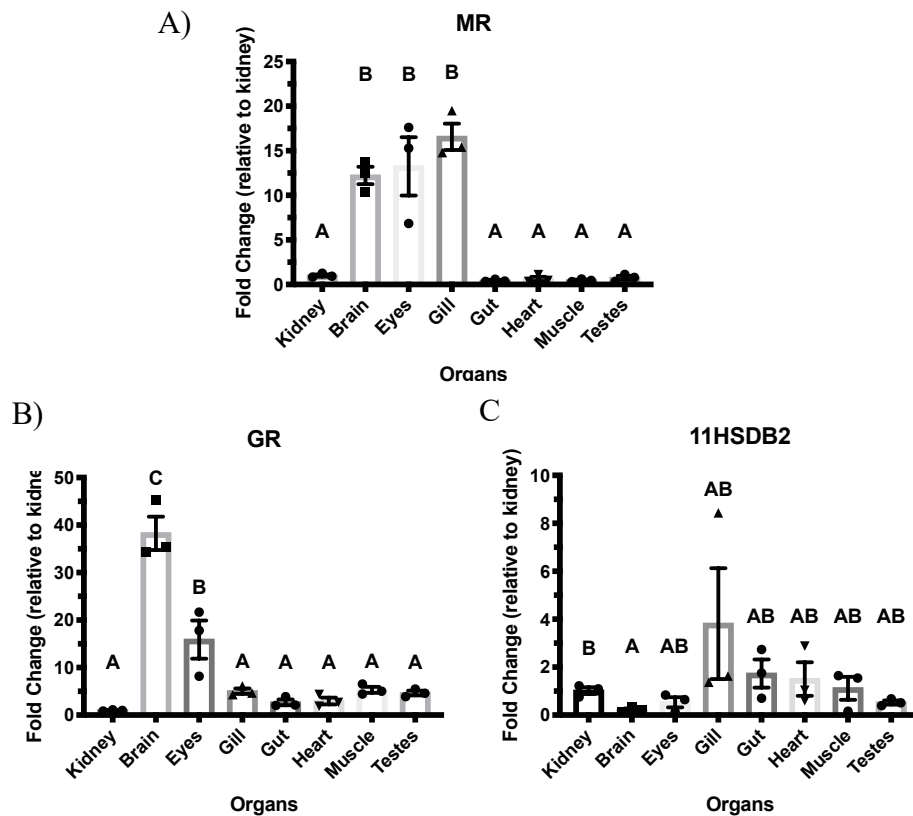
Figure 3.2. mRNA expression of *MR*, *GR* and *hsd11b2* in organs of adult wildtype AB zebrafish. qPCR was employed to measure the expression of two cortisol receptors and a cortisol-inducible gene in 8 organs throughout the body. Fold change for each organ's expression is relative to the kidney. A) The expression of MR was significantly higher in the brain (p=0.0004), eyes (p=0.0001) and gill (p<0.0001), than the kidney. There was no significant difference in MR expression in the gut, heart, muscle or testes in comparison to the kidney. B) A similar expression pattern was observed for GR, with a significant increase in expression in the brain (p<0.0001) and eye (p=0.0012) but not in the gill, relative to the kidney. C) Whereas the expression of hsd11b2 was significantly lower in the brain (p=0.0063) than the kidney. No other significant differences in *hsd11b2* expression were identified in other organs. All data points are mean ±SEM (n = 3). Results analysed by one-way ANOVA and Tukey's multiple comparison test. Letters signify statistical significance between organs (A<B<C).

3.2.3 - Targeted mutation of exon 3 of the zebrafish MR (nr3c2) gene to generate MR loss-of-function mutant alleles by CRISPR-Cas9

To investigate the function of *MR* (*nr3c2*) in zebrafish, a genetic knock-out approach was taken utilising CRISPR-Cas9 mutagenesis. *Nr3c2* encodes three protein coding transcripts, however two of these transcripts appear to be incomplete coding sequences. The largest and complete transcript *nr3c2*-203 is 3540bp in length and comprises of 9 exons, encoding a 970 amino acid protein (Yates et al., 2020). A guide RNA (gRNA) of 18 nucleotides was designed to target exon 3, which encodes the start of the functionally important DNA-binding domain (DBD) and lies upstream of the ligand binding domain (LBD). Nuclear receptors, such as MR, are a family of ligand-activated transcription factors. Thus, I aimed to disrupt the *MR*'s two functional domains to prevent ligand binding and DNA binding and I hypothesised this would generate an *MR* loss-of-function mutation. The gRNA consisted of a target specific CRISPR RNA (crRNA) that overlapped with a PAM site and a restriction enzyme (RE) target sequence (Figure 3.3). The tracrRNA scaffold sequence was included in this gRNA.

The *MR*-specific gRNA was injected along with Cas9 protein into the yolks of 50 1-cell stage zebrafish embryos. After incubation of injected embryos for 24hrs at 28.5°C, embryos aged 1-day post fertilisation (dpf) were culled, genomic DNA (gDNA) was extracted, and the targeted genomic DNA sequence was amplified by PCR to form a 250bp amplicon (Figure 3.4; positive control (+ve)). A restriction digest assay revealed that PCR amplicons generated from gDNA of non-injected embryos were completely digested into two discrete products identified as ~110bp and ~140bp bands (Figure 3.4; Uninjected). In contrast, the PCR of gDNA extracted from 10 of the 12 embryos injected with *MR* gRNA and Cas9 protein resulted in a 250bp amplicon, with very faint bands at ~110bp and ~140bp size. This indicates that mutations have been induced at the target site which has resulted in the disruption of the RE target site in a high percentage of the embryonic cells (Figure 3.4), suggesting a very efficient CRISPR-Cas9 mutagenesis. 1 of the 12 *MR* gDNA injected embryos was completely digested signifying no mutagenesis had occurred, and 1 of the 12 failed to amplify and no band is visualised (Figure 3.4). The remaining population of injected zebrafish embryos (F_0) were raised to adulthood and at 3 months of age they were screened for germline mutations (Figure 3.5). CRISPR-injected females were outcrossed with wildtype males and vice versa, and the resulting progeny were collected. The F_1 progeny were screened by PCR, restriction enzyme digestion and agarose gel electrophoresis, for the presence of mutant alleles (a second band) visually distinct from the wildtype allele identified as 200bp amplicon (Figure 3.5A). Two germline mutations were identified. Thus, in Outcross 1 a second, larger band is apparent in comparison to the wild-type band (Figure 3.5A; green

box). By contrast, in Outcross 2, a second smaller band is present (Figure 3.5A; red box). PCR products with distinct second bands were cloned into pCR 2.1-TOPO TA vectors, transformed into competent *E. coli*, colony PCR performed and visualised by agarose gel electrophoresis (Figure 5B). Highlighted in green are the two distinct alleles identified in Founder 1: the wild-type 200bp band and the larger mutated band. Highlighted in red are the two distinct alleles identified in Founder 2, the wild-type 200bp band and the smaller band (Figure 3.5B). The wild-type and mutant alleles were sequenced and a 25bp insertion with a 2bp substitution mutant allele was identified in Founder 1, and a 46bp deletion with a 2bp substitution was identified in Founder 2 (Figure 3.5C&D).

The 25bp insertion and 2bp substitution mutation leads to a frameshift at codon 597 and a premature stop codon 52 amino acids later (T597*fsX*52). By contrast, the 46bp deletion and 2bp substitution mutation leads to a frameshift at codon 597 and a premature stop codon 16 amino acids later (T597*fsX*16). These two mutations will be referred to as MR^{25Ins} and MR^{46Del} for future reference. It is predicted that the DNA binding domain of the wild-type allele is located between residues 597-674, and the ligand binding domain is located between residues 723-970. Accordingly, I predict that both mutations result in a loss of DNA-binding and ligand-binding domains (Yates et al., 2020).

These F_1 progeny were raised to sexual maturity, genotyped and sequenced; heterozygous fish carrying the same mutation were subsequently intercrossed. Founder 1 also carried other mutations visible by PCR in the germline which were not maintained. The resulting F_2 population was genotyped and genotype ratios indicated that the new alleles followed Mendelian inheritance principles (Figure 3.6).
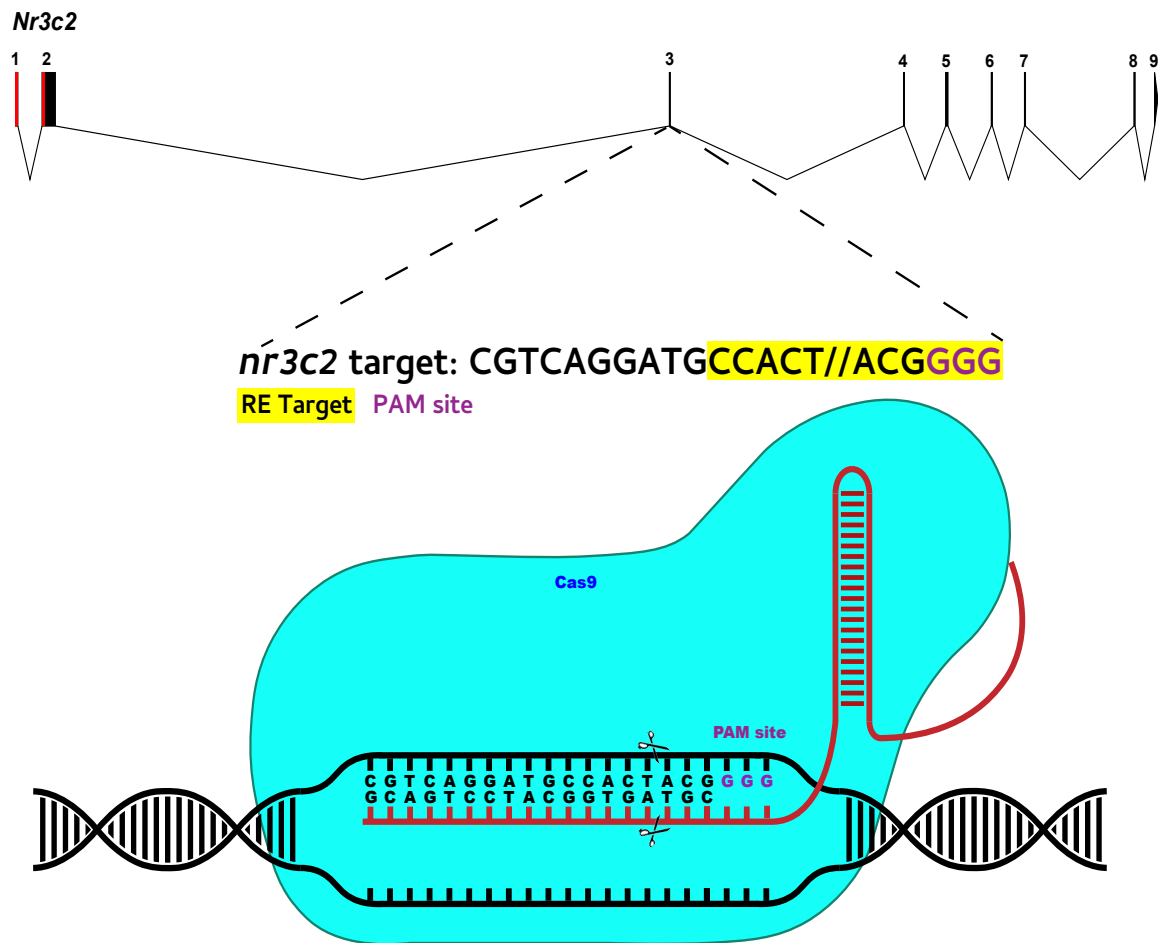
Figure 3.3. CRISPR-cas9 technology was utilised to generate a targeted mutation in *nr3c2*. Top) Exon 3 was targeted with a custom-designed 18 nucleotide guideRNA plus PAM site (purple) that would induce a DNA double-stranded break (//) that overlapped the restriction enzyme BsiYI's target sequence (yellow) at the start of the DNA binding domain. Bottom) Schematic of guideRNA (red) and Cas9 enzyme (blue) activity generating a DNA double-stranded break (scissors) 3 nucleotides from PAM site.
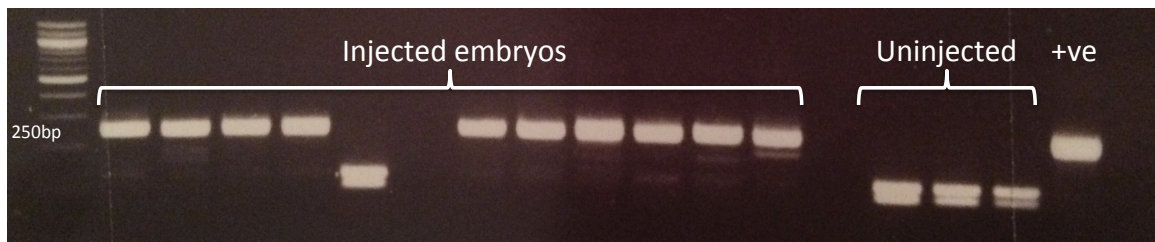
Figure 3.4. *MR (nr3c2)* CRISPR-Cas9 target validation assay. Restriction enzyme assay to screen for novel mutations in *MR*. DNA was extracted from twelve CRISPR gRNA injected and four uninjected zebrafish embryos and the targeted genomic region was subsequently amplified by PCR. The *MR* gRNA target sequence overlapped a restriction enzyme target site for BsiYI. All injected and three uninjected PCR products were digested with the restriction enzyme BsiYI. One uninjected sampled was used as an undigested positive control (+ve). The undigested PCR product is ~250bp. This ~250bp PCR product when digested, produces two products: ~110bp and ~140bp, seen as two discrete bands in the uninjected samples. In 10/12 injected samples, there is a single ~250bp band and very faint bands at ~110bp and ~140bp. This indicates that in 10/12 gRNA injected samples, the gRNA target has induced a mutation that has altered the DNA sequence and disrupted the restriction enzyme target site, which prevents digestion. 1/12 injected embryo's DNA was 100% digested signifying mutagenesis did not occur, and 1/12 injected embryos gDNA did not amplify by PCR.
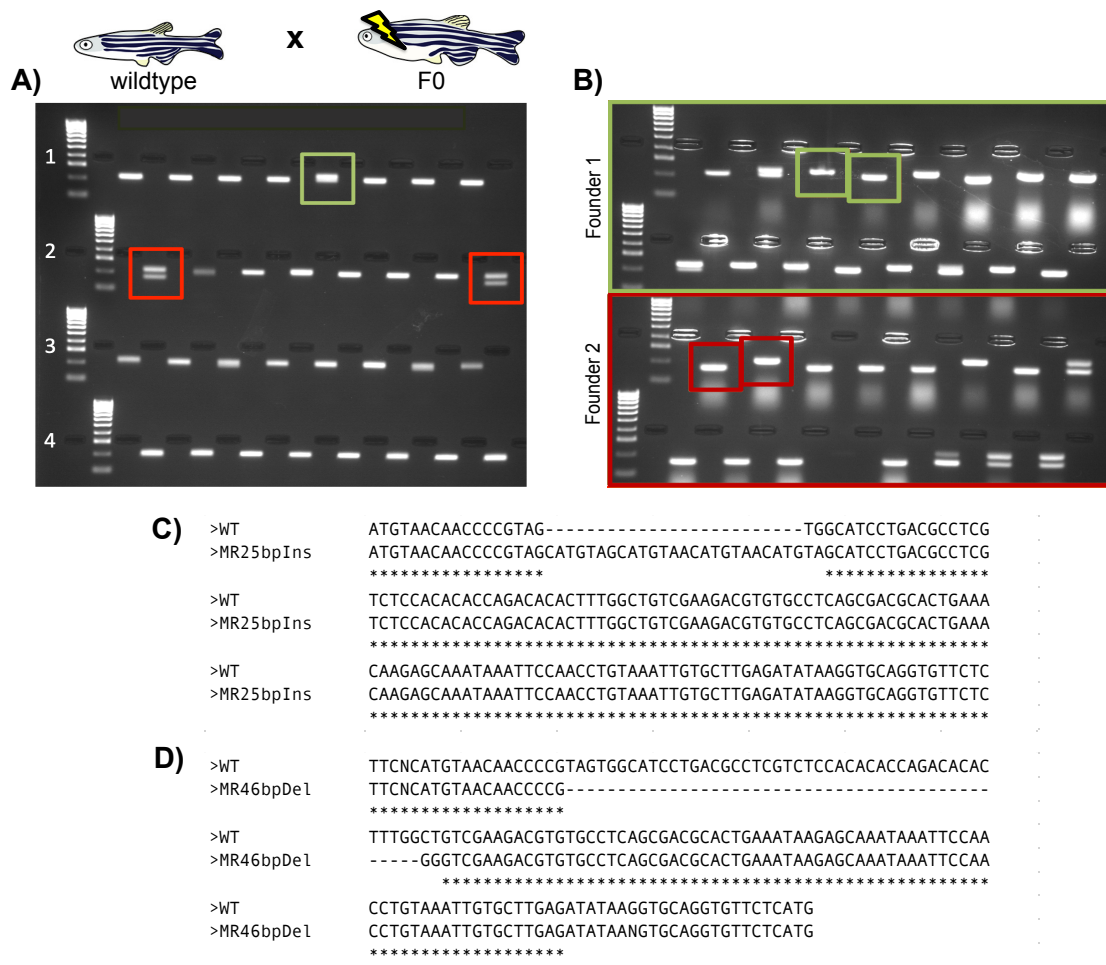
Figure 3.5. *MR* mutant founder screening. A) The CRISPR/Cas9-injected F0 generation was outcrossed with wildtype fish; progeny from four different outcrosses are represented here (rows 1-4). DNA was extracted from 8 progeny from each outcross and the targeted genomic region was amplified by PCR and visualised on an agarose gel. In Outcross 1, 1/8 progeny have a second allele band slightly larger in size than the expected wildtype 200bp allele band (green box). In Outcross 2, 2/8 progeny have a second allele band smaller than expected wildtype 200bp band (red box). B) TOPO TA cloning of Outcross 1 and Outcross 2 segregates wildtype and mutant allele bands for sequencing. C) *MR* genomic DNA sequencing of the mutant allele in Outcross 1 identified a 25bp insertion with a two base pair substitution. D) *MR* genomic DNA sequencing identified the mutant allele as a 46 base pair deletion and a two base pair substitution in progeny from the Outcross 2.
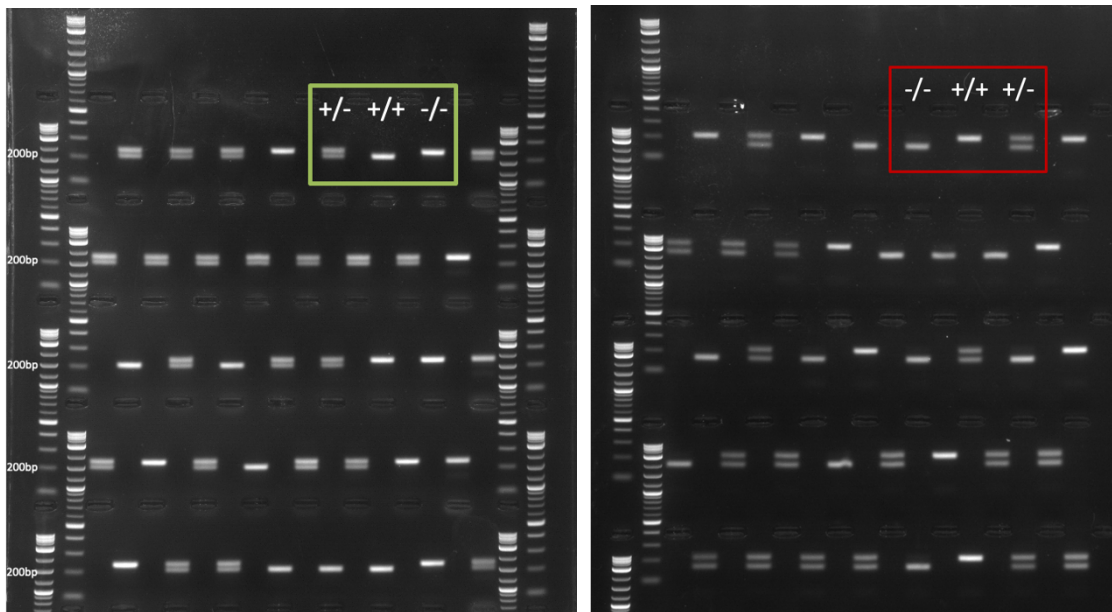
Figure 3.6. *MR^{25Ins}* and *MR^{46Del}* F$_2$ genotyping reveals adults are homozygous viable. F$_1$ *MR* zebrafish, heterozygous for the 25bp insertion (left) or 46bp deletion (right), were in-crossed. The F$_2$ progeny were genotyped at 3months old by PCR. Genotype ratios did not deviate from Mendelian inheritance. Left) Three individuals highlighted in the green rectangle are heterozygous (left), wildtype (middle) and homozygous (right) carrying the *MR* 25bp insertion mutation **(***MR^{25Ins}*). (Right) Three F$_2$ individuals highlighted in the red rectangle are homozygous (left), wildtype (middle), and heterozygous (right) carrying the MR 46bp deletion mutation (*MR^{46Del}*).

3.2.4 - $MR^{-/-}$ mutant larvae carrying either *46Del* or *25Ins* mutations do not exhibit impaired visual background adaption.

Glucocorticoid-resistant and glucocorticoid-deficient zebrafish models are well documented to display impaired visual background adaptation (VBA) in zebrafish larvae i.e. gr^{s357} mutants (Griffiths et al., 2012; Ziv et al., 2013), $GR^{-/-}$ mutants (Marchi et al., 2020) and glucocorticoid-deficient zebrafish published in our lab (Eachus et al., 2017a; Li et al., 2020a; Oakes et al., 2020b). These models exhibit a delay in the glucocorticoid-dependent neuroendocrine response of skin pigment contraction when exposed to bright light. Thus, mutants in which glucocorticoid signaling is defective display a darker skin pigment phenotype than wild-type siblings.

To investigate if the MR had a similar role as its sister receptor, GR, a VBA assay was performed to determine the impact of *MR* loss-of-function on glucocorticoid signaling. After a 1-hour dark period and subsequent 20-minute light period, there was no visual difference in any progeny of a $MR^{+/-}$ incross (Figure 3.7). In contrast, GR-resistant or glucocorticoid-deficient mutants e.g. my novel *cyp17a2*$^{-/-}$ mutant line in Chapter 8, appear darker than the rest of the population due to a lack of contraction of black pigmented skin cells on the dorsal head (Eachus et al., 2017a; Marchi et al., 2020). In addition, there was no significant difference in total length of 5dpf larvae between $MR^{+/+}$ wildtype and MR^{46Del} mutants and MR^{25Ins} mutants (Appendix Figure A1). This suggests that *MR* loss-of-function does not reduce glucocorticoid synthesis and cause glucocorticoid-deficiency, and that is it GR, not MR, that regulates skin pigment size adaptation to light conditions.
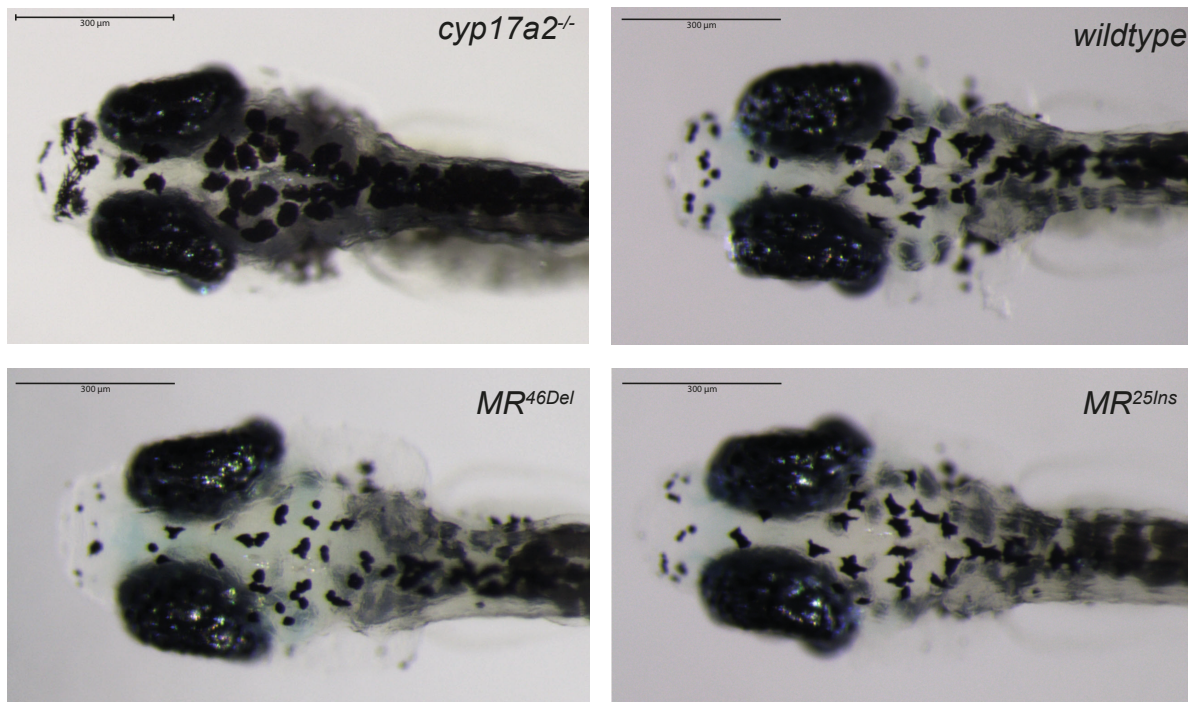
Figure 3.7. *MR$^{-/-}$* mutant 5dpf larvae exhibit normal visual background adaptation phenotype after exposure to the VBA stimulus. Top left) Representative image of *cyp17a2$^{-/-}$* glucocorticoid-deficient 5dpf larva after VBA stimulus with large black skin pigment cells indicating glucocorticoid-deficiency (VBA-) (Chapter 8). Top right) Representative image of age-matched wildtype 5dpf larva after VBA stimulus with contracted black skin pigment cells. Bottom) Representative images of age-matched *MR^{45Del}* and *MR^{25Ins}* mutant 5dpf larvae that exhibit wildtype-like contracted black skin pigment cells. Scale bar = 300μm. Wildtype n=20; *MR^{46Del}* n=20; *MR^{25Ins}* n=20.

3.2.5 *MR* loss-of-function alters the HPI axis during development of zebrafish larvae

The role of the GR and its ligand, cortisol, is well established in the stress response and HPA/I axis regulation (Charmandari et al., 2005; Wendelaar Bonga, 1997a). However, the role of the MR is less clear. My results show that MR and GR gene expression both greatly increase at the same time as HPI axis development and *de novo* cortisol synthesis post-hatch (Alsop and Vijayan, 2008). To further investigate the role of MR in HPI axis regulation, I investigated whether the loss of MR function affected basal HPI axis gene expression. Wholemount *in situ* hybridisation, staining for the ACTH-precursor *pomca* antisense RNA showed that $MR^{-/-}$ larvae exhibit increased *pomca* expression in a small number of anterior pituitary cells in the larval brain, suggesting a de-repression of the HPI axis in the pituitary (Figure 3.8A). In fish, the final consequence of an activated HPI axis is the production of the stress hormone, cortisol, in the interrenal tissue of the head kidney. In order to quantify steroid hormone concentrations in larvae, $MR^{+/+}$ and MR^{46Del} sibling adults were incrossed separately and progeny were raised to an age of 5dpf. 150 larvae were pooled per sample; and steroid hormones extracted and subsequently quantified using LC-MS/MS. Corticosteroid precursor 17-hydroxyprogesterone, and mineralocorticoid precursors 11-deoxycorticosterone and corticosterone were measured at negligible concentrations due to being at the limit of detection. The glucocorticoid precursor 11-deoxycortisol concentration was significantly increased ~1.5 fold in MR^{46Del} mutants (mean: $MR^{+/+}$=0.85; MR^{46Del}=1.34, p=0.0118), and the stress hormone cortisol was significantly increased ~3fold in MR^{46Del} mutants (mean: $MR^{+/+}$=13.45; MR^{46Del}=35.82, p<0.0001) (Figure 3.8B). Together, increased *pomca* staining in the anterior pituitary of 4dpf $MR^{-/-}$ larvae and cortisol concentrations of pooled 5dpf MR^{46Del} larvae suggest that the loss of MR function results in de-repression of the HPI axis.
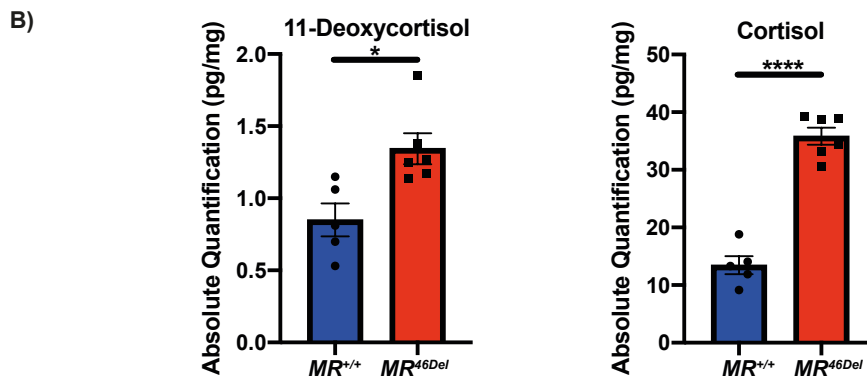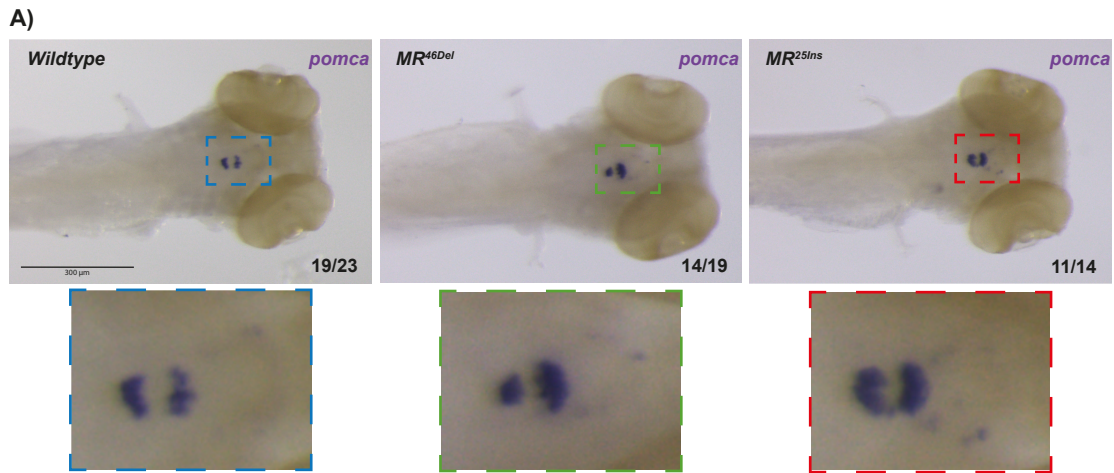
Figure 3.8. *MR^{-/-}* exhibit increased *pomca* staining in the anterior pituitary of 4dpf larvae and *MR^{46Del}* display significantly increased cortisol concentrations in 5dpf larvae. A) Representative images of whole mount *in situ* hybridisation staining for HPI axis gene *pomca* antisense RNA on 4dpf larvae shows increased pomca staining in the anterior pituitary of *MR^{46Del}* and *MR^{25Ins}* mutants in comparison to age-matched *MR^{+/+}*. Dashed box area is zoomed in below. The number of larvae that were represented by the image out of total larvae is noted on each image. Scale bar = 300µm. B) Concentrations of the glucocorticoid precursor 11-deoxycortisol and primary glucocorticoid cortisol in 5dpf larvae were measured by LC-MS/MS. Both 11-deoxycortisol (p=0.0118) and cortisol (p<0.0001) concentrations were significantly higher in *MR^{46Del}* mutants compared to age-matched *MR^{+/+}* larvae. (N=10, each N is a pool of 150 embryos). Steroid results were analysed using unpaired *t*-tests. * p<0.05, **** p<0.0001.

3.2.6 $MR^{-/-}$ mutant larvae exhibit an increased expression of *star* and glucocorticoid-responsive genes *hsd11b2, tsc22d3* and *fkbp5* expression

The rate limiting step of hormone biosynthesis is the translocation of cholesterol from the outer- to inner-mitochondria membrane in steroidogenic cells (Stocco, 2001). This step is performed by the steroidogenic acute regulatory (StAR) protein, whose expression is regulated by the HPI axis (Figure 1.4). ACTH activates cAMP-protein kinase A (PKA) signalling in adrenal cells, which results in increased expression of *StAR* and subsequent glucocorticoid synthesis. To investigate whether increased *pomca* staining in the pituitary of $MR^{-/-}$ larvae was associated with increased cortisol concentrations in MR^{46Del} larvae, *StAR* gene expression was measured in samples of 30 pooled 5dpf larvae from $MR^{+/+}$ and MR^{46Del} collected from separate sibling adult incrosses. *StAR* expression was significantly increased ~2.5 fold in MR^{46Del} larvae compared to age-matched $MR^{+/+}$ larvae (p=0.026) (Figure 3.9). This suggests that my previous finding that the loss of MR function results in de-repression of the HPI axis gene *pomca*, may cause ACTH-driven increased *StAR* expression and resulting in increased cortisol synthesis.

In order to assess the systemic consequences of elevated cortisol concentrations, I used qPCR to measure the expression of glucocorticoid-responsive genes in samples of 30 pooled 5dpf larvae from $MR^{+/+}$ and $MR^{-/-}$ separate in-crosses. Expression of the glucocorticoid-induced gene *pck1* was not significantly upregulated in MR^{46Del} or MR^{25Ins} larvae, however the expression of the well-established glucocorticoid-responsive gene *fkbp5* (Binder, 2009; Cassuto et al., 2005; Eachus et al., 2017a; Imai et al., 1990) was significantly upregulated in both MR^{46Del} and MR^{25Ins} 5dpf larvae (p<0.0001) (Figure 3.9). Likewise, the glucocorticoid-responsive gene expression of *hsd11b2* and *tsc22d3* was significantly upregulated in MR^{46Del} 5dpf larvae (Figure 3.9). *Fkbp5* expression was investigated at earlier timepoints, exhibiting a significant upregulation in MR^{46Del} larvae at ages 2dpf (p=0.0054; Welsh's unpaired t-test) and 4dpf (p=0.0286; Mann-Whitney test), whilst the same trend was observed that was not significant at 3dpf (p=0.0571; Mann-Whitney test) (n=8 each timepoint). Surprisingly, the expression of the mammalian glucocorticoid-responsive gene *pck1* was not increased in $MR^{-/-}$ mutants.

Currently, no specific mineralocorticoid receptor-target genes have been identified in teleosts, as mammalian targets are usually activated by aldosterone binding and associated with electrolyte regulation, the primary function of cortisol and the glucocorticoid receptor in fish (Cruz et al., 2013). To understand which molecular pathways are affected by the loss of MR DNA binding and ligand

binding function, transcriptomic analysis of MR^{46Del} 5dpf larvae may provide insights into systemic biological processes the MR plays a role in.
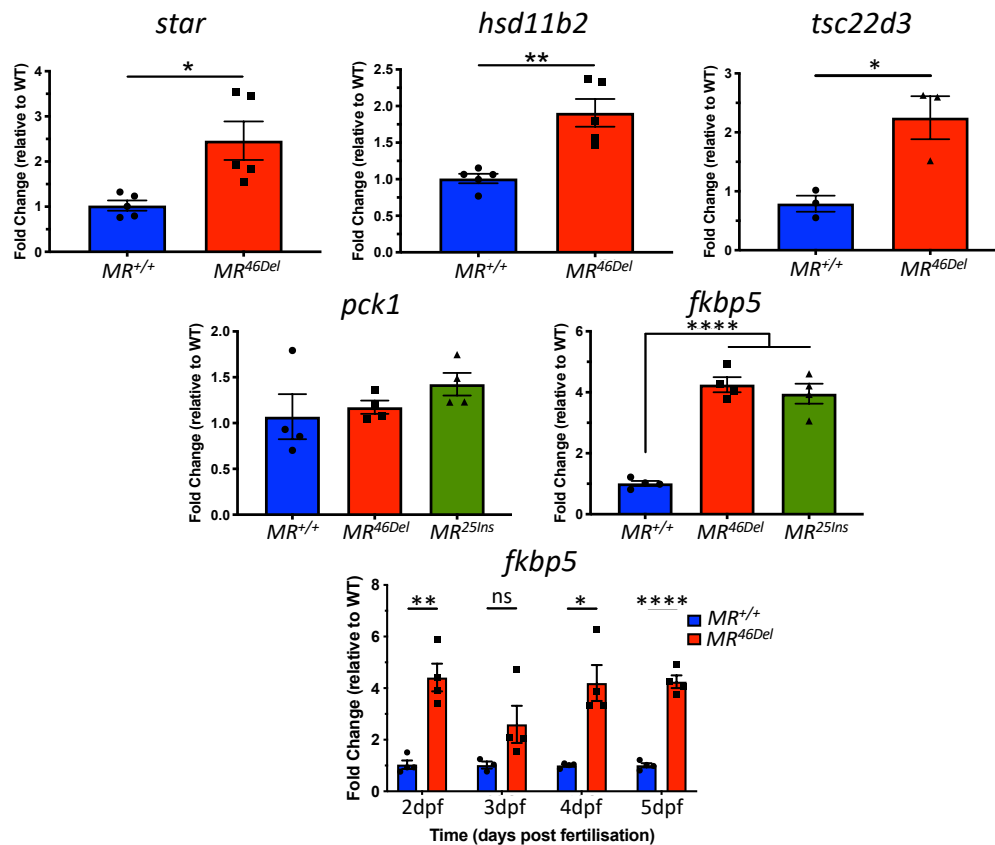
Figure 3.9. Loss of MR function results in an increase in the expression of the steroidogenic enzyme *StAR* and glucocorticoid-responsive genes *fkbp5, tsc22d3* and *hsd11b2* in 5dpf larvae. Top) The expression of the steroidogenic enzyme *star* (p=0.0021) and the glucocorticoid-responsive genes *hsd11b2* (p=0.026) and *tsc22d3* (p=0.02) were significantly increased in MR^{46Del} 5dpf larvae compared to age-matched $MR^{+/+}$ larvae (n=10, each n is a pool of 30 larvae; results analysed using unpaired t-tests). Middle) The expression of glucocorticoid-responsive gene *pck1* was not significantly upregulated in MR^{25Ins} or MR^{46Del} 5dpf mutant larvae compared to $MR^{+/+}$ age-matched larvae, whereas the glucocorticoid-responsive gene *fkbp5* was significantly upregulated in both MR^{25Ins} and MR^{46Del} mutants (p<0.0001) (n=12, each n is a pool of 30 larvae; results analysed using one-way ANOVA). Bottom) *fkbp5* expression was investigated at earlier timepoints, exhibiting a significant upregulation in MR^{46Del} larvae at ages 2dpf (p=0.0054; Welsh's unpaired t-test) and 4dpf (p=0.0286; Mann-Whitney test), whilst the same trend was observed that was not significant at 3dpf (p=0.0571; Mann-Whitney test) (n=8 each timepoint).

3.3 Discussion

The physiological role of the MR in zebrafish is poorly understood, whereas the role of the GR has been extensively studied and well defined in teleosts. Herein, I have described the HPI-associated molecular and endocrine impact resulting from the loss of MR DNA and ligand binding function in zebrafish.

To understand the temporal dynamics of both cortisol receptors, *MR* and *GR;* and the glucocorticoid-responsive gene *hsd11b2* mRNA expression during early zebrafish development, samples were collected and expression analysed between 24hpf to 120hpf. Low mRNA expression of *MR*, *GR* and *hsd11b2* was observed at 24hpf, with significant increased expression after hatch, measured at 72hpf. This finding supports previous research that found *GR* mRNA was maternally deposited but its abundance decreased from 1.5hpf to 25hpf and rebounded after hatch (~49hours), following closely with cortisol measurements during zebrafish development (Alsop and Vijayan, 2008). *MR* transcripts were also discovered to be maternally deposited, and expression increased 52-fold from 1.5hpf to 97hpf, a similar finding to my ~43 fold change between 24hpf to 96hpf (Alsop and Vijayan, 2008). My study measured cortisol concentration at the zebrafish development age of 5dpf and the gene expression of the glucocorticoid-responsive gene *hsd11b2*. HSD11B2 converts cortisol to its inactivate form, cortisone, and is important in facilitating other ligands binding MR in mammals. My results show that *hsd11b2* expression to dramatically increases ~200 fold from 24hpf to 72hpf, after hatching, where it peaks and is significantly reduced at 96 and 120hpf. This is supported by the previous finding that *hsd11b2* expression was similarly increased ~270 fold from 1.5hpf to 73hpf, however this study found *hsd11b2* expression peaked at 97hpf then subsequently significantly decreased (Alsop and Vijayan, 2008). Together, this expression data suggests both *MR* and *GR* transcripts are expressed at low levels at 24hpf and that their function is important when larvae are exposed to the external environment after hatch and during HPI axis development. Likewise, *hsd11b2* appears to be important in zebrafish larvae post-hatch and in the corresponding *de novo* cortisol synthesis due to the level of fold change seen both in this and a previous study (Alsop and Vijayan, 2008).

Organs were harvested from adult wildtype AB zebrafish and the mRNA expression of the two corticosteroid receptors *GR* and *MR*; and cortisol-inducible gene *hsd11b2* were investigated. Both *MR* and *GR* exhibited high mRNA expression in the brain and eyes relative to the kidney, with *MR* exhibiting a similar expression level also in the gill. This is surprising as it has previously been demonstrated that cortisol and the GR are the primary mechanism for osmoregulation in zebrafish (Kumai et al., 2012). These results build on the existing evidence that *MR* mRNA expression is relatively

high in both the brain and eyes in teleosts, as seen in other fish such as medaka, cichlid and midshipman (Arterbery et al., 2010; Greenwood et al., 2003; Sakamoto et al., 2016; Sturm et al., 2005). However, it was beyond the scope of this study to compare copy numbers of MR and GR, however it should be noted that GR CT values were generally lower than MR, suggesting a higher level of expression. One interesting finding was that high *MR* expression in the brain coincided with a low expression of *hsd11b2*. This is similar to mammalian findings, in which *hsd11b2* expression is high in the kidneys to facilitate aldosterone binding to the MR by inactivating cortisol, whereas in the brain, low expression of *hsd11b2* leads to cortisol acting as the main ligand for MR (Berger et al., 1998; Rozeboom et al., 2007). However, this poses the question: Is there another ligand for MR in zebrafish, or is MR just another GR in zebrafish? Addressing this question is beyond the scope of this study, but previous research has demonstrated activation of zebrafish MR transcriptional activity by various ligands *in vitro*, including aldosterone, cortisol, deoxycorticosterone and surprisingly the mammalian MR-inhibitor, spironolactone (Pippal et al., 2009). However, the circulating concentrations of 11-deoxycorticosterone, corticosterone and aldosterone in zebrafish are negligible, which we also found measuring steroids in whole fish.

To understand the function of the MR in zebrafish, I generated novel constitutive *MR* mutant alleles using CRISPR-Cas9 technology, aiming to disrupt nuclear transcription factor function: DNA and ligand binding. Both alleles encode nonsense mutations from the first amino acid of the DNA-binding domain in the MR, leading to premature stop-codons and putative-loss of function of the DNA and ligand binding domains. Currently, there is not an MR-specific target gene identified in zebrafish to assess the loss of nuclear transcription factor function. However, a distinct HPI-associated molecular and endocrine regulatory role for the MR was revealed.

The VBA assay revealed that $MR^{-/-}$ mutant larvae did not exhibit glucocorticoid-deficient or -resistant phenotypes such as the dark pigmentation seen in cortisol deficient $cyp17a2^{-/-}$ mutants (Chapter 8). Instead, $MR^{-/-}$ mutant larvae appeared to have an intact VBA response and exhibited skin pigment adaptation patterns resembling those of wildtype larvae; supporting previous findings that VBA is a GR-dependent neuroendocrine response (Kramer et al., 2001; Muto et al., 2005).

The role of the MR in the mammalian brain has previously been associated with the limbic system and the HPA axis (ter Heegde et al., 2015), however many studies report contradicting results and the restriction caused by neonatal lethality of $MR^{-/-}$ constitutive knockout rodent models has limited our understanding of MR function. Current knowledge has relied on a few conditional MR mutants that

alter expression or function, or tissue-specific mutations that provide a tunnel-vision approach to MR function and incomplete effects (Berger et al., 2006; Kolber et al., 2008; Usher et al., 2010). More recently, an MR-KO medaka mutant was created; the first adult-viable MR-KO animal (Sakamoto et al., 2016). This mutant exhibited defects in visual stimuli-induced behaviour, linking MR function with vision and brain-dependent behaviour in fish (Sakamoto et al., 2016), however the effect loss of *MR* function on the HPI axis was not investigated. Accordingly, I studied the expression of *pomca*, the precursor of ACTH, whose expression is induced during stress in the anterior pituitary cells of zebrafish brains, in these new mutants. My results show higher *pomca* mRNA hybridisation in both *MR^{46Del}* and *MR^{25Ins}* mutants compared to age-matched wild-type M*R$^{+/+}$* larvae. qPCR was attempted; however, CT values were very high and on the limit of detection with the intercalating dye SYBR green. In future, qPCR with TaqMan probes may provide a more sensitive and reliable result. However, this finding of HPI axis gene de-repression is further supported by steroid hormone analysis of 5dpf zebrafish larvae. LC-MS/MS glucocorticoid analysis of pooled *MR$^{+/+}$* and pooled *MR^{46Del}* 5dpf larvae revealed a significant increase in the stress hormone, cortisol, and its precursor 11-deoxycortisol. Systemic effects of hypercortisolaemia were demonstrated by the significantly elevated expression of glucocorticoid-responsive genes of *fkbp5* and *hsd11b2* at 5dpf in *MR^{46Del}* larvae. In fact, compared to age-matched *MR$^{+/+}$* larvae, *fkbp5* expression was increased in *MR^{46Del}* larvae throughout development: 24hpf, 48hpf, 96hpf and 120hpf. Together, these results suggest that MR loss-of-function mutations result in a de-repression of the HPI axis which results in systemic hypercortisolaemia. In support of our findings, mice deficient for MR in forebrain exhibited 40% higher levels of plasma corticosterone, the primary glucocorticoid for rodents (Cole and Young, 2017).

As this research was being undertaken, a study was published of a novel MR mutant and GR mutant zebrafish line and their impacts on the HPI axis (Faught and Vijayan, 2018). Their findings supported my own; loss of MR function resulted in de-repression of HPI axis gene expression, such as *crh* and *pomca*. However, one distinct difference was that their *MR* mutants with a de-repressed HPI axis, were not hypercortisolaemic, and only their *GR* mutant line had elevated cortisol at 5dpf. However, their targeted mutagenesis was at a different site, exon 2 of *nr3c2* (Faught and Vijayan, 2018). As the 5' NTD is the location for specific transcription factors binding, such as AF1, differences in phenotypes are expected (Pippal and Fuller, 2008; Rogerson et al., 2004). However, dimerization with other MR and GR molecules, nuclear localisation and binding of the chaperone HSP90 and the transcription factor AF2, all require the DBD and LBD regions of the MR, as does the primary nuclear receptor function, which is putatively lost in my *MR* mutant alleles and the previously described *MR$^{-/-}$* mutant zebrafish line (Faught and Vijayan, 2018)

For the MR^{25Ins} mutant allele, changes in total body length, steroid hormone concentrations, and *hsd11b2* gene expression were not yet investigated. Future work to complete these experiments, in addition to TaqMan qPCR of HPI axis genes: *crh* and *pomca,* will enable quantitative analysis to be performed. However, as our results generally support the findings of a recently developed MR-mutant zebrafish, and it is clear the MR has a repressive role on the HPI during early zebrafish development. To understand the systemic impact of MR loss-of-function and to search for a MR-specific target gene, the impact of the MR^{46Del} mutation on the 5dpf larval transcriptome was explored.

Chapter 4. Defining the implications of the loss of mineralocorticoid receptor function on 5dpf larval transcriptomes in *MR46Del* mutant zebrafish.

4.1 Introduction

Glucocorticoids play critical roles in the regulation of various physiological processes, including glucose, protein and lipid metabolism, the stress response and inflammation (Cruz-Topete and Cidlowski, 2014; Kuo et al., 2015; Reul and De Kloet, 1985; Timmermans et al., 2019; Vegiopoulos and Herzig, 2007). Many therapeutic synthetic glucocorticoids do not transactivate the MR, i.e. dexamethasone and betamethasone, which are widely used to treat many conditions, however, chronic glucocorticoid usage has significant adverse effects, leading to side effects such as osteoporosis, diabetes, growth retardation in children, hypertension in adults and abdominal obesity (Moghadam-Kia and Werth, 2010).

In mammals, the effects of cortisol-mediated activation of the Mineralocorticoid Receptor (MR) are tissue-specific, and rely heavily on the expression of the cortisol-inactivating enzyme 11beta-hydroxysteroid dehydrogenase type 2 (HSD11B2). The MR has a 10-fold higher affinity for cortisol than the canonical cortisol receptor GR. In tissues where aldosterone-specific MR-activation is essential, the cortisol-inactivating enzyme HSD11B2 is highly expressed, facilitating aldosterone binding by reducing active cortisol concentrations (Funder, 2005). However, throughout many tissues in the body, such as the brain and adipose tissue, HSD11B2 is expressed at low levels, where cortisol is the major ligand of both MR and GR (Faught and Vijayan, 2019b). Many studies of glucocorticoid signalling have been performed in murine models, however rats and mice produce negligible concentrations of cortisol due to the lack of an important enzyme, CYP17A1, in the adrenal gland. As such, corticosteroid precursors are directed through the mineralocorticoid biosynthetic pathway as the glucocorticoid biosynthetic pathway is blocked (Figures 1.1; 8.1) (Auchus et al., 2017). The dominant glucocorticoid in rodents is corticosterone. Corticosterone is a mineralocorticoid precursor of aldosterone that is known to bind both the glucocorticoid and mineralocorticoid receptor, and in rodents, acts as the principal glucocorticoid. The role of a key *CYP17* homolog gene in zebrafish, *cyp17a2*, important in correct mineralocorticoid and glucocorticoid biosynthesis in zebrafish will be investigated in a Chapter 8.

Zebrafish provide an opportune model to study the effects of Mineralocorticoid and Glucocorticoid Receptor functions as they synthesise the same glucocorticoid as humans, cortisol, and unlike other teleosts, there is only one gene copy of each, *nr3c1* (GR) and *nr3c2* (MR). However, in teleosts, aldosterone is hypothesised to not be synthesised, as no homolog of the aldosterone synthase gene has been discovered and aldosterone concentrations are measured at negligible concentrations (Colombo et al., 2006). Despite endogenous cortisol demonstrating higher affinity for MR than GR, the GR has been the main focus of research in metabolism and the stress response. However, more recently, MR has been shown to exhibit functions distinct from those of GR in regulating the stress axis response and triglyceride metabolism in zebrafish larvae (Faught and Vijayan, 2018, 2019b). However, the broader, systemic roles of the MR or GR in zebrafish have not been fully addressed.

Through both its receptors, GR and MR, cortisol exercises its functions through directly binding of the ligand binding domain (LBD) of these proteins to form an active transcription factor complex that may function in genomic and non-genomic mechanisms. To understand the whole-organism impacts of MR and GR on the zebrafish larval transcriptome, I have performed RNAseq analysis on pools of 5dpf larvae carrying either the *MR^{46Del}* mutation or the published *gr^{s357}* mutation, and wild-type larvae (Griffiths et al., 2012; Sireeni et al., 2020; Ziv et al., 2013a). In this chapter, I will explore the impact the *MR^{46Del}* mutation on the 5dpf zebrafish larval transcriptome. I hypothesise that despite lack of the mammalian primary MR ligand aldosterone, tissues identified as low HSD11B2-expressing and their related biological processes will be dysregulated in *MR^{46Del}* mutant zebrafish larvae. This is due to biological processes where cortisol-mediated activation of the MR, such as the HPA axis, is highly conserved between zebrafish and mammals.

4.2 Results

In Chapter 3, I have previously shown that *MR^46Del* mutant larvae exhibit increased levels of *pomca* mRNA, increased levels of glucocorticoid-responsive gene expression, and hypercortisolaemia in ≤5dpf larvae, all of which are consistent with elevated HPI axis activity. These observations are supported by recently published findings that also indicate an important role for MR in the regulation of HPI axis activity and the stress response (Faught and Vijayan, 2018). As cortisol and the HPI axis may influence many physiological systems, and to gain further insight into the molecular mechanisms regulated by the MR during development, I performed RNA sequencing of 5dpf wild-type and *MR^46Del* homozygous mutant larvae.

A tank of adult *MR^46Del* and a separate tank of adult sibling *MR^+/+* zebrafish were marbled and fertilized eggs were collected. Larvae were raised to 5dpf and pools of 30 larvae were taken for each sample. RNA was extracted using the Qiagen RNAeasy Kit and quality and purity were then assessed using the Agilent Bioanalyzer and the Thermo Scientific NanoDrop™. Library preparation and mRNA sequencing was performed by the Deep Sequencing Facility at Technische Universität, Dresden in Germany. Details of RNAseq analysis pathway of raw data processing, reference genome alignment and differential expression analysis is described previously in Chapter 2.

4.2.1 Quality control and STAR alignment of *MR^46Del* mutant and *MR^+/+* 5dpf larval RNAseq samples

It is necessary to identify error-types and evaluate the quality of sequence reads to reduce the impact that technical limitations of sequencing have on interpretation of downstream analysis. FastQC software was used before and after each sequence read manipulation (Andrews, 2010). Subsequent to rRNA removal and adaptor/quality trimming, FastQC revealed excellent sequence quality for *MR^+/+* (WTAB) 1-4 and *MR^46Del* mutants (MR) 1-4 with high Phred score quality (>30) (Figure 4.1A&B). Phred scores correspond to the probability of an incorrect base call during sequencing, i.e. a Phred score of 10 indicates there is an error in every 10-base calls (90% accuracy). It is generally accepted that a Phred score of >30 indicates quality sequencing. Per sequence quality scores skewed to high Phred scores supports high quality sequencing data. Per base N content presents the number of indistinguishable bases within each read. My results indicate a per base N content of ~0, verifying our data is of high quality. All samples passed the mean quality scores, per sequence quality scores and per base N content, however samples WTAB 1-4 and MR 3-4 had slightly high sequence GC content.

There were no overrepresented sequences in any samples, indicating rRNA had been successfully removed, a common source of high GC content. However, PCA, heatmap and dendrogram plots do not show that this is an issue in downstream analysis (Figure 4.2). All samples failed the per base sequence content metric, which assesses "the proportion of each base position for which each of the four normal DNA bases has been called", as all samples showed biased base composition for the first 12bp of each read (Figure A2). There are multiple explanations for this: i) hexamer primers during reverse transcription lead to positional bias, ii) polymerase sequence specificity, iii) artefacts of end-repair; a combination of these factors is also possible. However, this is expected for RNAseq libraries and is thought not to affect downstream analysis.

Samples were sequenced at a high depth 26-34million reads for exploratory transcriptomic analysis (Table A1). Post-sequencing quality control processing resulted in MR 1, 3 and 4 biological replicate samples, with samples WTAB1-4 and exhibiting a similar percentage of reduction in reads, and sample MR 2 exhibiting a higher % removed. Post-quality processing provided adequate read depth (~24-32 million reads) for downstream transcriptomic analysis of each biological. STAR software was used to performed alignment of reads to the zebrafish reference genome (GRCz11) (Dobin et al., 2013). STAR alignment details are documented and show a mapped alignment of between ~18-26 million reads to annotated genes.

4.2.2 mRNA sequencing quality control reveals an outlier MR^{46Del} mutant sample with a significantly low read depth.

Experimental quality control is an important initial assessment performed during early transcriptomic downstream analysis. Principal Component Analysis (PCA) revealed that sample MR 2 did not cluster with other samples of MR or WTAB genotypes by PCA analysis (Figure 4.1A) or cluster analysis by size (dendrogram; Figure 4.2C). This was supported by MR2 displaying a variation profile dissimilar to MR or WTAB genotypes, seen in a hierarchical clustering heatmap of normalised count data (Figure 4.2B). Sample MR 2 also contained the smallest number of reads aligned by STAR, seen by lowest total number of genecounts before and after DESeq2 normalisation (Figure 4.3A & B). Estimated size factor analysis indicated that MR2 displayed the smallest size factor of 0.532, compared to all other samples (Figure 4.3C). As such, MR 2 was be classed as an outlier and removed from any further downstream analysis.
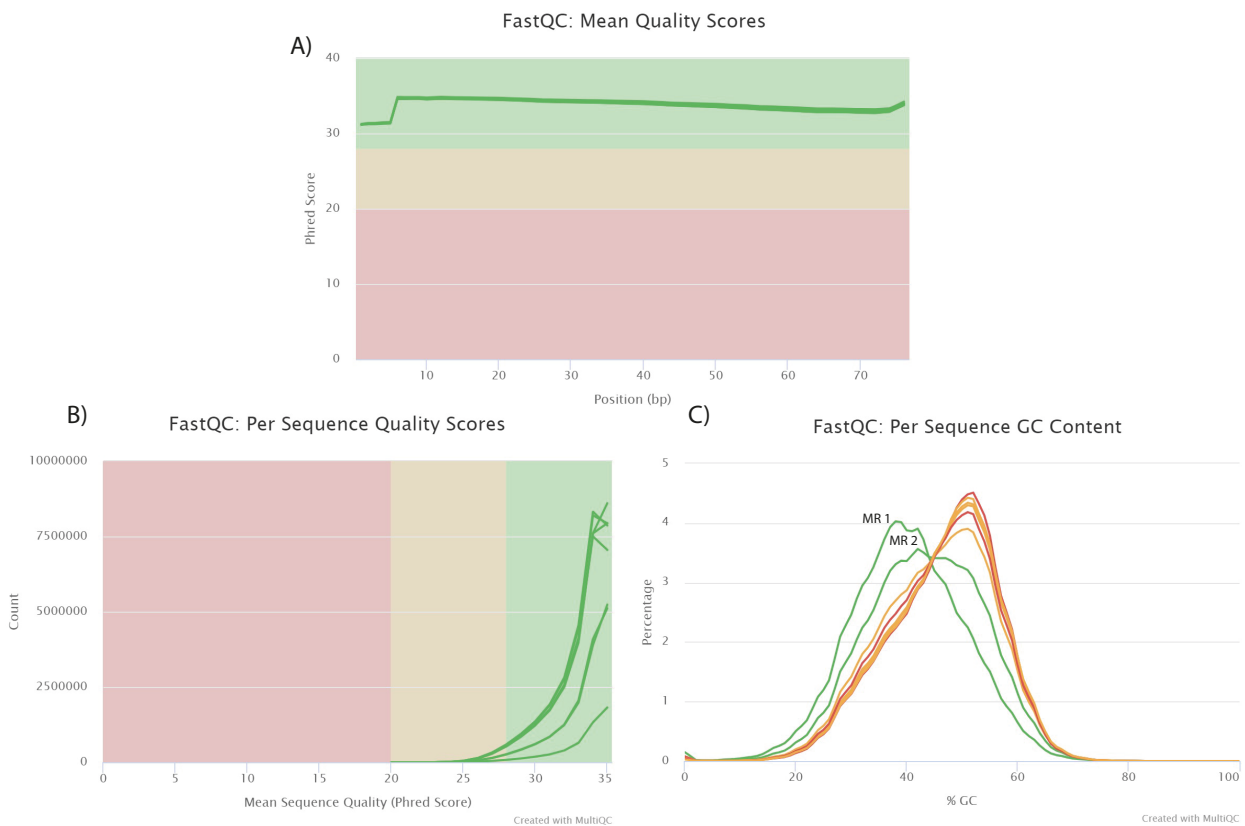
Figure 4.1. Quality control of RNA sequencing reads for MR (*MR^{46Del}*) and WTAB (*MR^{+/+}*) larvae samples after preliminary processing. Sample quality control was performed using FastQC and visualised using MultiQC after initial processing using Trimmomatic software to trim adaptors and poor-quality reads, and SortmeRNA software to remove rRNA reads that may be present. A&B) Quality scores indicate very high sequence quality with Phred scores above 30. C) Per sequence GC content indicates that all samples except MR 1 and MR 2 are slightly skewed to the right indicting high GC Content.
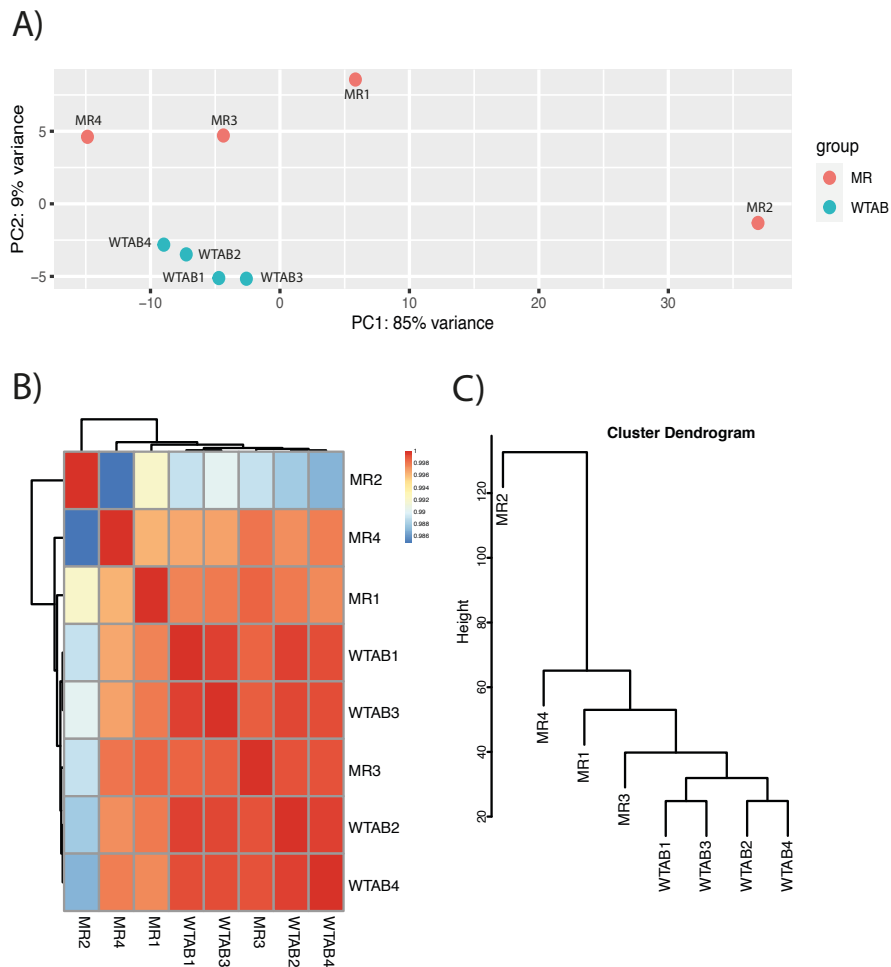
Figure 4.2. Biological QC using principal component analysis, heatmap and dendrogram clustering analysis of MR (*MR^46Del*) and WTAB (*MR^+/+*) reveals outlier sample MR2. A) PCA (ntop=500): MR2 is segregated from all other MR and WTAB samples by PC1 that accounts for 85% of total variation. B) Hierarchical clustering heatmap generated from the same data shows distinctly different profile of sample MR2 from all other samples. C) Cluster dendrogram of sample distances presents MR2 to be noticeably distanced from all other samples.
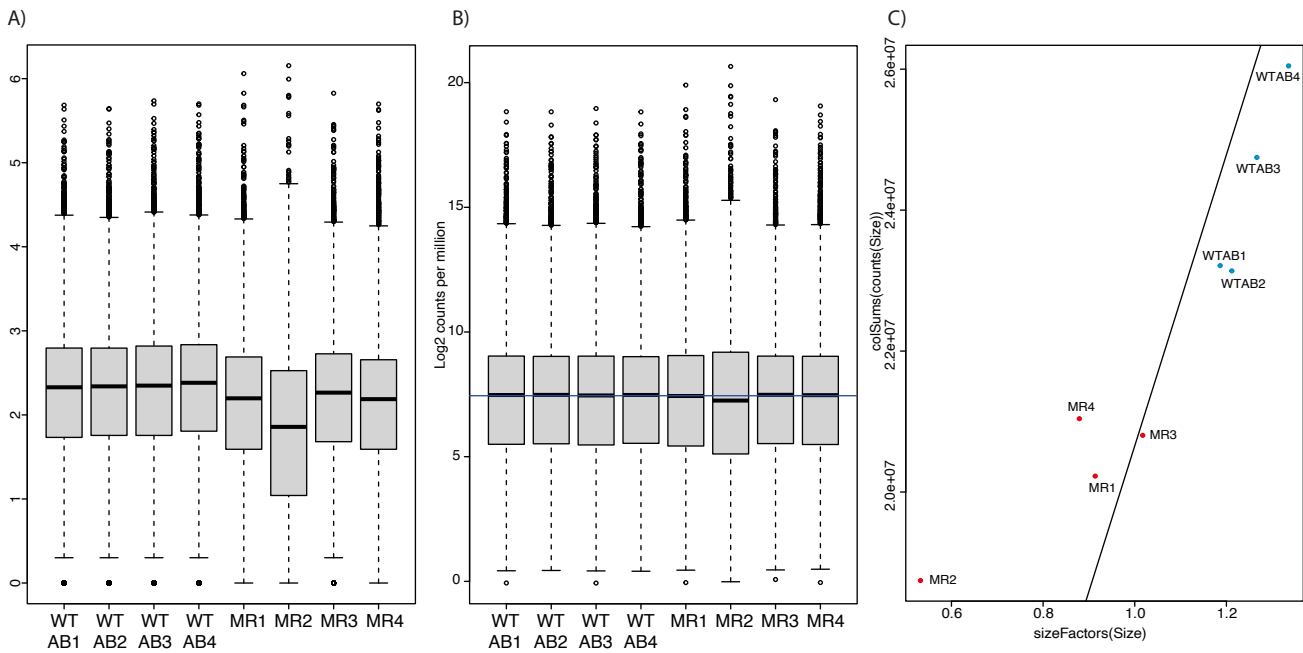
Figure 4.3. RNA sequencing depth reveals outlier sample MR2 has lower median gene counts than all other samples. A) Boxplot showing median raw counts for each gene. MR samples are display higher variability than WTAB samples, of note, sample MR2. B) Boxplot showing DESeq2 normalised median library size, MR2 sample still displays small library size. C) DESeq2 estimate size factor function presents MR2 with a low size factor of 0.532 compared to all other samples.
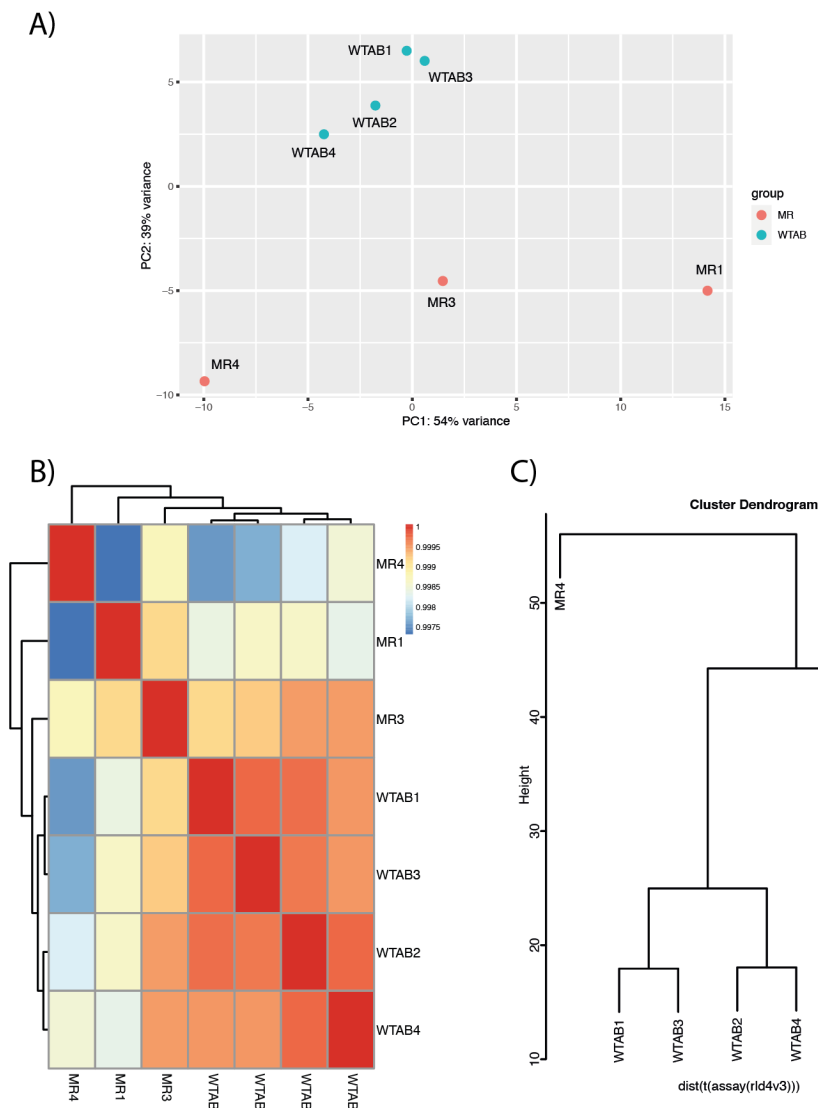
Figure 4.4. Biological QC using principal component analysis, heatmap and dendrogram clustering analysis of MR (*MR*^{*46Del*}) and WTAB (*MR*^{*+/+*}) after removal of MR2 outlier. A) PCA (ntop=500): WTAB samples cluster together and genotypes are segregated by PC2, accounting for 39% of total variation. B) Hierarchical clustering heatmap generated from the same data shows samples cluster by genotype. C) Cluster dendrogram of sample distances presents WTAB samples as a relatively tight cluster with higher variation with MR samples.

4.2.3 Initial analysis of the differential transcriptomic profile resulting from the *MR^46Del* mutation in 5dpf larvae.

PCA analysis (Figure 4.4A) revealed variation between the transcriptomic profiles of *MR^46Del* mutants (MR) and *MR^+/+* controls (WTAB), with considerable variation observed within the samples of MR genotype. Despite an absence of segregation by genotype in the first principal component, a clear segregation between the two genotypes was revealed in the second principal component; this accounted for 39% of the total variation within all samples. The high degree of intra-group variation seen within the MR samples along PC1 (54% total variation) and lack of clustering may reduce statistical power for downstream analysis, but also provide biologically appropriate transcriptomic differences between genotypes. This high intra-group variation between MR samples is further supported by the hierarchical clustering heatmap of normalised counts (Figure 4.4B) and clustering dendrogram (Figure 4.4C), which indicates that sample MR4 to have the greatest dissimilarity to all other samples. It is worth noting here that prior to removal of the MR2 outlier, sample MR3 clustered with samples of WTAB genotype in the heatmap (Figure 4.2B), however after MR2 removal, sample MR3 appropriately clustered with other MR samples (Figure 4.4B).

Differential expression analysis was performed using the DESeq2 package (Love et al., 2014b). However, a more stringent FDR value of 0.05 was used rather than DESeq2's default exploratory 0.1 FDR value. Initial DESeq2 analysis can be visualised with an MA plot and DESeq2 dispersion plot (within-group variability). The MA plot (Figure A3) plots each gene as a dot, with log2fold change between MR mutants and WTAB controls (y-axis); against normalised (gene) count (x-axis). Genes with an adjusted p-value (padj) below the 0.05 threshold are shown in blue. This MA plot displays an approximate equal distribution between and statistically significant upregulated and downregulated genes (blue dots). It also demonstrates that genes with a larger mean normalised count contain sufficient statistical power to confirm significance. It is important to note that DESeq2 performs shrinkage estimation of log fold changes, with resulting low count values "shrunken" towards 0 as they prevent accurate log fold change (LFC) calculation. Plotting dispersion estimates (Figure A3) demonstrates that as the normalised count increases, intra-group variability is reduced. This plot resembles the typical dispersion pattern required for the use of the DESeq2 package (Love et al., 2014b).

To assign statistically significance to a DEG, an adjusted p-value of <0.05 was used as a threshold. This revealed a total of 2129 differentially expressed genes (DEGs) between MR mutants and WTAB control

5dpf larvae, of which, 900 were upregulated and 1229 were downregulated in MR mutant larvae (Table 4.1). To provide a more robust list of DEGs, independent filtering was performed: a base mean of <40 reads and 0.58<Log2FoldChange<-0.58 (equivalent to ~1.5-fold change) were filtered out, resulting in 1609 DEGs (Table 4.1). Of these filtered DEGs, 636 were upregulated and 912 DEGs were downregulated.

To explore the distribution of differentially expressed genes between MR mutants and WTAB 5dpf larvae, visual tools such as a volcano plot and heatmaps were utilised. The volcano plot shows that more DEGs are downregulated than are upregulated in MR mutants, although numerous upregulated DEGs exhibit a higher statistical significance (Figure 4.5). In this volcano plot, 1502 genes are shown as red dots (0.58<Log2FoldChange<-0.58; padj<0.05), 520 genes are blue dots (-0.58<Log2Foldchange<-0.58; padj<0.05), 949 genes are green dots (0.58<Log2Foldchange<-0.58 padj>0.05) and 14650 genes are grey dots (-0.58<Log2Foldchange<0.58; padj>0.05). The top significant DEGs are labelled, including those upregulated: *si:ch211-239f4.6*/*muc4* (fold change=11.67, padj=4.81E-31), *socs1a* (fold change=2.63, padj=4.8E-16), *socs3a* (fold change=3.11, padj=2.09E-12) and *hmgcra* (fold change=2.8, padj=2.92E-11); and those downregulated: si:ch211-113e8.5/*gimap8* (fold change=0.0146, padj=1.88E-08), *myhz1.3* (fold change=0.31, padj=0.0001356), *nova1* (fold change=0.45, padj=4.45E-09) and the gene encoding the MR, *nr3c2* (fold change=0.379, padj=5.56E-07). To visualise inter- and intra-group variation of DEGs, heatmaps were utilised to present the normalised gene count of the top 30 most significant DEGs. Hierarchical clustering of samples (column) demonstrated genotype segregation; however, gene (row) hierarchical clustering was not performed to illustrate that neither upregulated nor downregulated genes are predominant in this ordered DEG list (Figure 4.6A). The second heatmap incorporates gene hierarchical clustering (row) and demonstrated a near symmetrical distribution of both up- and down-regulated genes in the top 30 most significant DEGs, and clustering of genes that express a similar variation profile between normalised transcript counts (Figure 4.6B).

Plots of normalised gene counts for a selection of top statistically significant DEGs i.e. *muc4*, *socs1a*, *socs3a*, *gimap8*, *ptprnb* and *nr3c2,* demonstrate the significance of differential expression seen in the MR mutants in comparison to WTAB control 5dpf larvae (Figure 4.7). A list of top DEGs by statistical significance (Table 4.2) and by fold change (Table 4.3) indicate an equal distribution of up- and down-regulated DEGs. One surprising result was that *fkbp5* (fold change=1.24; padj=0.22) was not identified as a DEG. However *pomca* (fold change=2.22; padj=0.023), *hsd11b2* (fold change = 1.41; padj=0.01) and *tsc22d3* (fold change= 1.75; padj= 0.000165) were significantly upregulated in MR mutants.

The initial analysis of the differential transcriptomic profile resulting from the MR^{46Del} suggests roles for the MR as both a putative transcriptional activator and repressor in 5dpf larvae, on the basis of a similar distribution and number of upregulated and downregulated DEGs. As the 5dpf larva is a complex multi-organ biological system, understanding which biological networks and molecular pathways are involved in the differential transcriptomic profile of MR^{46Del} mutants will help reveal what roles the MR has in the development of zebrafish.

Table 4.1. Number of DESeq2 differentially expressed genes between MR and WTAB 5dpf larvae; filtered for false discovery rate, adjusted p-value (padj) and fold change threshold filters.

DESeq2 FDR Cutoff	padj cutoff	No. of Total DEGs	No. of DEGs with fold change > 1.25x	No. of DEGs with fold change > 1.5x
FDR alpha = 0.1 (default)	padj < 0.1	3168	3110	2087
FDR alpha = 0.05	padj < 0.05	2129 (900↑ + 1229↓)	2119 (893↑+ 1226↓)	1609 (636↑+ 973↓)
Independent Filtering	padj < 0.05	2022 (854↑ + 1168↓)	2012 (847↑ + 1165↓)	1502 (590↑ + 912↓)
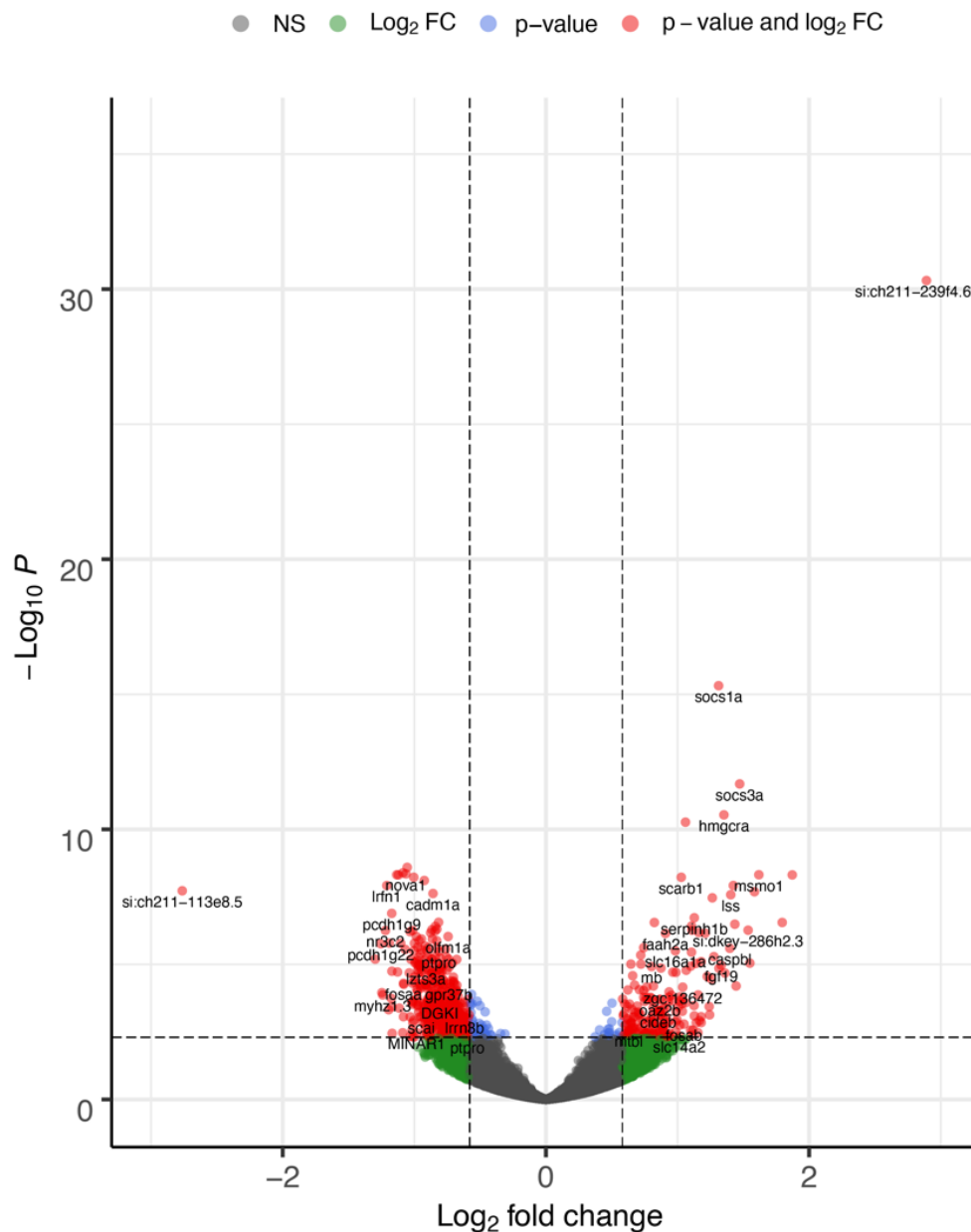
Figure 4.5. Volcano plot displaying predominantly symmetrical distribution of differentially expressed genes affected by the *MR^46Del* mutation in 5dpf zebrafish larvae. The statistical significance – padj values are plotted on the y axis against magnitude of differential expression – log2fold change. Dashed lines represent padj cutoff value < 0.05 and 0.58<Log2FoldChange<-0.58. Grey dots signify non-significant genes below Log2FoldChange threshold, green dots signify non-significant genes with Log2FoldChange >0, and red dots signify significant genes with Log2FoldChange >0.
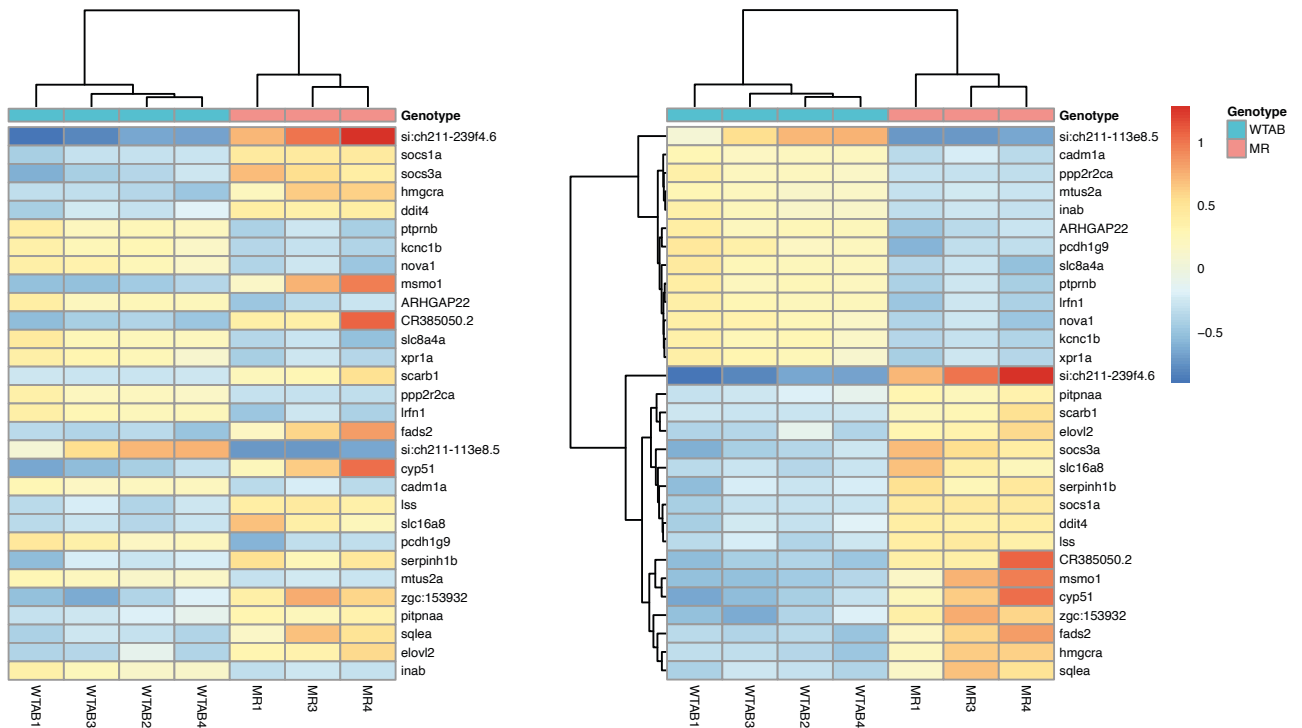
Figure 4.6. Top 30 most significant differentially expressed genes in 5dpf larvae between MR (*MR^46Del*) mutants compared to WTAB (*MR^+/+*). Left) Heatmap with hierarchical clustering of samples only in order of most significant genes. Right) Heatmap of hierarchical clustering of samples and genes of top 30 most significant DEGs.
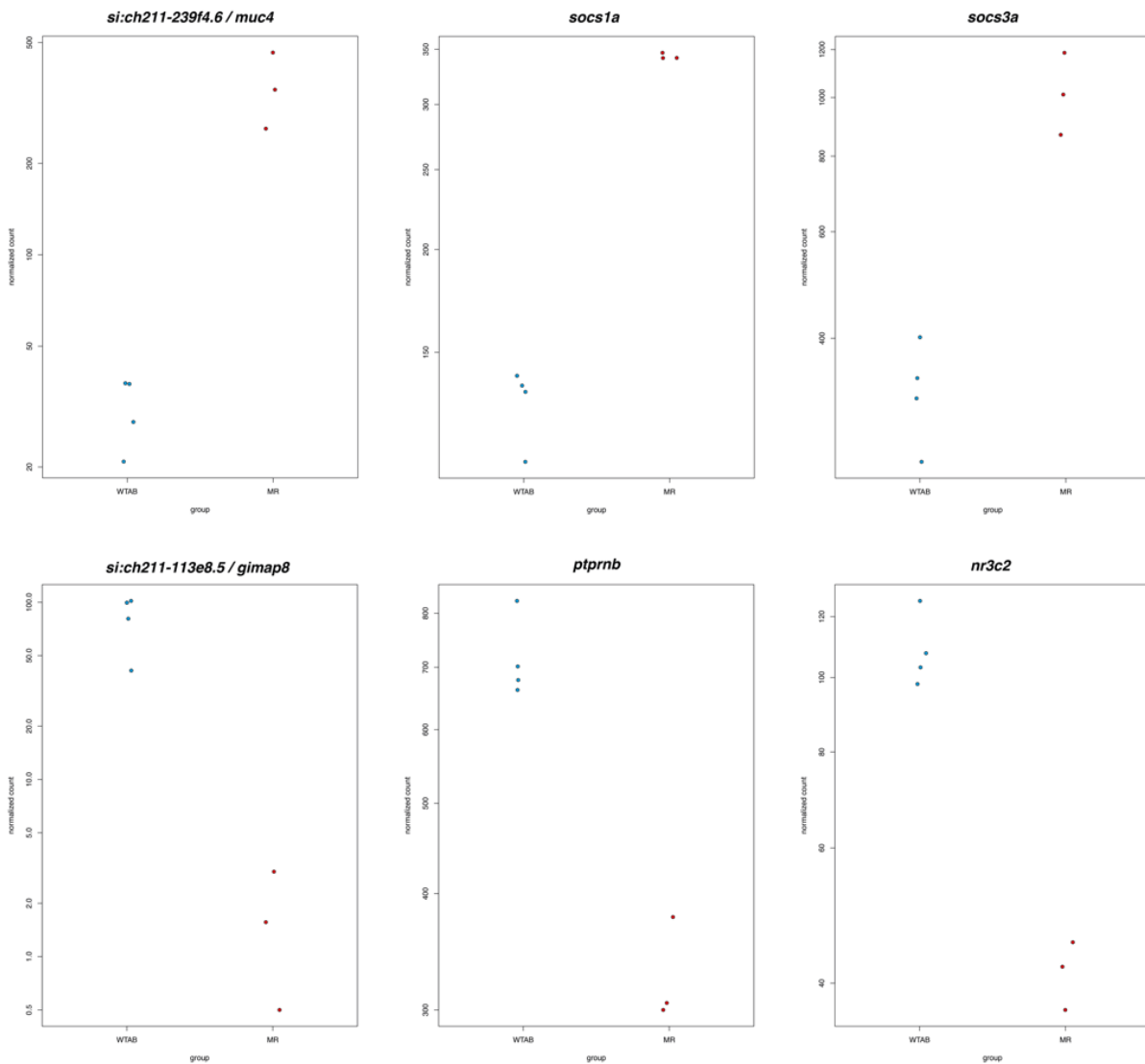
Figure 4.7. DESeq2 normalised gene expression plots for each sample of WTAB ($MR^{+/+}$) and MR mutant (MR^{46Del}) 5dpf larvae for a selection of top statistically significant DEGs. Normalised DESeq2 gene counts are plotted using the plotCounts function for genes *muc4*, *socs1a*, *socs3a*, *gimap8*, *ptprnb* and *nr3c2*. These illustrate the level of differential expression seen in MR^{46Del} mutants. See Table 2 for statistics.

Table 4.2. Top 20 most significant differentially expressed genes (padj<0.05) in *MR^46Del* vs *MR^+/+* 5dpf larvae. Colour indicates up-regulated (green) or down-regulated (red) gene expression.

Gene name	Fold change	p value	padj value	Ensembl gene ID
si:ch211-239f4.6 / muc4	11.6704471	2.39E-35	4.81E-31	ENSDARG00000093347
socs1a	2.63473726	4.77E-20	4.80E-16	ENSDARG00000038095
socs3a	3.11257121	3.11E-16	2.09E-12	ENSDARG00000025428
hmgcra	2.81025506	5.80E-15	2.92E-11	ENSDARG00000052734
ddit4	2.17923953	1.35E-14	5.44E-11	ENSDARG00000037618
ptprnb	0.45747976	7.62E-13	2.55E-09	ENSDARG00000077047
kcnc1b	0.44426915	1.41E-12	4.06E-09	ENSDARG00000032959
nova1	0.45275408	1.77E-12	4.45E-09	ENSDARG00000020178
ARHGAP22	0.42547883	2.22E-12	4.81E-09	ENSDARG00000076434
msmo1	3.93610001	2.39E-12	4.81E-09	ENSDARG00000055876
slc8a4a	0.43009363	2.73E-12	4.87E-09	ENSDARG00000055154
CR385050.2	5.98426149	2.90E-12	4.87E-09	ENSDARG00000117264
xpr1a	0.47547562	4.14E-12	5.95E-09	ENSDARG00000062449
scarb1	2.14559276	4.04E-12	5.95E-09	ENSDARG00000101557
ppp2r2ca	0.50804497	5.84E-12	7.84E-09	ENSDARG00000056797
lrfn1	0.39469194	9.56E-12	1.20E-08	ENSDARG00000027602
fads2	3.16315115	1.02E-11	1.20E-08	ENSDARG00000019532
si:ch211-113e8.5 / gibap8	0.01461962	1.69E-11	1.88E-08	ENSDARG00000069707
cyp51	3.89641593	1.93E-11	2.05E-08	ENSDARG00000042641
cadm1a	0.53499694	2.35E-11	2.37E-08	ENSDARG00000031075

Table 4.3. Top 20 significant differentially expressed genes ordered by magnitude of fold change caused by the *MR^{46Del}* mutation in 5dpf zebrafish larvae. Top 10 upregulated genes by magnitude (green) and subsequently, top 10 downregulated genes by magnitude (red).

Gene name	Fold change	p value	padj value	Ensembl gene ID
si:ch211-239f4.6 / muc4	11.6704471	2.39E-35	4.81E-31	ENSDARG00000093347
zgc:153932	6.7075724	3.77E-10	2.81E-07	ENSDARG00000052779
CR385050.2	5.98426149	2.90E-12	4.87E-09	ENSDARG00000117264
si:ch211-207n23.2	4.97700217	3.98E-08	9.00E-06	ENSDARG00000097157
si:dkey-247k7.2	4.810718	5.27E-07	6.32E-05	ENSDARG00000103199
zbtb20	4.1688258	0.00010342	0.003368	ENSDARG00000005586
CR855277.2	4.16119297	0.00054753	0.010876	ENSDARG00000092801
si:dkey-286h2.3	3.96786814	9.17E-10	5.43E-07	ENSDARG00000068290
msmo1	3.93610001	2.39E-12	4.81E-09	ENSDARG00000055876
cyp51	3.89641593	1.93E-11	2.05E-08	ENSDARG00000042641
si:ch211-113e8.5 / gimap8	0.01461962	1.69E-11	1.88E-08	ENSDARG00000069707
myhz1.3	0.31388984	1.38E-06	0.000136	ENSDARG00000067997
BX323458.2	0.33184797	2.48E-08	6.40E-06	ENSDARG00000094614
myhc4	0.33433911	5.48E-06	0.000369	ENSDARG00000035438
SYNDIG1	0.35208801	1.99E-06	0.00018	ENSDARG00000100751
pcdh1g22	0.35808968	4.46E-09	1.72E-06	ENSDARG00000103013
myhz2	0.36794192	6.41E-06	0.000416	ENSDARG00000012944
myha	0.3737677	1.69E-05	0.000866	ENSDARG00000095930
si:dkeyp-69b9.3 / myocd	0.37825196	1.04E-07	1.79E-05	ENSDARG00000088881
nr3c2	0.37917903	9.85E-10	5.56E-07	ENSDARG00000102082

4.2.4 Gene Ontology Analysis

Statistical overrepresentation analysis of all independently filtered all DEGs (Log2Foldchange <-0.58 | >0.85; padj<0.05), revealed 48 gene ontology (GO) terms related to Biological Process that were below the p<0.05 and FDR<0.05 thresholds. Of these, an overrepresentation of genes annotated to the term steroid biosynthesis and metabolic processes, ion transport, lipid metabolic processes and synaptic signalling were over-represented. Similarly, 43 GO terms related to Molecular Function were identified, including ion- and ligand-gated channel activity, monooxygenase activity, steroid hydroxylase activity, oxidoreductase activity and brain-related GABA receptor activity. In addition, 26 GO terms related to Cellular Components were overrepresented locations associated with plasma membrane components e.g., ion channels, neuron projections and synapses. All GO terms associated with all DEGs can be found in Appendix 1, including GOrilla maps, REViGO plots and KEGG pathway figures. To understand at a higher resolution which biological, molecular and cellular processes are dysregulated by the *MR^{46Del}* mutation in 5dpf zebrafish larvae, I separated GO analysis by upregulated and downregulated DEGs.

Statistical overrepresentation analysis of upregulated DEGs revealed 44 significant GO terms related to biological processes with an FDR<0.05, including steroid biosynthesis, lipid and cholesterol biosynthetic processes, many lipid metabolic processes including cholesterol, sterol, alcohol, organic acid pathways, as well as lipid transport, xenobiotic and sulphur metabolism, and aminoglycan catabolism (Figure 4.8 & 4.11; Table 4.4). Similarly, 16 Molecular Function-related GO terms were identified. Of these, an overrepresentation of genes involved in oxidoreductase and monooxygenase activity, haem binding, steroid hydroxylase activity, lipid binding and lipid transporter activity were identified (Figure 4.9 & 4.11; Table 4.4). Interestingly, upregulated genes were overrepresented in ontologies for Cellular Components such as the plasma membrane, extracellular space and protein-lipid complexes (Figure 4.10 & 4.11; Table 4.4). In addition, the important role of MR in metabolic processes, steroid biosynthesis and oxidative phosphorylation was identified in DAVID KEGG and reactome pathway analysis of upregulated DEGs in *MR^{46Del}* mutant 5dpf larvae (Table 4.5; Appendix 1). These GO terms suggest MR has an important role of in lipid metabolism and transport.

4.2.5. Genes involved in steroid and lipid metabolic processes are primarily upregulated in 5dpf *MR^{46Del}* mutant zebrafish larvae.

Cholesterol is the precursor to all steroid hormones, including glucocorticoids. Of the 44 biological process GO terms identified as overrepresented in my upregulated DEG population, the majority were

associated with steroid and lipid metabolism. Cholesterol synthesis occurs primarily at the endoplasmic reticulum, and has an important rate limiting step performed by the enzymes encoded by *hmgcs1* and *hmgcra* (Sharpe and Brown, 2013). In the first step, Hmgcs1 catalyses the condensation of acetyl-CoA to form HMG-CoA, which is converted to mevalonate by Hmgcra, which was identified as a top5 DEG (Table 4.2; Figure 4.5 & 4.6). The cholesterol synthesis pathway involves multiple modifications to a steroid backbone that leads to the synthesis lanosterol; genes encoding proteins responsible for these modifications, such as *msmo1* (fold change=3.94; padj=4.81E-09), *sqlea* (fold change=0.58<Log2FoldChange<-0.583.37; padj=3.23E-07) and *lss* (fold change = 3.13; padj=2.64E-08) were upregulated in MR^{46Del} mutant larvae (Figure 4.11). Further modifications by enzymes encoded by upregulated DEGs: *cyp51* (fold change = 3.90; padj=2.05E-08), *tm7sf2* (fold change = 1.65; padj=0.00087), *ebp* (fold change = 2.13; padj=0.00014), and *sc5d* (fold change = 2.41; padj=1.16E-05), result in the *de novo* synthesis of cholesterol. The cholesterol and lipid biosynthesis pathway is illustrated in Figure 4.12.

The transport of cholesterol from the outer to inner membrane of the mitochondrion is the rate limiting step of corticosteroid synthesis and is performed by StAR. In Chapter 3, I described a significant increase in expression of *star* in MR^{46Del} mutants using the technique of qRT-PCR. Similarly, in my transcriptomic analysis, *star* (fold change = 2.00; padj=0.00071) was a significantly upregulated in MR^{46Del} mutants. Likewise, *fdx1b* (fold change = 2.64; padj=0.0054), an essential electron-providing cofactor to mitochondrial steroidogenic enzymes and vital for glucocorticoid synthesis was also identified as a significantly upregulated DEG. In addition, *cyp21a2* (fold change = 1.79; padj=0.046), *hsd3b1* (fold change = 2.16; padj=0.042) and *cyp11a2* (fold change = 2.07; padj=0.011), genes encoding essential steroidogenic enzymes and fundamental in glucocorticoid synthesis were significantly upregulated in MR^{46Del} mutants (Figure 4.12) (Eachus et al., 2017a; Li et al., 2020b; Weger et al., 2018). This general increase of steroidogenic genes establishes a connection between increased expression of genes important for *de novo* cholesterol synthesis and the previously reported increased glucocorticoid steroid profiles of 11-deoxycortisol and cortisol MR^{46Del} mutant larvae. Further downstream, this transcriptomic analysis confirmed other results described in Chapter 3: both *tsc22d3* and *hsd11b2* were significantly upregulated in MR^{46Del} mutant larvae (Figure 4.12).

Genes encoding enzymes important for lipid synthesis, transport and lipolysis were also identified as upregulated DEGs in MR^{46Del} mutant larvae. These genes included *hsd17b12a*, important for the conversion of acetyl-CoA to the major saturated fatty acid palmitate, and *mogat2* and *dgat2*, important for the formation of triglycerides from glycerol (Figure 4.12). Similarly, the genes involved

in the synthesis of omega-3 fatty acid docosahexaenoic acid (DHA) from α-linolenic acid were also expressed at significantly higher levels in MR^{46Del} mutants than in $MR^{+/+}$ wild-type larvae (Figure 4.12). Likewise, in the linolenic acid to arachidonic acid pathway, there was an increase in downstream prostaglandin expression of *ptgs2b* and *ptgis*.

Multiple genes important for the transport of cholesterol from the ER to multivesicular endosomes/bodies were upregulated in MR^{46Del} mutants, including multiple annexins e.g. *anxa1a anxa1c, anxa2b*. Moreover, members of the apolipoprotein family, involved in cholesterol metabolism, such as *apoea, apoeba, apoe4a, apoa1a* and *apoc2* were also up-regulated in MR^{46Del} mutant larvae. The proteins encoded by these genes are important for transport of triglycerides, phospholipids, cholesteryl esters and cholesterol into cells (Figure 4.12). Similarly, the antigen *CD36* and scavenger receptor *scarb1* were significantly upregulated, which play a significant role in importing fatty acids into the cell. Not only were lipid biosynthesis genes upregulated, in addition, genes that initiate lipid catabolism through beta-oxidation such as *gcgb*, *acs15* and *decr2* also exhibited increased mRNA expression in MR^{46Del} mutants. The two most significant up-regulated genes, *socs1a* and *socs3a*, were included as genes associated with 'lipid metabolic processes'.

In addition, a collection of genes associated with vitamin A (retinol) metabolism, transport and conversion to 11-cis-retinaldehyde, the universal chromophore of visual pigments, were upregulated in MR^{46Del} mutants (Appendix 1 Figure A12). These include the retinol synthesis gene *lrata*, retinol transporter *stra6*, and catalysts of retinol to 11-cis-retinaldehyde conversion, *rbp4*, *rdh5* and *rpe65a*. Furthermore, a significant number of DEGs were overrepresented in the biological process GO terms 'Sulphation' and 'Sulphur compound metabolic process'. Many were members of the sulfotransferase family, including *sult1st1, sult1st2, sult1st3, sult1st6, sult3st2* and *sult6b1*. Additional upregulated DEGs were associated with post-translational modification of amino acids and steroid hormones, including *papss2a, cthl, cdo1, tpk1 and ggt1b*; multiple DEGs also exhibited sulfotransferase properties such as *gstp1*, *gstp2*, and *mat2al*. Together, the loss of MR function caused increased expression of genes important for steroid and lipid metabolism, which could be important for meeting the additional demands of stress.

Table 4.4. Significant Biological Processes (left), Molecular Function (middle) and Cellular Component (right) Gene Ontology terms significantly overrepresented in upregulated genes differentially expressed in *MR^46Del* mutant zebrafish larvae.

GO Term	Description	P-value	FDR q-value	Enrichment (N, B, n, b)
GO:0008202	steroid metabolic process	2.71E-16	2.23E-12	9.55 (11754,70,387,22)
GO:0006694	steroid biosynthetic process	3.26E-15	1.34E-11	12.59 (11754,41,387,17)
GO:0006629	lipid metabolic process	7.89E-15	2.16E-11	3.27 (11754,502,387,54)
GO:1901615	organic hydroxy compound metabolic process	1.49E-12	3.05E-09	5.19 (11754,158,387,27)
GO:0044281	small molecule metabolic process	3.82E-12	6.26E-09	2.45 (11754,829,387,67)
GO:1902652	secondary alcohol metabolic process	4.26E-12	5.82E-09	10.35 (11754,44,387,15)
GO:0016125	sterol metabolic process	4.92E-12	5.76E-09	9.35 (11754,52,387,16)
GO:0016126	sterol biosynthetic process	8.73E-12	8.95E-09	14.02 (11754,26,387,12)
GO:0008203	cholesterol metabolic process	4.58E-11	4.17E-08	9.89 (11754,43,387,14)
GO:0006805	xenobiotic metabolic process	7.61E-11	6.24E-08	10.67 (11754,37,387,13)
GO:0008610	lipid biosynthetic process	8.15E-11	6.08E-08	4.12 (11754,214,387,29)
GO:0006066	alcohol metabolic process	1.86E-10	1.27E-07	5.45 (11754,117,387,21)
GO:0006695	cholesterol biosynthetic process	2.86E-09	0.0000018	14.39 (11754,19,387,9)
GO:1902653	secondary alcohol biosynthetic process	2.86E-09	0.00000168	14.39 (11754,19,387,9)
GO:1901617	organic hydroxy compound biosynthetic process	5.5E-09	0.00000301	6.07 (11754,80,387,16)
GO:0044283	small molecule biosynthetic process	4.49E-08	0.000023	3.07 (11754,297,387,30)
GO:0006082	organic acid metabolic process	4.73E-08	0.0000228	2.59 (11754,458,387,39)
GO:0046165	alcohol biosynthetic process	2.54E-07	0.000116	6.39 (11754,57,387,12)
GO:0006869	lipid transport	9.46E-07	0.000408	4.26 (11754,114,387,16)
GO:0042737	drug catabolic process	0.00000102	0.000417	5.20 (11754,76,387,13)
GO:0042738	exogenous drug catabolic process	0.00000119	0.000466	9.35 (11754,26,387,8)
GO:0044255	cellular lipid metabolic process	0.00000145	0.000541	2.47 (11754,405,387,33)
GO:0006790	sulfur compound metabolic process	0.00000412	0.00147	3.64 (11754,142,387,17)
GO:0051923	sulfation	0.00000477	0.00163	12.15 (11754,15,387,6)
GO:0015850	organic hydroxy compound transport	0.00000521	0.00171	7.84 (11754,31,387,8)
GO:0019752	carboxylic acid metabolic process	0.0000327	0.0103	2.23 (11754,408,387,30)
GO:0006721	terpenoid metabolic process	0.0000331	0.0101	7.33 (11754,29,387,7)
GO:0043436	oxoacid metabolic process	0.0000352	0.0103	2.19 (11754,430,387,31)
GO:0034381	plasma lipoprotein particle clearance	0.0000354	0.01	30.37 (11754,3,387,3)
GO:0050896	response to stimulus	0.0000395	0.0108	1.65 (11754,1181,387,64)
GO:0016053	organic acid biosynthetic process	0.0000471	0.0125	3.16 (11754,154,387,16)
GO:0006720	isoprenoid metabolic process	0.0000568	0.0146	5.79 (11754,42,387,8)
GO:0016114	terpenoid biosynthetic process	0.0000729	0.0181	15.19 (11754,8,387,4)
GO:0046717	acid secretion	0.0000729	0.0176	15.19 (11754,8,387,4)
GO:0046394	carboxylic acid biosynthetic process	0.000145	0.034	3.00 (11754,152,387,15)
GO:0043207	response to external biotic stimulus	0.000154	0.035	3.50 (11754,104,387,12)
GO:0017144	drug metabolic process	0.000155	0.0344	2.50 (11754,243,387,20)
GO:0009605	response to external stimulus	0.000164	0.0354	2.49 (11754,244,387,20)
GO:0030301	cholesterol transport	0.000168	0.0354	8.93 (11754,17,387,5)
GO:0033993	response to lipid	0.000179	0.0368	4.41 (11754,62,387,9)
GO:0009607	response to biotic stimulus	0.000185	0.0369	3.44 (11754,106,387,12)
GO:0051704	multi-organism process	0.000202	0.0394	3.41 (11754,107,387,12)
GO:0033273	response to vitamin	0.000208	0.0396	12.15 (11754,10,387,4)
GO:0015918	sterol transport	0.000227	0.0422	8.44 (11754,18,387,5)

GO Term	Description	P-value	FDR q-value	Enrichment (N, B, n, b)
GO:0016491	oxidoreductase activity	5.27E-15	1.62E-11	3.16 (11754,547,387,57)
GO:0020037	heme binding	3.5E-12	5.38E-09	6.64 (11754,96,387,21)
GO:0046906	tetrapyrrole binding	8.1E-12	8.29E-09	6.38 (11754,100,387,21)
GO:0004497	monooxygenase activity	1.31E-11	0.00000001	6.60 (11754,92,387,20)
GO:0016705	oxidoreductase activity, acting on paired donors, with incorporation or reduction of molecular oxygen	5.22E-11	3.21E-08	5.52 (11754,121,387,22)
GO:0048037	cofactor binding	5.62E-11	2.88E-08	3.34 (11754,346,387,38)
GO:0005506	iron ion binding	4.26E-09	0.00000187	5.41 (11754,101,387,18)
GO:0008395	steroid hydroxylase activity	1.69E-08	0.00000651	9.03 (11754,37,387,11)
GO:0016712	oxidoreductase activity, acting on paired donors, with incorporation or reduction of molecular oxygen, reduced flavin or flavoprotein as one donor, and incorporation of one atom of oxygen	0.00000521	0.00178	7.84 (11754,31,387,8)
GO:0004062	aryl sulfotransferase activity	0.00000564	0.00173	24.30 (11754,5,387,4)
GO:0004364	glutathione transferase activity	0.00000829	0.00232	15.19 (11754,10,387,5)
GO:0015020	glucuronosyltransferase activity	0.0000231	0.00592	9.59 (11754,19,387,6)
GO:0008289	lipid binding	0.0000418	0.00989	2.47 (11754,295,387,24)
GO:0016209	antioxidant activity	0.0000809	0.0178	6.44 (11754,33,387,7)
GO:0071813	lipoprotein particle binding	0.000138	0.0283	22.78 (11754,4,387,3)
GO:0071814	protein-lipid complex binding	0.000138	0.0266	22.78 (11754,4,387,3)
GO:0005319	lipid transporter activity	0.000291	0.0527	4.14 (11754,66,387,9)

GO Term	Description	P-value	FDR q-value	Enrichment (N, B, n, b)
GO:0044425	membrane part	2.88E-08	0.000037	1.43 (11754,3577,387,168)
GO:0031224	intrinsic component of membrane	6.66E-08	0.0000428	1.47 (11754,3067,387,148)
GO:0016021	integral component of membrane	1.98E-07	0.000085	1.45 (11754,3036,387,145)
GO:0016020	membrane	0.00000632	0.00203	1.31 (11754,4116,387,177)
GO:0005576	extracellular region	0.0000222	0.0057	2.12 (11754,502,387,35)
GO:0005783	endoplasmic reticulum	0.0000335	0.00717	2.08 (11754,512,387,35)
GO:0005789	endoplasmic reticulum membrane	0.0000626	0.0115	2.36 (11754,322,387,25)
GO:0005615	extracellular space	0.000124	0.02	2.08 (11754,439,387,30)
GO:1990777	lipoprotein particle	0.000208	0.0296	12.15 (11754,10,387,4)
GO:0034358	plasma lipoprotein particle	0.000208	0.0267	12.15 (11754,10,387,4)
GO:0032994	protein-lipid complex	0.000208	0.0242	12.15 (11754,10,387,4)
GO:0044432	endoplasmic reticulum part	0.000464	0.0497	1.92 (11754,474,387,30)
GO:0044421	extracellular region part	0.000552	0.0546	1.84 (11754,546,387,33)
GO:0034364	high-density lipoprotein particle	0.000658	0.0604	15.19 (11754,6,387,3)
GO:0034385	triglyceride-rich plasma lipoprotein particle	0.000658	0.0563	15.19 (11754,6,387,3)
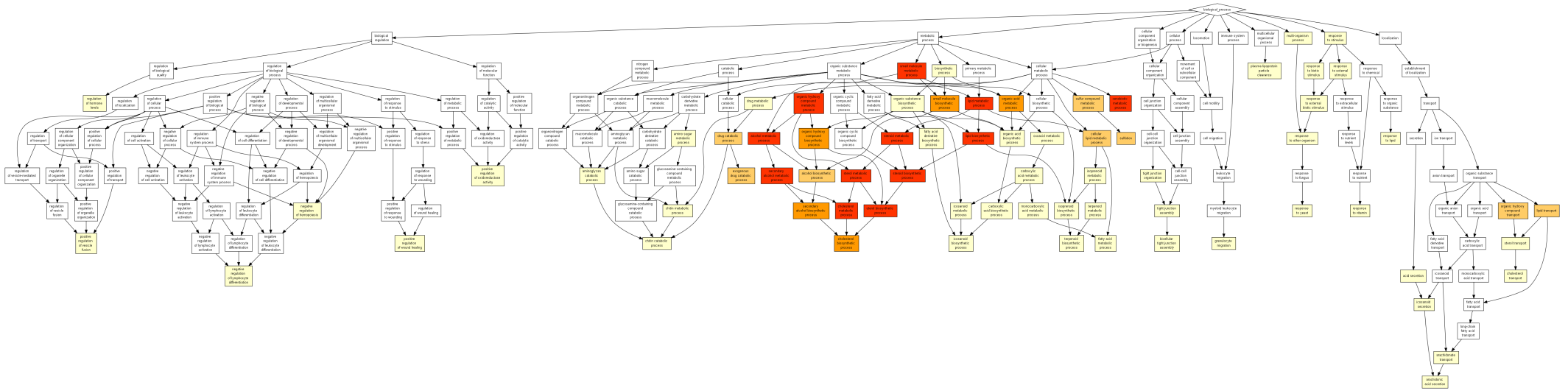
Figure 4.8. Biological Process GO-term visualisation of upregulated significantly differentially expressed genes resulting from the *MR^46Del* mutation in 5dpf zebrafish larvae. Enrichment of genes overrepresented in Biological Processes. All maps produced using GOrilla software. Legend indicates p-value colour scale.

Figure 4.9. Molecular Function GO-term visualisation of upregulated significantly differentially expressed genes resulting from the *MR^46Del* **mutation in 5dpf zebrafish larvae.** Enrichment of genes overrepresented in molecular functions. Map produced using GOrilla software. Legend indicates p-value colour scale

Figure 4.10. Cellular Component GO-term visualisation of upregulated significantly differentially expressed genes resulting from the *MR^46Del* **mutation in 5dpf zebrafish larvae.** Enrichment of genes overrepresented in Cellular Components. Map produced using GOrilla software. Legend indicates p-value colour scale

94

Figure 4.11. REVIGO GO-term visualisation of upregulated significantly differentially expressed genes resulting from the *MR^46Del* mutation in 5dpf zebrafish larvae. Enrichment of genes overrepresented in biological processes (top), molecular functions (bottom left) and cellular components (bottom right). All maps produced using REVIGO software.
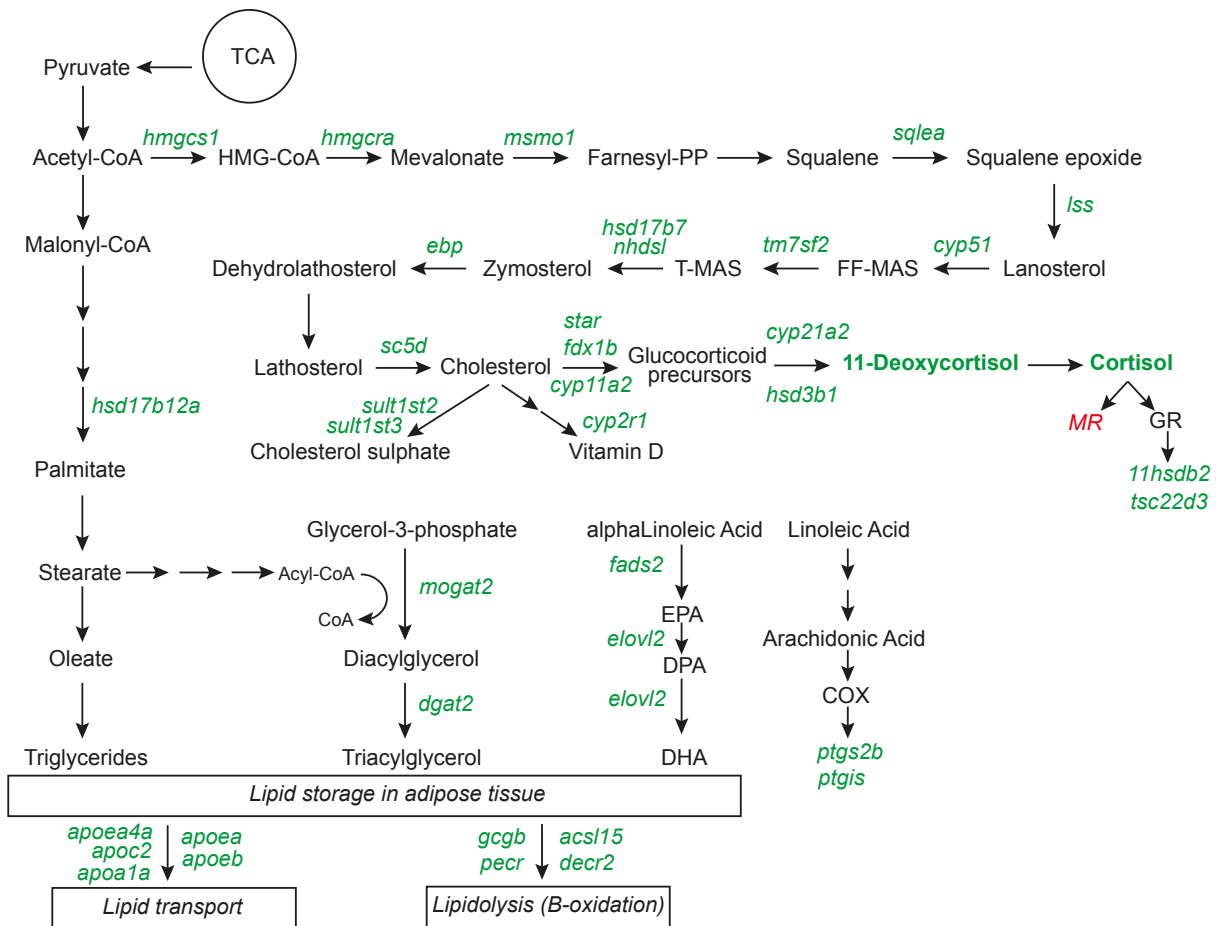
Figure 4.12. *MR^{46Del}* larval differentially expressed genes regulating metabolic pathways involved cholesterol and glucocorticoid synthesis, lipogenesis and lipolysis. Genes in green are upregulated in *MR^{46Del}* mutants; red are downregulated. Upregulated steroids described in Chapter 3, 11-deoxycortisol and cortisol, are highlighted in bold. Cortisol arrows to MR and GR indicate ligand binding. Figure made in Adobe illustrator.

Table 4.5. KEGG and Reactome enrichment analysis of biological pathways for upregulated DEGs in 5dpf *MR^46Del* mutant zebrafish larvae.

KEGG Term	Count	Fold Enrichment	Benjamini	FDR
Metabolic Pathways	82	1.94958124	5.58E-09	5.58E-09
Steroid Biosynthesis	10	14.2199421	9.63E-07	4.48E-07
Oxidative Phosphorylation	7	2.98618785	0.07678029	0.01330993
Retinol Metabolism	17	5.35982434	0.16785497	0.02622827

Reactome Term	Count	Fold Enrichment	Benjamini	FDR
Cholesterol biosynthesis	9	17.3583131	2.79E-06	2.79E-06
Glutathione conjugation	8	10.7336429	0.00136968	6.85E-04

4.2.6 Genes downregulated in the 5dpf larval *MR^46Del* mutant transcriptome encode proteins involved in synaptic signaling.

Statistical overrepresentation analysis of downregulated DEGs revealed 67 significant GO terms related to Biological Processes with an FDR<0.05, including synaptic signalling, regulation of ion transport, axon guidance, regulation of a membrane potential, regulation of neurotransmitter transport and glutamatergic signalling (Figures 4.13 & 4.16; Table 4.6). Similarly, 50 Molecular Function-related GO terms were identified. Of these, overrepresentation of genes involved in ion gated channel activity, transmembrane transport, GABA receptor and glutamate receptor activity, and JUN and SAP kinase activity were recognised (Figure 4.14 & 4.16; Table 4.6). As such, downregulated genes were overrepresented in ontologies for Cellular Components such as neurons, plasma membrane components, ion channel complexes, pre- and post-synapse, and dendrites. These GO terms suggest MR has an important role of neurodevelopment and synaptic signalling during zebrafish larval development (Figure 4.15 & 4.16; Table 4.6). In addition, KEGG pathway analysis revealed an enrichment of neural cell adhesion molecules downregulated in the *MR^46Del* mutant transcriptome (Appensix 1 Figure A17).

The synapse is a complex bridge between interacting neurons, or between a neuron and a muscle cell, where transmission of electrical or chemical impulses occurs (Südhof, 2018). In the pre-synaptic neuron this usually involves release of synaptic vesicles carrying cargoes of neurotransmitters, as well as voltage-gated ion channels, neurotransmitter transporters and synaptic adhesion molecules (SAMs) to stabilise close interactions with the post-synaptic cell (Südhof, 2018). A significant number of genes that encode important components of these junctions were downregulated in the *MR^46Del*

transcriptome. This included both excitatory metabotropic glutamatergic synapse receptors *grid2*, *grm3*, *grm4* and *grm6a*, and inhibitory GABAergic receptors *gabbr1b*, *gabbr2*, *gabrg2*, *gabrd*, *gabra1* and *gabra5*. As GABA receptors are ligand-gated chloride channels, an electrochemical gradient is required for regulation of GABAergic neurotransmission (Bormann, 2000). Genes essential for the formation of this gradient include potassium/chloride channels *kcnj3a, kcnj5,* and *kcnj6*, *slc12a5b*; calcium channels *cacnb4a cacnb1* and *cacna1ba*; and the sodium channel *scn1lab*, all of which were significantly downregulated in MR mutants. Similarly, multiple components important for synaptic vesicle function and exocytosis were identified in my downregulated DEG population, including *exoc4*, known to interact with DLG4 in glutamatergic synapses (Sans et al., 2003); *napba* a member a SNARE-complex, important for synaptic vesicle docking; *slc17a6a*, involved in the uptake of glutamate into synaptic vesicles at presynaptic nerve terminals; and amyloid beta precursor *apba1a*, a neuronal adapter protein. To initiate synapse formation, maturation and maintenance, synaptic adhesion molecules are required to provide mechanical support (Südhof, 2018). Two important synaptic adhesion molecule pairs, the GABAergic presynaptic neurexin (*nrxn2a*) and glutamatergic postsynaptic neuroligin (*nlgn1*) were downregulated in *MR^46Del* mutants. Other synaptic receptors were downregulated in *MR^46Del* mutants, including the dopamine receptor *drd2a*, cannabinoid receptor *cnr1*, circadian rhythm-associated receptor *mtnr1aa*; and the BDNF or neurotrophin receptor, *ntrk2b*.

An important synapse-type is the neuromuscular junction (NMJ), between the terminal end of a motor nerve and a muscle fibre. In vertebrates, the neurotransmitter acetylcholine is released from the presynaptic terminal, crosses the synaptic cleft and bind to nicotinic acetylcholine receptors located on the cell membrane of the muscle fibre (Wu et al., 2010). Many cholinergic ionotropic receptors were downregulated in *MR^46Del* mutants, including *chrm2a chrna2b chrm4a* and *chrna9*. Associated dystrophin proteins *dtna* and *dtnbb* were also identified as downregulated DEGs; these genes are known for their roles in formation and stability of synapses and organisation of nicotinic acetylcholine receptors (Pilgram et al., 2010). In addition, the mitogen-activated protein kinases (MAPK) *mapk8b*, *mapk9*, *mapk10* and *map3k12*, which function downstream of the c-Jun N-terminal kinase (JNK) pathway were downregulated in *MR^46Del* mutants. MAPKs may provide a non-genomic mechanism is which the MR may regulate transcription of various biological pathways.

Table 4.6. Significant Biological Processes (left), Molecular Function (middle) and Cellular Component (right) Gene Ontology terms overrepresented in downregulated genes differentially expressed in _MR46Del_ mutant zebrafish larvae.

Biological Processes (left)

GO Term	Description	P-value	FDR q-value	Enrichment (N, B, n, b)
GO:0099536	synaptic signaling	5.16E-13	4.23E-09	5.56 (11754,112,491,26)
GO:0023052	signaling	2.63E-12	1.08E-08	4.52 (11754,159,491,30)
GO:0043269	regulation of ion transport	6.03E-12	1.65E-08	4.38 (11754,164,491,30)
GO:0098660	inorganic ion transmembrane transport	7.78E-12	1.6E-08	3.41 (11754,281,491,40)
GO:0030001	metal ion transport	1.15E-11	1.88E-08	3.30 (11754,297,491,41)
GO:0034220	ion transmembrane transport	3.13E-11	4.27E-08	3.00 (11754,359,491,45)
GO:0051049	regulation of transport	5.06E-11	5.93E-08	3.16 (11754,311,491,41)
GO:0099537	trans-synaptic signaling	6.25E-11	6.41E-08	5.15 (11754,107,491,23)
GO:0032879	regulation of localization	8.28E-11	7.54E-08	2.57 (11754,512,491,55)
GO:0098916	anterograde trans-synaptic signaling	1.01E-10	8.3E-08	5.27 (11754,100,491,22)
GO:0007268	chemical synaptic transmission	1.01E-10	7.55E-08	5.27 (11754,100,491,22)
GO:0034762	regulation of transmembrane transport	1.12E-10	7.69E-08	4.45 (11754,140,491,26)
GO:0007267	cell-cell signaling	1.33E-10	8.37E-08	4.41 (11754,141,491,26)
GO:0006811	ion transport	1.8E-10	1.05E-07	2.38 (11754,614,491,61)
GO:0098662	inorganic cation transmembrane transport	1.89E-10	1.04E-07	3.39 (11754,247,491,35)
GO:0034765	regulation of ion transmembrane transport	2.33E-10	1.19E-07	4.47 (11754,134,491,25)
GO:0006812	cation transport	5.9E-10	2.84E-07	2.83 (11754,364,491,43)
GO:0098655	cation transmembrane transport	7.94E-10	3.62E-07	3.16 (11754,273,491,36)
GO:0007154	cell communication	5.26E-09	0.00000227	3.44 (11754,202,491,29)
GO:0015672	monovalent inorganic cation transport	1.11E-08	0.00000455	3.51 (11754,184,491,27)
GO:0055085	transmembrane transport	1.78E-08	0.00000696	2.20 (11754,609,491,56)
GO:0042391	regulation of membrane potential	3.57E-08	0.0000133	4.96 (11754,82,491,17)
GO:0098742	cell-cell adhesion via plasma-membrane adhesion molecules	7.51E-08	0.0000268	4.73 (11754,86,491,17)
GO:0007186	G protein-coupled receptor signaling pathway	9.61E-08	0.0000328	2.96 (11754,243,491,30)
GO:0007156	homophilic cell adhesion via plasma membrane adhesion molecules	1.06E-07	0.0000346	4.91 (11754,78,491,16)
GO:0007411	axon guidance	5.07E-07	0.00016	3.08 (11754,194,491,25)
GO:0097485	neuron projection guidance	5.59E-07	0.00017	3.07 (11754,195,491,25)
GO:0099177	regulation of trans-synaptic signaling	8.44E-07	0.000247	4.03 (11754,101,491,17)
GO:0050804	modulation of chemical synaptic transmission	8.44E-07	0.000239	4.03 (11754,101,491,17)
GO:0022610	biological adhesion	0.00000121	0.000331	2.45 (11754,332,491,34)
GO:0007155	cell adhesion	0.00000121	0.00032	2.45 (11754,332,491,34)
GO:0007214	gamma-aminobutyric acid signaling pathway	0.00000199	0.00051	13.06 (11754,11,491,6)
GO:0007188	adenylate cyclase-modulating G protein-coupled receptor signaling pathway	0.00000235	0.000583	4.18 (11754,86,491,15)
GO:0007187	G protein-coupled receptor signaling pathway, coupled to cyclic nucleotide second messenger	0.00000273	0.000658	4.13 (11754,87,491,15)
GO:0001508	action potential	0.00000453	0.00106	9.31 (11754,18,491,7)
GO:0051259	protein complex oligomerization	0.00000489	0.00111	4.19 (11754,80,491,14)
GO:0098609	cell-cell adhesion	0.0000103	0.00228	3.12 (11754,146,491,19)
GO:0050808	synapse organization	0.0000155	0.00335	4.35 (11754,66,491,12)
GO:0006810	transport	0.000017	0.00358	1.47 (11754,1746,491,107)
GO:0051234	establishment of localization	0.0000227	0.00465	1.45 (11754,1778,491,108)
GO:0051588	regulation of neurotransmitter transport	0.0000291	0.00582	7.29 (11754,23,491,7)
GO:0006814	sodium ion transport	0.0000331	0.00646	3.57 (11754,94,491,14)
GO:0051179	localization	0.0000384	0.00732	1.42 (11754,1945,491,115)
GO:0120039	plasma membrane bounded cell projection morphogenesis	0.0000419	0.00781	3.17 (11754,121,491,16)
GO:0048812	neuron projection morphogenesis	0.0000419	0.00763	3.17 (11754,121,491,16)
GO:0070206	protein trimerization	0.0000422	0.00752	15.96 (11754,6,491,4)
GO:0051260	protein homooligomerization	0.0000519	0.00905	4.18 (11754,63,491,11)
GO:0048858	cell projection morphogenesis	0.0000625	0.0107	3.06 (11754,125,491,16)
GO:0032412	regulation of ion transmembrane transporter activity	0.0000794	0.0133	4.35 (11754,55,491,10)
GO:0035725	sodium ion transmembrane transport	0.0000808	0.0133	3.99 (11754,66,491,11)
GO:0032990	cell part morphogenesis	0.000101	0.0162	2.95 (11754,130,491,16)
GO:1904062	regulation of cation transmembrane transport	0.000123	0.0193	3.82 (11754,69,491,11)
GO:0001505	regulation of neurotransmitter levels	0.000126	0.0195	3.55 (11754,81,491,12)
GO:0022898	regulation of transmembrane transporter activity	0.000127	0.0192	4.13 (11754,58,491,10)
GO:0070838	divalent metal ion transport	0.000138	0.0206	2.99 (11754,120,491,15)
GO:0072511	divalent inorganic cation transport	0.000138	0.0203	2.99 (11754,120,491,15)
GO:0070588	calcium ion transmembrane transport	0.000142	0.0205	3.50 (11754,82,491,12)
GO:0032409	regulation of transporter activity	0.000147	0.0208	4.06 (11754,59,491,10)
GO:0007254	JNK cascade	0.000184	0.0256	11.97 (11754,8,491,4)
GO:0006816	calcium ion transport	0.000189	0.0258	3.21 (11754,97,491,13)
GO:0099003	vesicle-mediated transport in synapse	0.000195	0.0263	4.31 (11754,50,491,9)
GO:0010959	regulation of metal ion transport	0.000196	0.0259	3.92 (11754,61,491,10)
GO:0071805	potassium ion transmembrane transport	0.000226	0.0294	3.34 (11754,86,491,12)
GO:0071804	cellular potassium ion transport	0.000226	0.0289	3.34 (11754,86,491,12)
GO:0007215	glutamate receptor signaling pathway	0.000264	0.0333	7.98 (11754,15,491,5)
GO:0051966	regulation of synaptic transmission, glutamatergic	0.000365	0.0453	5.98 (11754,24,491,6)
GO:0006813	potassium ion transport	0.000386	0.0472	3.16 (11754,91,491,12)

Molecular Function (middle)

GO Term	Description	P-value	FDR q-value	Enrichment (N, B, n, b)
GO:0022839	ion gated channel activity	5.18E-17	1.59E-13	4.81 (11754,199,491,40)
GO:0022836	gated channel activity	1.84E-16	2.82E-13	4.65 (11754,206,491,40)
GO:0005216	ion channel activity	1.28E-15	1.31E-12	4.30 (11754,228,491,41)
GO:0022838	substrate-specific channel activity	2.4E-15	1.84E-12	4.23 (11754,232,491,41)
GO:0022803	passive transmembrane transporter activity	2.25E-13	1.38E-10	3.72 (11754,264,491,41)
GO:0015267	channel activity	2.25E-13	1.15E-10	3.72 (11754,264,491,41)
GO:0005261	cation channel activity	2.93E-13	1.29E-10	4.46 (11754,177,491,33)
GO:0022890	inorganic cation transmembrane transporter activity	2.29E-12	8.8E-10	3.23 (11754,333,491,45)
GO:0046873	metal ion transmembrane transporter activity	2.38E-12	8.13E-10	3.68 (11754,247,491,38)
GO:0008324	cation transmembrane transporter activity	5.66E-12	1.74E-09	3.06 (11754,368,491,47)
GO:0015075	ion transmembrane transporter activity	7.61E-12	2.13E-09	2.64 (11754,525,491,58)
GO:0015318	inorganic molecular entity transmembrane transporter activity	2.94E-11	7.54E-09	2.67 (11754,484,491,54)
GO:0060089	molecular transducer activity	4.41E-10	1.04E-07	2.70 (11754,417,491,47)
GO:0005244	voltage-gated ion channel activity	5.93E-10	0.00000013	4.83 (11754,109,491,22)
GO:0038023	signaling receptor activity	8.84E-10	1.81E-07	2.71 (11754,397,491,45)
GO:0022832	voltage-gated channel activity	1.22E-09	2.35E-07	4.66 (11754,113,491,22)
GO:0004888	transmembrane signaling receptor activity	2.46E-09	4.45E-07	2.87 (11754,325,491,39)
GO:0022857	transmembrane transporter activity	2.83E-09	4.84E-07	2.17 (11754,707,491,64)
GO:0030594	neurotransmitter receptor activity	1.66E-08	0.00000269	5.55 (11754,69,491,16)
GO:0004930	G protein-coupled receptor activity	2.89E-08	0.00000444	4.12 (11754,122,491,21)
GO:0005215	transporter activity	3.64E-08	0.00000532	2.03 (11754,755,491,64)
GO:0015077	monovalent inorganic cation transmembrane transporter activity	6.01E-08	0.0000084	3.25 (11754,199,491,27)
GO:0022843	voltage-gated cation channel activity	2.62E-07	0.000035	4.61 (11754,83,491,16)
GO:0005272	sodium channel activity	0.00000167	0.000214	8.71 (11754,22,491,8)
GO:0022834	ligand-gated channel activity	0.00000203	0.00025	3.99 (11754,96,491,16)
GO:0015276	ligand-gated ion channel activity	0.00000203	0.00024	3.99 (11754,96,491,16)
GO:0005249	voltage-gated potassium channel activity	0.0000155	0.00176	5.20 (11754,46,491,10)
GO:0016917	GABA receptor activity	0.0000187	0.00205	9.58 (11754,15,491,6)
GO:0017080	sodium channel regulator activity	0.0000187	0.00198	9.58 (11754,15,491,6)
GO:0005267	potassium channel activity	0.0000274	0.00281	4.46 (11754,59,491,11)
GO:0015081	sodium ion transmembrane transporter activity	0.0000416	0.00413	3.70 (11754,84,491,13)
GO:0001640	adenylate cyclase inhibiting G protein-coupled glutamate receptor activity	0.0000422	0.00405	15.96 (11754,6,491,4)
GO:0098988	G protein-coupled glutamate receptor activity	0.0000422	0.00393	15.96 (11754,6,491,4)
GO:0099528	G protein-coupled neurotransmitter receptor activity	0.0000467	0.00422	10.88 (11754,11,491,5)
GO:0005248	voltage-gated sodium channel activity	0.0000467	0.0041	10.88 (11754,11,491,5)
GO:0022824	transmitter-gated ion channel activity	0.000057	0.00487	5.01 (11754,43,491,9)
GO:0022835	transmitter-gated channel activity	0.000057	0.00474	5.01 (11754,43,491,9)
GO:0015085	calcium ion transmembrane transporter activity	0.0000607	0.00491	3.58 (11754,87,491,13)
GO:0098960	postsynaptic neurotransmitter receptor activity	0.00007	0.00552	6.45 (11754,26,491,7)
GO:0008066	glutamate receptor activity	0.0000911	0.007	6.21 (11754,27,491,7)
GO:0005230	extracellular ligand-gated ion channel activity	0.000127	0.00949	4.13 (11754,58,491,10)
GO:0004705	JUN kinase activity	0.000281	0.0206	17.95 (11754,4,491,3)
GO:0016909	SAP kinase activity	0.000281	0.0201	17.95 (11754,4,491,3)
GO:0099529	neurotransmitter receptor activity involved in regulation of postsynaptic membrane potential	0.000283	0.0198	6.24 (11754,23,491,6)
GO:1904315	transmitter-gated ion channel activity involved in regulation of postsynaptic membrane potential	0.000283	0.0194	6.24 (11754,23,491,6)
GO:0016247	channel regulator activity	0.000349	0.0233	4.45 (11754,43,491,8)
GO:0015079	potassium ion transmembrane transporter activity	0.000386	0.0252	3.16 (11754,91,491,12)
GO:0099094	ligand-gated cation channel activity	0.000547	0.035	3.47 (11754,69,491,10)
GO:0008503	benzodiazepine receptor activity	0.00068	0.0427	14.36 (11754,5,491,3)
GO:0015280	ligand-gated sodium channel activity	0.00068	0.0418	14.36 (11754,5,491,3)

Cellular Component (right)

GO Term	Description	P-value	FDR q-value	Enrichment (N, B, n, b)
GO:0097458	neuron part	1.66E-19	2.13E-16	3.37 (11754,490,491,69)
GO:0005886	plasma membrane	2.67E-19	1.72E-16	2.24 (11754,1345,491,126)
GO:0031224	intrinsic component of membrane	6.14E-19	2.63E-16	1.69 (11754,3067,491,217)
GO:0016021	integral component of membrane	2.18E-18	7E-16	1.69 (11754,3036,491,214)
GO:0044425	membrane part	4.17E-18	1.07E-15	1.60 (11754,3577,491,239)
GO:0016020	membrane	3.46E-17	7.41E-15	1.52 (11754,4116,491,261)
GO:0044459	plasma membrane part	5.35E-16	9.82E-14	2.38 (11754,957,491,95)
GO:0031226	intrinsic component of plasma membrane	1.09E-14	1.76E-12	3.08 (11754,451,491,58)
GO:0043005	neuron projection	1.47E-14	2.1E-12	3.71 (11754,290,491,45)
GO:0005887	integral component of plasma membrane	2.33E-14	2.99E-12	3.10 (11754,432,491,56)
GO:0034702	ion channel complex	3.52E-13	4.12E-11	5.03 (11754,138,491,29)
GO:0034703	cation channel complex	9.28E-13	9.94E-11	5.92 (11754,97,491,24)
GO:1902495	transmembrane transporter complex	1.91E-12	1.89E-10	4.72 (11754,147,491,29)
GO:0044456	synapse part	3.33E-12	3.06E-10	3.43 (11754,286,491,41)
GO:1990351	transporter complex	5.46E-12	4.68E-10	4.54 (11754,153,491,29)
GO:0120025	plasma membrane bounded cell projection	6.75E-12	5.42E-10	2.84 (11754,438,491,52)
GO:0045202	synapse	1.01E-11	7.63E-10	3.76 (11754,223,491,35)
GO:0042995	cell projection	1.56E-11	1.11E-09	2.65 (11754,505,491,56)
GO:0098794	postsynapse	5.08E-08	0.00000344	6.48 (11754,48,491,13)
GO:0097060	synaptic membrane	0.00000111	0.0000712	3.61 (11754,126,491,19)
GO:0032590	dendrite membrane	0.00000199	0.000122	13.06 (11754,11,491,6)
GO:0098797	plasma membrane protein complex	0.00000336	0.000196	2.55 (11754,272,491,29)
GO:0001518	voltage-gated sodium channel complex	0.00000384	0.000215	11.97 (11754,12,491,6)
GO:0008076	voltage-gated potassium channel complex	0.00000703	0.000376	7.37 (11754,26,491,8)
GO:0030424	axon	0.0000096	0.000493	3.74 (11754,96,491,15)
GO:0034706	sodium channel complex	0.0000116	0.000574	10.26 (11754,14,491,6)
GO:0034705	potassium channel complex	0.000013	0.000616	6.84 (11754,28,491,8)
GO:0045211	postsynaptic membrane	0.0000153	0.000704	3.81 (11754,88,491,14)
GO:0032589	neuron projection membrane	0.0000187	0.000828	9.58 (11754,15,491,6)
GO:0043197	dendritic spine	0.0000483	0.00207	5.80 (11754,28,491,8)
GO:0044309	neuron spine	0.0000483	0.002	5.80 (11754,28,491,8)
GO:0031256	leading edge membrane	0.0000942	0.00378	5.32 (11754,36,491,8)
GO:0120038	plasma membrane bounded cell projection part	0.000116	0.00451	2.22 (11754,280,491,26)
GO:0044463	cell projection part	0.000116	0.00437	2.22 (11754,280,491,26)
GO:0043025	neuronal cell body	0.000288	0.0106	5.24 (11754,32,491,7)
GO:0044297	cell body	0.000428	0.0153	4.93 (11754,34,491,7)
GO:0098563	intrinsic component of synaptic vesicle membrane	0.000517	0.0179	9.58 (11754,10,491,4)
GO:0030054	cell junction	0.000587	0.0199	1.89 (11754,379,491,30)
GO:0031672	A band	0.00068	0.0224	14.36 (11754,5,491,3)

Figure 4.13. Biological Process GO-term visualisation of downregulated significantly differentially expressed genes resulting from the *MR^46Del* mutation in 5dpf zebrafish larvae. Enrichment of genes overrepresented in Biological Processes. All maps produced using GOrilla software. Legend indicates p-value colour scale.
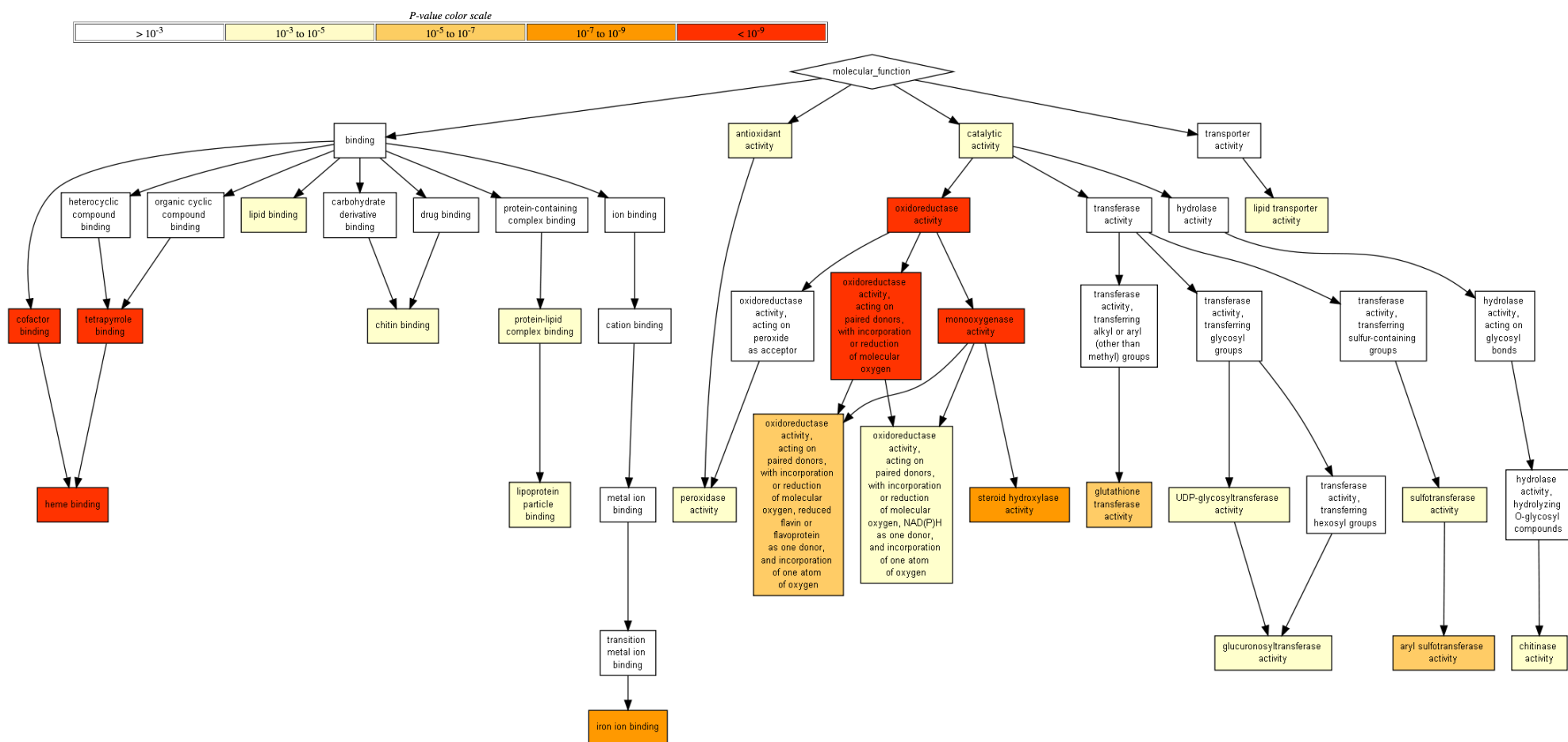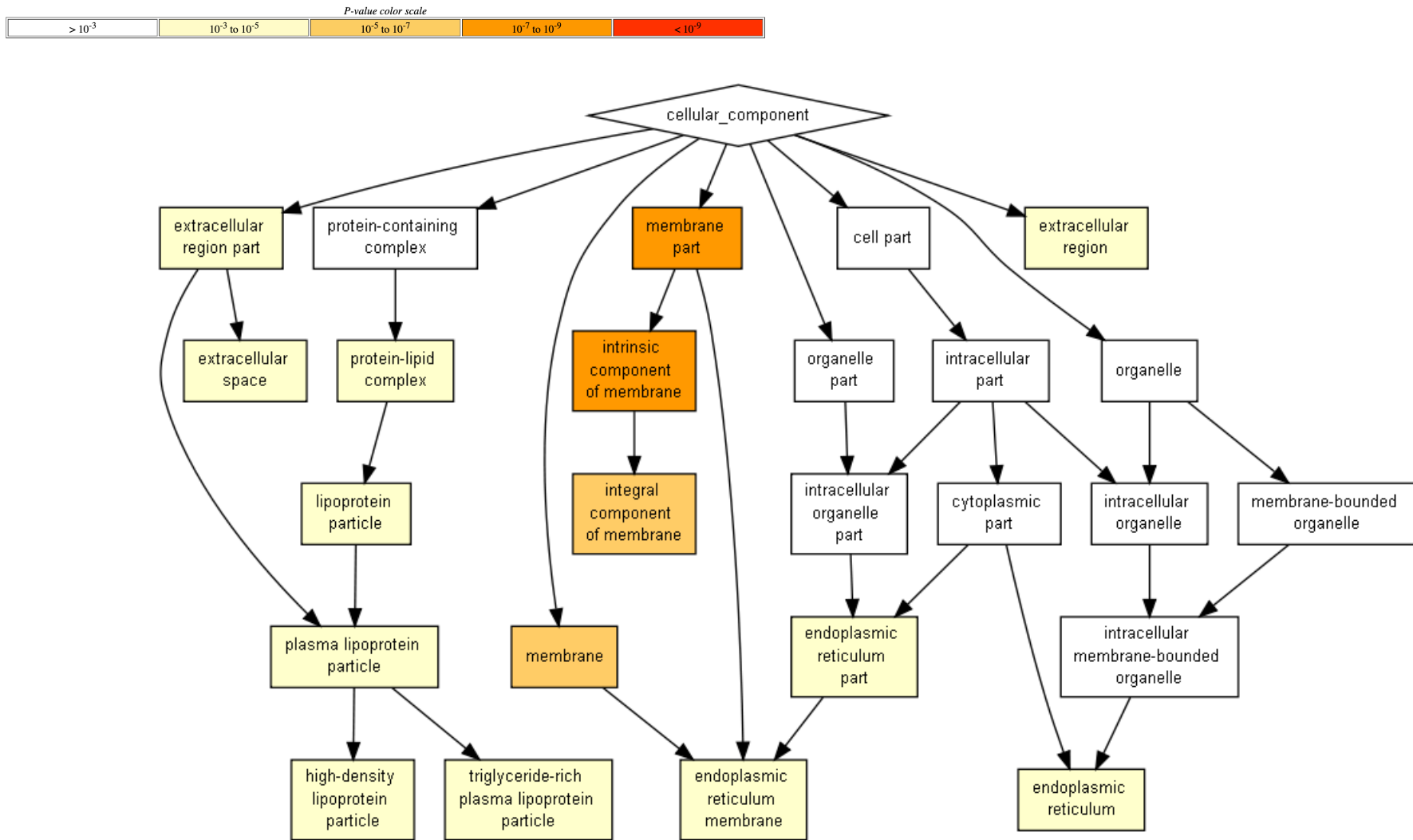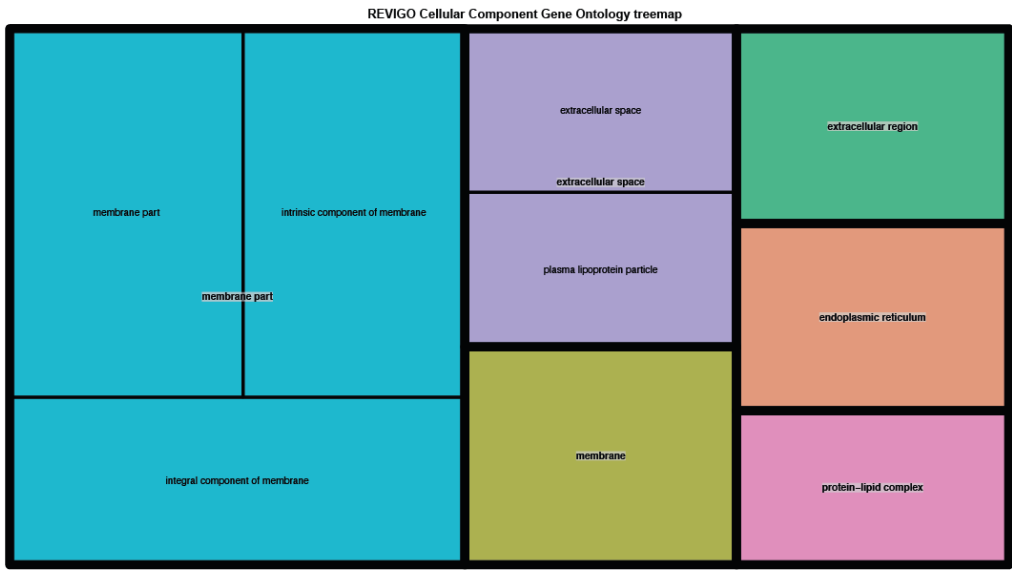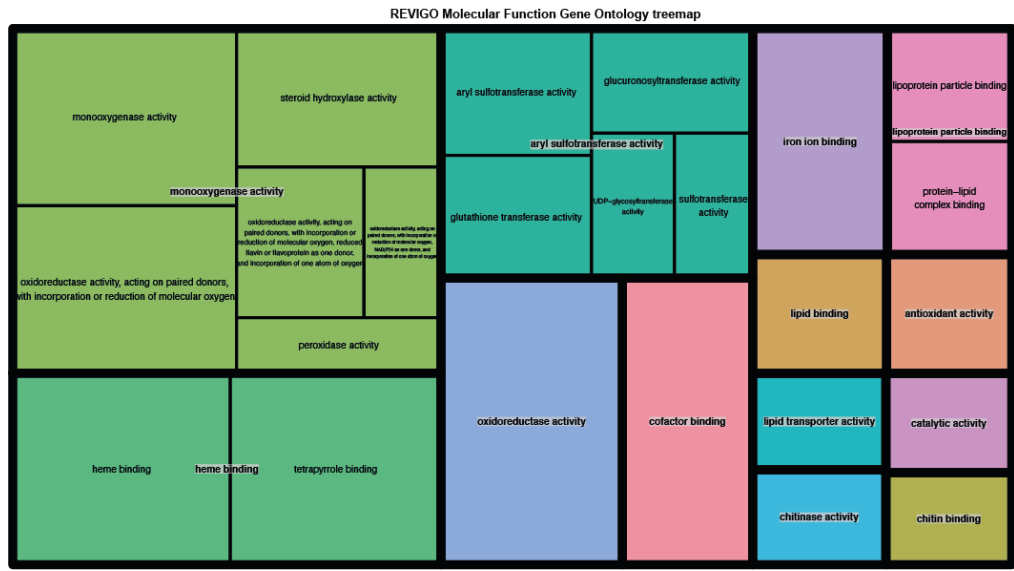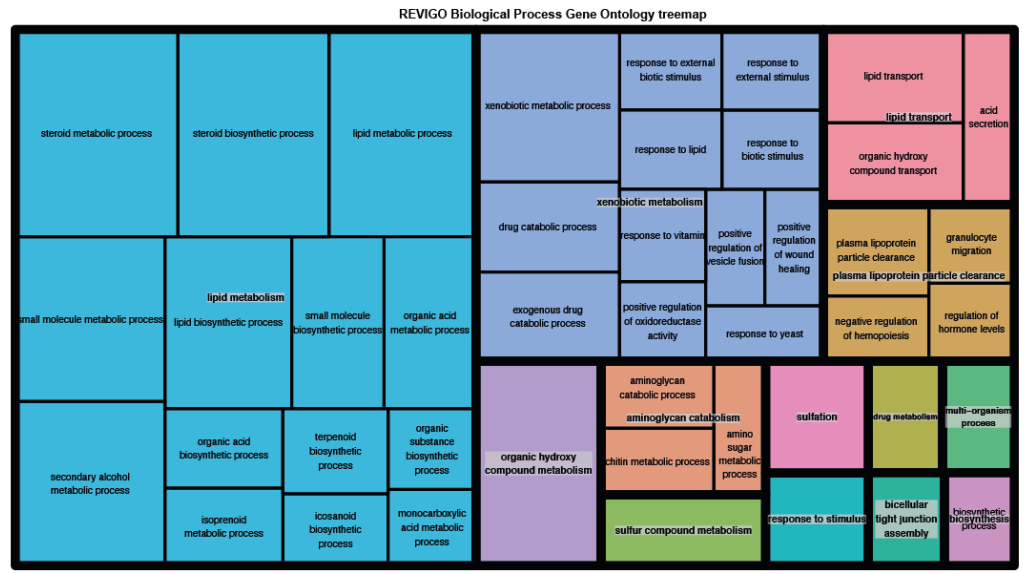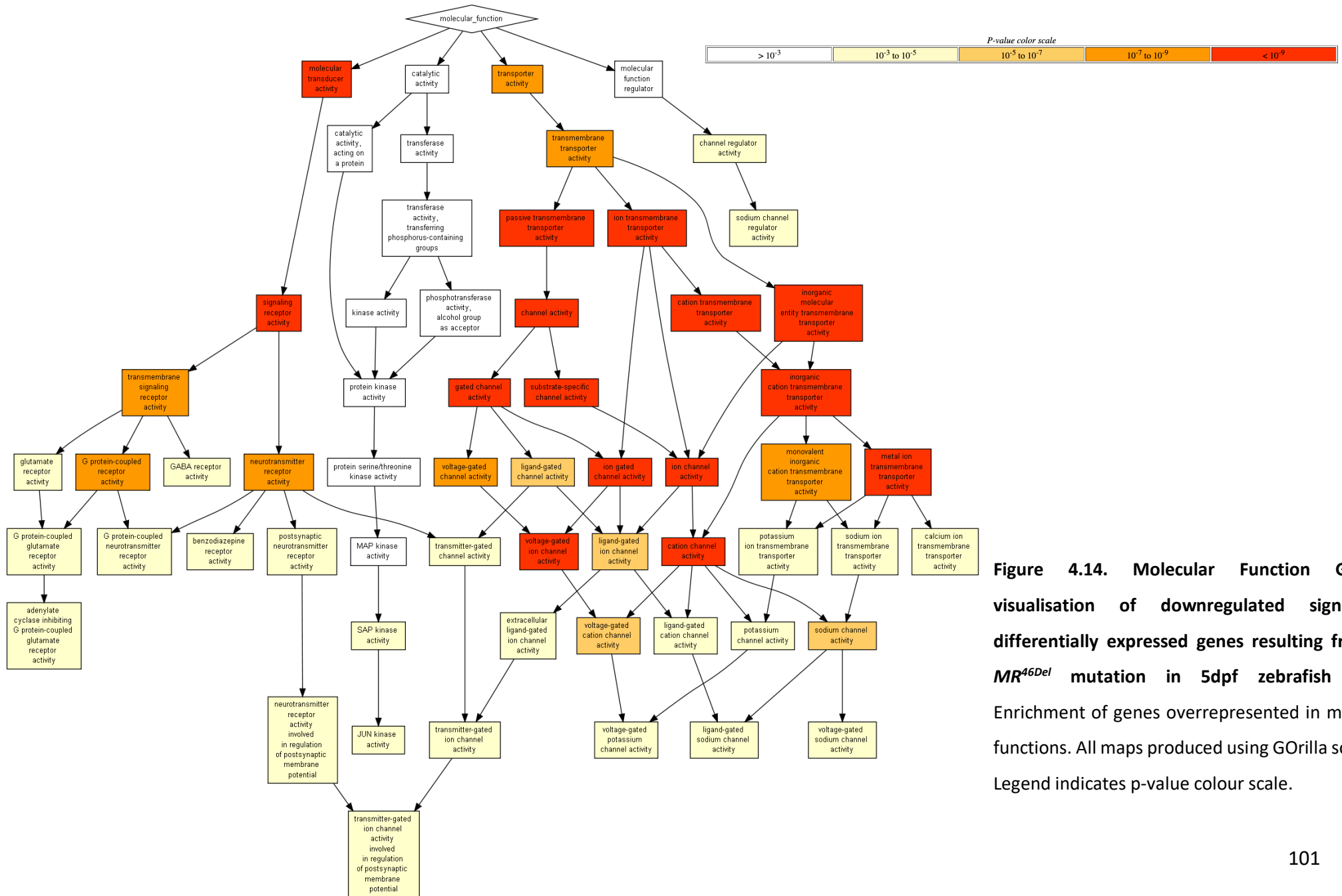
Figure 4.14. Molecular Function GO-term visualisation of downregulated significantly differentially expressed genes resulting from the *MR*[46Del] **mutation in 5dpf zebrafish larvae.** Enrichment of genes overrepresented in molecular functions. All maps produced using GOrilla software. Legend indicates p-value colour scale.

Figure 4.15. Cellular Component GO-term visualisation of downregulated significantly differentially expressed genes resulting from the _MR^46Del_ mutation in 5dpf zebrafish larvae. Enrichment of genes overrepresented in Cellular Components. All maps produced using GOrilla software. Legend indicates p-value colour scale.
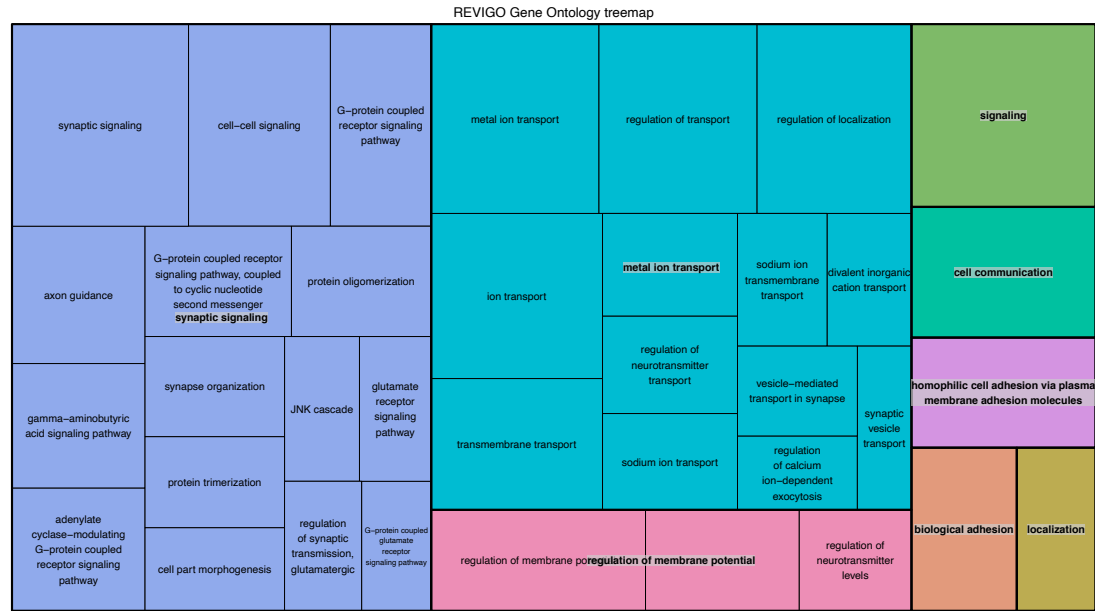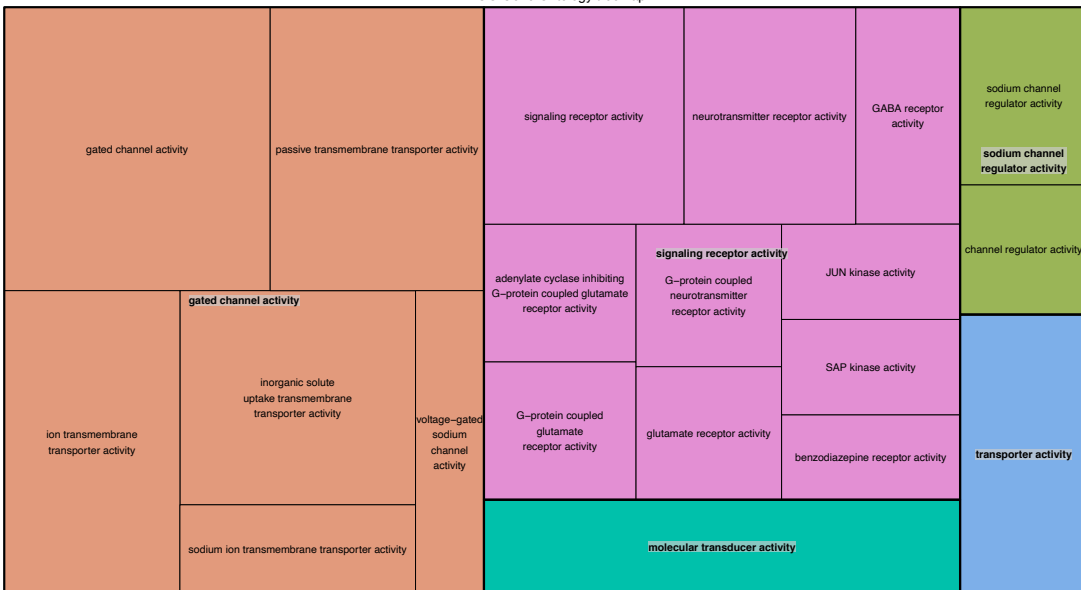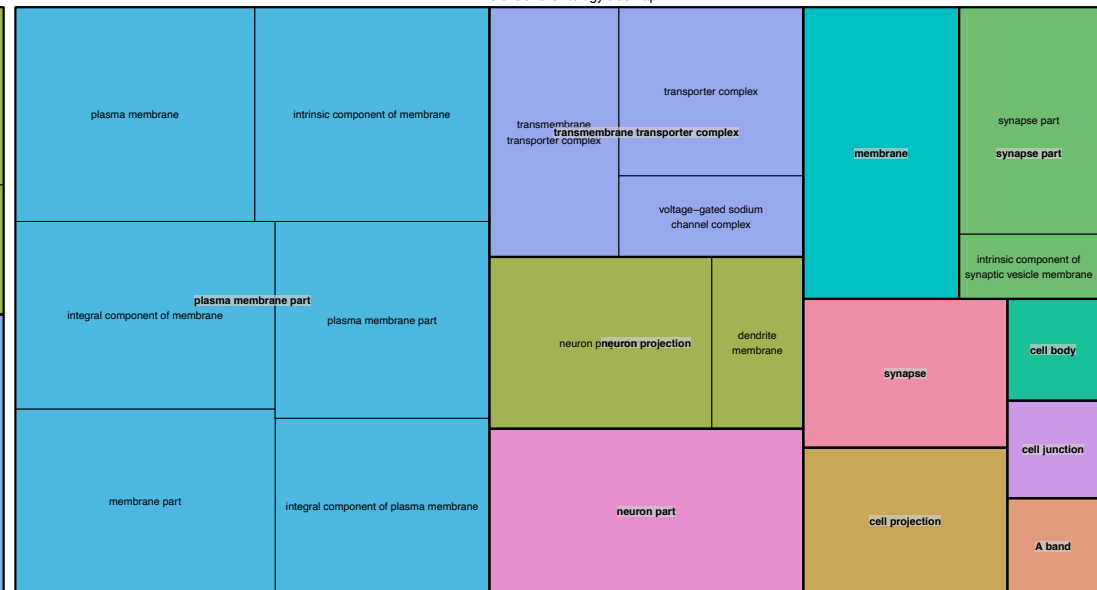
Figure 4.16. REVIGO GO-term visualisation of downregulated significantly differentially expressed genes resulting from the *MR^46Del* mutation in 5dpf zebrafish larvae.

Enrichment of genes overrepresented in biological processes (A), molecular functions (B) and cellular components (C). All maps produced using REVIGO software.

Table 4.7. KEGG and Reactome enrichment analysis of biological pathways for downregulated DEGs in 5dpf *MR⁴⁶ᴰᵉˡ* mutant zebrafish larvae.

KEGG Term	Count	Fold Enrichment	Benjamini	FDR
MAPK signaling pathway	27	2.69352159	3.92E-04	3.77E-04
Adrenergic signaling in cardiomyocytes	18	3.02481035	0.00234345	0.00225666
Cell adhesion molecules (CAMs)	15	3.46592852	0.00234345	0.00225666
Neuroactive ligand-receptor interaction	28	2.15657775	0.00334594	0.00322202

Reactome Term	Count	Fold Enrichment	Benjamini	FDR
Voltage gated Potassium channels	12	7.43653734	8.55E-05	8.29E-05

4.3 Discussion

In order to further explore the systemic molecular effects of a loss of MR function, de-repression of the HPI axis and whole body larval hypercortisolaemia identified in 5dpf *MR⁴⁶ᴰᵉˡ* mutants, I have performed RNA sequencing on pooled samples of *MR⁴⁶ᴰᵉˡ* 5dpf larvae, targeting poly-A tailed transcripts. Initial quality control assessment of mRNA sequencing data identified an outlier sample, MR2. This outlier was detected through multiple means of evidence, including PCA, heatmap hierarchical clustering, size estimation and dendrogram mapping (Figure 2). After the removal of outlier MR2, 5dpf larvae mRNA samples displayed a clear segregation between genotype in the second principal component and clustered by genotype in heatmap hierarchical clustering. Differential expression analysis results of 5dpf *MR⁴⁶ᴰᵉˡ* larvae identified a dysregulation of genes seen previously by qPCR and wholemount *in situ* hybridisation (WISH), such as *pomca*, *star*, *hsd11b2* and *tsc22d3*. The identification of previously characterised glucocorticoid-responsive genes as DEGs indicate reliable data analysis and accurate representation of the effects of this MR mutation in zebrafish.

In Chapter 3, I demonstrated that the stress-induced gene *pomca* exhibited an increase in WISH mRNA staining in the anterior pituitary of 4dpf larvae (Figure 3.8). This was supported by the identification of *pomca* as an upregulated DEG in 5dpf *MR⁴⁶ᴰᵉˡ* mutants. ACTH, a post-translation product of POMC and an essential component in the HPA/I axis, is known to induce *star* expression in adrenal/interrenal tissue, thus initiating the synthesis of the stress hormone, cortisol (Clark, 2016). Multiple essential genes in corticosteroid synthesis were identified as upregulated DEGs in *MR⁴⁶ᴰᵉˡ* mutants: *star*, *fdx1b, cyp11a2, hsd3b1* and *cyp21a2*. The discovery of gene encoding steroidogenic proteins important for multiple steps of corticosteroid synthesis, and the rate-limiting step performed by StAR, reinforces my previous findings by qPCR in Chapter 3 and supports my findings of elevated glucocorticoid steroid concentrations *MR⁴⁶ᴰᵉˡ* mutants. Furthermore, increased expression of glucocorticoid-responsive

genes *tsc22d3* and *hsd11b2* validate previous results (Figure 3.9) and this transcriptomic analysis. However, the highly glucocorticoid-regulated genes *fkbp5* and *pck1* were not identified as a DEG in my transcriptomic analysis. The *fkbp5* gene was detected with a base mean transcript value of 4098 reads, but no significant difference was reported. This may highlight general variation within groups, or an effect of sample collection time, as glucocorticoids are regulated by circadian rhythms. Despite the lack of fkbp5 increase, other glucocorticoid-responsive genes were upregulated.

Transcriptomic analysis of MR^{46Del} mutants revealed the systemic impact of the loss of MR's DBD and LBD. Gene ontology analysis of upregulated and downregulated DEGs identified roles for MR in regulating distinct molecular mechanisms. An overrepresentation of upregulated DEGs was associated with GO terms relating to steroid and lipid metabolic processes, whilst downregulated DEGs were primarily associated with synaptic signalling. An interesting finding was the general upregulation of genes throughout the *de novo* cholesterol biosynthesis pathway, such as initial steps performed by HMG CoA synthase (*hmgcs1*) and HMG CoA reductase (*hmgcra*) (Figure 4.10). Throughout the cholesterol biosynthesis pathway, at each major step, genes essential for conversion of precursors from mevalonate to farnesyl-PP, to squalene, to lanosterol, to lathosterol, and finally cholesterol, were upregulated in MR^{46Del} mutants. As cholesterol is the precursor to all steroid hormones, the discovery of its increased biosynthesis provides further supporting evidence that glucocorticoid synthesis is elevated in my MR mutant. Previously, it has been demonstrated that ACTH stimulates the transcription and activation of HMG CoA reductase, the rate limiting step in *de novo* cholesterol synthesis (Clark, 2016). In addition, it also promotes utilisation of other resources of cholesterol, through lipolysis and the uptake of LDL cholesterol esters (Carr and Simpson, 1981; Zhang et al., 2018). Together, this suggests that de-repression of *pomca* may lead to ACTH-induced cholesterol biosynthesis and resulting glucocorticoid synthesis in MR^{46Del} mutants.

The lipogenesis pathway from acetyl-CoA reveals a general upregulation of genes involved in fatty acid synthesis and corresponding triglyceride and triacylglycerol production (Figure 4.10). This includes *hsd17b12a*, important for the first fatty acid synthesised and palmitate; *mogat2*, when deficient in mice protect against development obesity (Nelson et al., 2011); *dgat2*, a lipogenic gene essential for mice survival due to early lipogenic defects (Smith et al., 2000; Stone et al., 2004). Genes involved in the synthesis of linoleic acid-derived polyunsaturated fatty acids were also upregulated, as were 2 downstream prostaglandin hormones. In addition, the scavenger receptor *scarb1* was significantly upregulated in MR^{46Del} mutants. This receptor mediates the transportation of cholesterol between the

cell surface and apoB-lipoproteins, increasing the cholesterol pool for steroid hormone synthesis (Shen et al., 2018).

Our results are at variance with the findings of another MRKO zebrafish line, in which MRKO larvae with and without cortisol treatment resulted in no significant differences in *hmgcs1*, *dgat2* or *elovl2* mRNA expression compared to wildtype controls, in 5dpf larvae by qPCR (Faught and Vijayan, 2019b). However, their MRKO (MR-knockout) mutants did have a significant increase in *lpl* mRNA expression, the lipoprotein lipase key in the hydrolysis of triglycerides (Faught and Vijayan, 2019b). Despite the contradictory qPCR results, Faught and Vijayan performed RNAseq on their MRKO and GRKO lines and identified that cholesterol and lipid metabolic pathways were dysregulated in both mutants. Here, they suggested a variety of genes were regulated through either MR or GR regulation. One distinct difference between the *MR^46Del* mutant described in this thesis and the MRKO mutant described by Faught and Vijayan, is that thle latter did not exhibit elevated levels of cortisol, only a de-repression of HPI axis genes such as *pomca* (Faught and Vijayan, 2018). However, transcriptomic comparison of wildtype larvae and their MRKO+cortisol treatment condition, which more closely mirrors my mutant phenotype, displayed a clear upregulation of cholesterol synthesis, lipogenesis and lipid transport and lipolysis associated genes. Many of which were also identified in my dataset, including *dgat2*, *apoea*, *apoeb*, *elovl2*, *msmo1*, *hmgcs1*, *hmgcra* and finally *sc5d* (Faught and Vijayan, 2019b).

Earlier research in the 1970s and 80s discovered that ACTH treatment in rats increased free fatty acids and glycerol in plasma, suggesting a regulatory role of ACTH on lipolysis (Blanchette-Mackie and Scow, 1985; Fan and Ho, 1981; Franz et al., 1983; Spirovski et al., 1975). There are also many similarities between central obesity and hypercortisolaemic patients diagnosed with Cushing's syndrome (Feelders et al., 2012; Ferraù and Korbonits, 2015). However, the effects of glucocorticoids and ACTH in vivo are complex, with many experimental studies administering higher than pathophysiological levels of glucocorticoids, without understanding the tissue-specific and temporal-specific impacts of such high concentrations of glucocorticoids on metabolism. Many studies involve treatment with high concentrations of dexamethasone and betamethasone, both of which are GR-specific agonists; which cannot therefore advance understanding of MR's role in lipid metabolism. However, whilst it is widely accepted that glucocorticoids are lipolytic, these hormones also simultaneously increase expression of genes in pathways of triglyceride synthesis, hydrolysis and lipolysis (Lee et al., 2014). Our experimental approach has enabled us to obtain a systems-level overview of the dysregulated biological processes that result from the *MR^46Del* loss-of-function mutation in 5dpf zebrafish larvae. It was beyond the scope of this study to measure triglycerides, free fatty acids and cholesterol

concentrations. As such, it is not known if this comprehensive upregulation of gene expression associated with lipid metabolism is translated to changes in concentrations of these lipids .

The top 2 characterised DEGs were *socs1a* and *socs3a* (Table 4.2). Suppressors of cytokine signalling (Socs) are negative regulators of the JAK signal inducer/STAT transcription activator pathway (Alexander, 2002). Previously, it has been demonstrated in teleosts that cortisol treatment stimulates: upregulation of *socs1* and *socs2* expression in hepatocytes, accompanied by a reduction in growth hormone signaling and suppression of cytokine immune system signaling through JAK/STAT signaling (Philip and Vijayan, 2015). Accordingly, it was proposed that Socs proteins may regulate a shift between energy-utilising growth and immune processes, to energy-producing metabolic pathways in order to meet increased energy demands resulting from exposure to stress (Faught and Vijayan, 2016). Together, the majority of the top DEGs were associated with steroid and lipid metabolism and indicate an increase in expression of components of metabolic energy producing pathways. Previously, it has been shown that many of these pathways are regulated by the GR in teleosts (Faught and Vijayan, 2016). However, in this thesis I have demonstrated that these processes are upregulated in zebrafish larvae lacking MR function. It will now be of interest to determine whether these phenotypes are directly linked to the transcriptional regulatory function of MR, or if they are indirectly linked by the elevated levels of cortisol I have demonstrated in MR mutant larvae.

Interestingly, the primary Biological Process downregulated in the MR^{46Del} mutant 5dpf larval transcriptome was synaptic signaling. This included synaptic components characteristic of glutamatergic and/or GABAergic neurons, as well as pre- and post-synaptic components and neuromuscular junctions. The majority of genes are associated with cell surface ionotropic receptors important for both exocytosis and endocytosis, and action potential generation. However, structural components maintaining synapse stability were also downregulated in MR^{46Del} mutants.

Many of the downregulated DEGs have human homologues that are linked to psychiatric disorders, depression and epilepsy, via dysregulation of synaptic signalling processes. Changes in the expression levels of *MR* has been documented in various psychiatric disorders: i) post-mortem examination of the brain of patients with Major Depressive Disorder revealed a reduction in *MR* expression in the hippocampus (Klok et al., 2011; Medina et al., 2013), ii) a decrease in *MR* expression in the prefrontal cortex was found in patients with schizophrenia and bipolar disorder (Xing et al., 2004), and iii) duration of psychotic illness was negatively correlated with *MR* expression (Xing et al., 2004). In addition, MR has also been observed at presynaptic terminals, dendritic spines and dendrites in

humans (Prager et al., 2010). Prager et al (2010) suggested that MR may be positioned to regulate both glutamate neurotransmission, and post-synaptic responses. As the MR is commonly associated with learning and memory (McCann et al., 2021); MR regulation of synapse signalling may be a potential mechanism in which the adrenal steroid hormones influence behaviour during stress.

In summary, this Chapter documents the use of RNA sequencing technologies to characterise the phenotypic consequences of a loss of function mutation in the *MR* gene in 5dpf zebrafish larvae. The results of the preceding chapter demonstrated that MR mutants exhibit a de-repressed HPI axis, resulting in upregulated larval *star* expression, increased glucocorticoid concentrations, and upregulation of glucocorticoid-responsive gene expression. In this chapter, I have described a general upregulation of genes essential for corticosteroid precursor pathways, such as *de novo* cholesterol synthesis, lipolysis to increase the free-cholesterol pool, and fatty acid synthesis, through RNAseq. In addition, the expression of components of glutamatergic and GABAergic synapses are upregulated. Taken together, these results implicate the MR in regulation of not only the HPI axis, but lipid metabolism and synaptic signaling in the brain. However, the role of the GR is intricately intertwined with the MR in the regulation of the HPI/A axis, lipid metabolism and neuronal functions. As such, it is of interest to assess the phenotypic consequences of a loss of GR function on the larval zebrafish transcriptome.

Chapter 5. Defining the implications of glucocorticoid-resistance on 5dpf larval transcriptomes in gr^{s357} mutant zebrafish.

5.1 Introduction

Glucocorticoids, such as cortisol, are steroid hormones that play an important role in many biological processes, including development, carbohydrate metabolism (Kadmiel and Cidlowski, 2013), glucose homeostasis, inflammatory responses and behaviour. A crucial function of GCs in these processes is to mediate biological responses to biological stressors (Chatzopoulou et al., 2016; Kadmiel and Cidlowski, 2013; Schaaf et al., 2009b).

Cortisol is the main endogenous GC in humans and zebrafish, whereas in rodents, the predominant GC is corticosterone. These steroid hormones are secreted by the adrenal cortex in mammals, and in teleosts the functional homologue is the interrenal gland, located in the fish head kidney. In teleosts, GC production is regulated by the Hypothalamic-Pituitary-Interrenal (HPI) axis, which is the equivalent to the Hypothalamic-Pituitary-Adrenal (HPA) axis in mammals, the main neuroendocrine pathway through which the stress response is activated and regulated (Pikulkaew et al., 2010; Wendelaar Bonga, 1997).

Perception, anticipation and reaction to stress-inducing stimuli occur within the central nervous system, where adaptive physiological responses such as energy store mobilisation, heightened cognition and locomotor behaviours, are initiated by interactions between the limbic system and HPA axis (McEwen, 2012; McEwen and Wingfield, 2010). In mammals, these adaptive responses are triggered through the activation of the HPA axis, resulting in the secretion of glucocorticoids from the adrenal gland. Glucocorticoid action is mediated by two corticosteroid receptors: its canonical receptor, the glucocorticoid receptor (GR), and the closely related mineralocorticoid receptor (MR). These GC-receptors are expressed in target tissues and cells, when ligand-bound, are activated DNA-binding transcription factors that regulate target gene expression (Kadmiel and Cidlowski, 2013).

In previous chapters 3 and 4, through the generation of an MR mutation carrying a 46bp deletion with a 2bp substitution (MR^{46Del}), I have discovered a multitude of biological functions that are dysregulated in 5dpf larvae, including a de-repression of the HPI axis, increased expression of steroidogenic genes, corresponding increased glucocorticoid concentrations and consequential upregulation of glucocorticoid-responsive genes. In addition, RNAseq analysis of 5dpf larvae

revealed an important role for the MR in steroid and lipid metabolism, synaptic signalling in glutamatergic and GABAergic neurons, and in neuromuscular junctions. However, many of these functions have also been shown to be at least partially regulated by the GR. As such, the question remains to be answered: Are there biological processes regulated by only MR, only GR, and regulated by both MR and GR?

In zebrafish, cortisol has been shown to signal via activation of the GR at very early stages of development, with maternal cortisol deposition in oocytes and presence of GR (*nr3c1*) mRNA detected (Pikulkaew et al., 2010, 2011; Wilson et al., 2013). Activation of the HPI axis through acute and GR-mediated chronic stress methods in zebrafish larvae illustrate the homology between mammalian and teleost models (Pavlidis et al., 2015). Previously, a loss-of-function GR mutation (*gr^s357^*) was discovered to disrupt the DNA-binding domain and prevent transcriptional activity (Ziv et al., 2013). This s357 allele is a single nucleotide substitution at position 443 that results in an amino acid substitution from a highly conserved arginine residue to cysteine in the second zinc-finger motif of the GR protein (Ziv et al., 2013). This s357 mutant was discovered through its impaired visual background adaptation (VBA) phenotype (Muto et al., 2005). VBA is a GR-dependent neuroendocrine response that causes the pigment cells of the skin to contract (reduce in size) in light conditions, whilst they are larger in the dark (Kramer et al., 2001). Homozygous *gr^s357^* mutant larvae are darker than *gr^wt^* siblings in the VBA assay, indicating a loss of GR function (Muto et al., 2005). In chapter 3, I determined that MR mutants resembled wildtype larvae after the VBA assay, confirming that this neuroendocrine response is GR and not MR-dependent.

Zebrafish carrying the *gr^s357^* mutation also exhibited a loss of GR-mediated negative feedback on the HPI axis, resulting in chronically activated HPI axis as seen by the increased expression of stress-induced responsive genes, such as *pomca* (pro-opiomelanocortin), and elevated concentrations of the stress hormone cortisol (Griffiths et al., 2012). A similar phenotype was exhibited by the *MR^-/-^* mutant I generated (chapter 3&4). This previous larval research led to the following questions: what other biological processes are affected by the loss of direct GR-DNA binding and what is the role of the GR during zebrafish development?

To understand the systemic effects of a dysfunctional GR on the developing zebrafish, RNA sequencing of whole *gr^s357^* and *gr^wt^* larvae at age 5dpf was performed. This was to identify biological pathways affected by loss of GR function at early stages of zebrafish development.

5.2. Results

Gr^s357 mutant zebrafish have a chronically activated HPI axis due to a loss of glucocorticoid-mediated negative feedback, resulting in elevated stress hormone (cortisol) production, and have been shown to have stress-related changes in their behaviour (Griffiths et al., 2012; Ziv et al., 2013). Several putative GR-downstream target genes, including *fkbp5*, *pomca* and *crh*, have been shown to be upregulated in *gr^s357* mutants. As cortisol and the HPI axis influence many physiological systems, I have performed RNA sequencing of 5dpf larvae to further understand the systemic impact of the *gr^s357* mutation and gain further insight into the molecular mechanisms regulated by the GR during development. Previously reported *gr^s357* mutant results were confirmed through the VBA assay (mutants were darker than controls), and qPCR, which showed that *fkbp5* mRNA expression was near ablated in 5dpf *gr^s357* mutant (Figure A18).

5.2.1 Quality control and STAR alignment of *gr^s357* mutant and *gr^wt* 5dpf larval RNAseq samples

As before, it is necessary to identify error-types and evaluate the quality of sequence reads to reduce the impact that sequencing technical limitations have on interpretation of downstream analysis. FastQC software was used before and after each sequence read manipulation (Andrews, 2010). Subsequent to rRNA removal and adaptor/quality trimming, FastQC revealed excellent sequence quality for *gr^wt* (WTTL) 1-4 and *gr^s357* mutant samples (GR) 1-4 (Figure 5.1), with the exception of a mildly high GC% in WTTL 2. All samples failed the per base sequence content that assesses "the proportion of each base position for which each of the four normal DNA bases has been called", as all samples showed biases base composition for the first 12bp of each read (Figure A19). There are multiple explanations for this: i) hexamer primers during reverse transcription leads to positional bias, ii) polymerase sequence specificity, iii) artefacts of end-repair; iv) a combination of these factors. However, this is expected for RNAseq libraries and is thought to not affect downstream analysis.

Samples were sequenced at a high depth 27-34 million reads for exploratory transcriptomic analysis (Table A4). Post-sequencing quality control processing resulted in a higher percentage reduction in total reads in GR 1-3, with WTTL1-4 and GR 4 resulting in similar reduction in reads. Post-quality processing provided adequate read depth (23-32 million reads) for downstream transcriptomic analysis. Read alignment to the zebrafish reference genome (GRCz11) was performed by STAR and alignment details are documented and show a mapped alignment of between 15-25 million reads to annotated genes (Table A5).

5.2.2 mRNA sequencing quality control reveals an outlier gr^{s357} mutant sample with a gr^{wt} transcriptomic profile

Experimental quality control is an important initial assessment performed during early transcriptomic downstream analysis. Principal component analysis (PCA) revealed a general segregation of samples by genotype by the first principal component, however there were two overlapping samples: WTTL 4 and GR 4 (Figure 5.2A). The GR 4 sample was located within the WTTL genotype cluster and distanced from the other GR samples, which were tightly grouped together (Figure 5.2A). The hierarchical clustering heatmap of normalised count data (Figure 5.2B) supports the PCA plot, which indicates that GR4 sample displays a transcriptomic profile similar to the other four WTTL samples and is clustered next to sample WTTL 4. Dendrogram clustering analysis demonstrated clustering by genotype for GR 1-3 and WTTL1-4, however also provided further insight into the close relationship between WTTL 4 and GR 4 (Figure 5.2C). Variation between WTTL samples is seen as WTTL 2 visually exhibits the least similarity with other sample patterns. Sample WTTL 2 has the highest sequence depth and slightly skewed GC content which may contribute to this variation (Figure 5.1A&B).

Raw data read depth, post-processing read depth and mapped STAR alignment read numbers of GR4 are very similar to that of WTTL4 and other WTTL samples in comparison to the other GR samples. Through read depth, STAR alignment counts, PCA, heatmap and a dendrogram, I have determined that sample GR 4 is most likely the same sample as WTTL 4. It is likely that WTTL 4 was aliquoted twice and labelled incorrectly as GR 4 and sent for mRNA sequencing. Consequently, GR 4 was removed from further downstream analysis.
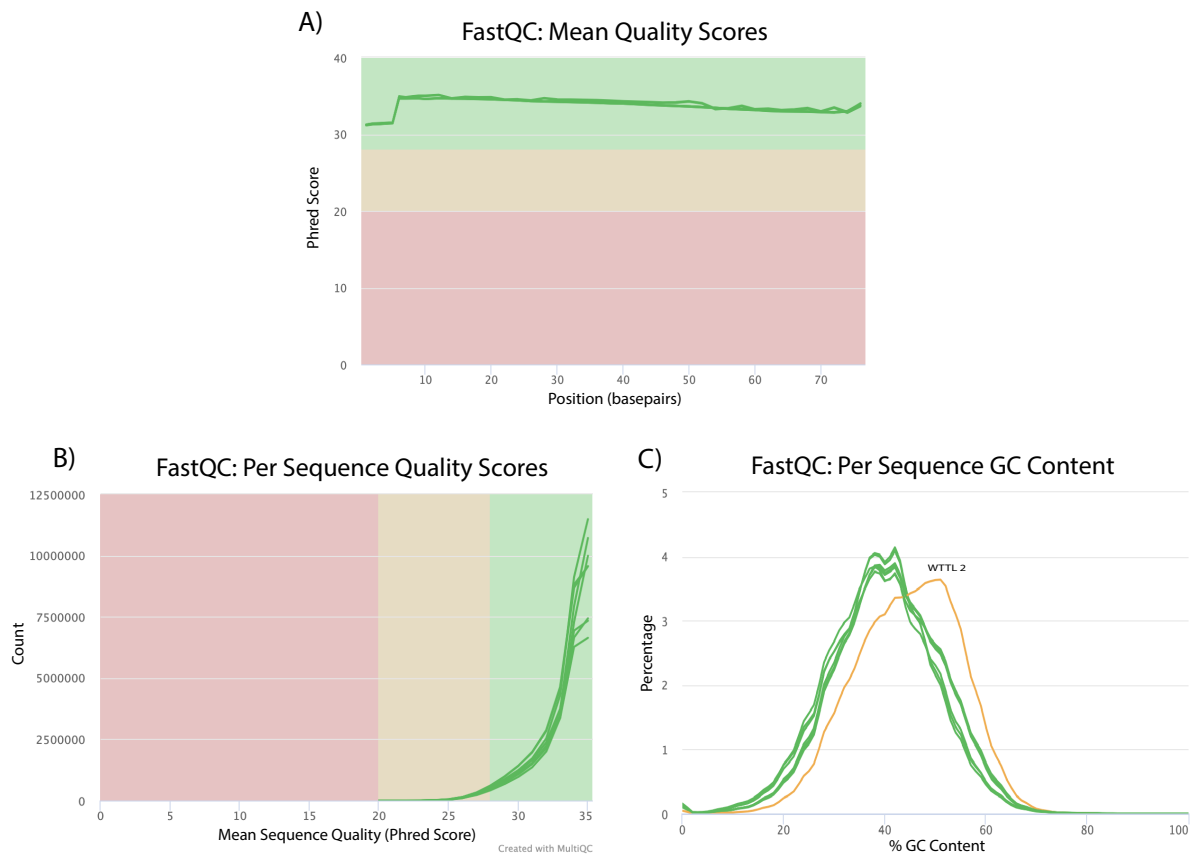
Figure 5.1. Quality control of RNA sequencing reads for GR (gr^{s357}) and WTTL (gr^{wt}) larvae samples after preliminary processing. Sample quality control was performed using FastQC and visualised using MultiQC after initial processing using Trimmomatic software to trim adaptors and poor-quality reads, and SortmeRNA software to remove rRNA reads that may be present. A&B) Quality scores indicate very high sequence quality with Phred scores above 30. C) Per sequence GC content indicates that all samples, except WTTL 2, are high quality. WTTL 2 displays a slight right skew but is within acceptable range.
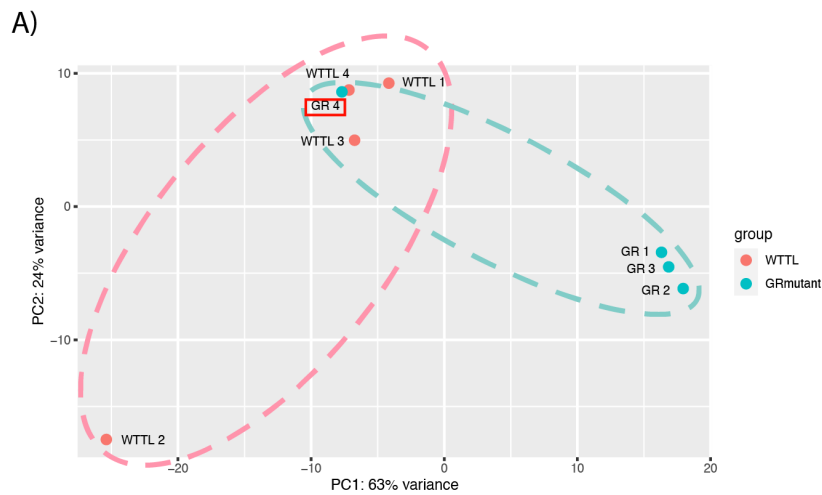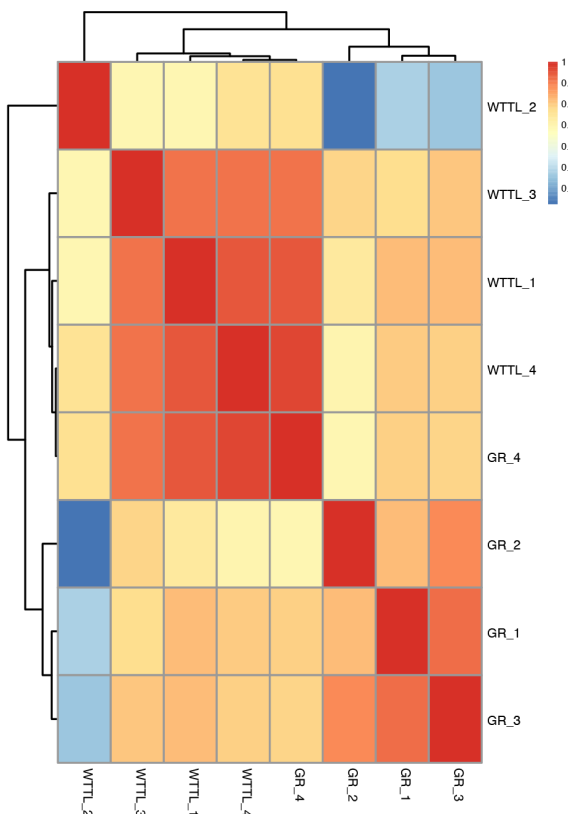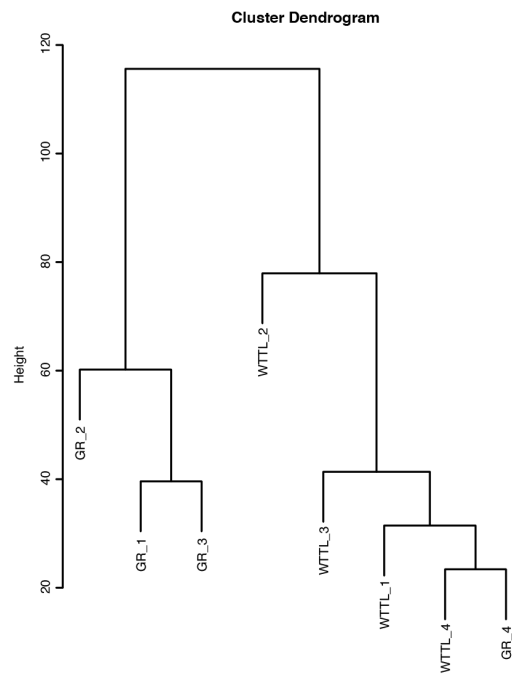
Figure 5.2. Principal component analysis, heatmap and dendrogram clustering of GR (*gr^s357*) and WTTL (*gr^wt*) 5dpf larval samples reveals outlier sample GR4. A) PCA (ntop=500): Overlap of GR and WTTL genotype clustering due to sample GR 4 overlapping the WTTL 4 sample. B) Clustering heatmap generated from the same data shows similar variation profiles of GR 4 to WTTL 4. C) Dendrogram demonstrates clustering by genotype, except for GR4 that is most related to WTTL4 GR4's variation profile aligns with the generalised WTTL genotype pattern rather than with the GR pattern.
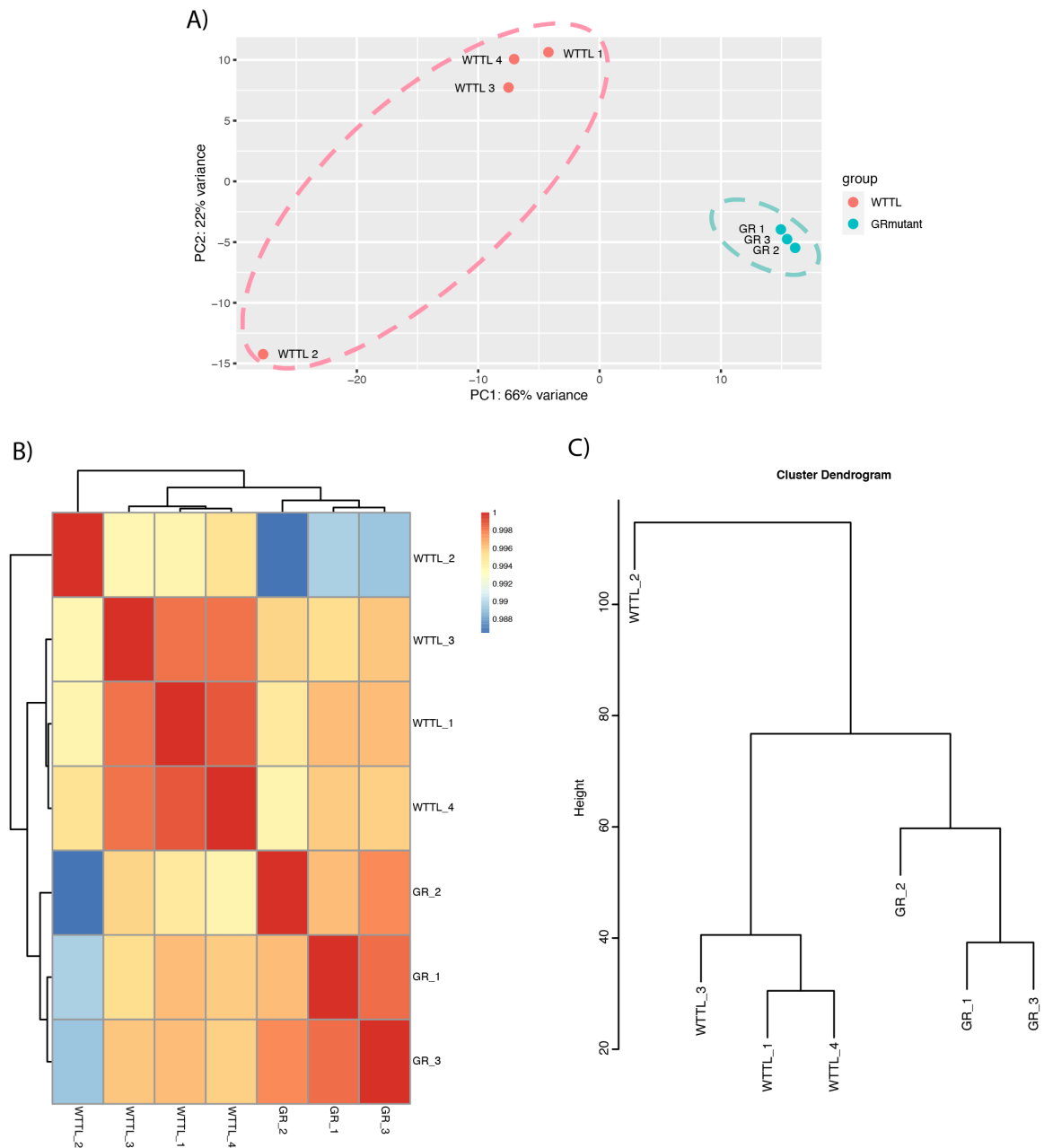
Figure 5.3. Principal component analysis, heatmap and dendrogram clustering reveals variation between GR (gr^{s357}) mutant and WTTL (gr^{wt}) 5dpf larval transcriptomes after removal of GR 4 outlier. A) PCA (ntop=500): despite gr^{wt} samples not being highly clustered, gr^{s357} mutants were. Genotypes were segregated by the first principal component accounting for 66% of total variation. B) Clustering heatmap generated from the same data. C) Dendrogram demonstrates clustering by genotype.
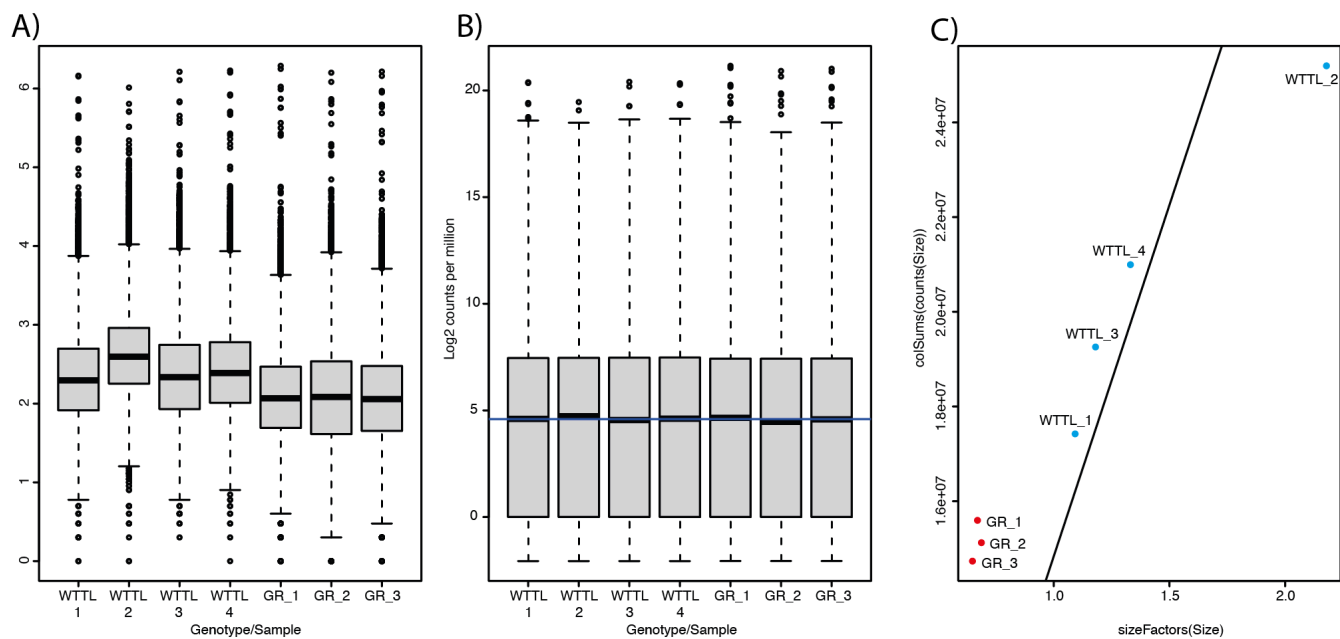
Figure 5.4. RNA sequencing depth reveals higher sequencing depth of WTTL samples. A) Boxplot showing median raw counts for each sample. WTTL samples display higher STAR alignment and intragroup variability than GR samples, of note, sample WTTL_2. B) Boxplot showing DESeq2 normalised median library size, all samples including WTTL_2 is normalised appropriately. C) DESeq2 estimate size factor function presents high variability within WTTL samples.

Table 5.1. Number of GR larvae DESeq2 differentially expressed genes filtered with false discovery rate, adjusted p-value (padj) and fold change threshold filters.

DESeq2 FDR Cutoff	padj cutoff	No. of Total DEGs	No. of DEGs with fold change > 1.5x	No. of DEGs with fold change > 2x
FDR alpha = 0.1 (default)	padj < 0.1	5515	5138	3469
FDR alpha = 0.05	padj < 0.05	3958	3848	2797
Independent Filtering	padj < 0.05	2836	1271↑ + 1565↓	N/A

5.2.3 Initial analysis of the differential transcriptomic profile resulting from the gr^{s357} mutation in 5dpf whole larvae.

PCA analysis (Figure 5.3A) revealed variation between the transcriptomic profiles of gr^{s357} mutants (GR) and gr^{wt} controls (WTTL), with considerable variation observed within the WTTL group. However, a clear segregation by genotype was revealed in the first principal component that accounts for 66% of the total variation. The intra-group variation within the WTTL genotype samples resulted in samples WTTL 1, 3 and 4 being clustered together, with the WTTL 2 sample distanced along the second principal component that accounts for 22% of total variation. This represents the biological intra-group variation between samples and is more likely to provide more robust biologically relevant transcriptomic differences between genotypes. This is further supported by the hierarchical clustering heatmap of normalised counts and dendrogram clustering (Figure 5.3B&C), where sample WTTL 2 visually exhibits the least similarity with other sample patterns. Sample WTTL 2 has the highest sequence depth and slightly skewed GC content which may contribute to this variation.

Differential expression analysis was performed using the DESeq2 package (Love et al., 2014b). As before, a more stringent FDR value of 0.05 was used rather than DESeq2's default exploratory 0.1 FDR value; analysis of DEG counts for both thresholds demonstrate the value of a more stringent acceptance threshold (Table 5.1). Initial DESeq2 analysis and an overview of the data can be visualised using an MA plot with dispersion (within-group variability). As before, the MA plot displayed an approximate equal distribution between total upregulated and downregulated genes (Figure A21). Dispersion estimates demonstrated that as normalised count increases, intra-group variability was reduced and resembles the typical dispersion pattern required for the use of the DESeq2 package (Figure A21) (Love et al., 2014). To visualise RNAseq data, distribution and boxplots of the median log gene counts for each sample were plotted. WTTL samples display a more variable and higher median count than GR samples (Figure 5.4A). However, after normalisation with DESeq2's rlog function, gene counts are correctly normalised for all samples (Figure 5.4B). Size factor against total gene count for each sample was plotted (Figure 5.4C). GR samples cluster together indicating low variability, whereas WTTL samples are spread along the regression line. WTTL 2 exhibited a large size factor, however due to the correct clustering by genotype on heatmaps and the dendrogram, and segregation by genotype in the first principal component by PCA, this sample was included for further downstream analysis.

To define statistically significant differentially expressed genes (DEGs), an adjusted p-value <0.05 was used as a threshold. This revealed a total of 3958 DEGs between gr^{s357} mutants and gr^{wt} 5dpf

larvae. To provide a more robust list of DEGs, independent filtering was performed: a base mean of <40 reads and 0.58<Log2FoldChange<-0.58 (equivalent to ~1.5-fold change) were filtered out, resulting in 2836 DEGs (Table 5.1). Of these filtered DEGs, 1271 DEGs were upregulated and 1565 DEGs were downregulated, displaying a near-symmetrical distribution of DEGs.

To explore the distribution of differentially expressed genes between the gr^{s357} mutants and gr^{wt} 5dpf larvae, visual tools such as a volcano plot and heatmaps were utilised. The volcano plot visually exhibits a near-symmetrical distribution of differentially expressed genes, with similar levels of significance and log2fold change (Figure 5.5). In the volcano plot: 2836 genes are highlighted as red dots (0.58<Log2FoldChange<-0.58; padj<0.05), 110 genes are blue dots (-0.58<Log2Foldchange<0.58; padj<0.05), 2309 genes are green dots (0.58<Log2Foldchange<-0.58 padj>0.05), and finally, 9439 genes are plotted as grey dots (-0.58<Log2Foldchange<0.58; padj>0.05). The top significant DEGs are labelled, including the most significant DEG *fkbp5* (fold change=0.0066, padj=1.76E-115), *kcnk5a* (fold change=42.7967, padj=2.46E-58) and *tsc22d3* (fold change=0.0822, padj=5.46E-47) (Figure 5.5). This illustrates the profound differential gene expression identified in gr^{s357} mutant 5dpf larvae.

Heatmaps display the top 30 most significant DEGs (Figure 5.6). Hierarchical clustering of samples confirmed genotype segregation. Gene hierarchical clustering was not performed to illustrate that neither upregulated nor downregulated genes are predominant in the top 30 ordered DEG list (Figure 5.6A). The second heatmap (Figure 5.6B) incorporates gene hierarchical clustering and demonstrates a near symmetrical distribution of both up- and down-regulated genes in the top 30 most significant DEGs. Both heatmaps plot each sample's gene normalised counts, providing a visual of intra- and inter-group variation. Plots of normalised gene counts for the top 5 significant DEGs (*fkbp5*, *kcnk5a*, *tsc22d3*, *ucp2* and *cyp2p9*) and gene of interest *klf9*, recently shown to be a key GR signalling regulator in zebrafish (Gans et al., 2020), demonstrate the significance of differential expression seen in the GR (gr^{s357}) mutants in comparison to WTTL (gr^{wt}) controls in 5dpf larvae (Figure 5.7). Tables 5.2 and 5.3 present the top 20 DEGs by p-adjusted statistical significance and by fold change, illustrating a near-symmetrical differential expression of up- and downregulated genes.

Initial analysis of the differential transcriptomic profile resulting from the gr^{s357} mutation has revealed the role of the glucocorticoid receptor as both a transcriptional activator and repressor in 5dpf larvae, indicated by a near symmetrical distribution of DEGs. As the 5dpf larva is a complex multi-organ biological system, understanding which biological networks and molecular

pathways are involved in the *gr^{s357}* mutant's differential transcriptomic profile will help reveal what roles the glucocorticoid receptor has in the development of zebrafish.

Figure 5.5. Volcano plot displaying predominantly symmetrical distribution of differentially expressed genes affected by the *gr^{s357}* mutation in 5dpf zebrafish larvae. The statistical significance – padj values are plotted on the y axis against magnitude of differential expression – log2fold change. Dashed lines represent cutoff: log2fold change >0.58 | <-0.58 (fold change of 1.5), and padj value < 0.05. Total of 32520 genes are plotted. Grey dots signify non-significant genes below Log2FoldChange threshold, green dots signify non-significant genes above Log2FoldChange threshold, blue dots signify significant genes with below Log2FoldChange threshold, and red dots signify significant genes above Log2FoldChange threshold.

Figure 5.6. Top 30 most significant differentially expressed genes in 5dpf larvae between GR (*gr^s357^*) mutants compared to WTTL (*gr^wt^*) controls. A) Heatmap with hierarchical clustering of samples only. B) Heatmap of hierarchical clustering of samples and genes.
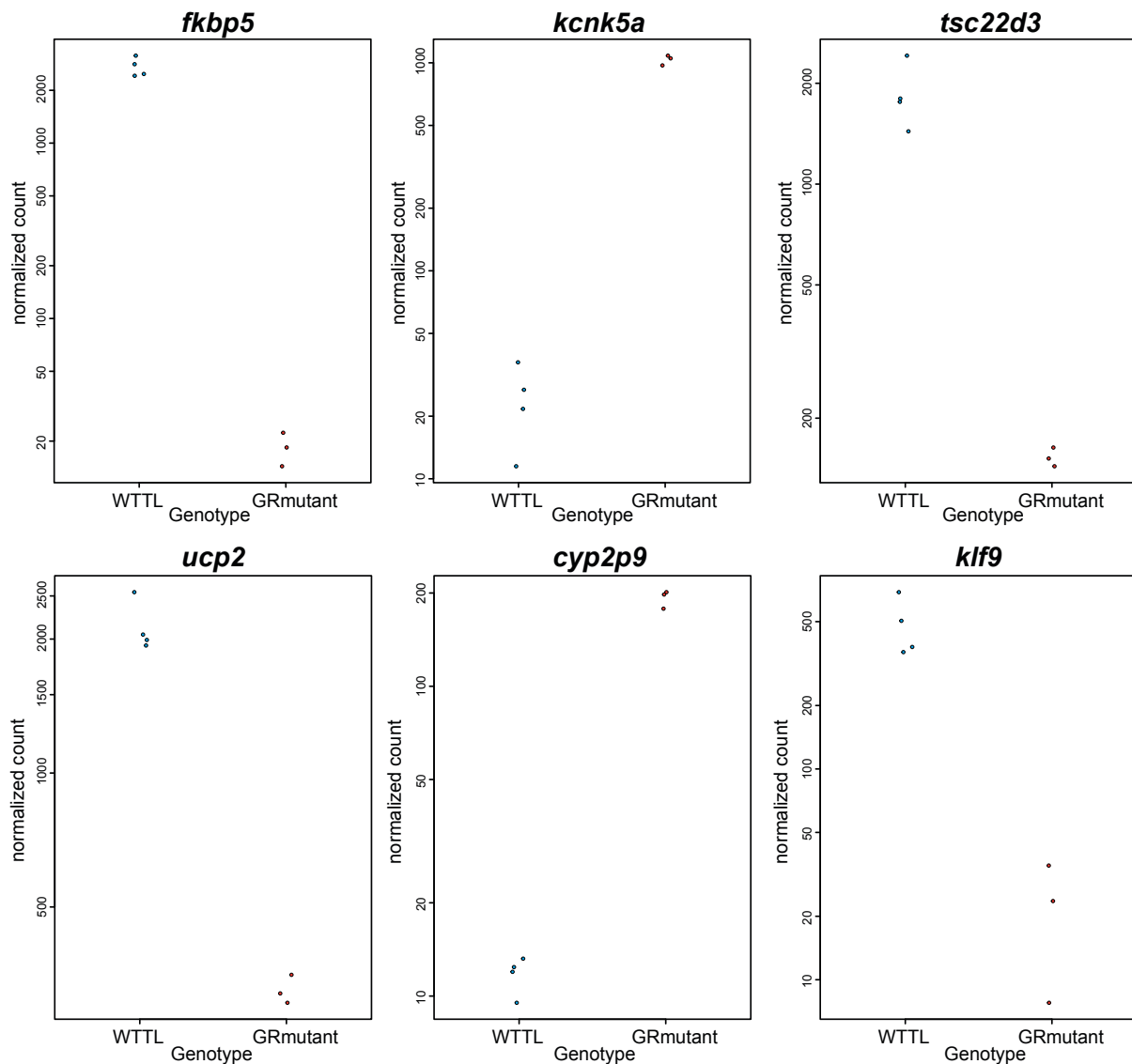
Figure 5.7. Normalised gene expression plots for each sample of WTTL (*gr^wt^*) and GRmutant (*gr^s357^*) 5dpf larvae for the top 5 most statistically significant characterised genes, and gene of interest *klf9*. Normalised DESeq2 gene counts are plotted using plotCounts function for genes *fkbp5, kcnk5a, tsc22d3, ucp2, cyp2p9* and *klf9*. See Table 4 for statistics.

Table 5.2. Top 20 most significant differentially expressed genes (padj<0.05) in *gr^s357* vs *gr^wt* 5dpf larvae. Colour indicates up-regulated (green) or down-regulated (red) gene expression direction.

Gene name	Fold change	p value	padj value	Ensembl gene ID
fkbp5	0.006598	7.61E-120	1.76E-115	ENSDARG00000028396
kcnk5a	42.7966674	2.12E-62	2.46E-58	ENSDARG00000023587
tsc22d3	0.08223874	7.07E-51	5.46E-47	ENSDARG00000075666
ucp2	0.15244644	6.87E-48	3.98E-44	ENSDARG00000043154
si:ch211-121a2.2	110.538936	2.02E-45	9.37E-42	ENSDARG00000039682
cyp2p9	17.0616408	9.36E-44	3.62E-40	ENSDARG00000022631
BX469930.1	0.00921278	1.24E-42	4.11E-39	ENSDARG00000092358
si:dkey-159f12.2	0.0620115	1.19E-41	3.44E-38	ENSDARG00000093606
CCDC134	12.2455314	9.90E-40	2.55E-36	ENSDARG00000103285
asic1c	27.6837554	6.67E-37	1.55E-33	ENSDARG00000098428
si:dkey-88j15.3	57.6768095	2.97E-35	6.25E-32	ENSDARG00000076573
bnip4	0.03910396	7.24E-32	1.40E-28	ENSDARG00000022832
impg1a	5.42368016	1.04E-31	1.86E-28	ENSDARG00000077187
si:ch1073-429i10.1	14.3321284	6.14E-30	1.02E-26	ENSDARG00000075664
smpd5	5.68358789	7.06E-30	1.09E-26	ENSDARG00000059811
AL928650.3	19.6877774	1.28E-26	1.85E-23	ENSDARG00000096599
rrm2	6.55418604	2.31E-25	3.15E-22	ENSDARG00000020711
CABZ01084081.1	69.3083424	4.70E-25	6.05E-22	ENSDARG00000111522
klf9	0.0445582	5.03E-25	6.14E-22	ENSDARG00000068194
zgc:195170	23.0958451	1.01E-24	1.17E-21	ENSDARG00000076264

Table 5.3. 20 significant differentially expressed genes ordered by magnitude of fold change caused by the *gr^s357* mutation in 5dpf zebrafish larvae. Top 10 upregulated genes by magnitude (green) and subsequently, top 10 downregulated genes by magnitude (red).

Gene name	Fold change	p value	padj value	Ensembl gene ID
si:ch211-121a2.2	110.538936	2.02E-45	9.37E-42	ENSDARG00000039682
CABZ01084081.1	69.3083424	4.70E-25	6.05E-22	ENSDARG00000111522
si:dkey-88j15.3	57.6768095	2.97E-35	6.25E-32	ENSDARG00000076573
kcnk5a	42.7966674	2.12E-62	2.46E-58	ENSDARG00000023587
asic1c	27.6837554	6.67E-37	1.55E-33	ENSDARG00000098428
AL928650.2	23.9205445	1.99E-19	1.44E-16	ENSDARG00000096526
zgc:195170	23.0958451	1.01E-24	1.17E-21	ENSDARG00000076264
pla2g3	19.9411612	9.59E-18	4.94E-15	ENSDARG00000008948
AL928650.3	19.6877774	1.28E-26	1.85E-23	ENSDARG00000096599
cyp2p9	17.0616408	9.36E-44	3.62E-40	ENSDARG00000022631
si:ch211-209l18.4	0.00097569	6.90E-17	3.33E-14	ENSDARG00000090847
zgc:194659	0.00175827	2.53E-14	8.77E-12	ENSDARG00000079347
CABZ01088274.1	0.00188953	1.09E-13	3.52E-11	ENSDARG00000098174
CABZ01065076.1	0.00230968	1.98E-12	4.63E-10	ENSDARG00000099056
CR855277.2	0.00236937	1.37E-11	2.79E-09	ENSDARG00000092801
znf1156	0.00309318	5.54E-12	1.18E-09	ENSDARG00000098800
CABZ01069162.1	0.00344353	2.08E-11	4.16E-09	ENSDARG00000115161
si:ch211-212k18.15	0.00447668	1.56E-10	2.51E-08	ENSDARG00000089432
fkbp5	0.006598	7.61E-120	1.76E-115	ENSDARG00000028396
BX469930.1	0.00921278	1.24E-42	4.11E-39	ENSDARG00000092358

5.2.4 Gene Ontology analysis of differentially expressed genes in 5dpf zebrafish larvae carrying the *gr^s357* mutation.

Statistical overrepresentation analysis of differentially expressed genes (0.58<Log2FoldChange<-0.58) revealed 25 gene ontology (GO) terms related to biological processes that were below the adjusted p<0.05 threshold. However, only 7 of these GO terms was also below the FDR<0.05 threshold (Table 5.4). Of these, an overrepresentation of genes was recognised to be involved in extracellular matrix structure and organisation, biological and cell adhesion, and cell surface receptor signalling. 7 GO terms related to molecular function contained overrepresented genes, including: extracellular matrix structure, transmembrane signalling receptor activity and cytokine activity (Table 5.6). Finally, 21 cellular components GO terms were related to the extracellular matrix region and space, and integral and intrinsic components of the plasma membrane (Table 5.7). The biological, molecular and cellular component GO pathways of enriched DEGS are visually displayed in Figures 5.8, 5.9, 5.10 and 5.11. Similarly, KEGG and Reactome pathway analysis revealed an enrichment of genes associated with ECM-receptor interaction and focal adhesions, and three Reactome pathways: ECM degradation and associated laminin interactions, and PDGF signalling (Table 5.7). To understand in higher resolution what is transcriptionally activated or repressed by the GR in 5dpf zebrafish larvae, I separated the DEG list into two populations: upregulated and downregulated DEGs.

Table 5.4. Significant Biological Process Gene Ontology terms overrepresented in all genes differentially expressed in *gr^s357* mutant zebrafish larvae. Red line indicates FDR<0.05 cut off.

GO Term	Description	P-value	FDR q-value	Enrichment (N, B, n, b)
GO:0030198	extracellular matrix organization	1.05E-11	8.22E-08	2.57 (10396,107,1892,50)
GO:0043062	extracellular structure organization	3.28E-11	1.29E-07	2.48 (10396,113,1892,51)
GO:0007166	cell surface receptor signaling pathway	1.02E-09	2.68E-06	1.57 (10396,531,1892,152)
GO:0022610	biological adhesion	2.66E-08	5.22E-05	1.72 (10396,290,1892,91)
GO:0007155	cell adhesion	2.66E-08	4.18E-05	1.72 (10396,290,1892,91)
GO:0009653	anatomical structure morphogenesis	1.39E-06	1.83E-03	1.33 (10396,896,1892,217)
GO:0035567	non-canonical Wnt signaling pathway	4.47E-05	5.01E-02	2.96 (10396,26,1892,14)
GO:0048562	embryonic organ morphogenesis	8.37E-05	8.22E-02	1.93 (10396,91,1892,32)

N, number genes in background list; B, genes un background annotated with GO term; n, genes in target list; b, genes in target list annotated with GO term. Enrichment = (b/n)/(B/N).

Table 5.5. Significant Molecular Function Gene Ontology terms overrepresented in all genes differentially expressed in *gr^s357* mutant zebrafish larvae. Red line indicates FDR<0.05 cut off.

GO Term	Description	P-value	FDR q-value	Enrichment (N, B, n, b)
GO:0005201	extracellular matrix structural constituent	5.02E-07	1.46E-03	2.69 (10396,51,1892,25)
GO:0004888	transmembrane signaling receptor activity	6.40E-07	9.30E-04	1.71 (10396,241,1892,75)
GO:0038023	signaling receptor activity	8.98E-07	8.70E-04	1.62 (10396,298,1892,88)
GO:0060089	molecular transducer activity	1.93E-06	1.40E-03	1.58 (10396,316,1892,91)
GO:0005102	signaling receptor binding	1.97E-06	1.15E-03	1.56 (10396,338,1892,96)
GO:0005125	cytokine activity	8.52E-06	4.12E-03	2.83 (10396,35,1892,18)
GO:0004896	cytokine receptor activity	3.77E-05	1.56E-02	3.30 (10396,20,1892,12)
GO:0048018	receptor ligand activity	7.18E-05	2.61E-02	1.80 (10396,122,1892,40)
GO:0019955	cytokine binding	7.75E-05	2.50E-02	2.98 (10396,24,1892,13)
GO:0005178	integrin binding	1.35E-04	3.91E-02	2.86 (10396,25,1892,13)
GO:0030545	receptor regulator activity	1.91E-04	5.06E-02	1.73 (10396,127,1892,40)
GO:0008395	steroid hydroxylase activity	2.25E-04	5.44E-02	2.75 (10396,26,1892,13)
GO:0022857	transmembrane transporter activity	5.47E-04	1.22E-01	1.30 (10396,549,1892,130)
GO:0015291	secondary active transmembrane transporter activity	6.62E-04	1.37E-01	1.70 (10396,113,1892,35)
GO:0017147	Wnt-protein binding	6.89E-04	1.33E-01	2.75 (10396,22,1892,11)
GO:0005215	transporter activity	9.11E-04	1.65E-01	1.28 (10396,585,1892,136)

N, number genes in background list; B, genes un background annotated with GO term; n, genes in target list; b, gene sin target list annotated with GO term. Enrichment = (b/n)/(B/N).

Table 5.6. Significant Cellular Component Gene Ontology terms overrepresented in all genes differentially expressed in *gr^s357* mutant zebrafish larvae.

GO Term	Description	P-value	FDR q-value	Enrichment (N, B, n, b)
GO:0044421	extracellular region part	6.22E-26	7.91E-23	2.10 (10396,470,1892,180)
GO:0005576	extracellular region	1.71E-21	1.08E-18	2.07 (10396,412,1892,155)
GO:0005615	extracellular space	5.73E-20	2.43E-17	2.08 (10396,372,1892,141)
GO:0031012	extracellular matrix	7.69E-18	2.44E-15	2.61 (10396,162,1892,77)
GO:0062023	collagen-containing extracellular matrix	3.84E-12	9.77E-10	2.88 (10396,80,1892,42)
GO:0005887	integral component of plasma membrane	2.21E-08	4.68E-06	1.67 (10396,335,1892,102)
GO:0016021	integral component of membrane	2.32E-08	4.22E-06	1.21 (10396,2470,1892,543)
GO:0031224	intrinsic component of membrane	6.55E-08	1.04E-05	1.20 (10396,2497,1892,545)
GO:0005581	collagen trimer	1.67E-07	2.36E-05	3.12 (10396,37,1892,21)
GO:0031226	intrinsic component of plasma membrane	1.74E-07	2.21E-05	1.61 (10396,352,1892,103)
GO:0005604	basement membrane	4.86E-06	5.61E-04	3.01 (10396,31,1892,17)
GO:0044459	plasma membrane part	1.31E-05	1.39E-03	1.32 (10396,778,1892,187)
GO:0043235	receptor complex	1.52E-05	1.48E-03	1.75 (10396,163,1892,52)
GO:0005886	plasma membrane	1.55E-05	1.41E-03	1.26 (10396,1113,1892,255)
GO:0016020	membrane	5.11E-05	4.33E-03	1.12 (10396,3451,1892,701)
GO:0044425	membrane part	8.76E-05	6.96E-03	1.13 (10396,2958,1892,606)
GO:0044420	extracellular matrix component	1.26E-04	9.44E-03	3.18 (10396,19,1892,11)
GO:0005921	gap junction	3.73E-04	2.63E-02	3.30 (10396,15,1892,9)
GO:0030054	cell junction	4.20E-04	2.81E-02	1.41 (10396,323,1892,83)
GO:0008305	integrin complex	6.89E-04	4.38E-02	2.75 (10396,22,1892,11)
GO:0009986	cell surface	7.26E-04	4.39E-02	1.94 (10396,65,1892,23)

N, number genes in background list; B, genes un background annotated with GO term; n, genes in target list; b, gene sin target list annotated with GO term. Enrichment = (b/n)/(B/N).

Table 5.7. KEGG and Reactome enrichment analysis of biological pathways for all DEGs in 5dpf *gr^s357* mutant zebrafish larvae.

KEGG Term	Count	Fold Enrichment	Benjamini	FDR
ECM-receptor interaction	34	2.8883513	2.74E-07	2.70E-07
Focal adhesion	71	1.96172003	2.74E-07	2.70E-07

Reactome Term	Count	Fold Enrichment	Benjamini	FDR
Laminin interactions	17	3.76019002	1.04E-04	1.04E-04
Signaling by PDGF	15	3.31781473	0.00380775	0.00377492
Degradation of the ECM	14	2.97752604	0.01760372	0.01745196

Figure 5.8. Biological Process GO-term visualisation of ALL significantly differentially expressed genes resulting from the *gr^s357* mutation in 5dpf zebrafish larvae. Enrichment of genes encompassing biological processes. Map produced using GOrilla software. Legend indicates p-value colour scale.

126

Figure 5.9. Molecular Function GO-term visualisation of ALL significantly differentially expressed genes resulting from the *gr^s357* **mutation in 5dpf zebrafish larvae.** Enrichment of genes encompassing Moleculr Functions. Map produced using GOrilla software. Legend indicates p-value colour scale.

Figure 5.10. Cellular Component GO-term visualisation of ALL significantly differentially expressed genes resulting from the *gr^s357* mutation in 5dpf zebrafish larvae. Enrichment of genes encompassing Cellular Components. Map produced using GOrilla software. Legend indicates p-value colour scale.
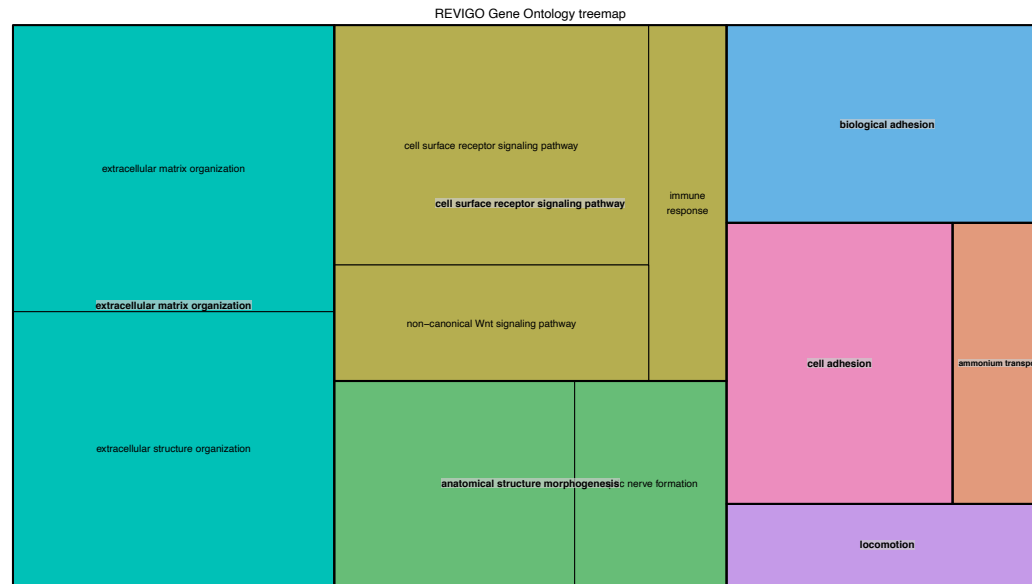
Figure 5.11. REVIGO GO-term visualisation of ALL significantly differentially expressed genes resulting from the *gr^s357* mutation in 5dpf zebrafish larvae. Top) Enrichment of genes encompassing Biological Processes. Bottom left) Enrichment of genes encompassing Molecular Functions. Bottom right) Enrichment of genes encompassing Cellular Components. All maps produced using REVIGO treemap software. Box size is reflects p-value.

5.2.5 Genes associated with cellular components of the neuron are primarily upregulated in *gr^s357* mutant zebrafish larvae

Surprisingly, despite a near symmetrical distribution of up- and downregulated genes in my differential expression analysis of the *gr^s357* mutant larval transcriptome, no specific GO pathway terms relating to biological processes or molecular functions were identified within our thresholds ($p<0.05$ and FDR<0.05). Likewise, analysis of enriched biological pathways present in the population of upregulated DEGs identified no significant KEGG or Reactome pathways. However, upregulated DEGs were overrepresented in the location of their translated protein's function (GO: cellular component). Three terms were specified: axon, cell projection and neuron part (Table 5.8; Figure 5.12). As GO analysis of upregulated genes uncovered no GO terms within my thresholds, the thresholds were relaxed to p-value only of <0.05.
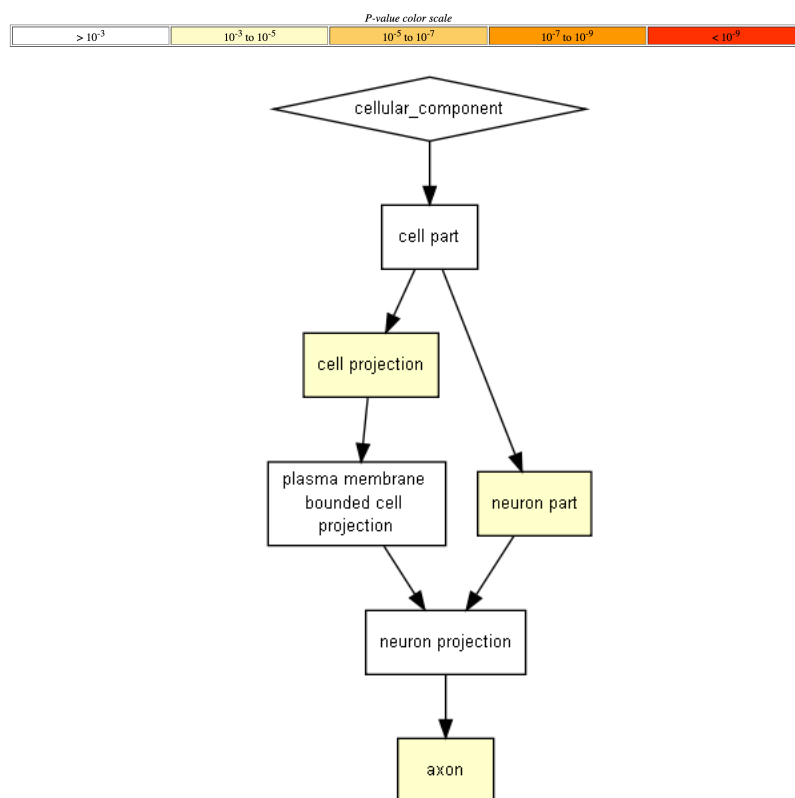
Figure 5.12. Cellular Component GO-term visualisation of upregulated significantly differentially expressed genes resulting from the *gr^s357* mutation in 5dpf zebrafish larvae. Enrichment of upregulated genes encompassing Cellular Components. Map produced using GOrilla software. Legend indicates p-value colour scale.

In our upregulated DEG population, genes involved in many neuronal development processes were identified. Genes were upregulated in GABA and glutamate signalling in synapses, including the GABA neurotransmitter transporters *slc6a1a* and *slc6a1b*; GABA receptor *gabrp*, and glutamate receptors *gria1a* and *grin2da*. Moreover, many synaptic scaffold proteins essential for correct synaptic signalling, including *shank3a* (scaffold of excitatory glutamatergic synapses), *map1aa* (microtubule-associated protein), *dlg2* (important for postsynaptic receptor clustering), *bsnb* (scaffold protein for presynaptic terminal active zone) and *syt7b* (important for neurotransmitter release at synapses) were found upregulated in *gr^s357* mutant larvae. In addition, the serotonin receptor *htr1aa* was also identified in the upregulated DEG population. Genes important in correct neuronal development such as *bdnf* (Brain-Derived Neurotrophic Factor), its receptor *ntrk3a* (Tropomyosin receptor kinase) and components of its downstream signalling *rab5ab* were upregulated in *gr^s357* mutant larvae (Cohen-Cory et al., 2010). Many other genes important for neuronal differentiation and survival were upregulated, including *mettl5*, essential for myelination (Wang et al., 2020).

Genes involved in the axon skeleton, axon guidance, migration and growth were upregulated in *gr^s357* mutant larvae including neurofilaments *neflb, neflb* and *nefmb*, axonal skeletal proteins such as *dctn1b* (dynactin), *myo16 and spg11* (spastic paraplegia 11), scaffold proteins for filapodia such as *gpm6aa* and *lin7b*, adaptor proteins such as *itsn2a*, *maptb* (Tau b) and *pacsin1a* (interacts with Tau), genes that interact with microtubules (*dbnla and dscama)* and commonly known tyrosine kinase genes *lrrk2* and *ret*. The most significantly upregulated gene in *gr^s357* mutant larvae, *kcnc5a* (Figure 5.5,5.6&5.7; Table 5.2&5.3), encodes a potassium voltage-gated channel involved in axon action potential generation (Pannasch et al., 2006). Other genes that encode channels were also upregulated in *gr^s357* mutant larvae, including *kcnd3*, *znrf2b* (regulates Na+/K+ pumps), and sodium/calcium transporters *slc8a1b* and *slc8a2b*. Together, a multitude of neuronal and axon cellular components are dysregulated in *gr^s357* mutant larvae.

5.2.6 Genes involved in ECM composition, morphogenesis, angiogenesis, locomotion and the immune response are primarily downregulated in the 5dpf larval *gr^s357* mutant transcriptome.

DEGs that were downregulated in the *gr^s357* mutants were overrepresented in a striking 49 GO terms relating to biological processes, including extracellular matrix organisation, morphogenesis, angiogenesis, locomotion and the immune response (Figure 5.15;Table A6). These downregulated DEGs were overrepresented in 16 molecular function GO terms, including

extracellular matrix structure, cytokine activity, growth factor activity, Wnt signalling and receptor-ligand activity (Figures 5.13&5.15; Table A7). These downregulated DEGs were overrepresented in 23 GO terms relating to cellular components, including the extracellular matrix and integral or intrinsic components of the plasma membrane (Figures 5.14&5.15;Table A8). These GO terms suggest a transactivation role of the GR for extracellular matrix formation and organisation, as well as cell surface signalling through mechanisms such as growth factor and cytokine binding. Likewise, enrichment of biological pathways in the downregulated DEGs list identified 3 significant KEGG pathways: Focal adhesions (Figure 5.15), ECM-interactions (Figure 5.16) and the regulation of the actin cytoskeleton (Table 5.9). In addition, Reactome analysis recognised 6 significantly enriched pathways for overrepresented downregulated genes: laminin interactions, signalling by PDGF, degradation of the ECM, ECM proteoglycans, molecules associated with elastic fibres and activation of metalloproteinases (Table 5.9).

Table 5.8. Significant Cellular Component Gene Ontology terms overrepresented in upregulated genes differentially expressed in *gr^s357* mutant zebrafish larvae.

GO Term	Description	P-value	FDR q-value	Enrichment (N, B, n, b)
GO:0030424	axon	3.09E-05	3.92E-02	2.90 (10396,81,796,18)
GO:0042995	cell projection	4.08E-05	2.59E-02	1.69 (10396,456,796,59)
GO:0097458	neuron part	8.96E-05	3.79E-02	1.68 (10396,428,796,55)
GO:0045202	synapse	5.36E-04	1.70E-01	1.93 (10396,189,796,28)

N, number genes in background list; B, genes un background annotated with GO term; n, genes in target list; b, gene sin target list annotated with GO term. Enrichment = (b/n)/(B/N).

Table 5.9. KEGG and Reactome enrichment analysis of biological pathways for downregulated DEGs in 5dpf *gr^s357* mutant zebrafish larvae.

KEGG Term	Count	Fold Enrichment	Benjamini	FDR
Focal adhesion	63	2.69688493	5.40E-12	5.24E-12
ECM-receptor interaction	32	4.21176628	2.94E-11	2.86E-11
Regulation of actin cytoskeleton	39	1.81966688	0.0101525	0.00986034

Reactome Term	Count	Fold Enrichment	Benjamini	FDR
Laminin interactions	17	5.91790654	1.03E-07	1.02E-07
Signaling by PDGF	14	4.87357009	6.79E-05	6.68E-05
Degradation of the ECM	14	4.68612509	1.04E-04	1.03E-04
ECM proteoglycans	14	3.4811215	0.00388506	0.00382274
Molecules associated with elastic fibres	10	4.14419226	0.01348912	0.01327272
Activation of matrix metalloproteinases	8	4.97303071	0.01953893	0.01922547

5.2.6.1 Genes encoding ECM composition and ECM organisation are primarily downregulated in 5dpf *gr^s357* mutant zebrafish larvae.

56 genes annotated with the GO term "Extracellular matrix organisation" were significantly enriched in the population of downregulated DEGs in *gr^s357* mutant larvae. Genes encoding ECM structural components such as multiple collagens: *col1a1b*, *col28a1a*, *col4a5*, *col4a4*, *col1a2*, *col4a1-6*, *col11a1b*, *col8a2* etc; myosin: *myh9a*; and laminins: *lamb1b*, *lamb1a*, *lama4*, *lac1*, *lamc3*, were downregulated in the *gr^s357* mutants. This was recognised in the KEGG and Reactome analysis performed on the downregulated population of DEGs, identifying overrepresented genes in pathways such as: "regulation of actin cytoskeleton", "laminin interactions" and "ECM proteoglycans" (Figures 5.13,5.14,5.15&5.16).

Genes that regulate ECM metabolism were also overrepresented in the population of downregulated DEGs in *gr^s357* mutants. Reactome analysis identified "degradation of the ECM" and "activation of metalloproteinases" as terms overrepresented in downregulated DEGs. Genes such as calcium-activated proteases *capn2a*, *capns1a*, *cast* and *ctsk*; glycoproteins such as fibronectin, *fn1;* decorin, *dcn*; and *nid1a*, and matrix metallopeptidases: *mmp2, mmp9, mmp14b, mmp15a* and *mmp30* were downregulated in *gr^s357* mutants. Many of these genes are additionally associated with GO term "collagen catabolic process". Previous literature has shown the effects of glucocorticoids on collagen synthesis in mammals e.g. dexamethasone treatment increases collagen synthesis, mediated through GR signaling in bovine aortic smooth muscle cells in vitro (Leitman et al., 1984), and cortisol treatment of fetal rat calvariae cultured increases collagen synthesis (Gazzerro et al., 1998). Together, this suggests this GR-mediated regulation of collagen is conserved in zebrafish.

5.2.6.2 Genes encoding biological and cellular focal adhesions are primarily downregulated in 5dpf *gr^s357* mutant zebrafish larvae.

Various cellular and extracellular components important for cell-ECM and cell-cell interactions are downregulated in *gr^s357* mutant larvae (Figures 5.13,5.14,5.15&5.17). Scaffold components of basement membranes such as laminins (*lamb1b, lamc1, lamb1a, lamc3*) and collagens (reported previously) and nidogen (*nid1a, nid1b*), in addition to other glycoproteins of the ECM such as fibronectin (*fn1b*), fibrillin (*fbn2b*), thrombospondins (*thbs4b, thbs3a, thbs2b, thbs3b and thbs4a*) and periostin (*postna, postnb*) are downregulated in *gr^s357* mutant zebrafish larvae. Many of these ECM components are used as ligands for cell receptor adhesion. The principal receptors to bind cells to the ECM are integrins. Similarly, many integrins are downregulated in *gr^s357* mutants, such as *itgb1b, itgb4, itga1, itga8, itgb1b.2, itga11a, itgb1a, itga3b, itgbl and, itga6b*. Numerous proteins that are important in cell-cell adhesions to form tight junctions or normal tissue structures are also downregulated in the *gr^s357* mutant, including transmembrane proteins such as claudins (*cldn11a, cldn11b, cldn1, cldnh, cldnb, cldni*), important for tight junction integrity, desmoplakin (*dspb*), important for desmosome structure, epithelial cell adhesion molecule (*epcam*) and talin-1 (*tln1*). It is interesting to note that not only are ECM components downregulated in *gr^s357* mutants but associated cellular-adhesion molecules are also downregulated. Previous literature has shown the effects of glucocorticoids on focal adhesions, including glucocorticoid-induced thrombospondin-1 protein expression (Barclay et al., 2016), fibronectin biosynthesis (Oliver et al., 1983) and integrin expression (Lowin et al., 2009).

5.2.6.3 Genes encoding Wnt signalling are primarily downregulated in 5dpf *gr^s357* mutant zebrafish larvae.

The relationship between Wnt signalling and glucocorticoid signalling has previously been reported but results are varied. These range from the GR demonstrating a repressive role in Wnt signalling in the endothelium (Zhou et al., 2020), to disrupted glucocorticoid signalling reducing Wnt signalling in osteoblasts (Zhou et al., 2009). Several Wnt signalling related gene ontology terms were enriched in the population of DEGs downregulated in *gr^s357* mutant zebrafish larvae (Figures 5.13&5.15). Downregulated genes included: Wnt genes *wnt4a, wnt5b, wnt11* and *wif1* (Wnt inhibitory factor 1), respective frizzled receptors *fzd2, fzd4, fzd6, fzd7a, fzd7b, sfrp1a, sfrp1b* and *sfrp2,* LRP coreceptors *lrp5* and *lrp6*, and downstream Wnt signalling genes such as *dvl2* (dishevelled homolog 2) and *rock2a*.

The wnt/planar cell polarity (PCP) pathway is initiated through Wnt5 and Wnt11 signalling via frizzled receptors that activate Dvl to form effector complexes, including the Dvl-Daam1-RhoA complex which leads to rock2 kinase activation (Semenov et al., 2007). Other Wnt/PCP-associated genes were downregulated, including the *prickle1a* (Prickle Planar Cell Polarity Protein 1), the Wnt-coreceptor *ryk*, the inhibitory Wnt signalling *tax1bp3* and *amotl2*, the beta catenin-activated transcription factor *tcf7l1*, the Wnt signalling regulators *notum1a* and *rspo3* (R-spondin), *psen1* (presenilin-1), and the Wnt ligand-dependent activation of its negative feedback regulator *nkd1*. Interestingly, multiple pathways downstream of Dvl regulate actin cytoskeleton/cell adhesion, providing a hypothetical connection between the downregulation of Wnt signalling genes and ECM/cell adhesion genes identified in *gr^s357* mutant zebrafish larvae.
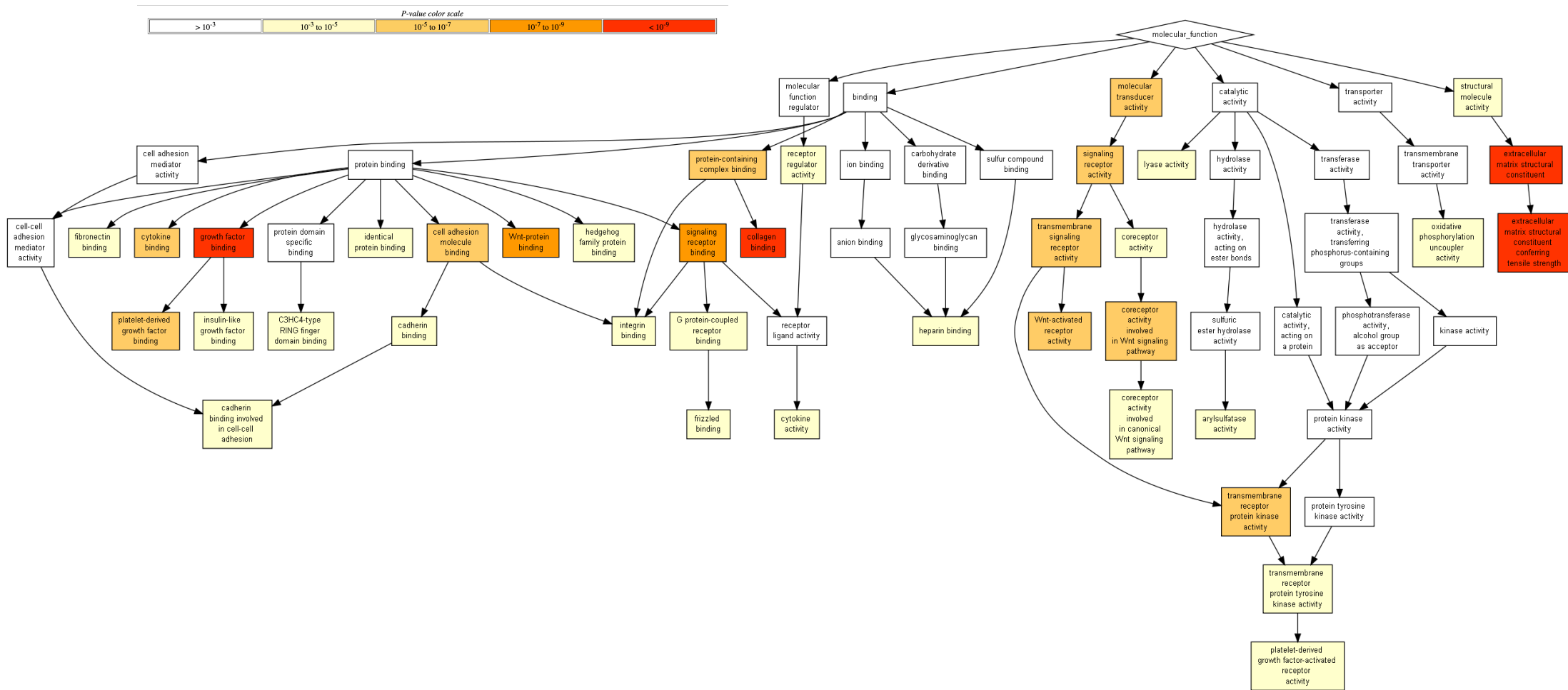
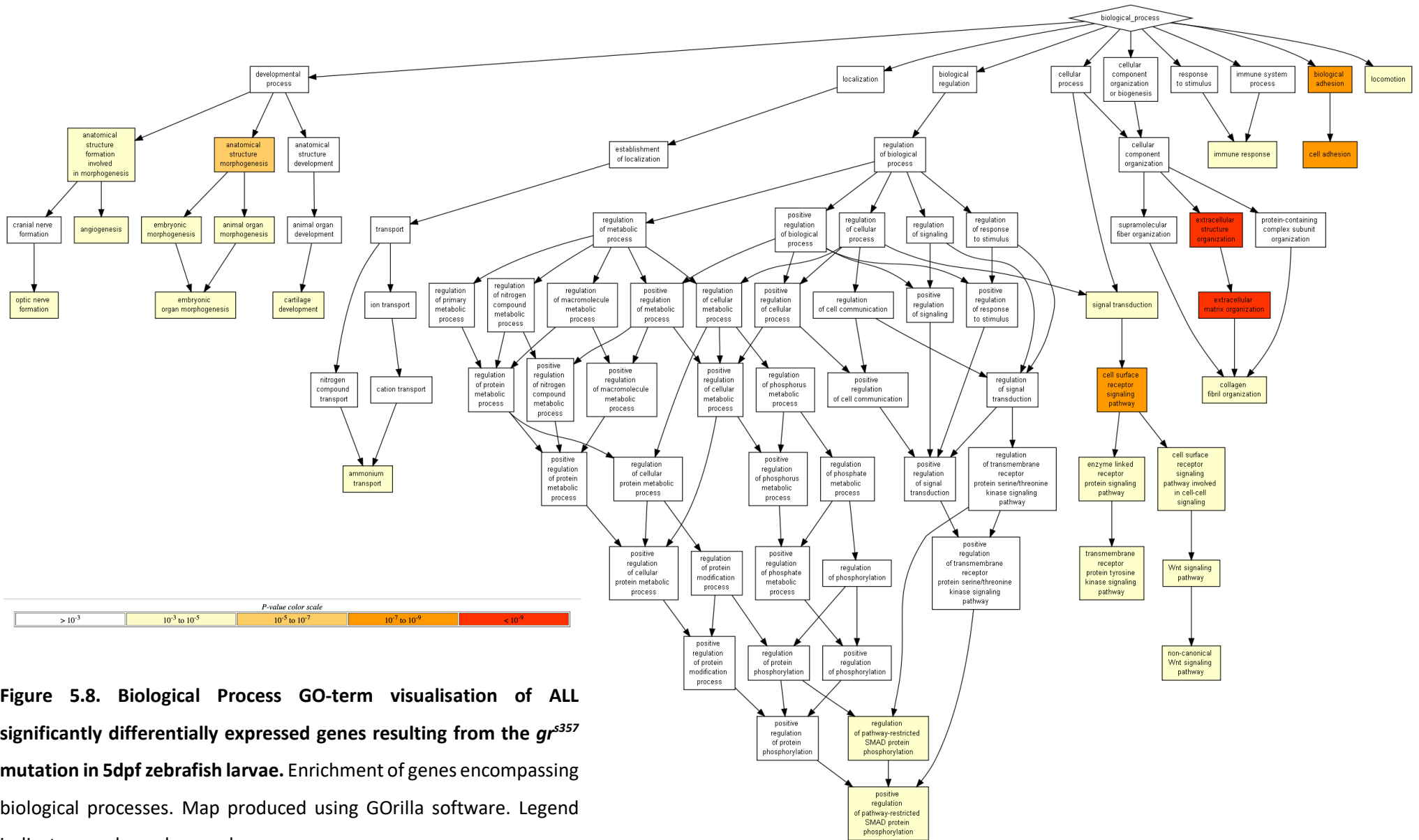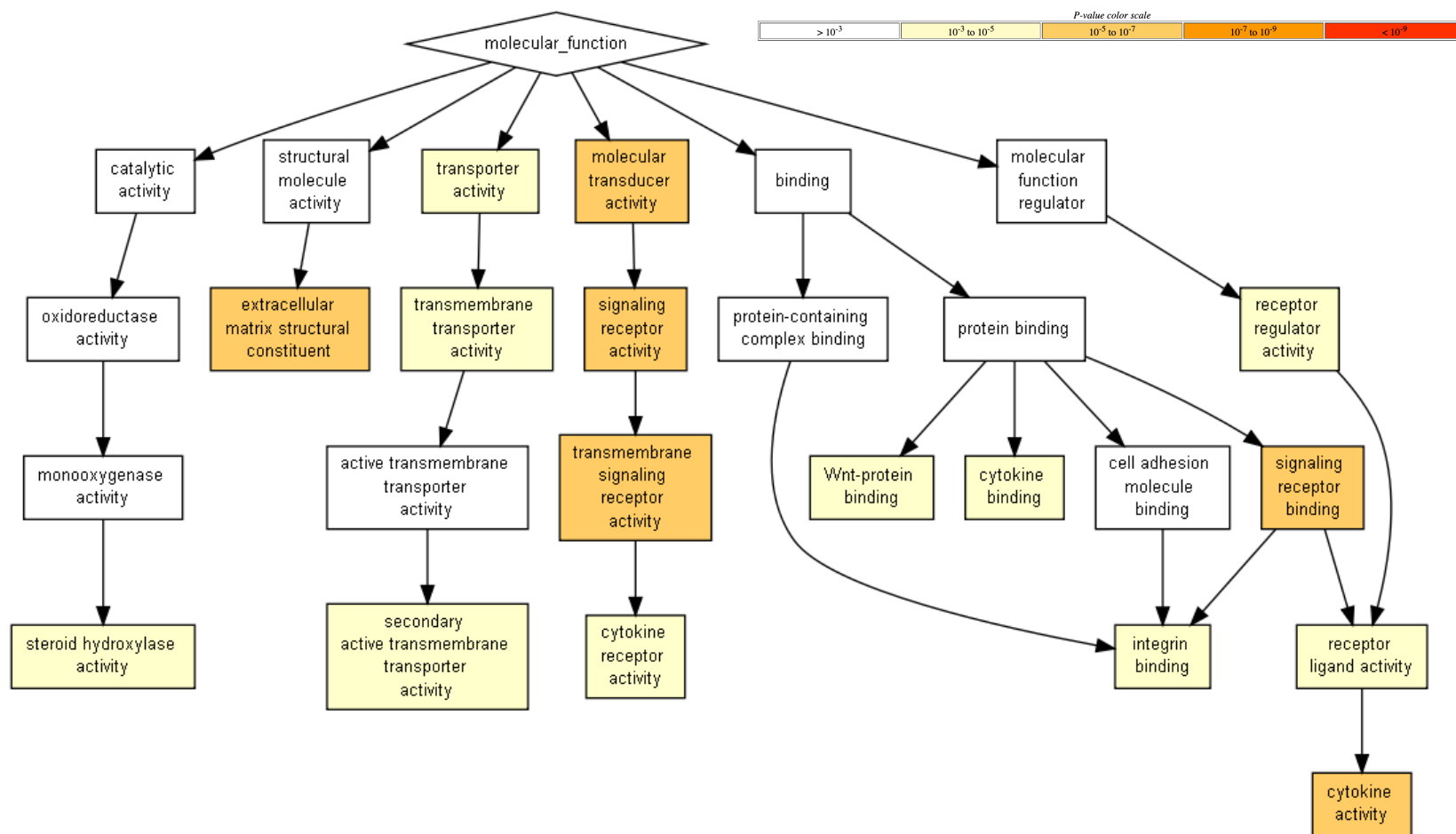**Figure 5.13. GO-term visualisation of significantly downregulated differentially expressed genes resulting from the *gr^s357* mutation in 5dpf zebrafish larvae.** Enrichment of genes encompassing Molecular Functions. Map produced using GOrilla software. Enrichment of genes encompassing biological processes not shown due to size. Legend indicates p-value colour scale.
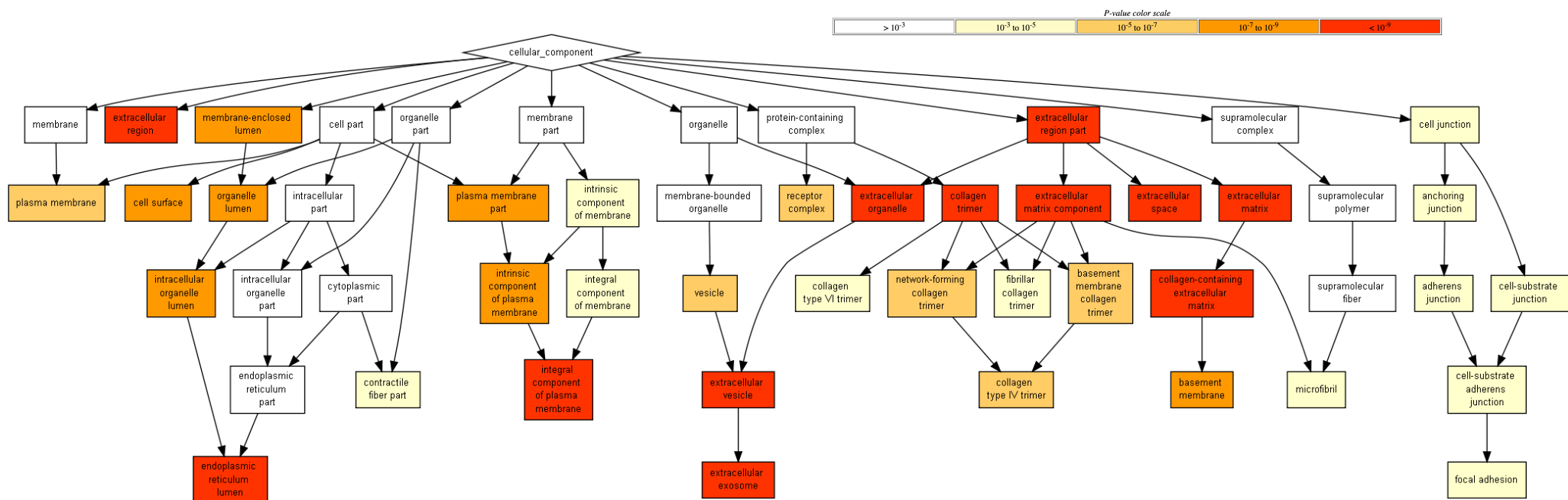
Figure 5.14. GO-term visualisation of significantly downregulated differentially expressed genes resulting from the *gr^s357* mutation in 5dpf zebrafish larvae. Enrichment of genes encompassing Cellular Components. Map produced using GOrilla software. Legend indicates p-value colour scale.
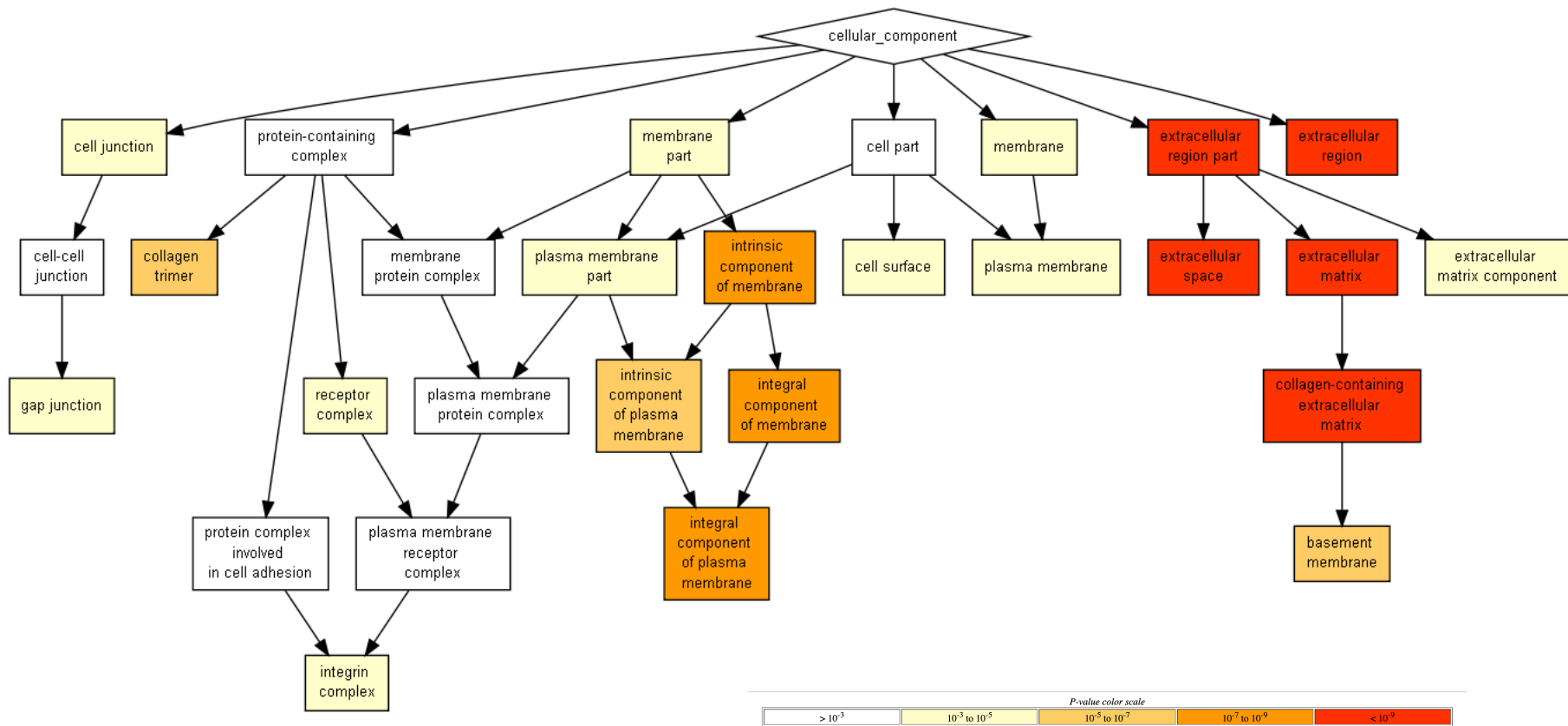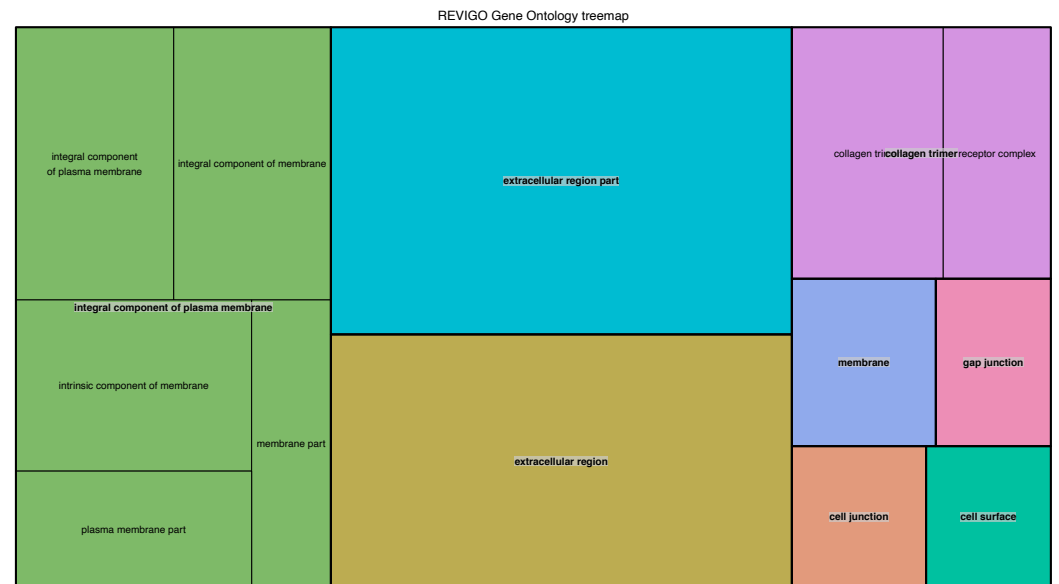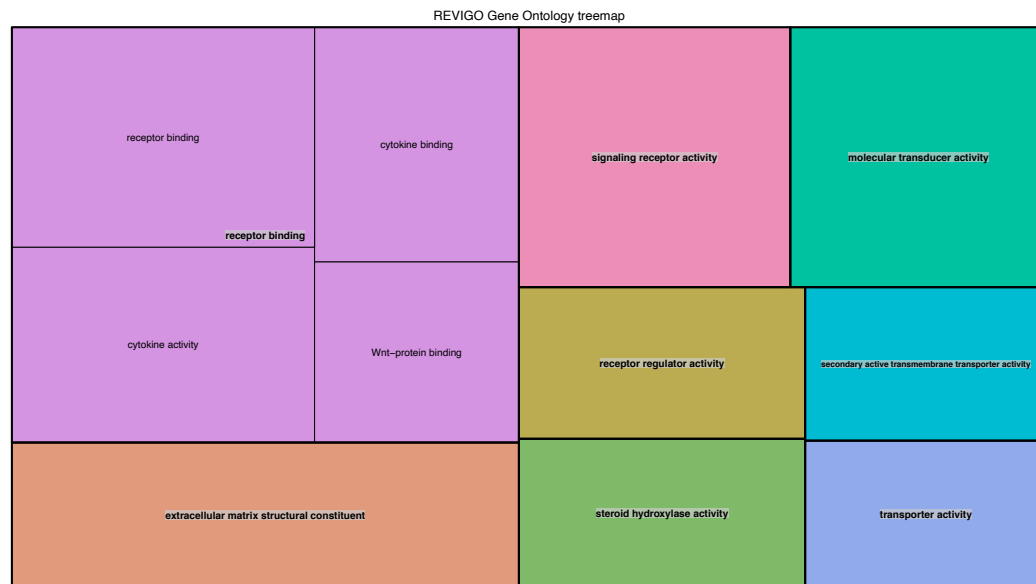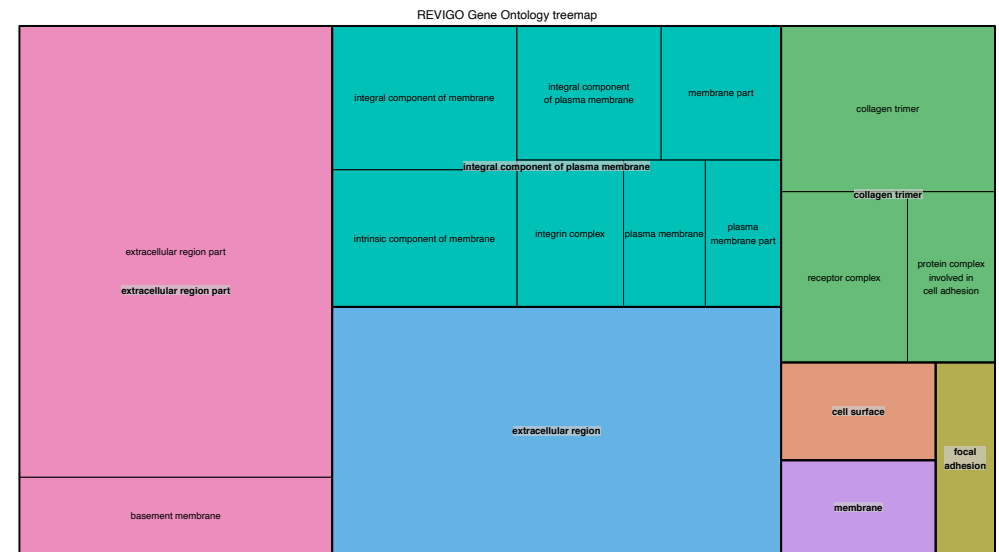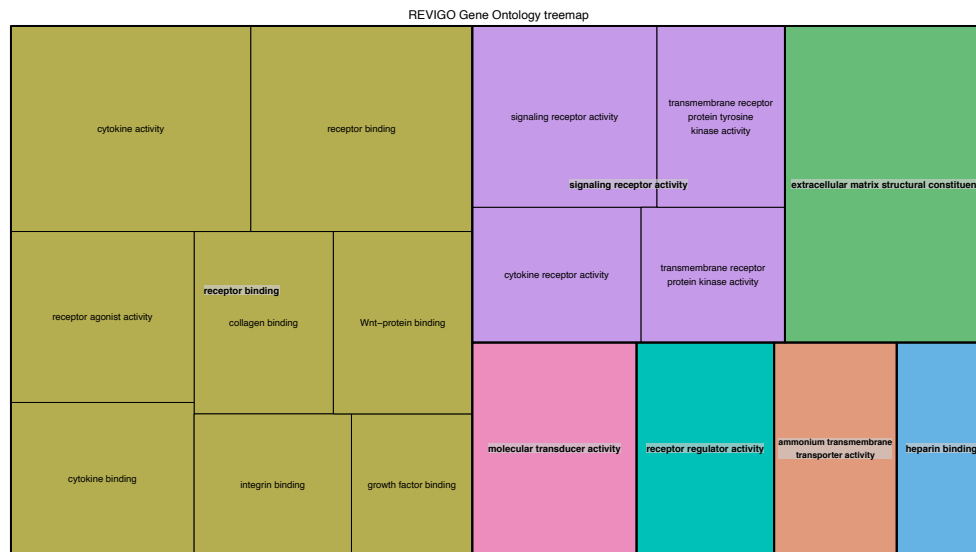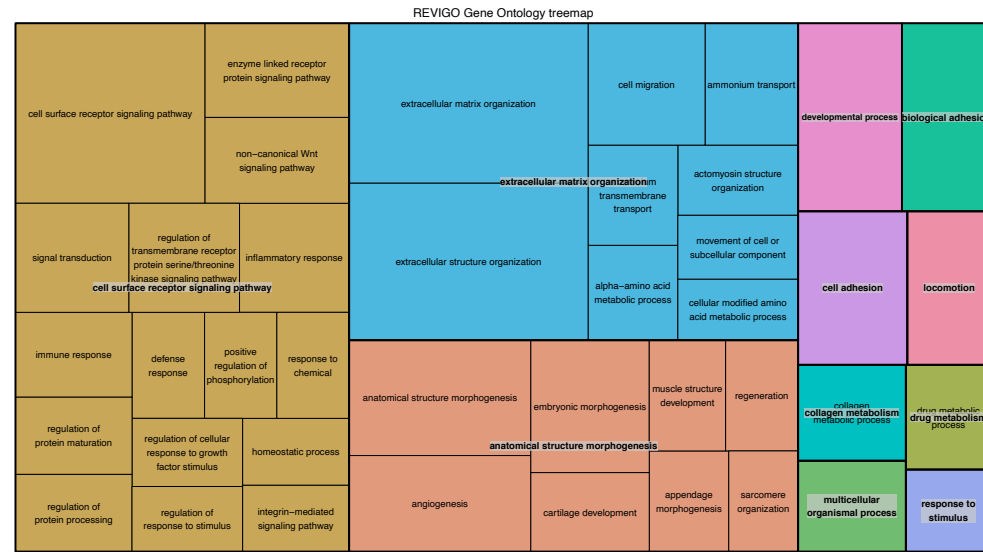
Figure 5.15. REVIGO GO-term visualisation of downregulated significantly differentially expressed genes resulting from the *gr^s357* mutation in 5dpf zebrafish larvae. Top) Enrichment of downregulated genes encompassing Biological Processes. Bottom left) Enrichment of downregulated genes encompassing Molecular Functions. Bottom right) Enrichment of downregulated genes encompassing Cellular Components. All maps produced using REVIGO treemap software. Box size is reflects p-value.
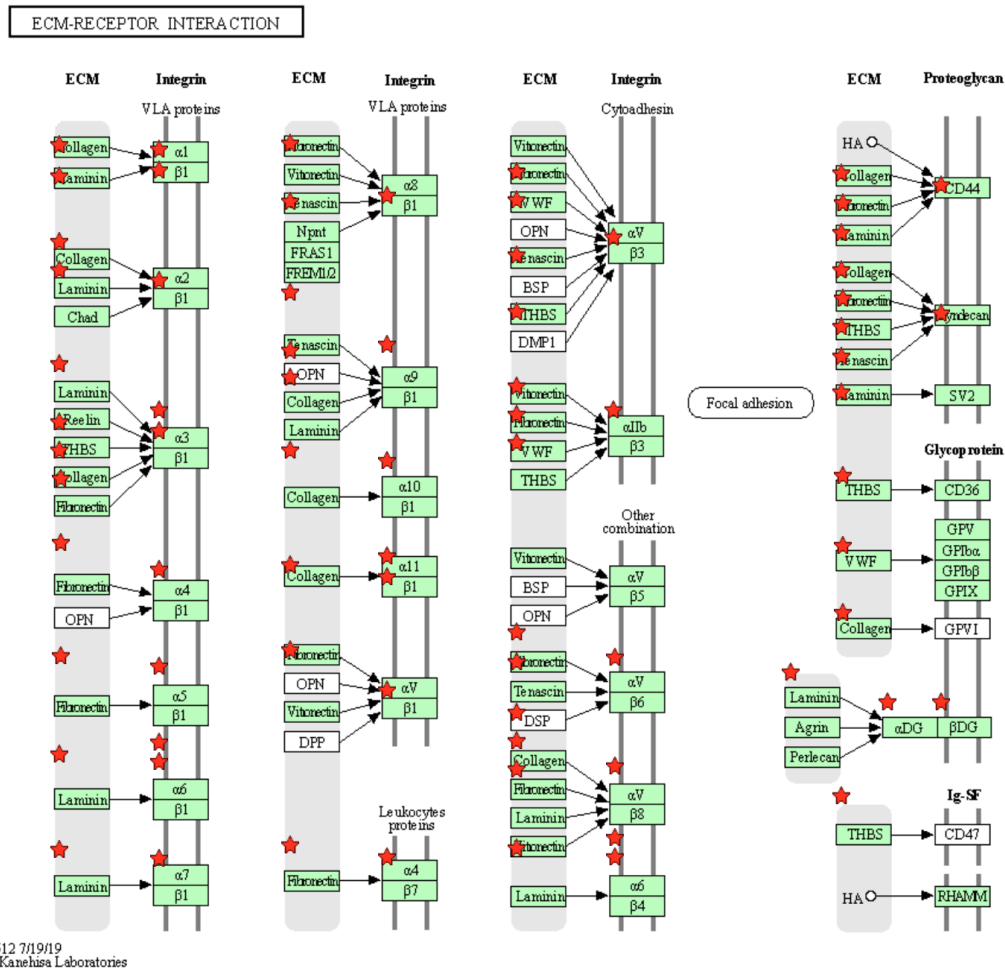
Figure 5.16. Genes annotated to the ECM Interaction KEGG pathway were significantly enriched in downregulated genes in the *gr^s357* 5dpf larval transcriptome. Differentially expressed pathway components are indicated with red stars.
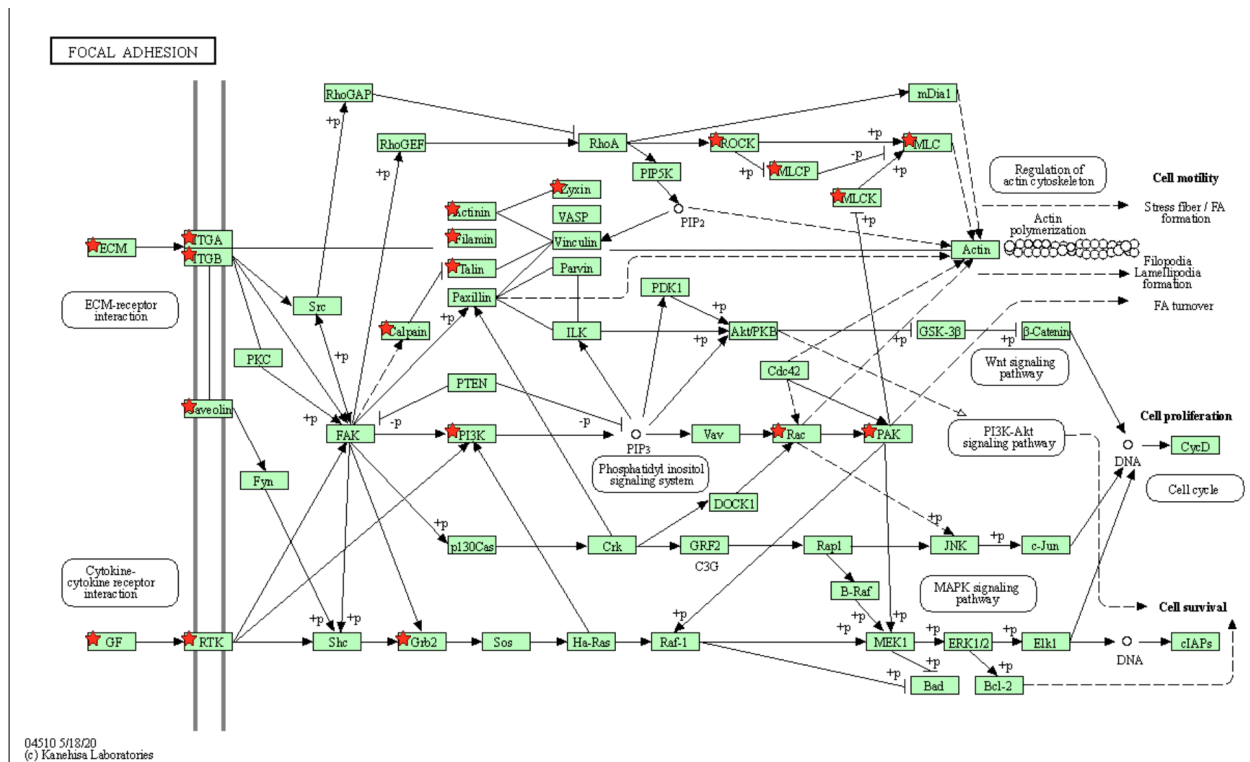
Figure 5.17. Genes annotated to the Focal Adhesion KEGG pathway were significantly enriched in downregulated genes in the *gr^s357* 5dpf larval transcriptome. Differentially expressed pathway components are indicated with red stars.

Figure 5.18. Genes annotated to the Regulation of Actin Skeleton KEGG pathway were significantly enriched in downregulated genes in the *gr^s357* 5dpf larval transcriptome. Differentially expressed pathway components are indicated with red stars.

5.2.6.4 Genes encoding positive regulation of transmembrane receptor protein serine/threonine kinase signalling are primarily downregulated in 5dpf *gr^s357* mutant zebrafish larvae.

Several "transmembrane receptor protein serine/threonine kinase signalling" related GO terms were enriched in the population of downregulated DEGs in *gr^s357* mutant zebrafish larvae (Figure 5.15; Table A6). Members of the transforming growth factor-β (TGF-β) superfamily, such as TGF-β isoforms, activins and bone morphogenetic proteins (BMPs), regulate growth, cell differentiation and cell death, which are important for embryonic development (Moustakas et al., 2001). These superfamily ligands bind respective heteromeric complexes of serine/threonine kinase receptors. The intracellular effectors, known as Smads, transduce these ligand-mediated signals acting as transcription factors by translocating to the nucleus and forming transcriptional complexes with other nuclear partners (Massagué et al., 2005). Many superfamily ligands-encoding genes associated with positive regulation of SMAD phosphorylation are downregulated in the in *gr^s357* mutant zebrafish larvae, including *bmp3, bmp4, bmp5, bmp16, tgfb1a, tgfb3, gdf10a, gdf10b, igfbp3* (insulin-like growth factor binding protein 3) and the activin subunit *inhbb*. In addition, the gene encoding the receptor *osr1*, was downregulated. *Osr1* is part of a receptor complex, which includes the TGF-β receptor, that signals through non-canonical TGF-β pathways. Major regulators of the TGF-β/Smad signalling pathway were also identified in the population of downregulated DEGs: *skib* (Sloan-Kettering Institute b), a Smad interacting protein that negatively regulates TGF-β/Smad signalling by disrupting the formation of Smad complexes and recruitment of coactivators (Tecalco-Cruz et al., 2018), and *vasnb*, a membrane protein that binds TGF-β and attenuates signalling. Furthermore, there was a downregulation of BMP antagonists such as *sostdc1a*, *ost*, and *twsg1a* (twisted gastrulation homolog). Interestingly, the gene *tsc22d3/gilz* was severely downregulated in the *gr^s357* mutants. This gene has been shown to be a direct target of GR and mediates crosstalk between glucocorticoids and TGF-β signalling by binding and promoting phosphorylation of Smad2 and activation of FoxP3 expression, important for T cell immune responses (Bereshchenko et al., 2014). *Tsc22d3* was also discovered significantly upregulated in my hypercortisolaemic *MR^46Del* mutant transcriptome. Whilst foxp3 was not a significant DEG in this analysis, many other Forkhead box transcription factor encoding genes were significantly downregulated, including *foxd1, foxf2a, foxj3, foxq1b, foxj2, foxq1a, foxd2, foxf1, foxk1* and *fox1l*.

**5.2.6.5 Genes regulating the 'immune response' are primarily downregulated in 5dpf *gr^s357*
mutant zebrafish larvae.**

Two GO terms relating to the immune system were identified during GO enrichment analysis:
"immune response" and "cytokine-mediated signalling pathway" (Figure 5.15; Table A6&A7). The
role of the glucocorticoids and the GR in the immune response has been heavily researched.
Glucocorticoids have various roles in regulating the immune system, through inhibiting
inflammation to inhibiting B cell and T cell production at high concentrations. Glucocorticoid
receptor signalling improves pathways involved in the innate immunity but dampens those
involved in adaptive immunity (Cain and Cidlowski, 2017).

The differential expression analysis of *gr^s357* mutant zebrafish larvae revealed an enrichment in
genes associated with the immune response. Genes encoding immune-associated cytokines, such
as *ccl25b*, *cxcl12a* and *crlf1a* (cytokine receptor-like factor 1a), were downregulated in *gr^s357*
mutants. Likewise, multiple receptors that transduce signalling of immune pathways were
significantly reduced, including *tlr5b* (important for bacterial flagellin recognition), *agtr2*
(angiotensin II receptor), *il13ra2* (interleukin 13 receptor) and *adipor2*. Genes encoding proteins
that function as components to an important receptor complex composed of *lifrb*, *il6stb* and *cntfr,*
which regulate IL-6 signal transduction, were also downregulated. These have also been shown
bound by *crlf1a* (Dembic, 2015). Downstream of this receptor complex, *stat6* expression was also
significantly downregulated. Within the population of downregulated DEGs were those
associated with TLR signalling, including inducers such as *fn1b* (fibronectin), the receptor *tlr5b*
and *mapkapk2a,* a regulator of IL-6 production which is also involved in TLR signalling pathway.
Additionally, other genes involved in T cell responses, the inflammasome and innate immunity
were also downregulated, including *myd88*, *ptgs1* (cox-1), *ptgs2a* (cox-2), *caspb*, *gbp3*, *elf3* and
slc27a1b (fatp1). Genes enriched in both the immune response and coagulation were
downregulated in *gr^s357* mutant zebrafish larvae such as coagulation factors *f3a* and *f3b*.
Interestingly, the coagulation pathway and immune system have been shown to be directly linked
(Burzynski et al., 2019).

5.2.6.6 Genes associated with 'signalling by PDGF' are primarily downregulated in 5dpf *gr^s357* mutant zebrafish larvae.

Gene enrichment Reactome analysis revealed a significant number of genes enriched in platelet-derived growth factor (PDGF) signalling that were downregulated in our differential expression analysis of 5dpf *gr^s357* mutant zebrafish larvae. Genes upstream of PDGF secretion such as *col4a1*, *col4a2*, *col4a3*, *col4a4*, *col4a5*, *col4a1*, *col6a*, *col6b* that bind to integrins (previously seen downregulated) were downregulated in *gr^s357* mutants. Collagen-integrin interactions are known regulators of PDGF-A expression (Tan et al., 1995). In addition, key PDGF receptors, *pdgfra, pdgfb* and *pdgfrl*, multiple secreted glycoproteins *thbs2a*, *thbs2b*, *thbs3a*, *thbs3b and thbs4b* (thrombospondins), known to bind PDGFs, and *furina,* which is required for PDGF synthesis, are present within the downregulated population of DEGs. However, it was observed that *furinb* was significantly upregulated in *gr^s357* mutants. In previous studies, exogenous dexamethasone treatment has been shown to inhibit platelet-derived growth factor signalling through GR signalling (Son et al., 2001). My results support these findings, as shown by the reduced PDGF signalling in *gr^s357* mutants, most likely due to the elevated cortisol concentration exhibited by the *gr^s357* mutants as consequence of the HPI axis negative feedback loss.

5.2.6.7 Genes associated with 'angiogenesis' are downregulated genes in 5dpf *gr^s357* mutant zebrafish larvae.

GO enrichment analysis revealed an overrepresentation of genes associated with angiogenesis in our population of downregulated DEGs. In my population of downregulated DEGs, 5 genes encoding angiopoietin ligands (*angpt1*, *angptl2a*, *angptl2b*, *angptl4 andangptl7)*, their receptors *tie1 and tek* (Tie2), other receptors associated with angiogenesis such as *flt4,* and the previously reported *pdgfrb* were identified. The transcription factor encoding genes *twist1a* and *twist1b,* which are known to regulate angiogenesis through the angiopoietin-Tie2 pathway, were also downregulated in *gr^s357* mutants. Genes involved in common mechanisms of angiogenesis such as cell migration and cell-junction remodelling were identified within the downregulated DEG population as described previously.

The most commonly recognised angiogenic pathway is VEGF signalling. In *gr^s357* mutants, *kdrl* (vegfr2) was downregulated, as were genes involved in the regulation of the VEGF signalling pathway, including components of an angiogenic protein complex: *rab13*, *grb2a* and *amotl2a* (angiomotin receptor) (Aase et al., 2007). Genes known to regulate the expression of VEGF

ligands were also downregulated, including *lpar1* (LPA receptor) and *lpar6a*, the transcription factor *nfkb2*, and associated inhibitors *nfkbiaa*, and *nfkbiab*, downstream of VEGF signalling. The transcription factor *foxf1* was also downregulated, which regulates VEGFR2 expression. Other genes that are associated with the VEGF pathway and are known to regulate angiogenesis were identified within the downregulated DEG population, including *igfbp7*, *hspa12b, ackr3b* (cxcr7), *kif11* and *fli1a.*

Genes involved in vessel remodelling and tip cell formation were downregulated in *gr^s357* mutants, including *ptprb*, *myh9a*, *sema3e*, *ramp2*, *igf2b*, *acvrl1* and *sdc2* (syndecan2), which bind both VEGF and PDGF, as well as collagens and laminins, whose expression is regulated by TGF-beta and IL-6. Genes involved in the regulation of angiogenesis through cross-linking and scaffolding of collagen IV were downregulated, including *loxl2a* and *loxl2b*, important for TGF-B signalling and angiogenesis.

5.2.6.8 Genes 'ammonium transport' are downregulated genes in early staged 5dpf *gr^s357* mutant zebrafish larvae.

Glucocorticoids and ammonia metabolism have previously been shown to have a complex relationship (Weiner, 2016). In the population of downregulated DEGs, a number of genes were overrepresented for ammonium transport function. These included *rhcga*, *rhcgb*, *rhag* and *rhbg, all of which* mediate ammonia excretion through ionocytes in the zebrafish (Shih et al., 2013). Also downregulated were solute carriers such as *slc25a47a*, *slc25a48*, *slc6a4a* (serotonin transporter) and *aqp1a.1* (aquaporin 1a), involved in acid secretion.

5.2.7 Comparative analysis between the *gr^s357* transcriptome and *MR^46Del* transcriptome.

To compare the *gr^s357* transcriptome to the *MR^46Del* transcriptome, a Venn diagram approach was employed, identifying DEGs that overlapped in both mutant transcriptomes and exploring common dysregulated biological processes (Figure 5.19). It should be noted that the *gr^s357* mutation is in a wildtype TL (Tüpfel long fin) genetic background (WTTL), whereas the *MR^46Del* mutation is in a wildtype AB (WTAB) background. Previous studies have highlighted key differences in behaviour and baseline HPI-axis activity within the two wildtype genetic backgrounds (Van Den Bos et al., 2017; Gorissen et al., 2015). However, transcriptomic analysis of individual mutation vs control was performed within the same strain.

A total of 200 genes were differentially expressed in both transcriptomic datasets, of which 15 genes were upregulated in both *MR46Del* and *grs357* transcriptomes, 71 genes were downregulated in both, and 114 genes were expressed in opposing directions *in MR46Del and grs357* transcriptomes (Table 5.10). Of these 114 genes, 53 were upregulated in *grs357* mutants and downregulated in *MR46Del* mutants, and 61 were vice versa. These included previously noted steroidogenic gene *star* and glucocorticoid responsive gene *tsc22d3*.

DEGs that were downregulated in *grs357* and upregulated in *MR46Del* transcriptomes were among the top30 most significant genes in either *grs357* or *MR46Del* transcriptomes, such as *CR855277.2/znf687a*, a zinc finger domain ablated in *grs357* mutants and upregulated ~4fold in *MR46Del* mutants, *rhcgl1* and *rhcga*, ~90% reduced in *grs357* mutants and upregulated ~2.2fold in *MR46Del* mutants, and *socs3a*, ~75% reduced in *grs357* mutants and upregulated ~3fold in *MR46Del* mutants (Table 5.10). Interestingly, GO analysis of this population of overlapping genes revealed multiple significant GO terms, including 'carbohydrate biosynthetic process', 'response to stimulus', 'steroid metabolic process' and 'organic hydroxy compound transport'. DEGs associated with response to stimulus included *tnfaip8l2b* (tumour necrosis factor alpha-induced protein), *nfkbiaa* (nuclear factor of kappa inhibitor), *rab13*, heat shock proteins *hsp90aa1.1* and *hsp70l*, and *ucp2*. Similarly, we see steroid metabolism-associated genes *star and apoeb*, and the vitamin D activator *cyp2r1* identified in this overlapping population. Interestingly, both *star* and *tsc22d3* were downregulated in *grs357* mutant and upregulated in *MR46Del* mutant larval transcriptomes.

DEGs that were upregulated in *grs357* and downregulated in *MR46Del* transcriptomes were predominantly associated with neuronal cell adhesion, axon guidance and neurotransmitter release. This included glutamate receptors *grm4* and *neto2b*, netrin receptor *unc5da*, synaptic vesicle-associated neurotransmitter release genes *rims1b*, *clvs2, pacsin1a* and *srcin1 and* neuronal cell surface proteins such as *nrxn2*, *spon1a*, *pcdh1g22*, *trim46a* and *cntn2*.

DEGs upregulated in both *grs357* and *MR46Del* transcriptomes were mitochondrial DNA-associated genes, including *mt-atp6, mt-atp8, mt-co1, mt-co2, mt-co3, mt-cyb, mt-nd1, mt-nd2, mt-nd3, mt-nd4, mt-nd4l, mt-nd5* and *mt-nd6*. These genes encode essential components of the oxidative phosphorylation pathway, producing energy for the cell. Together, this suggests the presence of an activated HPI axis with consequential elevated glucocorticoid levels, causing an increase in transcription of mitochondrial genes. This supports previous findings that dexamethasone treatment induces transcription of mitochondrial genes, through mitochondrially localised GR (Psarra and Sekeris, 2011). The largest upregulation of overlapping DEGs in both *grs357* and *MR46Del* was *zbtb20*, a zinc finger binding domain that regulates developmental neurogenesis. The

few DEGs that were downregulated in both gr^{s357} and MR^{46Del} larval transcriptomes were associated with Rho signalling and focal adhesions. However, *hsp90aa1.1*, the chaperone protein important for both MR and GR signalling, was also identified as significantly downregulated in both gr^{s357} and MR^{46Del} larval transcriptomes.
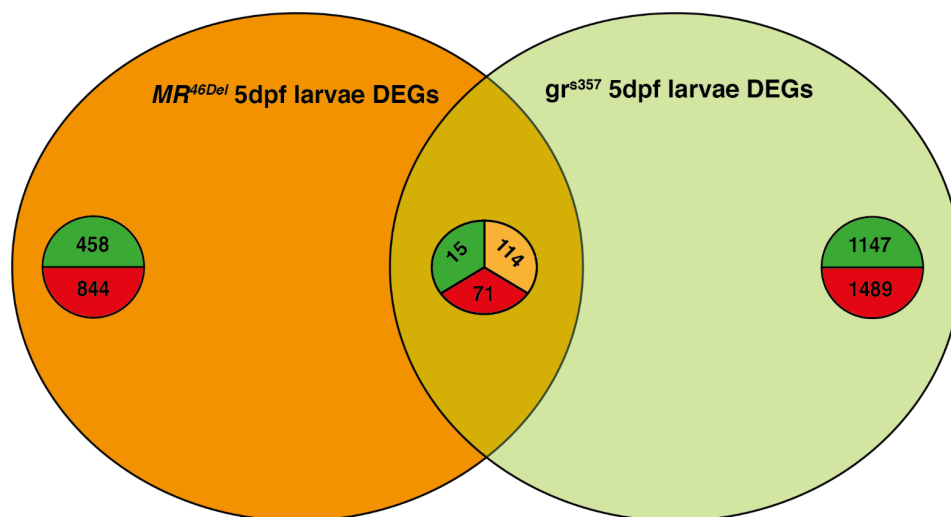
Figure 5.19. Venn diagram of differentially expressed genes in the transcriptomes of both gr^{s357} and MR^{46Del}. Number of genes upregulated are highlighted in green, downregulated in red, and alternative expression direction in orange.

Table 5.10. Venn diagram results of differentially expressed genes in the transcriptomes of both gr^{s357} and MR^{46Del}. Number of genes upregulated are highlighted in green, downregulated in red, and alternative expression direction in orange.

Gene name	GR Fold change	MR Fold change	Trend
abcc2	1.93456551	1.50351948	UP
ace2	2.05950783	1.58412904	UP
acsl5	1.73644186	1.6813979	UP
AL831745.1	2.00110498	1.919613	UP
anxa2b	1.70294253	1.76113707	UP
aoc1	2.21051909	1.59272889	UP
aqp8a.2	2.73434866	2.17447166	UP
asah2	1.73582712	1.52858082	UP
C1H4orf33	2.17206856	1.82332277	UP
CABZ01079192.1	2.66116982	1.82906886	UP
cd36	1.72601724	1.64741672	UP
cldn15a	1.99192303	1.85114536	UP
cldn15la	3.16364576	1.78344956	UP
cpo	3.09229053	1.8040565	UP
CR383676.2	2.90026578	2.50898403	UP
cyp2k18	3.57849304	2.33418345	UP
cyp2p8	2.45834884	1.59601052	UP
cyp3a65	2.33965979	1.66079687	UP
dhrs13l1	2.41046297	2.50843362	UP
fam133b	2.57260526	1.83088866	UP
gch2	1.62039484	1.5117981	UP
lrrc59	1.86287707	1.59400111	UP
med19a	2.18850049	1.5374353	UP
mgst2	2.50935134	1.71727504	UP
mgst3b	1.56946483	1.8151685	UP
mt-atp6	2.86913284	2.22976811	UP
mt-atp8	2.9026174	2.2693809	UP
mt-co1	2.30667287	2.11627413	UP
mt-co2	2.5183222	2.14984205	UP
mt-co3	2.54233954	2.1589955	UP
mt-cyb	2.32617968	2.23295062	UP
mt-nd1	2.41891112	2.20685699	UP
mt-nd2	2.53801121	2.16454139	UP
mt-nd3	2.75168457	2.30731603	UP
mt-nd4	2.61670607	2.03233503	UP
mt-nd4l	2.43683587	2.02110437	UP
mt-nd5	2.21471057	2.09382705	UP
mt-nd6	2.94901939	2.15154627	UP
muc13b	2.46144327	2.00691262	UP
NC_002333.17	3.23420852	2.42040199	UP
NC_002333.24	2.43205206	2.72337745	UP
NC_002333.9	3.52203596	2.37615422	UP
pla2g12b	2.0447628	1.79780946	UP
pon1	2.4940408	2.01575186	UP
ppp1r14aa	1.60491142	1.56961298	UP
prozb	3.67235691	2.24061408	UP
psma6l	2.210906	2.36891147	UP
rnf34a	1.64557377	2.14093537	UP
scarb1	1.6871225	2.14559276	UP
scg5	2.55480514	2.28603495	UP
sec62	2.04549874	1.50727275	UP
si:ch211-117h7.7	1.75922777	1.61660957	UP
si:ch211-133l5.7	1.75674388	1.95309501	UP
si:ch73-248e21.1	1.79158732	1.65521024	UP
slc15a1a	1.94564118	1.84179886	UP
slc35b4	1.61267452	1.71844417	UP
slc7a7	1.76893812	1.62947312	UP
snx6	2.18012811	1.72157621	UP
stoml3b	1.92093668	2.0866807	UP
stxbp6l	2.00297646	1.63697561	UP
tm4sf4	2.46385819	1.82196607	UP
tmprss15	3.44358745	1.68578663	UP
tmsb4x	1.50663233	1.5441812	UP
tnks1bp1	3.04345323	1.6219429	UP
ugt1a1	2.84823253	1.89767426	UP
ugt2a4	2.71640009	1.66674574	UP
ugt5b2	2.32632872	2.35619848	UP
zbtb20	3.07799294	4.1688258	UP
zgc:136472	2.75108917	2.31480142	UP
zgc:153896	2.7573782	2.0744282	UP
zgc:174935	1.716456	1.78020209	UP

Gene name	GR Fold change	MR Fold change	Trend
thbs3b	0.17677043	0.61395464	DOWN
hsp90aa1.1	0.20292099	0.51605611	DOWN
adgrd2	0.26602976	0.62530714	DOWN
unc45b	0.32970148	0.55087915	DOWN
aglb	0.32980859	0.4659109	DOWN
smyd2b	0.40488673	0.57210042	DOWN
cdk5	0.41527896	0.65702384	DOWN
sema3c	0.41596048	0.65794879	DOWN
myhz1.3	0.41769892	0.31388984	DOWN
mri1	0.44516501	0.60514436	DOWN
svilc	0.48666792	0.56057364	DOWN
arhgap33	0.50767975	0.63626687	DOWN
rhobtb2b	0.52686493	0.65018445	DOWN
slc6a15	0.52746951	0.57839743	DOWN
actn3a	0.59358142	0.48980343	DOWN

Gene name	GR Fold change	MR Fold change	Trend
apoa4b.2	0.49111278	2.09486726	Change
apoeb	0.60605174	1.67610895	Change
b3gnt7l	0.49432412	1.73585416	Change
BX248331.2	0.32453865	1.73110471	Change
BX322618.1	0.07211564	2.44266171	Change
caspb	0.43413183	2.15762494	Change
ckba	0.50102787	1.59936231	Change
cldn1	0.32524406	1.69454502	Change
clec3ba	0.25646652	2.41398748	Change
CR753876.1	0.11281616	1.78945279	Change
CR855277.2	0.00236937	4.16119297	Change
crip1	0.4344383	1.82001927	Change
ctsla	0.64517045	1.51719479	Change
cyp1c2	0.27662129	1.75718517	Change
cyp2r1	0.08776327	1.58944639	Change
dusp1	0.61359133	1.71744117	Change
f3b	0.49011107	1.65606315	Change
fbp2	0.1692908	1.82064982	Change
foxq1b	0.29649069	1.91871467	Change
g6pca.2	0.35235153	1.63019874	Change
gstp2	0.19819524	2.05265876	Change
hsd20b2	0.44839724	1.57196702	Change
hsp70l	0.18678315	1.76475244	Change
ifitm1	0.32706165	1.71548673	Change
il13ra2	0.38111027	1.63984232	Change
il13ra2	0.42973777	1.5193413	Change
mylk5	0.50292077	1.52185022	Change
nfkbiaa	0.46465239	1.86286977	Change
oaz2b	0.41343038	1.95672705	Change
papss2a	0.497251	1.56615184	Change
plac8.1	0.47482763	2.27953644	Change
rab13	0.60975121	1.51351222	Change
rbp4	0.33046354	1.55268047	Change
rhcga	0.09528243	2.27496792	Change
rhcgl1	0.01848864	2.17301681	Change
sat1b	0.44479688	1.59235379	Change
sb:cb1058	0.46038472	1.66017401	Change
sh3d21	0.40931792	1.50124218	Change
si:ch211-106h4.12	0.28625951	1.81640073	Change
si:dkey-4e7.3	0.51381095	1.65666268	Change
si:dkey-73p2.3	0.03481436	2.0954692	Change
si:dkey-7c18.24	0.29150563	3.49128667	Change
si:dkey-85k7.7	0.52796661	1.50558284	Change
si:dkeyp-1h4.6	0.1976097	2.74992662	Change
slc13a3	0.30612911	1.50638295	Change
slc22a7b.1	0.29731746	1.61486222	Change
smim14	0.64631071	1.80903474	Change
socs3a	0.26637369	3.11257121	Change
sostdc1a	0.30644643	1.78913937	Change
spam1	0.30267821	1.60536001	Change
star	0.37794927	2.00082939	Change
sult1st1	0.40454324	1.58337285	Change
sult1st3	0.42495888	1.95526809	Change
tnfaip8l2b	0.29319151	1.49531089	Change
tpm4a	0.55011241	1.49927204	Change
tsc22d3	0.08223874	1.74293936	Change
ucp2	0.15244645	1.5195766	Change
urahb	0.30898551	2.27301879	Change
wbp1lb	0.2993502	1.50548341	Change
zgc:162730	0.54166472	1.66743147	Change
zgc:195173	0.41221761	1.5661777	Change
abrab	2.3169587	0.41610927	Change
adam22	3.12124236	0.55977261	Change
ARHGAP22	4.26489587	0.42547883	Change
CABZ01088308.1	2.83823219	0.53391924	Change
cacna1c	2.05420787	0.56957588	Change
CDK18	1.93658843	0.66211337	Change
celsr3	2.30419363	0.58901284	Change
citb	2.13276105	0.61065963	Change
clvs2	2.14854333	0.46492861	Change
cntn2	1.82924569	0.52280679	Change
CR381531.2	2.4619248	0.48750305	Change
csmd2	1.90708427	0.57112263	Change
dab2ipa	2.84892095	0.63467451	Change
dscama	2.05256913	0.64496846	Change
elovl4a	2.00866639	0.6115752	Change
erc2	2.1007071	0.53175121	Change
fam131bb	2.18478241	0.6656361	Change
fam161b	2.30511887	0.60960072	Change
fynb	2.12546475	0.65084266	Change
grm4	2.4431254	0.62546872	Change
ica1	2.36760091	0.66822235	Change
kcnd3	2.37029034	0.56451766	Change
kif3ca	1.96032516	0.54147497	Change
kif5ba	1.85466282	0.63945651	Change
lhx2b	2.1403953	0.60889346	Change
mafaa	1.88171729	0.66583779	Change
MAPK8IP1	1.90136648	0.61319976	Change
mtus2a	2.15935118	0.55130081	Change
myo16	2.17489668	0.51572424	Change
neto1l	2.05405396	0.53196919	Change
neto2b	1.82777789	0.62419509	Change
NRXN2	2.31689382	0.47815942	Change
pacsin1a	2.29912814	0.60474126	Change
pcdh1g22	3.75709356	0.35808968	Change
pcdh1gc6	2.00858796	0.49267754	Change
ppp2r2ca	1.98025107	0.50804497	Change
rims1b	2.05546729	0.65043183	Change
scn2b	4.3261974	0.5690803	Change
sez6l2	2.10591616	0.45557152	Change
shank1	2.78255427	0.54403742	Change
si:ch211-113g11.6	1.95005864	0.62919322	Change
si:ch73-290k24.6	2.22259576	0.56224776	Change
slc8a1b	2.07365975	0.56844533	Change
slco5a1a	2.61386139	0.63301895	Change
smc1a	2.47369628	0.42225495	Change
spock2	1.82302557	0.64513364	Change
spon1a	3.58926902	0.61509038	Change
SRCIN1	1.902655	0.56071797	Change
TRAPPC9	1.89107505	0.63307962	Change
trim46a	2.23771793	0.49821327	Change
ttbk1b	2.27234229	0.58035321	Change
unc5da	2.03473239	0.62942518	Change
znf362b	1.63462747	0.6333888	Change

5.3. Discussion

This chapter describes the results of an experiment to explore further the molecular mechanisms affected by glucocorticoid resistance in whole zebrafish larvae. The transcriptomes of whole *gr^s357* 5dpf larvae were compared to those of their wild-type larval siblings.

Initial quality control assessment of 5dpf larvae mRNA sequencing data identified an outlier sample, GR4, labelled *gr^s357*, which had a similar profile to those of *gr^wt* samples (Figure 5.2). Through multiple means of evidence, including PCA, heatmap hierarchical clustering, dendrogram clustering and sequencing read depth I have demonstrated that that GR4 has the same characteristics as WTTL samples, and is therefore incorrectly labelled. After the removal of the GR4 outlier, 5dpf larvae mRNA samples displayed a clear segregation between genotypes in the first principal component. A similar segregation was seen between genotypes in the first principal component in adult brain mRNA samples. Differential expression analysis results of both 5dpf *gr^s357* larvae and adult *gr^s357* brains identified common GR-target genes previously described in the literature, including *fkbp5*, *pck1*, *tsc22d3* and *klf9* (Chinenov et al., 2014). The identification of well-characterised glucocorticoid-responsive genes as DEGs confirms the efficient data analysis and accurate representation of the effects of this GR mutation in zebrafish.

Previously, *fkbp5* has been well-characterised as a direct GR-target gene that is inducible by glucocorticoid treatment of zebrafish larvae (Marchi et al., 2020). In chapter 2, *fkbp5* was shown to be upregulated in the hypercortisolaemic *MR^46Del* mutant. My results identified *fkbp5* as the most significant DEG in *gr^s357* larval transcriptomic analysis, exhibiting almost complete extinction of gene expression in *gr^s357* mutant larvae. These results are supported by previous research in glucocorticoid-deficient or glucocorticoid-resistant mutant zebrafish, which exhibit a significant reduction in *fkbp5* mRNA expression (Eachus et al., 2017b; Marchi et al., 2020), and build on existing evidence that *fkbp5* is a direct GR-target gene; its expression is near-extinct in *gr^s357* mutants, yet upregulated in the hypercortisolaemic *MR^46Del* mutant I generated. Previous research has demonstrated that FKBP5 acts as a short negative feedback loop on the GR, partially regulating its sensitivity (Binder, 2009). FKBP5 is a co-chaperone of HSP90, and when bound to the GR protein, it alters the conformation of the GR protein and reduces its sensitivity to cortisol through lowering its affinity for cortisol, thereby reducing the efficiency of GR translocation to the nucleus in response to cortisol (Binder, 2009). It is beyond the scope of this study to investigate the function of GR-fkbp5 regulation, but it would be intriguing to inhibit Fkpb5 protein pharmacologically in *gr^s357* and *gr^wt* to investigate GR sensitivity to exogenous cortisol treatment, i.e. SAFit1 and SAFit2 (Gaali et al., 2015). Interestingly, the gene which encodes HSP90, *hsp90aa1.1*, was significantly downregulated in both MR and GR mutants.

Another gene of interest, *klf9*, was identified as a highly significant DEG in *gr^s357* larvae. *Klf9* was severely downregulated in *gr^s357* mutants compared to wildtype controls. These results build on the evidence that *klf9* expression is regulated by glucocorticoid signalling, upregulated with cortisol treatment and suppressed with GR-loss of function in 5dpf zebrafish larvae (Gans et al., 2020). In this study, *klf9^-/-* mutant zebrafish larvae were shown to downregulate glucocorticoid-induced genes relating to the immune response, endopeptidase activity and ammonium transport (Gans et al., 2020). All of these processes were identified during the gene ontology analysis in zebrafish larvae, building on the evidence that *klf9* is important in GR-dependent signalling for a multitude of biological processes (Gans et al., 2020).

The loss of GR function in the *gr^s357* 5dpf larvae resulted in the downregulation of genes that are linked to GO terms such as ECM organisation, cell-surface receptor signalling and biological cell adhesion. Genes encoding multiple ECM components such as collagens, laminins and myosin were downregulated in *gr^s357* mutant larvae. In addition, genes associated with ECM metabolism such as numerous matrix metallopeptidases were downregulated in *gr^s357* mutants. These downregulated components, alongside various downregulated transmembrane glycoproteins, are important for cell-ECM interactions. Previous research leads to some controversy around the role of glucocorticoid signaling and ECM regulation, with most studies demonstrating that exogenous cortisol treatment decreases collagen synthesis. For example, dexamethasone treatment of human fibroblasts decreased TGF-ß-induced collagen synthesis (Zhou et al., 2011). Moreover, dexamethasone treatment of rats resulted in reduced expression of collagen type I and III in rat dorsal skin (Oishi et al., 2002), and betamethasone treatment of human skin decreased expression of collagen I and III levels and expression (Oikarinen et al., 1998). By contrast, dexamethasone treatment on bovine trabecular meshwork (TM) cells increased collagen type IV and fibronectin levels (Zhou et al., 1998). The presented data suggests that the GR positively regulates ECM organisation in zebrafish larvae, since loss of GR DNA-binding function, decreased expression of ECM-associated genes. This finding is supported by previous studies of the pharmacological GR antagonist treatment with mifepristone, in which mifepristone treatment inhibited progesterone-induced collagen synthesis *in vitro* in leiomyoma cells (Patel et al., 2016) and *in vitro* in human cervical tissue (Bokström and Norström, 1995).

The interaction between cells and their surrounding ECM occurs primarily through focal adhesions, which regulate the actin cytoskeleton and are important for cell migration. Interestingly, both focal adhesions and actin cytoskeleton regulation were identified as two significant enriched KEGG pathways in the population of downregulated DEGs in *gr^s357* larvae. In

gr^s357 mutant larvae, genes encoding scaffold components of basement membranes and ECM components that are ligands for cell receptor adhesion were downregulated. This includes genes encoding multiple laminins, fibronectin, fibrillin and thrombospondins. Similarly, many integrins, the principal cellular receptors of ECM ligands, were downregulated in *gr^s357* mutant larvae. Integrins are responsible for intracellular signalling to regulate cellular shape, mobility and mediate the interaction between the ECM and the cytoskeleton (Huttenlocher and Horwitz, 2011; Vicente-Manzanares et al., 2009). Not only were numerous ECM ligands and integrin receptors downregulated, downstream Rho signalling pathways that regulate actin cytoskeleton polymerisation, such as the Rho effector *rock2a*, were also downregulated in *gr^s357* mutant larvae. In line with these findings, previous research in human lung carcinoma cells *in vitro* has identified direct GR-target genes that encode proteins which regulate the properties of actin filaments, such as Caldesmon (Mayanagi et al., 2008). In my results, Caldesmon (*cald1b*) was significantly upregulated in *gr^s357* larvae, suggesting a role for GR in transcriptional repression of this gene. Further studies have shown that dexamethasone treatment stabilises the synaptic F-actin cytoskeleton in hippocampal neurons (Yang et al., 2019, 2020). Likewise, components of the Wnt signalling planar cell polarity pathway, which also regulate the actin cytoskeleton (Skoglund and Keller, 2010), was highlighted as significantly enriched in genes that were downregulated in *gr^s357* mutant larvae. Wnt ligands, respective frizzled and LRP receptors, and downstream Wnt signalling genes *dishevelled* and *rock2*, were all downregulated in *gr^s357* larvae. Thus, my results build on the existing evidence that GR regulates the actin cytoskeleton and organisation of the ECM, and show that a loss of DNA-binding function of the GR results in a generalised reduction in ECM and actin cytoskeleton-associated gene expression, potentially through direct GR-DNA binding or through intermediate pathways such Wnt signaling. It is unlikely to be due to the resulting hypercortisolaemia, as these GO enriched genes were not differentially expressed in our hypercortisolaemic *MR^46Del* mutant transcriptome.

Other cell receptor signalling pathways were highlighted as significantly enriched in genes downregulated in *gr^s357* mutant larvae, including members of the transforming growth factor-β (TGF-β) superfamily, including TGF-β isoforms, activins and bone morphogenetic proteins (BMPs). Members of this ligand-superfamily are responsible for cell growth, cell differentiation and death, as well as other important developmental processes (Weiss and Attisano, 2013). Multiple BMP, TGF-β and insulin-like growth factors were downregulated in *gr^s357* larvae. These ligands bind to serine/threonine kinase receptors on the cell membranes and induce TGF-β/Smad signalling. These results build on existing evidence that there is crosstalk between glucocorticoid signalling and TGF-β signalling, previously shown to be mediated by Gilz (glucocorticoid induced leucine zipper; *tsc22d3*) (Bereshchenko et al., 2014). Interestingly,

tsc22d3, which encodes the Gilz protein*,* was the second most significantly downregulated gene after *fkbp5* in my *gr^s357* mutant larvae. Multiple genes encoding SMADs and other -TGF-β-induced target genes were downregulated in *gr^s357* larvae. My results suggest glucocorticoid-resistance leads to a dysregulation of TGF-β superfamily ligand signalling, which may be mediated potentially through the previously recognised transcription factor protein, Tsc22d3.

One important biological process regulated by TGF-β and glucocorticoid signalling is the immune response to infectious pathogens. In the *gr^s357* larval transcriptomic analysis, a significant enrichment of genes associated with the immune response were downregulated in *gr^s357* mutants. These included cytokine factors, interleukins, toll-like receptor, and genes associated with the inflammasome. My results indicate that GR signalling is important for immune responses and systemic cell signalling, primarily through cytokine signalling. Current understanding suggests that beneficial glucocorticoid-induced anti-inflammatory action is achieved through GR-mediated transrepression (De Bosscher et al., 2010), yet many anti-inflammatory genes require direct transactivation, such as *gilz* (*tsc22d3*) (Riccardi, 2015) or indirect activation such as the Stat6-regulated *inhibitor kappa B-alpha* genes(*nfkbiaa*, *nfkbiab*) (Nelson et al., 2003), all of which were significantly downregulated in *gr^s357* mutants. Understanding what immune responses are regulated via GR-mediated transrepression may be beyond the scope of this study, as this GR mutation does not inhibit ligand binding in the cytosol, or other transcription factor binding to DNA, rather it appears to solely impede its own binding to DNA. However, a protein that is usually subject to transrepression by the GR is NFκB *(nfkb2)*, which was identified as a significant downregulated DEG in our *gr^s357* mutants zebrafish. *Nfkb2^{-/-}* mice exhibit various immune defects e.g. decreased B-lymphocyte maturation and impaired T-cell function (Beinke and Ley, 2004). As such, regulation of this gene may differ between mammals and zebrafish. Further studies utilising one of the many GR functional knock-out models may provide further insights into the role of the GR in systemic immune responses. Nevertheless, the results presented here provide an insight into the immune response-related genes that are regulated by the GR, for both pro- and anti-inflammatory responses.

Surprisingly, despite a near symmetrical distribution of up- and downregulated genes in my differential expression analysis of the *gr^s357* mutant larvae transcriptome, no specific GO, KEGG or Reactome pathway terms relating to Biological Process or Molecular Function were identified in the upregulated population of DEGs, within my original criteria. Yet interestingly, the majority of genes identified in the population of upregulated DEGs in *gr^s357* larvae were associated with cellular components located in neurons and axons. This included genes associated with GABA and glutamate signalling in synapses, synapse scaffolds important for neurotransmitter release, and

neuronal development, including axon guidance, migration and growth. My results suggest that either increased circulating cortisol concentrations in gr^{s357} mutant larvae, or impaired GR signaling has increased neurogenesis and/or neuronal signaling during development. However, based on the findings that chronic cortisol treatment on mice reduces neurogenesis in the hippocampus (Sawamoto et al., 2016), it is more plausible that loss of GR function is directly responsible for increased expression of neurogenesis and signaling, or alternatively that elevated cortisol enhances neuronal gene expression by acting via the MR. Interestingly, in the MR^{46Del} transcriptome, neuron-specific gene expression was significantly decreased, strongly suggesting that elevated cortisol enhances neuronal gene expression by acting via the MR in zebrafish larvae.

Previous literature studying the effects of cortisol on neuronal signalling provide a wide range of outcomes, dependent on the type and duration of stress, area in the brain studied and the model used, i.e. chronic cortisol treatment on mice reduced neurogenesis in the hippocampus (Sawamoto et al., 2016); acute behavioural stress on rats lead to increased cortisol concentrations and a significant potentiation of glutamate receptor surface expression and excitatory synaptic currents (Yuen et al., 2009); and psychosocial stress on humans found no correlation with GABA and glutamate levels in vivo (Houtepen et al., 2017). Despite this, the widely accepted theory is that acute stress rapidly increases glutamate release from the presynaptic membrane (Popoli et al., 2012). GR and MR-downstream mechanisms regulating this release are unknown. It has been shown that this increased acute stress-induced glutamatergic signalling is through both genomic and rapid non-genomic pathways, with both MR and GR identified in the cytoplasm and the synapse terminal (Popoli et al., 2012). However, as the gr^{s357} mutation results in a missense mutation in the DBD, this may be a restrictive model to study the role of membrane-bound GR in non-genomic signalling. To conclude, my results suggest that the MR is required for transcriptional activation of synapse-associated genes, whereas in the hypercortisolaemic gr^{s357} mutants, cortisol is likely to induce neuronal gene transcription by activating the MR.

Through transcriptomic and functional analysis of loss of MR or GR function, I have highlighted their important roles in maintaining a functional HPI axis, which, when lost, results in HPI hyperactivation and resulting hypercortisolaemia. Both mutants have exhibited opposing dysregulation of genes encoding neuron-specific components, specifically genes associated with glutamatergic and GABAergic synaptic signalling. Together, this strongly suggests that elevated cortisol enhances neuronal gene expression by acting via the MR in zebrafish larvae.

Early life stress is known to influence the development of the HPA axis, neural networks, cognitive function and is strongly correlated with later life occurrence of major depressive disorder, anxiety disorders and PTSD (Heim et al., 2010; Kessler et al., 1997, 2010). Similarly, reduced *gr* transcription and GR function in the brain correlates with childhood abuse and depression (McGowan et al., 2009) and rats deprived of postnatal maternal care (Weaver et al., 2006). Likewise, the genetic disorder Chrousos Syndrome that encodes gr inactivation is characterised by hypercortisolaemia, chronic fatigue, anxiety and depression (Charmandari et al., 2013). Many aspects of the molecular mechanisms through which the GR regulates genomic targets in the adult brain, and the impact of chronic stress from early development, have not yet been elucidated. In order to obtain new insights into the impacts of GR function on the vertebrate brain, I investigated the impact of the *gr^s357* mutation on the transcriptome of eighteen-month-old adult zebrafish brains.

Chapter 6. Defining the implications of chronic glucocorticoid-resistance on the adult brain transcriptome in gr^{s357} mutant zebrafish.

6.1 Introduction

Glucocorticoids are fundamental elements of the neuroendocrine system, modulating adaptive physiology and behaviour in response to interactions between an organism and its environment. The brain is a prominent target of glucocorticoids, acting through either the MR or GR, whose expression is variable throughout different regions of the brain (Viho et al., 2019). Glucocorticoids have a pleiotropic effect on the brain, influencing behaviour, energy regulation, cognition, memory, learning, and the stress response. This provides a multifaceted approach to adapting to demands of stressors (Fietta and Fietta, 2007; Kino, 2015). On a cellular level, glucocorticoids are important for neuronal development and growth, synaptic signaling and motor control (Fietta et al., 2009; Liston and Gan, 2011). However, there are distinct differences between acute and chronic glucocorticoid treatment on stress paradigms and neural circuits such as dendritic remodelling (Magariños et al., 1996; Mitra and Sapolsky, 2008; Radley et al., 2006; Wellman, 2001; Yang et al., 2020). To unravel the molecular mechanisms regulated by GR in the vertebrate brain, I carried out a comparative transcriptome analysis of brains of age-matched sibling gr^{wt} and gr^{s357} adult male zebrafish.

Previously, an adult behavioural phenotype was also reported in gr^{s357} mutants. Homozygous gr^{s357} mutants displayed reduced swimming activity, periods of 'freezing'/immobility and reduced exploratory behaviour when placed in a novel tank (Ziv et al., 2013). Whether this is due to metabolic dysfunction, glucose availability, or changes in neural or endocrine signalling is yet to be determined. However, these results pose an interesting question: Does the GR have a role in zebrafish behaviour, and if so, what changes in the brain result in these abnormalities? In mammalian models, it is well known that corticosteroids are potent modulators of neurons and other brain cells. There are many examples of glucocorticoids influencing brain function, such as altered pain sensitivity with glucocorticoid treatment (Pinto-Ribeiro et al., 2009), and Cushing's disease, where there is a pathological increase in circulating cortisol, and patients present with neuropsychiatric disturbances and neurocognitive deficits (Chen et al., 2013; Feelders et al., 2012). Moreover, abundant expression of GR and MR is seen throughout different cell types in the mammalian brain, including the hypothalamus, amygdala and hippocampus, indicating an important role for corticosteroid signaling (Meijer et al., 2019). In our lab, we have confirmed previously reported behavioural changes in locomotion using the zebrafish model (i.e reduced swimming speed) and thigmotaxis in adult gr^{s357} mutants (Eachus, unpublished). These changes

indicate a difference in neural and endocrine signalling in adult gr^{s357} mutant zebrafish compared to their wild-type siblings. As GR is highly expressed in the brain, the gr^{s357} mutant can be utilised to understand which neural molecular pathways are regulated through identifying GR genomic targets in the adult zebrafish brain.

To understand further the brain-specific role of the GR in the zebrafish, mRNA sequencing of age-matched gr^{s357} and gr^{wt} adult brains was performed. This approach aimed to identify transcriptomic changes caused by a loss of GR signalling, and thus determine which brain-specific functions are regulated by the GR. In addition, I took advantage of the opportunity to perform a comparative analysis of GR function in zebrafish 5dpf larvae and in adult brain, by comparing the differentially expressed genes in these tissues of wild-type and gr^{s357} homozygous mutants.

6.2 Results

Understanding implications of glucocorticoid-resistance on adult brain transcriptomes in gr^{s357} mutant zebrafish.

Glucocorticoids have important effects on brain function and behaviour. As seen in my gr^{s357} mutant larval transcriptomic analysis, upregulated DEGs were associated with cellular components located in axons and neurons (Chapter 5). Similarly, in hypercortisolaemic MR^{46Del} mutants, both glutamatergic and GABAergic synaptic signaling was identified as upregulated in the 5dpf larval transcriptome (Chapter 4).

To investigate the role of GR-regulated transcription in the brain, we have performed RNA sequencing of the adult brain of both gr^{s357} and sibling gr^{wt} zebrafish. Initially, 18-month old male adult gr^{wt} and gr^{s357} sibling brains were dissected; RNA was extracted and quality assessment performed by student Dheemanth Subramanya. Library preparation and mRNA sequencing was performed by the Deep Sequencing Facility at Technische Universität, Dresden. RNAseq analysis from raw data processing to genome alignment and differential expression analysis was performed by myself.

However, one caveat was discovered post-dissection: the pituitary was not dissected out of the sphenoid, as such, pituitary-specific gene transcripts are not detected in my analysis. Nonetheless, glucocorticoids and the GR have been associated with neuronal and metabolic functions, as well as cognitive function such as behaviour. Thus, studying the brain transcriptome may provide novel insights into GR-regulation of the zebrafish adult brain.

6.2.1 Quality control and STAR alignment of gr^{wt} and gr^{s357} mutant adult zebrafish brain RNAseq samples

As before, to evaluate the quality of sequence reads, FastQC software was used before and after each sequence read manipulation (Andrews, 2010). Subsequent to rRNA removal and adaptor/quality trimming, FastQC revealed excellent sequence quality for gr^{wt} (WTTL) 1-4 and gr^{s357} mutant samples (GR) 1-4 (Figure 6.1). As with larval samples, all brain samples failed the per base sequence content as all samples showed biased base composition for the first 12bp of each read. However, as before, it is not thought to affect downstream analysis (Figure A22).

Samples were sequenced at a high depth 28-32million reads for exploratory transcriptomic analysis. Post-sequencing quality control processing resulted in a similar percentage reduction in total reads in all samples. Post-quality processing provided adequate read depth (27-31 million reads) for downstream transcriptomic analysis. Read alignment to the zebrafish reference genome (GRCz11) was performed by STAR and exhibit a mapped alignment of between 19-21 million reads to annotated genes (Tables A9&A10).
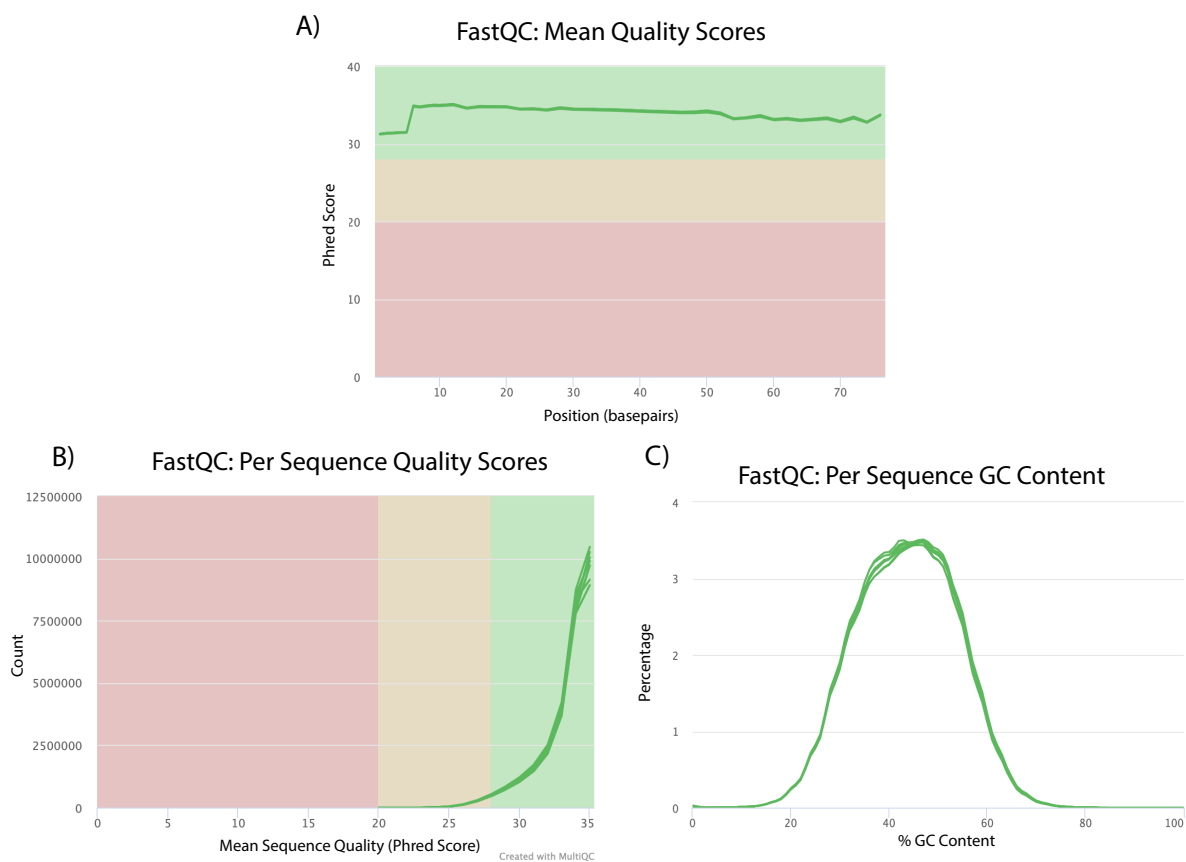
Figure 6.1. Quality control of RNA sequencing reads for gr^{s357} and gr^{wt} adult brain samples after preliminary processing. Sample quality control was performed using FastQC and visualised using MultiQC after initial processing using Trimmomatic software to trim adaptors and poor-quality reads, and, SortmeRNA software to remove rRNA reads that may be present. A&B) Quality scores indicate very high sequence quality with Phred scores above 30.**C)** Per sequence GC content indicates that all samples, are high quality.

6.2.2 Initial analysis of the differential transcriptomic profile resulting from the gr^{s357} mutation in adult zebrafish brains.

PCA analysis (Figure 6.2) revealed variation between the transcriptomic profiles of gr^{s357} mutants (GR) and gr^{wt} controls (WTTL), including substantial variation observed within the GR genotype. However, a clear segregation of samples with the two different genotypes was revealed in the first principal component that accounts for 40% of the total variation. However, the intra-group variation within the samples of GR genotype resulted in samples GR 1, 2 and 4 clustered together, with GR 3 distanced along the second principal component, which accounts for 36% of total variation. Despite sample GR3 displaying similar WTTL variation in the second principal component, the hierarchical clustering heatmap of normalised counts (Figure 6.2B) and dendrogram (Figure 6.3C) indicate GR3 does cluster closest with samples of GR genotype. Unlike in Chapters 4 and 5, library depth of all samples is relatively similar, and hierarchical clustering demonstrates segregation by genotype. As such, this represents the biological intra-group variation between samples and is more likely to provide more robust biologically relevant transcriptomic differences between genotypes.

As was done for the larval comparative analysis, differential expression analysis was performed on adult brain transcriptomes with a more stringent FDR value of 0.05 than DESeq2's default exploratory 0.1 FDR value. Unlike previous chapters, DESeq2 experimental overview by MA plot displays a predominant distribution of downregulated DEGs in gr^{s357} mutant brains (Figure A24). Dispersion estimates demonstrate that, as normalised count increases, intra-group variability was reduced; the plot resembles the typical dispersion pattern required for the use of the DESeq2 package (Figure A24) (Love et al., 2014b). Boxplots of the median log gene counts for each sample were plotted. All WTTL and GR samples exhibit similar library depth before DESeq2 normalisation and after (Figure 5.3A&B). Similarly, the size factor plot displays little variation between samples, as seen by the small range plotted on the x axis compared to previous chapters (Figure 5C).

As previously stated, to identify a statistically significant DEG, an adjusted p-value <0.05 was used as the threshold. This revealed a total of 1696 DEGs between gr^{s357} mutant and gr^{wt} adult brains. To provide a more robust list of DEGs, independent filtering was performed: a base mean of <40reads was filtered out, resulting in 1676 DEGs (Table 6.1). Independent filtering of 0.32<Log2FoldChange<-0.32 (~1.25 fold change) DEGs was used rather than previously used 0.58<Log2FoldChange<-0.58 (~1.5fold change), due to substantially less DEGs identified in brain transcriptomes in comparison to 5dpf larval transcriptomes previously analysed. Fold change

cutoffs are an arbitrary choice, dependent on the goals of an investigator. This less stringent threshold identified considerably more DEGs than the previously used cut off and will provide a more exploratory depth of transcriptomic analysis (Table 6.1). After independent filtering, 1059 DEGs were recognised in the adult male gr^{s357} neural transcriptome. Of these filtered DEGs, 438 were upregulated and 621 downregulated in gr^{s357} brains.

Table 6.1. Number of differentially expressed genes between gr^{s357} mutant and gr^{wt} adult brains filtered with false discovery rate, adjusted p-value (padj) and fold change threshold cut offs.

DESeq2 FDR Cutoff	padj cutoff	No. of Total DEGs	No. of DEGs with fold change > 1.25x	No. of DEGs with fold change > 1.5x
FDR alpha = 0.05	padj < 0.05	1696	1111 (460↑ + 641↓)	476 (174↑ + 302↓)
Independent Filtering	padj < 0.05	1676	1059 (438↑ + 621↓)	424 (152↑ + 272↓)

To explore the distribution of differentially expressed genes between the gr^{s357} mutant and gr^{wt} adult male brains, volcano plot and heatmap visual tools were utilised. The volcano plot visually displays a predominant downregulation of gene expression within the DEG list, of which also exhibit larger fold changes and higher significance values (Figure 6.4). In the volcano plot: 1059 genes are highlighted as red dots (0.32<Log2FoldChange<-0.32; padj<0.05), 585 genes are blue dots (-0.32<Log2Foldchange<0.32; padj<0.05), 1700 genes are green dots (0.32<Log2Foldchange<-0.32 pad>0.05), and finally, 13519 genes are plotted as grey dots (-0.32<Log2Foldchange<0.32; padj>0.05). The top significant DEGs are labelled, including the most significant DEG *fkbp5* (fold change=0.0214, padj=1.73E-229), *socs3a* (fold change=0.0821, padj=2.9E-176) and *oaz2b* (fold change=0.1688, padj=1.79E-98) (Figure 6.4).

Heatmaps display the top 30 most significant DEGs ordered; hierarchical clustering of samples confirmed genotype segregation (Figure 6.5A&B). Gene (row) hierarchical clustering was not performed to illustrate distribution of upregulated and downregulated DEGs. Only 1 upregulated DEG, *rxfp1* (fold change=3.4425, padj=3.46E-35), was present in the top 30 significant DEGs (Figure 6.5A). The second heatmap incorporates gene (row) hierarchical clustering (Figure 6.5B). DEGs *fkbp5* and *klf9* (fold change=0.0193, padj=1.65E-51) cluster together, as do *socs3a* and *oaz2b*. Plots of normalised gene counts for the top 5 significant DEGs (*fkbp5*, *socs3a*, *oaz2b*, *nfkbiab* and *cebpd*) and gene of interest *klf9*, demonstrate the significance of differential expression seen in the gr^{s357} (GR) mutants in comparison to gr^{wt} (WTTL) controls (Figure 6.6). Tables 5.2 and 5.3 present the top 20 DEGs by padj statistical significance and by foldchange.

The initial analysis of the differential transcriptomic profile resulting from the gr^{s357} mutation in adult zebrafish brains has revealed the glucocorticoid receptor's role as a transcriptional activator in the brain, indicated by the general downregulation of DEGs in gr^{s357} mutants. It has also revealed *fkbp5* as the most significant DEG, similar to gr^{s357} mutant 5dpf larvae. *Fkbp5* mRNA expression is ablated in both the adult male zebrafish brain and 5dpf larvae, suggesting strong GR regulation by genomic signaling. Similarly, *klf9*, *socs3a*, *hsd11b2*, and *tsc22d3* were initially recognised as significantly downregulated in both adult male brains and 5dpf larvae of gr^{s357} mutants. Therefore, this provides a basis in understanding which biological networks and molecular pathways are dysregulated in the gr^{s357} neural transcriptome and highlights the role the GR has in the adult zebrafish brain.
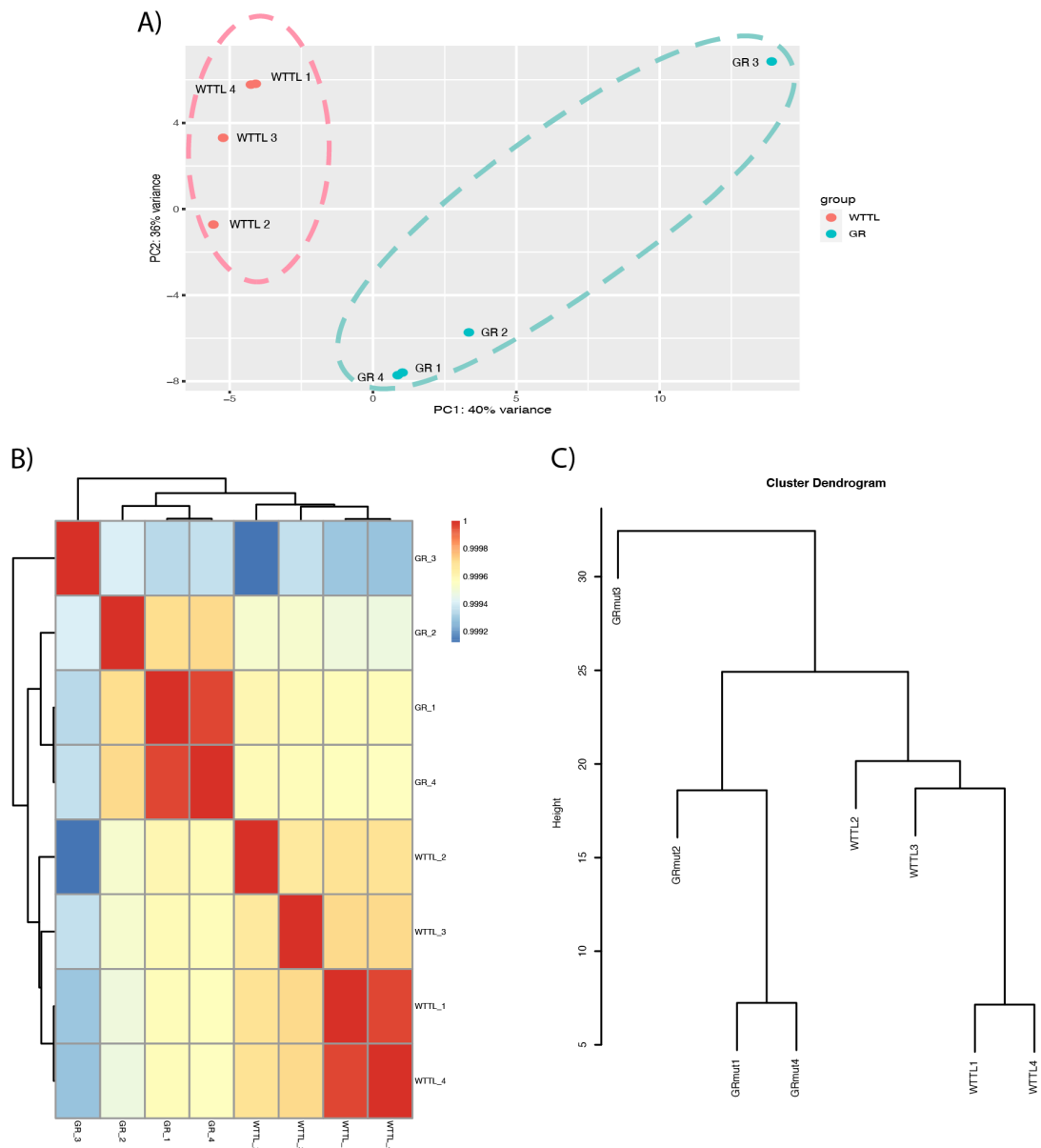
Figure 6.2. Principal component analysis and heatmap clustering reveals variation between *gr*^{s357} **mutant and** *gr*^{wt} **adult brain transcriptomes. A)** PCA (ntop=500): despite *gr*^{wt} samples not being highly clustered, *gr*^{s357} mutants were, and the two groups were segregated by the first principal component. **B)** Clustering heatmap generated from the same data.
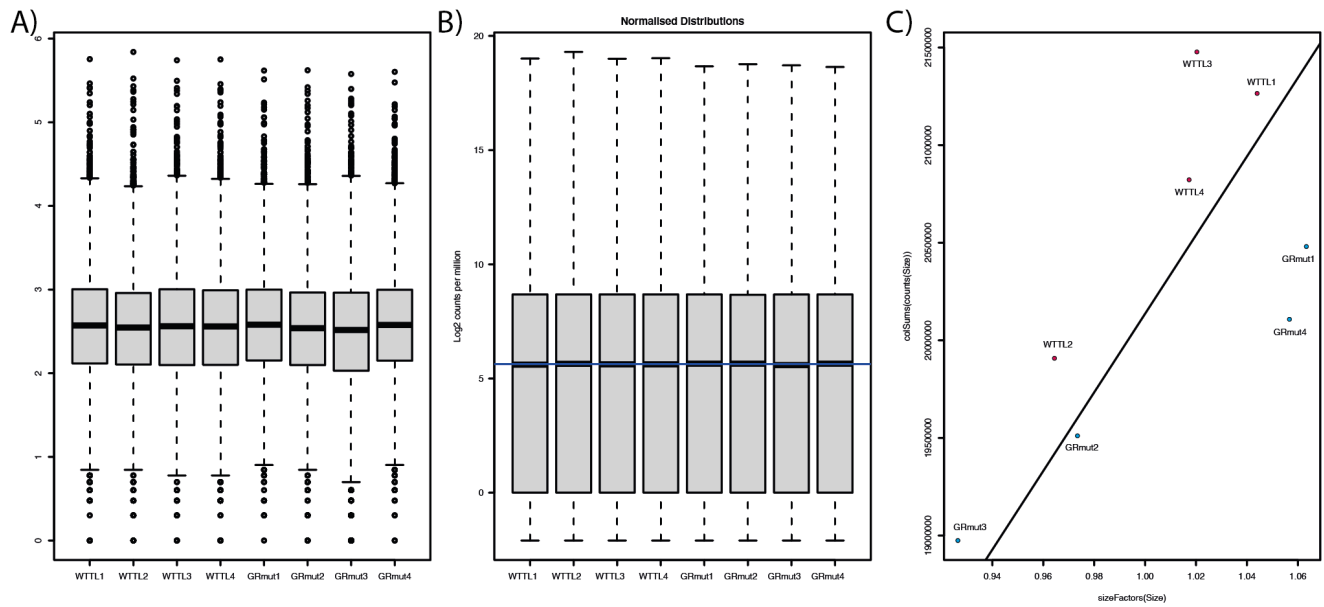
Figure 6.3. STAR alignment gene counts reveal similar library depths in *gr^wt* (WTTL) and *gr^s357* (GRmut) samples. A) Boxplot showing similar median raw counts and variability for each sample. B) Boxplot displaying DESeq2 normalised median library size, all samples are normalised appropriately. C) DESeq2 estimate size factor function presents low variability within all samples.
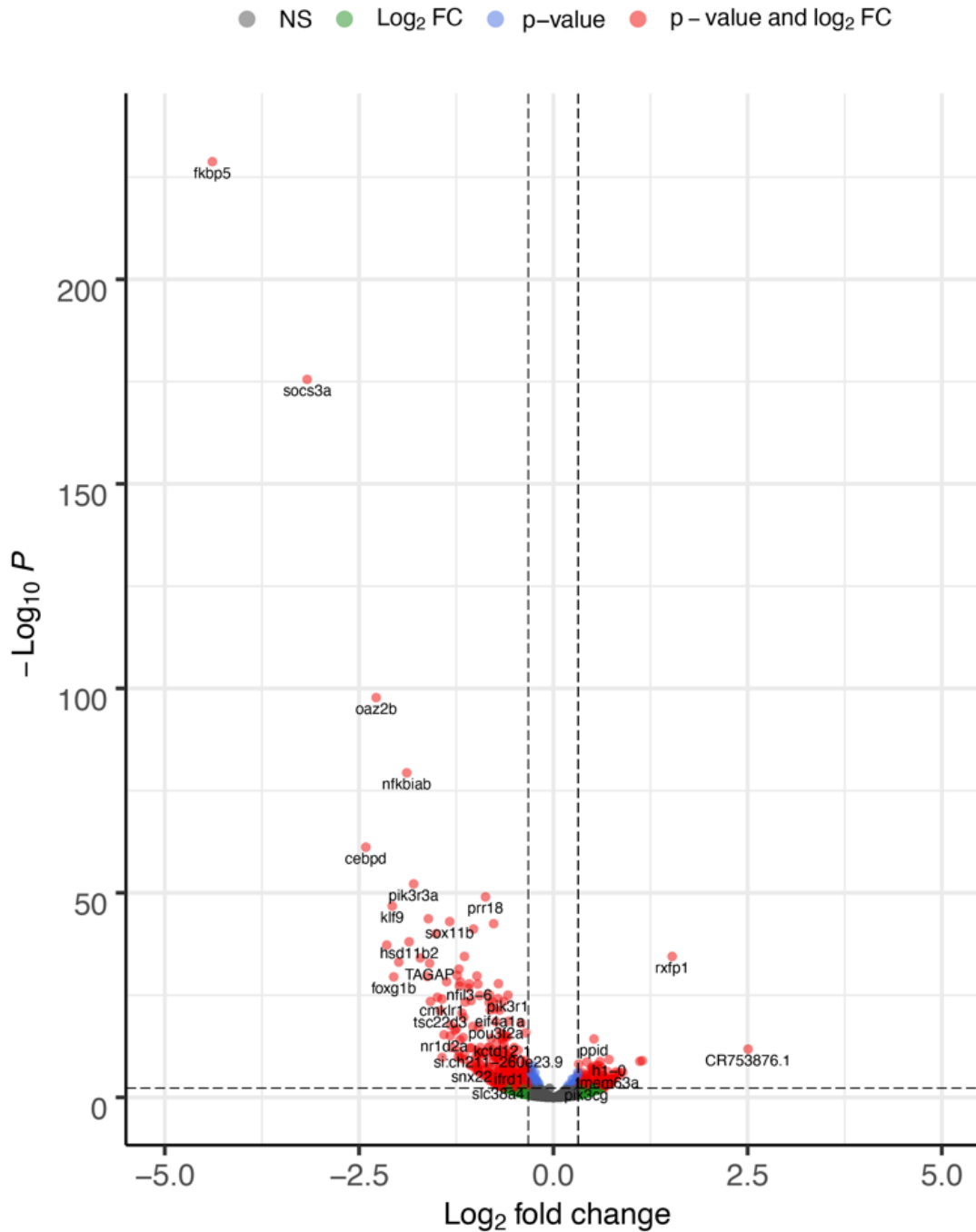
Figure 6.4. Volcano plot displaying predominantly asymmetrical distribution of significantly differentially expressed genes affected by the *gr^s357* mutation in adult male zebrafish brains. The statistical significance – padj values are plotted on the y axis against magnitude of differential expression – log2fold change. Dashed lines represent cutoff: 0.32<Log2FoldChange<-0.32, and, padj value < 0.05. Total of 32520 genes are plotted. Grey dots signify non-significant genes below Log2FoldChange threshold, green dots signify non-significant genes above Log2FoldChange threshold, blue dots signify significant genes with below Log2FoldChange threshold, red dots signify significant genes above Log2FoldChange threshold. Top DEGs are labelled.
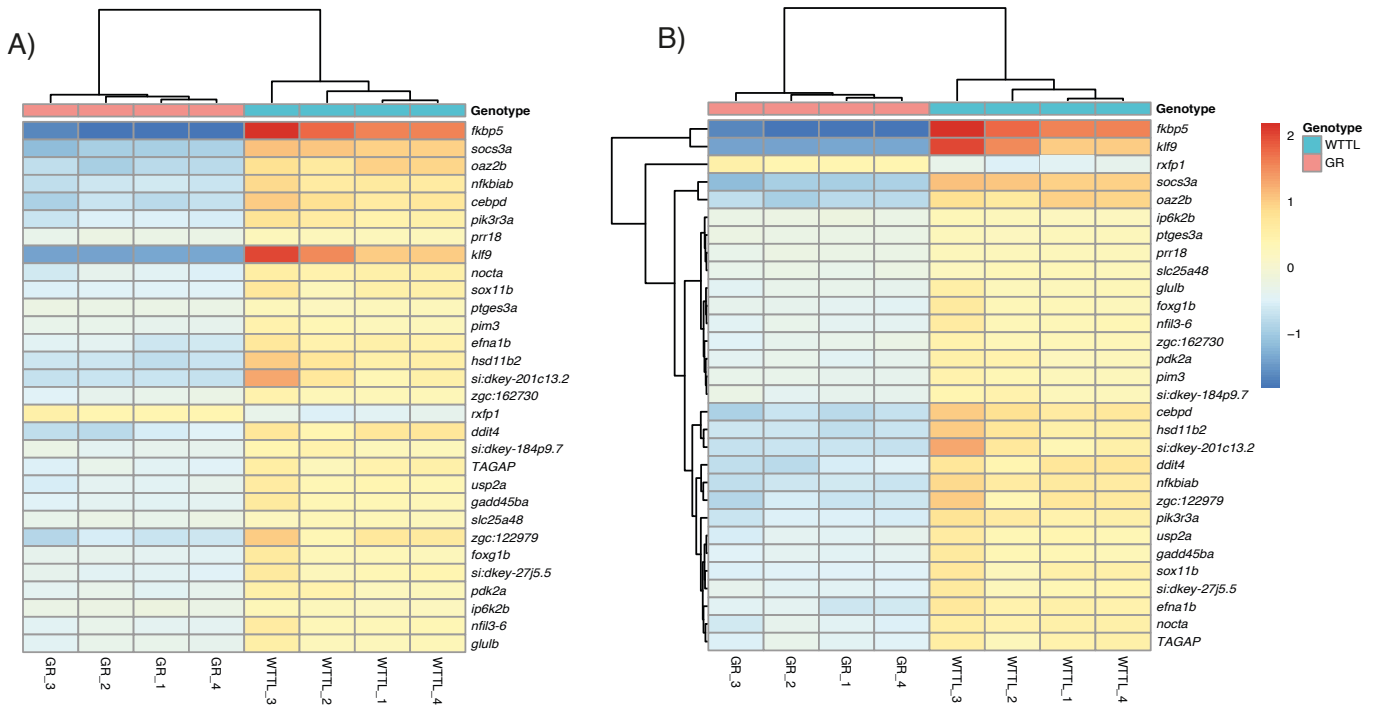
Figure 6.5. Top 30 most significant genes differentially expressed in adult brains of *gr^s357* **mutants compared to *gr^wt* siblings .** A) Heatmap with hierarchical clustering of samples (columns) only ordered by significance. B) Heatmap of hierarchical clustering of samples (columns) and genes (rows).
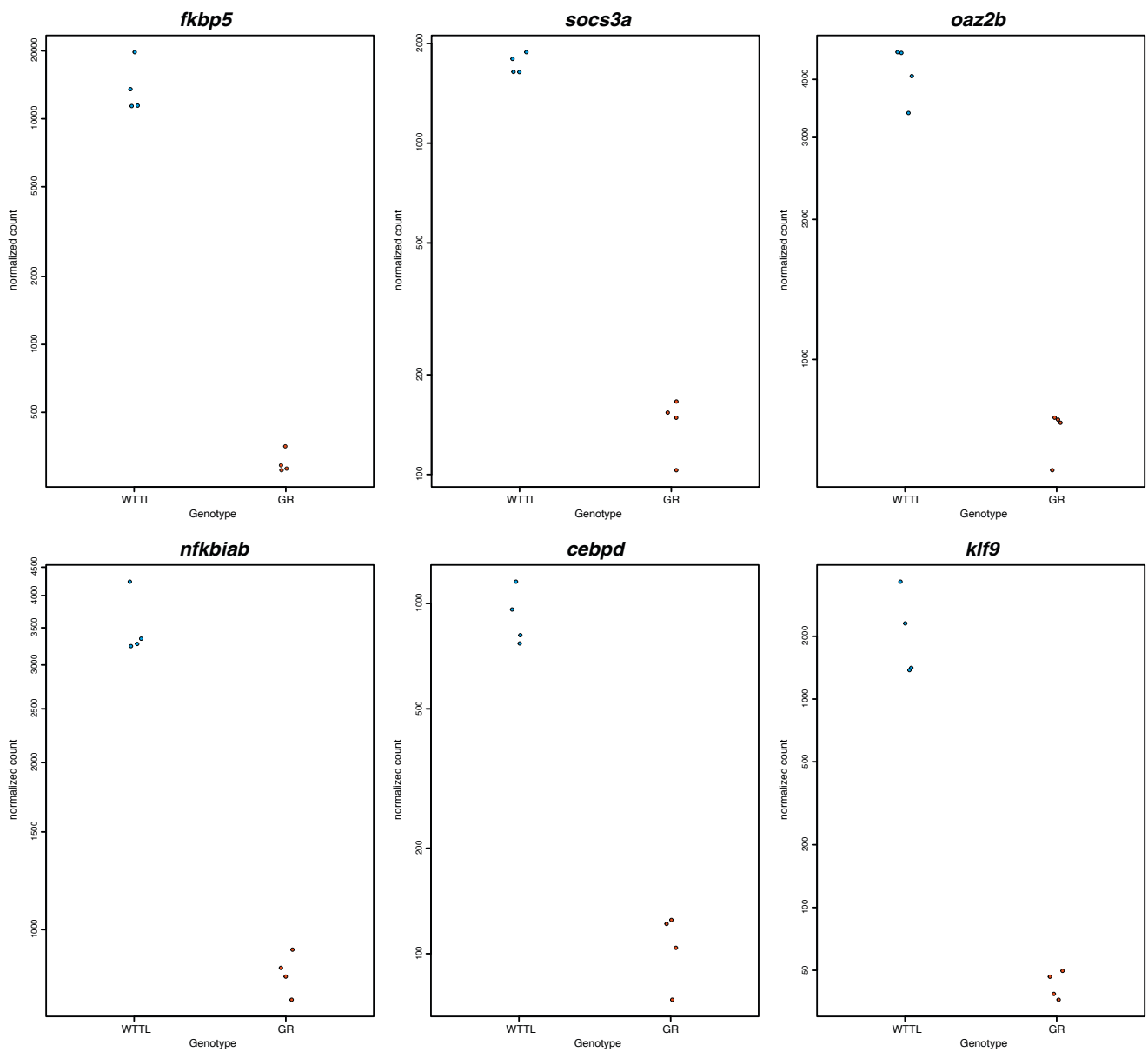
Figure 6.6. Normalised gene expression plots for each sample of *gr^wt* (WTTL) and *gr^s357* (GR) adult zebrafish brains for the top 5 most statistically significant differentially expressed genes, and an gene of interest *klf9*. Normalised DESeq2 gene counts are plotted using plotCounts function for genes *fkbp5*, *socs3a*, *oaz2b*, *nfkbiab*, *cebpd* and *klf9*. See Table 6.2 for statistics.

Table 6.2. Top 20 most significant differentially expressed genes (padj<0.05) in gr^{s357} mutant vs gr^{wt} sibling adult brains are predominantly downregulated. Colour indicates upregulated (green) or downregulated (red) gene expression direction.

Gene name	Fold change	p value	padj value	Ensembl gene ID
fkbp5	0.02140315	9.06E-234	1.73E-229	ENSDARG00000028396
socs3a	0.08209458	3.04E-180	2.90E-176	ENSDARG00000025428
oaz2b	0.16880121	2.81E-102	1.79E-98	ENSDARG00000059815
nfkbiab	0.2370985	9.15E-84	4.37E-80	ENSDARG00000007693
cebpd	0.11454568	1.79E-65	6.82E-62	ENSDARG00000087303
pik3r3a	0.23866668	2.04E-56	6.49E-53	ENSDARG00000103038
prr18	0.53609422	3.52E-53	9.59E-50	ENSDARG00000093768
klf9	0.01933028	6.90E-51	1.65E-47	ENSDARG00000068194
nocta	0.28054329	1.02E-47	2.16E-44	ENSDARG00000077726
sox11b	0.36522448	5.40E-47	1.03E-43	ENSDARG00000095743
ptges3a	0.57887597	1.97E-46	3.41E-43	ENSDARG00000037284
pim3	0.4726281	4.40E-45	6.99E-42	ENSDARG00000055129
efna1b	0.306196	6.58E-44	9.66E-41	ENSDARG00000018787
hsd11b2	0.19644758	6.92E-42	9.43E-39	ENSDARG00000001975
si:dkey-201c13.2	0.01960572	4.53E-41	5.76E-38	ENSDARG00000094696
rxfp1	3.44257389	2.90E-38	3.46E-35	ENSDARG00000090071
zgc:162730	0.42460163	3.14E-38	3.53E-35	ENSDARG00000103720
ddit4	0.22961079	7.68E-38	8.15E-35	ENSDARG00000037618
si:dkey-184p9.7	0.13970533	8.20E-37	8.23E-34	ENSDARG00000092726
TAGAP	0.26549439	1.76E-36	1.68E-33	ENSDARG00000043475

Table 6.3. Top 20 significant differentially expressed genes ordered by magnitude of fold change caused by the gr^{s357} mutation in zebrafish adult brains. Top 10 upregulated genes by magnitude (green) and subsequently top 10 downregulated genes by magnitude (red).

Gene name	Fold change	p value	padj value	Ensembl gene ID
CR753876.1	283.848035	6.68E-15	1.55E-12	ENSDARG00000097137
atp2a1	9.1695515	0.0029418	0.03750061	ENSDARG00000020574
pvalb4	8.06713298	2.40E-08	2.26E-06	ENSDARG00000024433
mylpfa	7.47320927	0.00049355	0.0102709	ENSDARG00000053254
nit1	6.99426104	4.99E-05	0.00173753	ENSDARG00000070116
f13a1a.1	6.34278071	4.28E-05	0.00154447	ENSDARG00000045453
atp2a1l	4.17280643	0.00025817	0.00639192	ENSDARG00000035458
timm23b	3.81873379	6.50E-12	1.04E-09	ENSDARG00000100375
CABZ01074307.1	3.80704124	3.91E-06	0.00020328	ENSDARG00000099775
tnnt3b	3.61239128	0.00054472	0.01107017	ENSDARG00000068457
zgc:194659	283.848035	6.68E-15	1.55E-12	ENSDARG00000079347
si:dkey-167k11.5	9.1695515	0.0029418	0.03750061	ENSDARG00000039752
klf9	8.06713298	2.40E-08	2.26E-06	ENSDARG00000068194
si:dkey-201c13.2	7.47320927	0.00049355	0.0102709	ENSDARG00000094696
fkbp5	6.99426104	4.99E-05	0.00173753	ENSDARG00000028396
itga2.3	6.34278071	4.28E-05	0.00154447	ENSDARG00000086838
foxg1b	4.17280643	0.00025817	0.00639192	ENSDARG00000032705
socs3a	3.81873379	6.50E-12	1.04E-09	ENSDARG00000025428
cebpd	3.80704124	3.91E-06	0.00020328	ENSDARG00000087303
si:dkey-242g16.2	3.61239128	0.00054472	0.01107017	ENSDARG00000069377

6.2.3 Gene Ontology analysis of differentially expressed genes in adult male zebrafish brains carrying the *gr^s357* mutation.

GO analysis of DEGs identified in *gr^s357* adult male brains revealed an overrepresentation in biological processes such as cell differentiation and cell fate commitment, and regulation of phosphorylation and developmental processes (Figure 6.7; Figure 6.9A; Table 6.4). Interestingly, molecular function GO analysis revealed an overrepresentation in multiple functions of the oxidative phosphorylation pathway, including cytochrome-c oxidase activity, oxidoreductase activity and electron transfer activity (Figure 6.8B; Figure 6.9B; Table 6.5). Corresponding to molecular function, cellular component GO analysis revealed an overrepresentation in genes encoding mitochondrial parts, including inner mitochondrial membrane protein complex, NADH dehydrogenase complex, respiratory chain complex I and the extracellular space (Figure 6.8B; Figure 6.9C; Table 6.6).

6.2.3.1 Genes encoding components of the oxidative phosphorylation pathway are primarily downregulated in *gr^s367* mutant brains.

GO, KEGG and Reactome analysis of *gr^s357* adult brain DEGs revealed overrepresentation of DEGs involved in numerous aspects of the electron transport chain, including the initial NADH dehydrogenase and ubiquinone activity, subsequent cytochrome complex activity and ATP synthesis (Table 6.5, 6.6&6.7; Figure 6.7,6.8,6.9&6.10). Various genes involved in the essential complex I component of the respiratory chain, including NADH dehydrogenase subunits (*mt-nd1, mt-nd2, mt-nd3, mt-nd4, mt-nd4l, mt-nd5, mt-nd6*), ubiquinone oxidoreductase subunits (*ndufa2, ndufa3, ndufa6, ndufa7, ndufab1a, ndufab1b, ndufaf6, ndufb10, ndufa11, ndufb11, ndufb5, ndufb8, ndufs5, ndufs6, ndufv2*), ubiqionone subunit *coq5* and *etfa* (electron-transferring-flavoprotein dehydrogenase) were significantly downregulated in *gr^s357* brains (Figure 6.10). However, *etfdh* was significantly upregulated.

Expression of genes associated with the respiratory system's complex II and III, succinate dehydrogenase and cytochrome b-c1 complex, were also decreased in *gr^s357* brains, including succinate dehydrogenase subunits, *sdhdb and sdhaf1, sdhaf3;* and cytochrome b-c1 subunit *mt-cyb*. Furthermore, expression of *cycsb* (cytochrome c), and multiple subunits of the cytochrome oxidase complex: *mt-co1, mt-co2, mt-co3, cox5aa, cox6b2, cox6c, cox7a2a, cox7a2l, cox7b, cox7c, cox11, cox16, cox17, cox18*, were significantly down regulated in *gr^s357* brains. In addition to a general downregulation of genes associated with proton concentration gradient across the

mitochondria membrane, sixteen genes that encode ATP synthase subunits (*atp1a3b*, *atp1b1a*, *atp5f1c*, *atp5f1e*, *atp5l*, *atp5mc3b*, *atp5mf*, *atp5pf*, *atp5po*, *atp7a*, *atpv0e2*, *mt-atp6*, *mt-atp8*) were significantly downregulated in *gr^s357* brains. Only two ATP synthase subunits, *atp2a1*, *atp2al*, were significantly upregulated in *gr^s357* brains.

A comprehensive downregulation of multiple components of the electron transport chain were identified in *gr^s357* brains (Figure 6.10), suggesting an association between glucocorticoid-resistance and mitochondrial dysfunction in *gr^s357* adult zebrafish brains. Interestingly, supporting the mitochondrial dysfunction conclusion, the expression of the neuroprotective gene *prkn* (parkin) was significantly increased in *gr^s357* brains. This has been seen in previous studies, where stress paradigms including mitochondrial dysfunction led to an increase in parkin expression (Winklhofer and Haass, 2010). Mitochondrial dysfunction and parkin signalling have been associated with neurodegenerative diseases and neuroinflammation such as Parkinson's, Alzheimer's and amyotrophic lateral sclerosis (AML) (Quinn et al., 2020). As the glucocorticoid receptor is known to translocate to the mitochondria and regulate transcription of mt-DNA genes, it is possible that glucocorticoid-GR signalling may affect neurodegenerative diseases and neuroinflammation (Lapp et al., 2019; Psarra and Sekeris, 2011).

In addition to an enrichment of genes of the electron transport chain located to the mitochondria, genes involved in cellular metabolism through the Krebs cycle, including pyruvate availability, glycolysis and the citrate acid cycle, were also identified. Genes that regulate pyruvate dehydrogenase activity, *pdk2a*, *pdk2b* and *pdk4;* and monocarboxylic acid transport of metabolic products, *slc16a9a*, *slc16a12b* and *slc38a4*, were significantly downregulated in the brains of *gr^s357* mutants, except *scl16a9a*, which was significantly upregulated.

Table 6.4. Significant biological processes gene ontology terms overrepresented in genes differentially expressed in *gr^s357* adult zebrafish brains.

GO Term	Description	P-value	FDR q-value	Enrichment (N, B, n, b)
GO:0045595	regulation of cell differentiation	1.12E-07	8.96E-04	2.23 (11040,343,692,48)
GO:0051093	negative regulation of developmental process	2.98E-06	1.20E-02	2.91 (11040,126,692,23)
GO:0045596	negative regulation of cell differentiation	4.07E-06	1.09E-02	3.38 (11040,85,692,18)
GO:0010453	regulation of cell fate commitment	8.59E-06	1.72E-02	7.98 (11040,14,692,7)
GO:0050793	regulation of developmental process	1.04E-05	1.67E-02	1.74 (11040,579,692,63)
GO:0042325	regulation of phosphorylation	2.14E-05	2.86E-02	2.01 (11040,309,692,39)
GO:2000026	regulation of multicellular organismal development	3.20E-05	3.68E-02	1.77 (11040,478,692,53)
GO:0019220	regulation of phosphate metabolic process	6.44E-05	6.47E-02	1.90 (11040,336,692,40)
GO:0051174	regulation of phosphorus metabolic process	6.44E-05	5.75E-02	1.90 (11040,336,692,40)
GO:0051241	negative regulation of multicellular organismal process	8.53E-05	6.86E-02	2.50 (11040,134,692,21)
GO:0065007	biological regulation	1.11E-04	8.09E-02	1.16 (11040,4813,692,349)
GO:0043549	regulation of kinase activity	1.35E-04	9.06E-02	2.18 (11040,190,692,26)
GO:0048585	negative regulation of response to stimulus	1.65E-04	1.02E-01	1.84 (11040,339,692,39)
GO:0051338	regulation of transferase activity	1.78E-04	1.02E-01	2.11 (11040,204,692,27)
GO:0022904	respiratory electron transport chain	1.80E-04	9.63E-02	4.22 (11040,34,692,9)
GO:0030334	regulation of cell migration	2.46E-04	1.24E-01	2.38 (11040,134,692,20)
GO:0060284	regulation of cell development	2.82E-04	1.34E-01	1.99 (11040,232,692,29)
GO:0022900	electron transport chain	2.88E-04	1.29E-01	3.99 (11040,36,692,9)
GO:0061387	regulation of extent of cell growth	2.89E-04	1.22E-01	3.19 (11040,60,692,12)
GO:0030516	regulation of axon extension	3.07E-04	1.24E-01	3.37 (11040,52,692,11)
GO:0050768	negative regulation of neurogenesis	3.07E-04	1.18E-01	3.37 (11040,52,692,11)
GO:0042659	regulation of cell fate specification	3.21E-04	1.17E-01	7.25 (11040,11,692,5)
GO:0050794	regulation of cellular process	3.73E-04	1.30E-01	1.16 (11040,4157,692,303)
GO:0006935	chemotaxis	4.07E-04	1.36E-01	2.92 (11040,71,692,13)
GO:0010721	negative regulation of cell development	4.35E-04	1.40E-01	3.25 (11040,54,692,11)
GO:0031345	negative regulation of cell projection organization	4.46E-04	1.38E-01	3.78 (11040,38,692,9)
GO:0048640	negative regulation of developmental growth	6.26E-04	1.86E-01	3.99 (11040,32,692,8)
GO:0007411	axon guidance	6.30E-04	1.81E-01	2.05 (11040,187,692,24)
GO:0051239	regulation of multicellular organismal process	6.36E-04	1.76E-01	1.54 (11040,602,692,58)
GO:0031399	regulation of protein modification process	6.36E-04	1.70E-01	1.76 (11040,326,692,36)
GO:2000145	regulation of cell motility	6.42E-04	1.66E-01	2.22 (11040,144,692,20)
GO:0048523	negative regulation of cellular process	6.64E-04	1.67E-01	1.39 (11040,1018,692,89)
GO:0045926	negative regulation of growth	6.68E-04	1.63E-01	3.59 (11040,40,692,9)
GO:0097485	neuron projection guidance	6.81E-04	1.61E-01	2.04 (11040,188,692,24)
GO:0051961	negative regulation of nervous system development	7.06E-04	1.62E-01	3.08 (11040,57,692,11)
GO:0007219	Notch signaling pathway	7.06E-04	1.58E-01	3.08 (11040,57,692,11)
GO:0071526	semaphorin-plexin signaling pathway	7.82E-04	1.70E-01	3.87 (11040,33,692,8)
GO:0006091	generation of precursor metabolites and energy	7.93E-04	1.68E-01	2.43 (11040,105,692,16)
GO:0032102	negative regulation of response to external stimulus	8.09E-04	1.67E-01	3.50 (11040,41,692,9)
GO:0045665	negative regulation of neuron differentiation	8.09E-04	1.63E-01	3.50 (11040,41,692,9)
GO:0050922	negative regulation of chemotaxis	8.48E-04	1.66E-01	4.30 (11040,26,692,7)
GO:0050789	regulation of biological process	8.69E-04	1.66E-01	1.14 (11040,4438,692,318)
GO:0050767	regulation of neurogenesis	8.82E-04	1.65E-01	1.94 (11040,214,692,26)
GO:0048638	regulation of developmental growth	9.11E-04	1.66E-01	2.69 (11040,77,692,13)
GO:0040013	negative regulation of locomotion	9.14E-04	1.63E-01	3.19 (11040,50,692,10)
GO:0051271	negative regulation of cellular component movement	9.14E-04	1.60E-01	3.19 (11040,50,692,10)
GO:0040012	regulation of locomotion	9.28E-04	1.59E-01	2.11 (11040,159,692,21)
GO:0042661	regulation of mesodermal cell fate specification	9.35E-04	1.57E-01	11.97 (11040,4,692,3)
GO:1905770	regulation of mesodermal cell differentiation	9.35E-04	1.53E-01	11.97 (11040,4,692,3)
GO:1905902	regulation of mesoderm formation	9.35E-04	1.50E-01	11.97 (11040,4,692,3)
GO:0046850	regulation of bone remodeling	9.35E-04	1.47E-01	11.97 (11040,4,692,3)

Table 6.5. Significant molecular function gene ontology terms overrepresented in genes differentially expressed in *gr^s357* adult zebrafish brains.

GO Term	Description	P-value	FDR q-value	Enrichment (N, B, n, b)
GO:0004129	cytochrome-c oxidase activity	1.52E-05	4.60E-02	7.45 (11040,15,692,7)
GO:0016675	oxidoreductase activity, acting on a heme group of donors	1.52E-05	2.30E-02	7.45 (11040,15,692,7)
GO:0016676	oxidoreductase activity, acting on a heme group of donors, oxygen as acceptor	1.52E-05	1.53E-02	7.45 (11040,15,692,7)
GO:0015002	heme-copper terminal oxidase activity	1.52E-05	1.15E-02	7.45 (11040,15,692,7)
GO:0009055	electron transfer activity	2.34E-05	1.42E-02	4.39 (11040,40,692,11)
GO:0003700	DNA-binding transcription factor activity	1.93E-04	9.73E-02	1.53 (11040,742,692,71)
GO:0031434	mitogen-activated protein kinase kinase binding	2.45E-04	1.06E-01	15.95 (11040,3,692,3)
GO:0015078	proton transmembrane transporter activity	2.89E-04	1.09E-01	3.19 (11040,60,692,12)
GO:0019956	chemokine binding	3.21E-04	1.08E-01	7.25 (11040,11,692,5)
GO:0005507	copper ion binding	8.48E-04	2.56E-01	4.30 (11040,26,692,7)
GO:0051087	chaperone binding	8.48E-04	2.33E-01	4.30 (11040,26,692,7)
GO:0016491	oxidoreductase activity	8.87E-04	2.23E-01	1.58 (11040,494,692,49)
GO:0016530	metallochaperone activity	9.35E-04	2.17E-01	11.97 (11040,4,692,3)

Table 6.6. Significant cellular component gene ontology terms overrepresented in genes differentially expressed in *gr^s357* adult zebrafish brains.

GO Term	Description	P-value	FDR q-value	Enrichment (N, B, n, b)
GO:0044429	mitochondrial part	3.93E-15	5.01E-12	2.75 (11040,406,692,70)
GO:0098798	mitochondrial protein complex	5.72E-13	3.65E-10	3.93 (11040,146,692,36)
GO:0044455	mitochondrial membrane part	6.85E-13	2.91E-10	4.21 (11040,125,692,33)
GO:0098800	inner mitochondrial membrane protein complex	1.22E-10	3.88E-08	5.01 (11040,70,692,22)
GO:0030964	NADH dehydrogenase complex	4.08E-10	1.04E-07	7.70 (11040,29,692,14)
GO:0045271	respiratory chain complex I	4.08E-10	8.68E-08	7.70 (11040,29,692,14)
GO:0005747	mitochondrial respiratory chain complex I	4.08E-10	7.44E-08	7.70 (11040,29,692,14)
GO:0005743	mitochondrial inner membrane	1.34E-09	2.13E-07	3.39 (11040,146,692,31)
GO:0098803	respiratory chain complex	1.36E-09	1.93E-07	5.77 (11040,47,692,17)
GO:0019866	organelle inner membrane	8.51E-09	1.08E-06	3.15 (11040,157,692,31)
GO:0031966	mitochondrial membrane	1.05E-08	1.22E-06	2.66 (11040,240,692,40)
GO:0005739	mitochondrion	1.94E-08	2.07E-06	1.98 (11040,563,692,70)
GO:0070469	respiratory chain	6.38E-08	6.26E-06	7.31 (11040,24,692,11)
GO:1990204	oxidoreductase complex	5.32E-07	4.84E-05	4.25 (11040,60,692,16)
GO:0044421	extracellular region part	2.11E-04	1.80E-02	1.73 (11040,415,692,45)
GO:0005576	extracellular region	2.14E-04	1.71E-02	1.77 (11040,379,692,42)
GO:0005746	mitochondrial respiratory chain	2.45E-04	1.84E-02	15.95 (11040,3,692,3)
GO:0005615	extracellular space	4.51E-04	3.19E-02	1.78 (11040,332,692,37)

Figure 6.7. Gene Ontology Biological Process visualisation of significantly differentially expressed genes resulting from the *gr^s357* mutation in adult male brains. Enrichment of genes encompassing significantly overrepresented Biological Processes in zebrafish are highlighted. Maps produced using GOrilla software. Legend indicates p-value colour scale.

Figure 6.8. GO-term visualisation of significantly differentially expressed genes resulting from the *gr^s357* mutation in adult male brains. A) Enrichment of genes encompassing Molecular Functions. B) Enrichment of genes encompassing Cellular Components. All maps produced using GOrilla software. Legend indicates p-value colour scale.
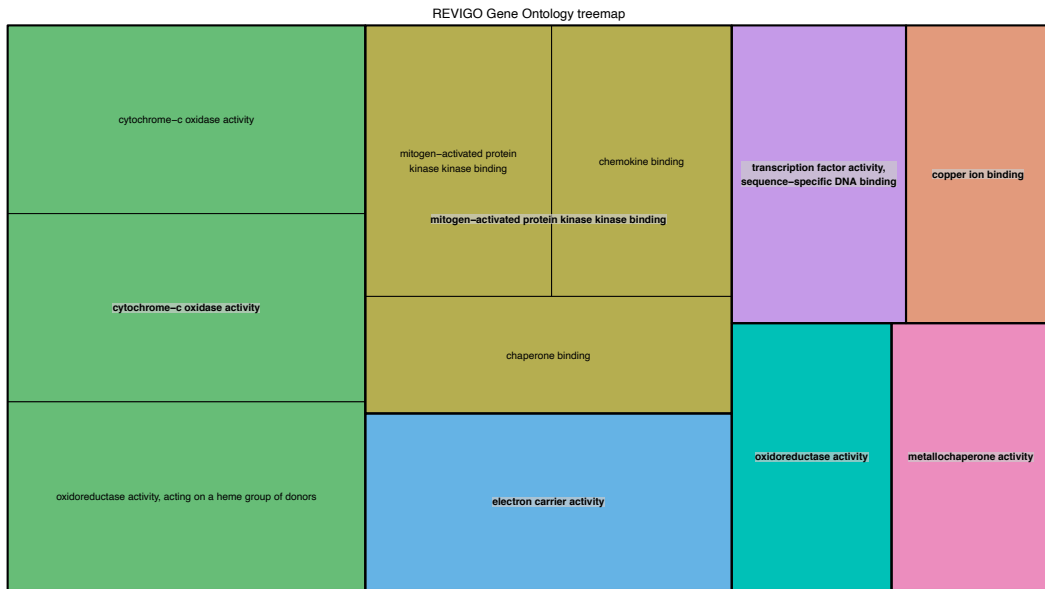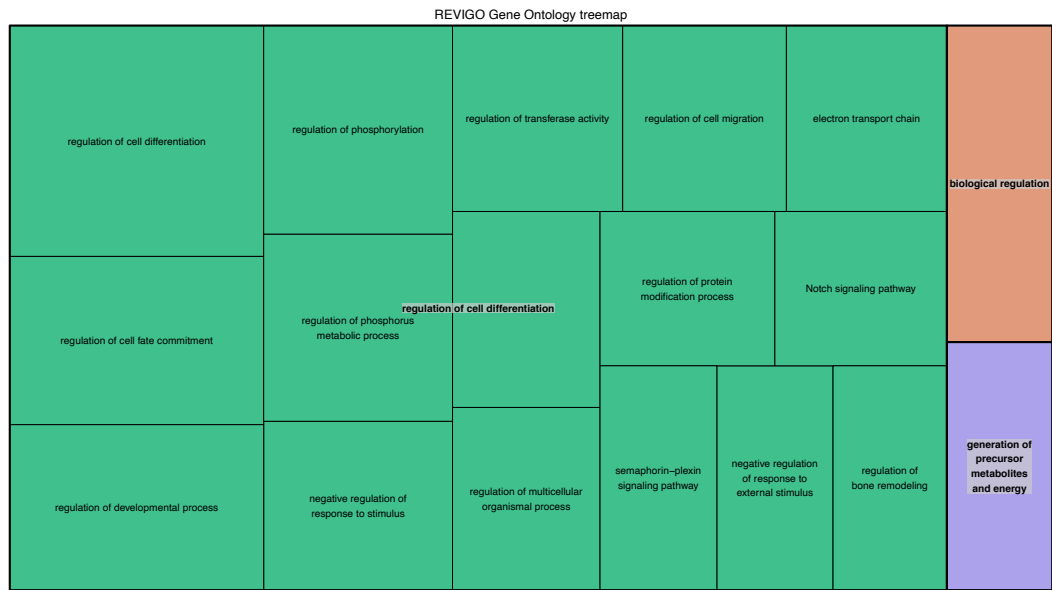
Figure 6.9. REVIGO GO-term treemap visualisation of significantly differentially expressed genes resulting from the *gr^s357* mutation in adult male zebrafish brains. Enrichment of genes encompassing Biological Processes (Top), Molecular Functions (Bottom left) and Cellular Components (Bottom right). All maps produced using REVIGO software. Size of box indicates p-value.

Table 6.7. KEGG and Reactome enrichment analysis of biological pathways for all DEGs in *gr^s357* **adult zebrafish brains.**

KEGG Term	Count	Fold Enrichment	Benjamini	FDR
Oxidative phosphorylation	87	5.57766902	3.97E-48	3.88E-48
Proteasome	27	4.52179782	2.40E-10	2.35E-10
Cardiac muscle contraction	28	3.59022374	5.12E-08	5.01E-08
Metabolic pathways	156	1.27761597	0.00700693	0.00685349

Reactome Term	Count	Fold Enrichment	Benjamini	FDR
Respiratory electron transport	43	7.69808991	1.25E-30	1.17E-30
Complex I biogenesis	37	6.62393783	6.47E-22	6.05E-22
Mitochondrial translation elongation	27	3.28959075	5.43E-07	5.08E-07
Mitochondrial translation termination	27	3.20068289	9.76E-07	9.13E-07
Formation of ATP by chemiosmotic coupling	11	5.07866642	1.80E-04	1.68E-04

6.2.3 Glucocorticoid catabolism and protein catabolism is downregulated in adult male *gr^s357* mutant brains

Another important group of oxidoreductase enzymes are the hydroxysteroid dehydrogenases that catalyse the dehydrogenation of hydroxysteroids. These genes are important for regulating steady-state levels of steroid hormones. Genes associated with the GO term 'steroid dehydrogenase activity' were enriched our list of DEGs in the brain of *gr^s357* mutant zebrafish. For example, two glucocorticoid-induced genes *hsd11b2* and *hsd20b2*, which are responsible for the inactivation of the glucocorticoid cortisol and regulate glucocorticoid catabolism, were downregulated in *gr^s357* mutants. Expression of other glucocorticoid-responsive genes was decreased in *gr^s357* mutant brains, including *hsd17b10*, important for the metabolism of neuroactive steroids and GABAergic neuronal function; *hsd3b7*, important for modification of the steroid hormone precursor, cholesterol; and *hsd17b3*, a gene responsible for the conversion of androstenedione to testosterone. Not only was glucocorticoid catabolism downregulated in brains of *gr^s357* mutants, expression of genes associated with protein catabolism were also significantly decreased, including proteosome subunits *psma5*, *psma6a*, *psmb1*, *psmb8a*, *psmb9a psmb10*, *psmb12*, *psmb13a*, *psmd8* and *psmd10*.

6.2.4 Neural circuits are dysregulated in the transcriptome of adult male *gr^s357* mutants

As expected, various genes involved in neural circuits, were identified as differentially expressed in brains of *gr^s357* mutants compared to *gr^wt* brains. Genes involved in neurological inflammation and apoptosis were downregulated, including n*fkbiab* and *socs1a* (suppressor of cytokine signaling); and the stress-inducible growth arrest and DNA-damage-inducible genes *gadd45ab, gadd45ba, gadd45bb* and *gadd45ga*. Expression of *prl2* (prolactin), important for stress adaption and neurogenesis, was also decreased in *gr^s357* mutant brains.

However, upregulated genes in the brains of adult *gr^s357* mutant zebrafish mirrored *gr^s357* mutant larvae gene ontology. An overrepresentation of genes was associated with the GO terms related to neuron projection guidance and differentiation, and axon guidance and extension. A significant increase in expression of genes involved in semaphorin-plexin receptor signaling was discovered, such as *sema3ab sema3bl, sema3gb sema6dl sema6d* and *sema6ba* (semaphorin subunits) and *plxna1a plxna3, plxnb3*, (plexin subunits). In addition, common axon guidance receptors such as *robo2*, *robo4*, corresponding *slit1a* (slit guidance ligand) and *ntn2* (netrin chemotropic factor) were upregulated in brains of adult *gr^s357* mutants.

Various genes associated with neuroactive ligand-receptor systems were identified to be differentially expressed in *gr^s357* mutant brain, including downregulation of serotonergic (*htr5ab*) and adrenergic systems (*adra1d*, *adrb2a* and *adra2da*), and upregulation of GABAergic (*gabbr1b, gabrg2*) and glutamatergic (*grid2*) systems; and upregulation of relaxin/insulin-like signaling (*rxfp1*), the most significant upregulated DEG in the brain of *gr^s357* mutant zebrafish.

6.2.5 Mitogen-activated protein kinase signaling is primarily downregulated in adult male *gr^s357* mutant brains

Gene ontology analysis revealed an overrepresentation of mitogen-activated protein kinase (MAPK) signaling in DEGs of adult male *gr^s357* mutant brains. MAPK signaling is an important signaling mechanism, which integrates extracellular signals such as neurotrophins, neurotransmitters and brain derived neurotrophic factor, to intracellular mechanisms affecting differentiation and synapse plasticity (David Sweatt, 2001; Vreugdenhil and Berezikov, 2010). Multiple MAPK phosphatases are downregulated in *gr^s357* neural transcriptomes, including *dusp1*, *dusp2*, *dusp6*, *dusp19b* and *dusp23b*. Likewise, a family of three tribble proteins, *trib1*, *trib2* and *trib3*, which regulate mapk kinase activation were significantly downregulated in *gr^s357* mutants.
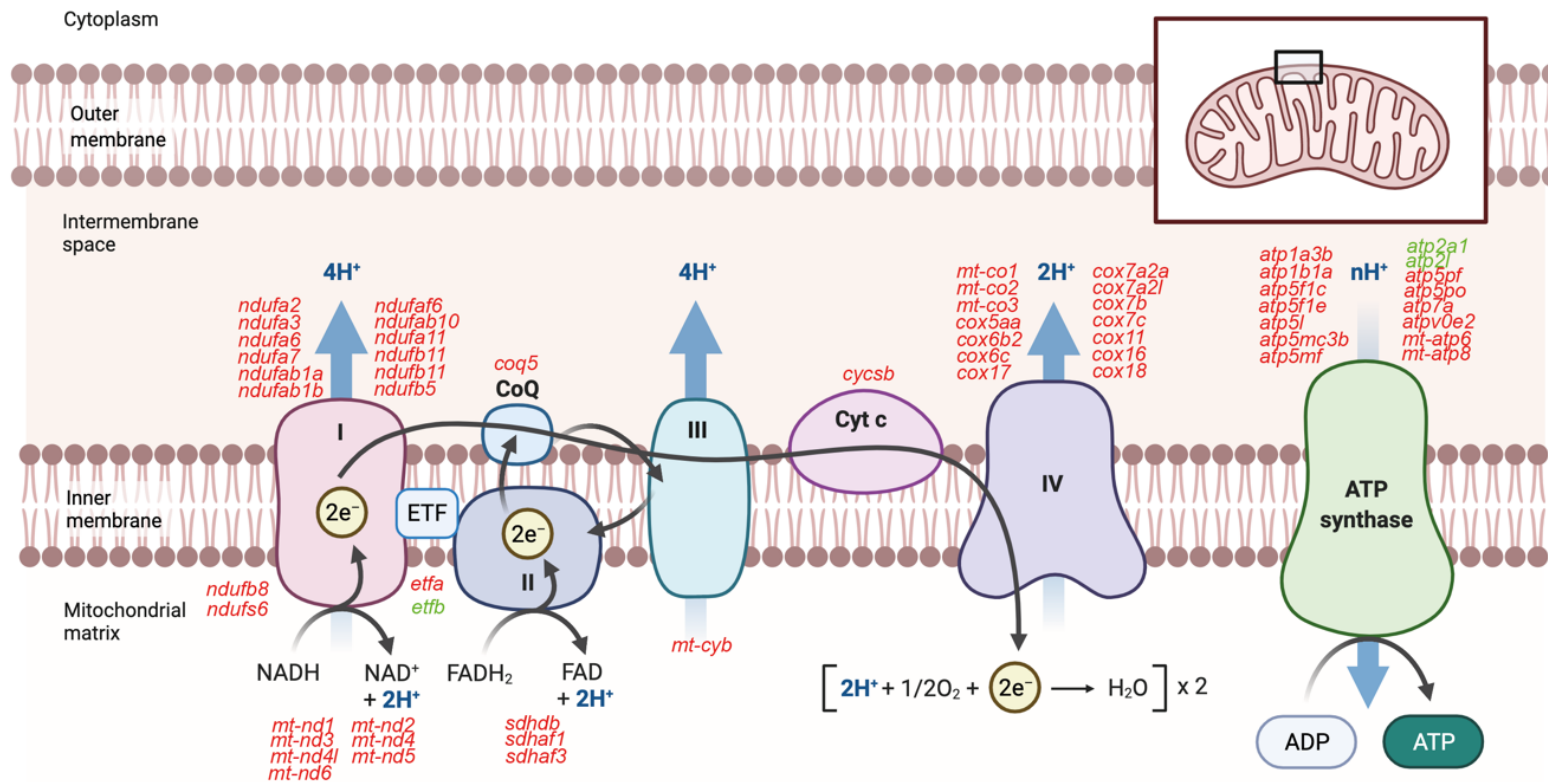
Figure 6.10. Diagram of mitochondrial electron transport chain annotated with differentially expressed genes significantly enriched in the oxidative phosphorylation pathway in the brains of adult male *gr^s357* mutant zebrafish. I, NADH dehydrogenase complex; ETF, electron transfer flavoprotein; II, succinate dehydrogenase; CoQ, coenzyme ubiquinone; III) cytochrome bc1 complex; Cyt c, Cytochrome C; IV, Cytochrome c oxidase complex; ATP synthase, adenosine triphosphate synthase.

6.2.6 A comparative analysis between the transcriptomes of 5dpf larvae and adult male brains carrying the *gr^s357* mutation

A Venn diagram approach was used to compare the transcriptomic changes discovered in 5dpf larvae and adult male zebrafish brains carrying the *gr^s357* mutation. This exploratory approach identified DEGs that overlapped in both mutant transcriptomes to explore common dysregulated biological processes (Figure 6.10). I used the *gr^s357* adult brain DEG list which was filtered by baseMean read counts >40; 0.32<Log2FoldChange<-0.32; padj<0.05, and compared it to *gr^s357* 5dpf larvae DEG list filtered by baseMean read counts >40; 0.58<Log2FoldChange<-0.58; padj<0.05.

This approach identified a total of 225 genes that were significantly differentially expressed in both *gr^s357* 5dpf larvae and *gr^s357* adult brain transcriptomes (Figure 6.10). 32 were upregulated in both *gr^s357* 5dpf larvae and adult brains, 113 downregulated in both and 80 DEGs were expressed in opposing directions in 5dpf larvae and adult brain transcriptomes. Of the 80 DEGs with opposing expression direction, 28 were upregulated in *gr^s357* 5dpf larvae and downregulated in *gr^s357* adult male brains, and 52 were vice versa.

DEGs that were downregulated in both *gr^s357* 5dpf larvae and adult brain transcriptomes included the most significant DEG in both datasets, *fkbp5*; and previously established glucocorticoid-responsive genes *tsc22d3*, *klf9* and *hsd11b2*. Previously described MAPK kinases *dusp1*, and *dusp23b*, glucocorticoid catabolism enzyme *hsd20b2*, NF-kappa-B inhibitor, *nfkbiab*, and *socs3a*. Unsurprisingly, common downregulated DEGs in both *gr^s357* larvae and adult brains are associated with the regulation of transcription. This includes *cebpd* (CCAAT/enhancer binding protein), transcriptional regulators such as *tsc22d3*, *bzw1b* (basic leucine zipper), *tp53inp1* (tumor protein p53 inducible nuclear protein 1), *tefb*, *mych* and *hif1al* (hypoxia-inducible factor 1). Furthermore, common downregulated DEGs were also associated with various pathways, including: the biosynthesis of amino acids, e.g. *glulb* (glutamate synthase), *gpt2l* (glutamic pyruvate transaminase) and *tha1* (threonine aldolase 1); regulation of ornithine decarboxylase e.g. the top 5 DEG *oaz2b* (ornithine decarboxylase antizyme), *azin1b* (antizyme inhibitor) and *slc25a15b* (ornithine transporter); insulin resistance e.g. *irs2a* (insulin receptor substrate), *nfkbiab* (nuclear factor of kappa light polypeptide), and associated kinases *pik3r3a*, *rps6kb1a* and *gbp* (glycogen synthase); and amino acid transport across the plasma membrane e.g. mitochondria transporters *slc25a23a* and *slc25a3b*, solute channel regulator *sgk3* and *ucp2*.
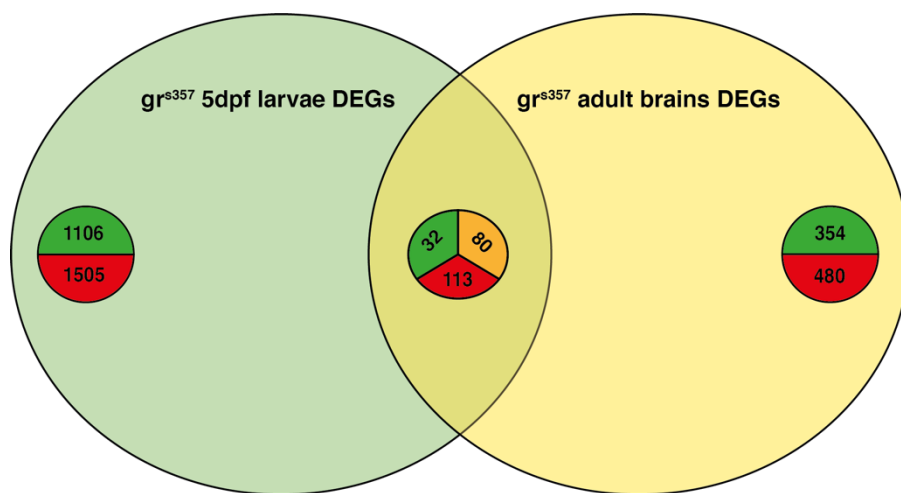
Figure 6.11. Venn diagram illustrating commonality and dissimilarities between significant DEGs identified in *gr^s357* larvae (green circle) and *gr^s357* brains (yellow circle). Within Venn circles, number of upregulated genes are denoted in green, downregulated genes denoted in red, and a change in expression direction denoted in orange

To investigate the DEGs identified as severely downregulated in both larvae and brain datasets this, the FIMO motif search tool was used to identify potential glucocorticoid response element (GRE) sequences (<u>AGAACA</u>NNN<u>TGTTCT</u>) in the 2000bp upstream of the 5' UTR of each gene (putative promoters) (Bailey et al., 2009). A single putative GRE sequence was discovered in genes: *fkbp5* (GGAACACAGTGTTCC+ or GGAACACTGTGTTCC- p= 9.95e-06 q=0.0294), *tsc22d3* (AGAACACGTTGTTCC+ or GGAACAACGTGTTCT- p=8.35e-07 q=0.00494) and *cebpd* (ACAACACGCAGTTCT+ or AGAACTGCGTGTTGT- p=1.22e-05 q=0.0578).

The most significant upregulated DEG in *gr^s357* adult brains, *rxfp1* (relaxin receptor), was also significantly upregulated in *gr^s357* 5dpf larvae. Other genes upregulated in both datasets were predominantly associated with transcriptional regulation, such as the chromatin regulators *bcorl1* and *histh1l*, transcriptional repressor *cica* and activators *ebf3a* and *lhx2b*; and putative zinc fingers *znf512b*, *znf1009* and *baz2ba*. DEGs that were upregulated in *gr^s357* 5dpf larvae but downregulated in adult brain transcriptomes included those associated with the electron transport chains: *mt-nd1*, mt-*nd2, mt-nd3, mt-nd4, mt-nd4l, mt-nd5 mt-nd6, mt-atp6, mt-atp8, mt-co1, mt-co2, mt-co3* and *taco1*. In conclusion, comparative analysis of *gr^s357* 5dpf larval and adult brain transcriptomes has highlighted robust GR-specific downstream target genes such as *fkbp5*, *tsc22d3* and *hsd11b2*. It has also highlighted the role of the GR as regulator of both transcriptional activators and repressors, with both types upregulated and downregulated in *gr^s357* mutants. Surprisingly, it has demonstrated an opposing dysregulation of the electron transport chain between *gr^s357* larvae and adult brains.

6.3 Discussion

This chapter describes the results of experiments to explore further the molecular mechanisms affected by glucocorticoid resistance in the neural transcriptome, and a comparative analysis against the larval transcriptome. The transcriptomes of dissected gr^{s357} adult brains were compared to those of their wild-type adult sibling brains. However, one caveat was discovered after sequencing the pituitary gland was not harvested during dissection of the brain and remained encapsulated within the sphenoid bone as part of the skull. Consequently, no pituitary-derived transcripts were sequenced in this analysis and understanding the impact of chronic high levels of cortisol and glucocorticoid resistance on the functioning of the HPI axis will therefore be incomplete. Nonetheless, my analysis of the impact of the gr^{s357} mutation on the adult zebrafish brain transcriptome has provided many novel insights into the molecular mechanisms regulated by the GR in the brain.

Initial quality control assessment by Principal Component Analysis of adult brain mRNA-seq data revealed the gr^{s357} mutation has a significant effect on gene expression, such that gr^{s357} samples are distinctly segregated from grwt samples. Differential expression analysis identified approximately 1000 genes exhibiting statistically significant differential expression in wild-type and gr^{s357} mutant adult brain samples. At the top of the list is *fkbp5*, closely accompanied by other genes such as *klf9* and *tsc22d3*, *hsd11b2*, and *pck1* which were also identified as differentially expressed in 5dpf gr^{s357} larvae. However, one surprising difference was that in gr^{s357} adult brains, the vast majority of statistically significant DEGs exhibited a decrease in expression, and relatively few exhibited an increase in transcript abundance in gr^{s357} mutant brains. This was something of a surprise as, amongst the upregulated DEGs in gr^{s357} mutant larvae, there was an enrichment in genes associated with cellular components located in neurons and axons. The identification of well-characterised glucocorticoid-responsive genes as DEGs confirms the efficient data analysis and accurate representation of the effects of this GR mutation in zebrafish (Chinenov et al., 2014).

As before in chapter 3 and chapter 5, *fkbp5* has been identified as differentially expressed, exhibiting increased expression in the hypercortisolaemic MR^{46Del} mutant, and almost complete extinction of gene expression in both the gr^{s357} mutant larval transcriptome and gr^{s357} mutant adult zebrafish brain transcriptome. Using the FIMO motif search tool, I identified a putative GRE upstream of the 5' UTR of the zebrafish *fkbp5* gene, suggesting direct GRE-binding and transcriptional regulation of *fkbp5* by GR. My results are supported by previous research, including studies of glucocorticoid-deficient or glucocorticoid-resistant mutant zebrafish, which exhibit a significant reduction in *fkbp5* mRNA, and GREs were located in intron 1 and intron 2 of

the human *FKBP5* gene (Eachus et al., 2017; Marchi et al., 2020; U et al., 2004). My results build on previous evidence that *fkbp5* is a direct GR-target gene, but also provides novel insight into *fkbp5*'s GR-mediated regulation during early development and in mature brains of the zebrafish.

GO, KEGG and Reactome analysis of the *gr^s357* adult brain DEGs revealed an overrepresentation of genes involved oxidative phosphorylation and the electron transport chain (Figures 6.7,6.8,6.9&6.10; Tables6.4-6.6). DEGs were enriched in cellular components associated with the mitochondria, including inner and outer membrane and the respiratory chain complexes (Figures 6.7 & 6.8; Tables 6.5, 6.6 & 6.7). Genes associated with cellular components of the mitochondria were primarily downregulated in *gr^s357* mutants suggesting an association between loss of GR function and mitochondrial dysfunction in *gr^s357* adult zebrafish brains. Genes encoding subunits of the electron chain such as: mitochondrial NADH dehydrogenases, ubiquinone oxidoreductases, cytochrome complexes and ATP synthase subunits, as well as genes that encode pyruvate dehydrogenase activity and monocarboxylic acid transporters of metabolic products were significantly downregulated in *gr^s357* brains compared to *gr^wt* brains. A common paradigm is that mitochondrial dysfunction is intrinsically linked with oxidative stress and ageing. Unfortunately, experiments to determine the extent of mitochondrial DNA damage and ROS production could not be included within the scope of this study, but this could be a focus of future research. Published research has demonstrated that the GR is translocated to brain mitochondria in a complex with Bcl-2 protein (Du et al., 2009), whereas other studies also indicate that mt-DNA contains putative GRE sequences (Sekeris, 1990) and that stress/glucocorticoids exposure induces changes in mt-DNA transcription and mitochondrial physiology in vitro (Hunter et al., 2016; Psarra and Sekeris, 2011). However, to my knowledge this is the first *in vivo* study to demonstrate that loss of GR DNA-binding function results in significant changes in mt-DNA transcription e.g. *mt-nd1, mt-nd2, mt-nd3, mt-nd4, mt-nd4l, mt-nd5, mt-nd6, mt-co1, mt-co2, mt-co3 mt-atp6*, *mt-atp8*. Moreover, in support of the argument that impaired GR signaling leads to mitochondrial dysfunction, expression of the neuroprotective gene *parkin* was significantly increased in *gr^s357* adult brains(Pickrell and Youle, 2015).

Mitochondrial function and the stress response are intrinsically connected. Physiological responses to an activated HPI include elevated blood glucose, metabolism changes and reallocation of cellular resources utilised by mitochondria to provide energy required for a stress response (Lapp et al., 2019). There are many correlations between the stress and mitochondrial function, including decreased mtDNA copy number in male veterans with PTSD (Bersani et al., 2016) and decreased mtDNA copy number and mitochondria function in individuals who experienced chronic caregiving stress (Picard et al., 2018). The role of the GR as a transcription

factor in mitochondria was suggested first by in silico studies and then demonstrated through *in vitro* mammalian cell culture methods. GREs were identified in the mitochondrial genome by virtue of their sequence similarity to the canonical GRE, and then demonstrated to mediate dexamethasone induced transcription of genes such as *mt-COX1*, *mt-COX3* and *mt-ND1* (Psarra and Sekeris, 2011). These genes were all downregulated in my *gr^s357* adult brain transcriptomic analysis. However, according to the type of stress studied and the duration, the direction of mtDNA transcriptional change appears to vary for a wide range of mitochondrial genes (Lapp et al., 2019). Similarly, in the *gr^s357* larvae and *gr^s357* adult brain comparison, twelve mitochondrial genes exhibited increased transcription in *gr^s357* mutant larvae and decreased transcription in *gr^s357* adult mutant brains. Previous mechanistic studies have shed some light on the effects of acute stress (Hunter et al., 2016), but more work is required to illuminate the effects of chronic, long term stress on mt-DNA transcription, copy number and mitochondrial function. My transcriptomic analysis provides novel insights into the effects of GR function on the vertebrate brain and 5dpf larvae *in vivo*, demonstrating that loss of GR function dysregulated mt-DNA transcription. Further functional analysis into mt-DNA copy number, epigenetic regulation of mtDNA expression and mitochondrial function in *gr^s357* mutant zebrafish will provide greater understanding of the impact of stress hormones on mitochondrial function.

One important function of mitochondria is the synthesis of steroid hormones, including glucocorticoids. The mitochondrion is the location for the rate limiting synthesis step where the steroidogenic acute regulatory protein (STAR) enables the movement of cholesterol across the mitochondrial membrane into the mitochondrial matrix (Bose et al., 2002). Whilst *star* was not significantly differentially expressed in *gr^s357* adult brains, an important group of oxidoreductase enzymes that catalyse the dehydrogenation of hydroxysteroids were downregulated in *gr^s357* adult brains. This included *hsd3b7*, important for modification of the steroid hormone precursor cholesterol, two glucocorticoid-induced genes, *hsd11b2* and *hsd20b2*, that regulate glucocorticoid catabolism (Tokarz et al., 2013), *hsd17b3* important for testosterone synthesis (Kimoto et al., 2010) and interestingly, *hsd17b10,* a mitochondrial protein important for mitochondrial tRNA function and mitochondrial protein production (He et al., 2018). My data suggests that glucocorticoid signaling regulates genes important for steroid hormone biosynthesis in the mitochondrion. This glucocorticoid regulation is vital for the physiological stress response initiated in the brain via the HPA axis. In mammals, physiological responses to an activated HPA axis include elevated blood glucose, metabolism changes and reallocation of cellular resources utilised by mitochondria to provide energy required for a stress response (Lapp et al., 2019).

In addition to a downregulation of genes regulating glucocorticoid catabolism i.e. *hsd11b2* and *hsd20b2*, various genes associated with protein catabolism were downregulated in *gr^{s357}* adult brains. Previous mammalian research has demonstrated the effects of glucocorticoid treatment on protein synthesis and breakdown in skeletal muscle. For instance, glucocorticoid treatment results in skeletal muscle atrophy, through a decrease in protein synthesis rates (Britto et al., 2014) and increased Ubiquitin-proteasome-dependent proteolysis, partially through increased mRNA expression of proteosome subunits (Combaret et al., 2004). Interestingly, I discovered sixteen genes encoding subunits of the 20S proteome that were significantly downregulated in *gr^{s357}* adult brains, suggesting a role of the GR in proteosome regulation. This relationship between glucocorticoid signaling and protein synthesis and breakdown has previously been suggested in zebrafish, as GR knockout mutant zebrafish exhibited an increase in total body weight and protein content in muscle tissue (Faught and Vijayan, 2019a). The authors demonstrated that a lack of GR function in zebrafish promoted protein synthesis and attenuated protein catabolism (Faught and Vijayan, 2019a). My results provide a novel insight into the GR's regulation of proteosome subunits in the brain, however due to the lack of available data on functional protein breakdown assays in the *gr^{s357}* adult, we cannot say protein catabolism was decreased, however it would be an interesting line of enquiry for future experiments.

Investigating the effect of the *gr^{s357}* mutation on both 5dpf larvae and brain has provided novel insights into the function of the GR in zebrafish development and in the fully developed adult brain. A comparison of DEG lists provided an interesting overlap of genes that were present in both datasets. Sixty genes were significantly upregulated in both *gr^{s357}* larvae and *gr^{s357}* brains, including the relaxin receptor *rxfp1*. This was the most significant upregulated DEGs in adult brain and has previously been associated with GR function. The relaxin peptide family is a ligand for Rxfp1, and regulates a multitude of biological processes, including collagen turnover, renal and myocardial functions, the immune system, reproduction and central nervous process (Nistor et al., 2018). Relaxin has been shown to be a GR agonist, resulting in GR phosphorylation, nuclear translocation and DNA binding at GRE locations, thus relaxin signalling is independent of *rxfp1* function (Dschietzig et al., 2004, 2009a; Halls et al., 2007). In addition, there is an autoregulatory relationship between glucocorticoids and relaxin concentrations, because exogenous glucocorticoid induced an increase of relaxin-2 concentration in HeLa cells, and relaxin-activated GR binds to to GRE sites in the *rln2* promoter region (Dschietzig et al., 2009b). However, r*elaxin 2* (*rln2*) was not identified as a DEG in either *gr^{s357}* larvae or *gr^{s357}* brains. This transcriptomic analysis of both *gr^{s357}* larvae and *gr^{s357}* brains provides a novel insight into the GR's regulation of the relaxin receptor, suggesting that GR acts as a transcriptional repressor of *rxfp1*, thus revealing an additional regulatory interaction between glucocorticoid and relaxin signaling. Further

research into potential GRE sites in the promoter and genomic DNA of *rxfp1* may provide important insights into how GR regulates *rxfp1* transcription.

In addition to *rxfp1*, many DEGs present in both *gr^s357* larvae and *gr^s357* brain datasets were associated with the regulation of transcription. This included common downregulated genes, such as *cebpd*, *tsc22d3* and *hif1al*; and common upregulated genes, such as *nfia* (nuclear factor I/A), *histh1l* (histone H1), *tbx2b* (T-box transcriptional repressor). The complicated nature of GR-regulated transcription has been revealed through various experimental approaches, including treatment with GR agonists and antagonists. As the GR is known to regulate many transcription factors, as seen in previous studies and this study, a plethora of secondary pathways are also affected, creating a vast interconnected network of transcriptional regulation affected by GC signaling (Chinenov et al., 2014). As many GR and other transcription factors can either activate or repress the same gene in a tissue-specific manner (Hunter et al., 2016), the common downregulated and common upregulated DEGs in *gr^s357* larvae and *gr^s357* brains provides a list of genes that strongly suggest GR target gene regulation in a specific direction. Interestingly, one hundred genes were found to be differentially expressed in opposing directions in *gr^s357* larvae and *gr^s357* brains, many of which were associated with the electron transport chain and mt-DNA. Previously I stated that the direction of mtDNA differential expression depends on type and duration of stress studied and is specific to each gene (Hunter et al., 2016). In my comparative analysis, specific mt-DNA associated genes were differentially expressed in opposing directions, i.e. upregulated in *gr^s357* larvae and downregulated in *gr^s357* brains. It is beyond the scope of this study to speculate on the possible reasons for this major difference, but it could be due to differences in the the duration of exposure to hypercortisolaemia, or due to tissue-specific or developmental stage-specific GR regulation of genes encoded by mt-DNA.

Concluding remarks

This chapter describes the use of RNA sequencing technologies to identify and characterise differentially expressed mRNAs in 5dpf larvae and adult brain tissue of zebrafish carrying the *gr^s357* mutation. The loss of GR DNA-binding capacity in *gr^s357* mutant larvae resulted in mRNA expression changes in genes associated with ECM organisation, focal adhesions and intracellular signaling including various components of the TGF-ß superfamily. By contrast, loss of GR function in adult *gr^s357* mutant zebrafish brains resulted in a dysregulation of genes associated with mitochondrial function, including the electron transport chain and steroid hormone biosynthesis. The most significant DEG in both *gr^s357* larvae and *gr^s357* brains was *fkbp5*, exhibiting almost complete extinction of gene expression compared to wild-type controls. Common genes dysregulated in the same direction were associated with transcriptional regulation, whereas

common genes dysregulated in opposing directions were associated with the mitochondrial electron transport chain. As such, my work suggests that the GR influences the transcription of a wide network of genes, some of which are specific to developmental stage or tissue, and others that are highly conserved between 5dpf larvae and adult zebrafish brains. The major challenge will be to understand when during development and where (which tissues) the switch occurs.

Whilst I have not performed RNA sequencing on the brains of $MR^{-/-}$ adult zebrafish, I have generated a double $MR^{-/-};GR^{-/-}$ mutant to establish the level of compensation that occurs when one of the cortisol-binding receptors is non-functional. Initial gross morphological characterisation of double mutants compared to wildtype and single mutant siblings display apparent compensation between MR and GR in regulating zebrafish growth.

Chapter 7. Generation of a double $MR^{-/-};GR^{-/-}$ mutant line and initial biometric characterisation

7.1 Introduction

To further understand the level of redundancy between MR and GR, I utilised a GR-KO mutant allele gr^{sh551}, created by fellow PhD student Davide Marchi (Freek van Eeden's laboratory, Bateson Centre, TUoS), using CRISPR-Cas9 mutagenesis, and subsequently maintained on a wild-type AB genetic background, at the University of Sheffield. I chose this mutant line instead of previously described gr^{s357} for three reasons: i) it was created in the same wildtype genetic background as the MR^{46Del} mutant I created, eliminating the variable of genetic background which could influence downstream analysis; ii) a complete loss of DBD and LBD function may provide a less complex phenotype to characterise than the previously described gr^{s357} mutants as the gr^{s357} alelle could in principle possess a degree of low but nevertheless functional ligand-binding and transcriptional activity.

This GR-KO mutant zebrafish line targeted exon 3 of the *nr3c1* gene which encodes the DBD domain of the GR protein (Marchi et al., 2020). This mutant carries an 11bp deletion that creates an out-of-frame missense mutation starting at codon 377, leading to a premature stop codon 12 residues later at codon 379 (A377fsX12). As the DBD starts at codon 384, the mutation putatively codes a truncated GR protein lacking the DBD and LBD. Homozygous GR-KO mutants named $gr^{sh551/sh551}$ exhibited well-established glucocorticoid signaling-defective phenotypes, such as exhibiting darker pigmentation after the VBA assay, increased expression of the HPI axis component *pomca* in the anterior pituitary, elevated concentrations whole-body cortisol and the ablation of *fkbp5* mRNA expression (Figure 7.1.; Marchi et al., 2020).

I hypothesised that the double mutant $GR^{-/-};MR^{-/-}$ would be homozygous lethal, due to loss of corticosteroid receptor compensation in various biological processes e.g loss of maternal *gr* and *mr* transcripts during embryogenesis, loss of ion homeostasis, and loss of a systemic response to a stress stimulus.
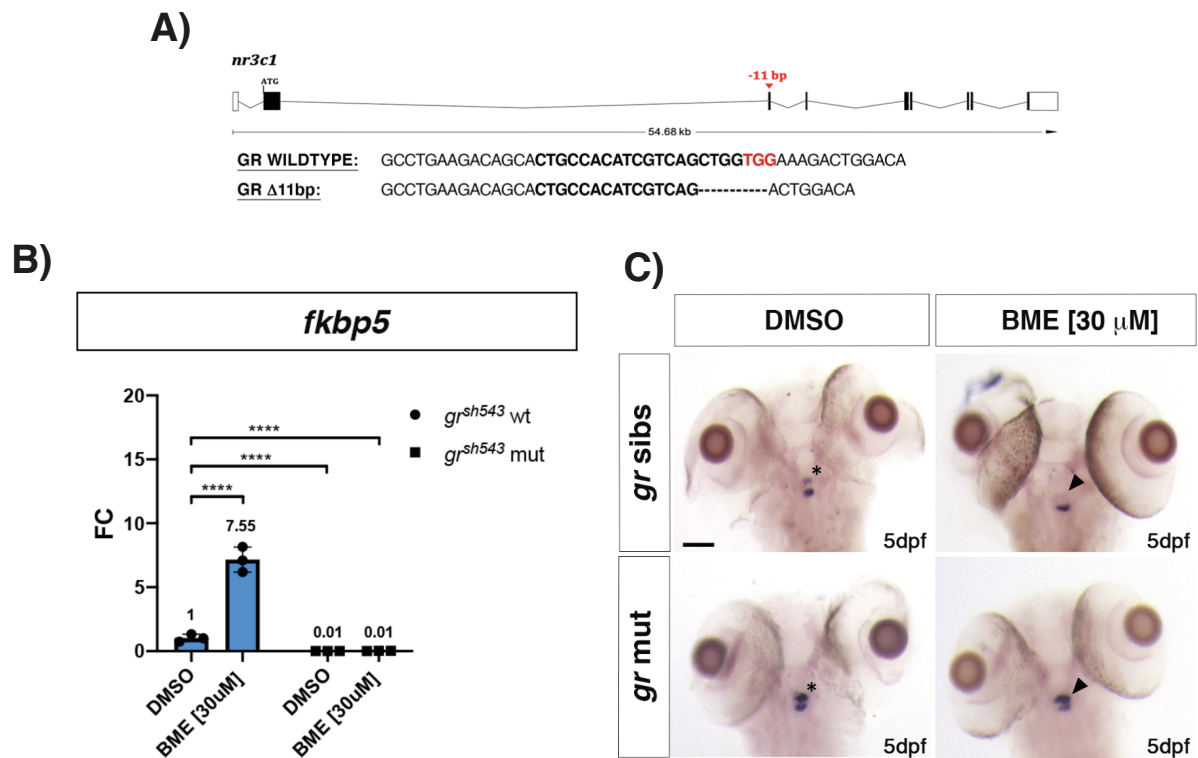
Figure 7.1. The *gr^sh551/sh551*mutant zebrafish generated by PhD student Davide Marchi. A) Schematic representative of zebrafish *GR* (*nr3c1*) gene. Exons are boxes and introns are lines. The 11bp deletion allele located in exon 3, which encodes the DNA binding domain, is highlighted. In this sequence, the crRNA target is in bold, red letters are PAM sequence; dotted line indicates deletion. B) qRT-PCR of glucocorticoid-target gene *fkbp5* in 5dpf larvae of *gr^sh551* mutants and wildtype siblings, with and without betamethasone (BME) treatment. C) Wholemount in situ hybridisation staining for antisense *pomca* RNA in the anterior pituitary of 5dpf larvae (all panels adapted from Marchi et al., 2020).

7.2. Results

7.2.1 Double mutant $GR^{-/-};MR^{-/-}$ zebrafish are viable but infertile at adulthood

To generate the double mutant line, homozygous $GR^{sh543/sh543}$ male and females were outcrossed by pair-mating with homozygous $MR^{46Del/46Del}$ female and male fish, respectively. Progeny were collected and raised to 3 months of age and genotyped by fin-clipping to confirm $GR^{sh543/+};MR^{46Del/+}$ genotype (Figure 7.2). F_1 generation $GR^{+/-};MR^{+/-}$ adult fish were then incrossed to generate all possible F_2 genotype combinations. Two clutches of F_2 generation fish were raised to adulthood.

Genotyping by PCR of the F2 population tail biopsies of both clutches revealed that double mutants $GR^{-/-};MR^{-/-}$ were viable at 9 months of age. To confirm previous glucocorticoid-signaling phenotypes, the VBA assay was performed on progeny of incrossed genotypes: $GR^{+/+};MR^{+/+}$ (WT), $GR^{-/-};MR^{+/+}$ (GR), $GR^{+/+};MR^{-/-}$ (MR) and $GR^{-/-};MR^{-/-}$ (double mutants). At 5dpf, MR mutant progeny displayed a similar response to the VBA assay as WT progeny (VBA+) at age 5dpf. By contrast, 100% of GR mutant progeny presented as dark (VBA-), indicative of defective glucocorticoid-signaling. Surprisingly, double-mutant females did not lay any eggs. Moreover, it was observed that male and female double mutant fish did not perform stereotypical breeding behaviour, i.e. engage in intimate contacts or chasing, and presented as lethargic with reduced general locomotor activity when visually compared to the other three genotypes. Double mutant males also displayed feminised secondary sex characteristics, including prominent blue stripes and large round bellies. On 4 repeated occasions when double mutants were pair-mated, they did not produce any eggs.

7.2. Zebrafish body weight, size and visceral fat: GR function can fully compensate for loss of MR function whereas MR can only partially compensate for loss of GR function.

It was observed during F_2 genotyping that GR mutants were bigger than WT and MR mutants, and double mutants of both sexes were profoundly larger than GR mutants. In collaboration with PhD student Davide Marchi, nine-month-old zebrafish of the aforementioned F_2 progeny were anaesthetised with tricaine, gently patted dry with a paper towel, and weighed on an analytical balance before returning to their tank. The results confirmed that there was no significant difference between weights of adult WT and MR mutant fish in either clutch 1 (p=0.9957) or clutch 2 (p=0.879) (Figure 7.2A&B). However, GR mutants exhibited a significant increase in weight compared to WT fish (clutch 1 p=0.0052; clutch 2 p=0.048), as previously reported (Marchi et al., 2020), and a similar trend was observed in comparison to MR mutants (clutch 1

p=0.0062; clutch 2 p=0.07). Of note, clutch 1 and clutch 2 were born 3 weeks apart, stocked at similar densities and fed the same amount of food. Therefore, weights of fish from both clutches were combined (Figure 7.2C). Interestingly, double mutants weighed profoundly more than all other genotypes (mean = 0.933g), ~2.5x more than WT (mean = 0.384g; p<0.0001), 2.5x more than MR mutants (mean = 0.396g; p<0.0001), and ~2x more than GR mutants (0.5054; p<0.0001). Moreover, GR mutants weighed significantly more than either WT (p=0.0038) or MR mutants (p=0.0043).

A similar pattern was observed at 18-months of age, after fish have been separated by genotype for 9 months. Zebrafish were culled and bodyweight and body length were recorded (Figure 7.4). As the two clutches were from the same genetic stock, born within the same month, and stocked at similar densities in identical tanks, data was combined. As before, no difference in weight was observed between WT and $MR^{-/-}$ fish (p=0.6753), also there was no difference in body size. Whereas $GR^{-/-}$ mutants were significantly heavier and longer than both WT (weight p=0.0289; length p<0.0001) and $MR^{-/-}$ fish (weight p=0.0015; length p<0.0001). Interestingly, double mutants were significantly heavier and longer than all other genotypes, as seen in Figures 7.4 and 7.5.

Interestingly, during dissection an observation was made regarding the quantity of visceral fat deposits in the abdominal cavity. $MR^{-/-}$ mutants have similar quantities of visceral fat to WT fish. $GR^{-/-}$ mutants displayed higher quantities of visceral fat than WT or $MR^{-/-}$ mutant fish. Whereas $MR^{-/-}$; $GR^{-/-}$ double mutants exhibited the highest quantity of visceral fat, more than all other genotypes (Figure 7.6). This suggests both MR and GR play an important role in the regulation of adipose tissue in the adult zebrafish.

These results indicate that loss of MR function alone has no appreciable effect on body weight, size or visceral fat accumulation, whereas loss of GR function causes a slight but significant increase in body weight, body size and fat deposits, indicating that GR activity limits these factors. However, loss of both GR and MR markedly increases body weight to over twice that of wild-type fish, indicating that both GR and MR are required to limit body weight. Similarly, body size and visceral fat quantity was significantly greater in double mutants than all other genotypes. Thus, whilst GR function can fully compensate for loss of MR function, MR can only partially compensate for loss of GR function. Taken together these results imply that GR and MR may share some common target genes that regulate body weight, size and adipose tissue expansion. However, GR is also likely to regulate additional genes that MR cannot target.
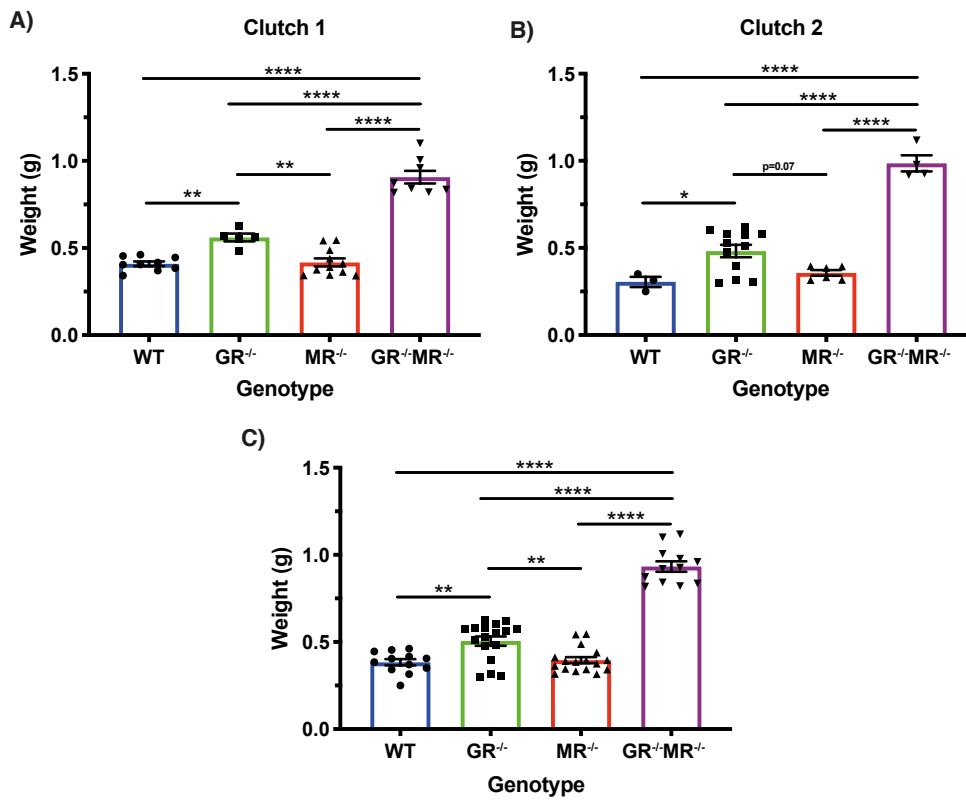
Figure 7.2. Body weights of zebrafish aged 9 months for wildtype (WT), *MR^{-/-}* and *GR^{-/-}* mutants, and *GR^{-/-};MR^{-/-}* double mutants. Two F_2 generations of an $GR^{sh543/+};MR^{46Del/+}$ incross, born 3 weeks apart, were stored in the same size tanks and stocks at similar densities. At 9 months they were genotyped and weighed. A) Clutch 1: *GR^{-/-}* fish weighed significantly more than WT (p=0.0052) and *MR^{-/-}* fish (p=0.0062). No difference in weight was observed between WT and *MR^{-/-}* fish. Double mutants weighed significantly more than WT, *MR^{-/-}* and *GR^{-/-}* mutants (p<0.0001). B) Clutch 2: *GR^{-/-}* fish weighed significantly more than WT (p=0.048) and displayed the same trend compared to *MR^{-/-}* fish (p=0.07). No difference in weight was observed between WT and *MR^{-/-}* fish. Double mutants weighed significantly more than WT, *MR^{-/-}* and *GR^{-/-}* mutants (p<0.0001). C) As the two clutches were from the same genetic stock, within the same month, stocked at similar densities in identical tanks, data was combined, and similar results were observed. *GR^{-/-}* fish weighed significantly more than WT (p=0.0038) and *MR^{-/-}* fish (p=0.0043). No difference in weight was observed between WT and *MR^{-/-}* fish. Double mutants weighed significantly more than WT, *MR^{-/-}* and *GR^{-/-}* mutants (p<0.0001). Results were analysed with one-way ANOVA with post-hoc Tukey test (* p<0.05, **p<0.01, ***p<0.001, ****p<0.0001). N=58.

7.2.2 Zebrafish locomotion: GR function can fully compensate for loss of MR function, whereas MR can only partially compensate for loss of GR function.

After observations of lethargic and reduced general locomotor activity in the double mutant adult fish in comparison to the other three genotypes, I measured WT, *MR⁻/⁻*, *GR⁻/⁻* and *GR⁻/⁻;MR⁻/⁻* locomotor activity for a 5 minute duration in the open field test (Figure 7.3). No significant difference of either total swim distance or fast swim distance (>10cm/s) was observed between WT and *MR⁻/⁻* fish. Where *GR⁻/⁻* mutants displayed a near significant reduction in total swim distance, and significant reduction in fast swim distance when compared to WT (total p=0.0546; fast p=0.0171) and *MR⁻/⁻*(total p=0.0528; fast p=0.0275) fish. Interestingly, double mutants swam significantly less total distance than WT (p<0.0001), *GR⁻/⁻* (p=0.0063) or *MR⁻/⁻* (p<0.0001) fish, and significantly less fast swim speed distance than WT (p<0.0001), *GR⁻/⁻* (p=0.001) or *MR⁻/⁻* (p<0.0001) fish. A similar trend to zebrafish body weight was seen in the open field zebrafish locomotion test. Loss of MR function alone had no appreciable effect on zebrafish locomotor activity, whereas loss of GR function caused a slight decrease in general locomotor activity and significant decrease in fast swim speed activity, indicating that GR activity promotes locomotor activity. However, loss of both GR and MR profoundly decreases locomotor activity, to over half that of wild-type fish, indicating that both GR and MR are required for normal levels of locomotor activity. Thus, whilst GR function can fully compensate for loss of MR function, MR can only partially compensate for loss of GR function. Taken together these results imply that GR and MR may share some common target genes that positively promote locomotor activity. However, GR is also likely to regulate additional behavioural genes that MR cannot target.
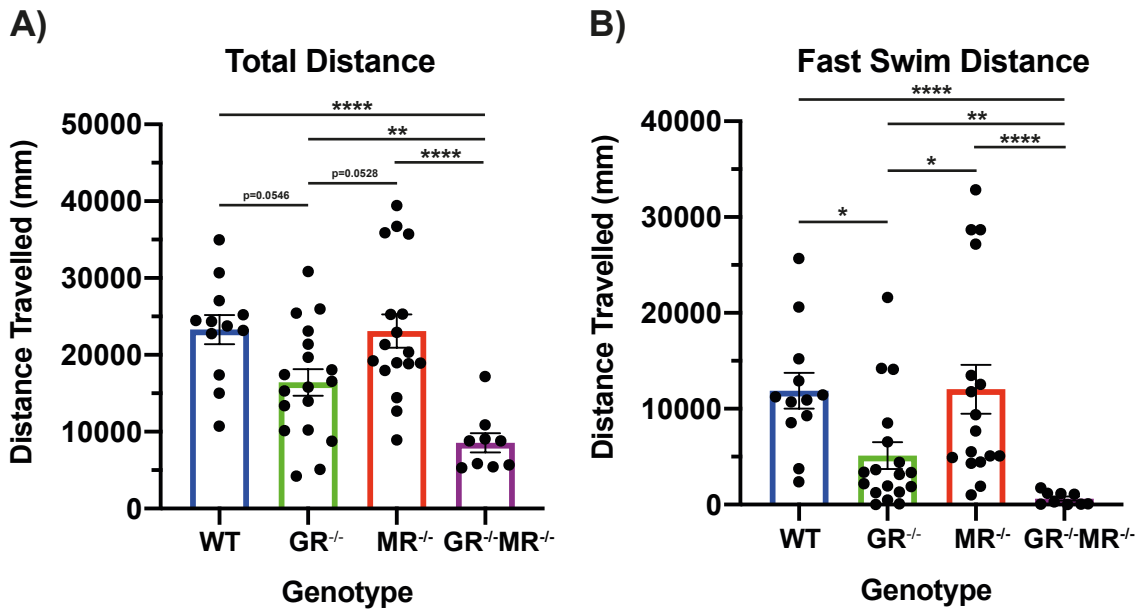
Figure 7.3. Response of WT, *GR*^{-/-}, *MR*^{-/-} and *GR*^{-/-};*MR*^{-/-} 9month old adult zebrafish to open field tests. Total distance and fast swim distance were recorded for a 5-minute period for clutch 1 and clutch 2. Results combined are shown. A) *GR*^{-/-} fish showed a trend of less total distance swam than WT siblings (p=0.0546) and *MR*^{-/-} mutants (p=0.0528). No significant difference in total distance swam was observed between WT and *MR*^{-/-} fish. Double mutants swam significantly less total distance than WT (p<0.0001), *GR*^{-/-} (p=0.0063) and *MR*^{-/-} (p<0.0001) fish. B) *GR*^{-/-} fish swam significantly less distance at a fast swim speed (>10cm/s) than WT siblings (p=0.0171) and *MR*^{-/-} mutants (p=0.0275). No significant difference in distance swam at a fast speed was observed between WT and *MR*^{-/-} fish. Double mutants swam significantly less distance at fast speeds than WT (p<0.0001), GR^{-/-} (p=0.001) and *MR*^{-/-} (p<0.0001) fish. Results were analysed with one-way ANOVA with post-hoc Tukey test (* p<0.05, **p<0.01, ***p<0.001, ****p<0.0001). N=58.
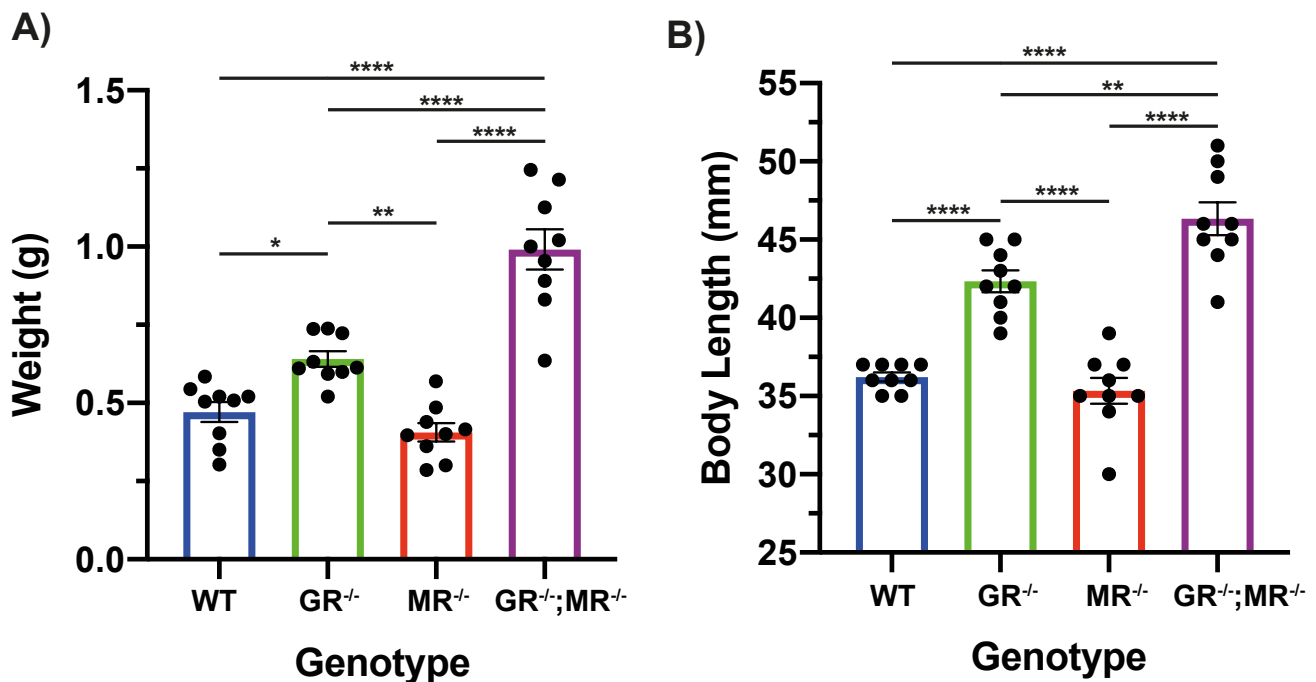
Figure 7.4. Body weight and length of zebrafish aged 18-months for wildtype (WT), *MR*^{-/-} and *GR*^{-/-} single mutants, and *GR*^{-/-};*MR*^{-/-} double mutants. Aged 18-months, zebrafish maintenance was reduced; fish were weighed and measured. As the two clutches were from the same genetic stock, within the same month, stocked at similar densities in identical tanks, data was combined, and similar results were observed. A) *GR*^{-/-} fish weighed significantly more than WT (p=0.0289) and *MR*^{-/-} fish (p=0.0015). No difference in weight was observed between WT and *MR*^{-/-} fish (p=0.6753). Double mutants weighed significantly more than WT, *MR*^{-/-} and *GR*^{-/-} mutants (p<0.0001). B) *GR*^{-/-} fish were significantly longer than WT and *MR*^{-/-} fish (p<0.0001). No difference in length was observed between WT and *MR*^{-/-} fish (p=0.8472). Double mutants were significantly longer than WT and *MR*^{-/-} mutants (p<0.0001) and *GR*^{-/-} mutants (p<0.0047). Results were analysed with one-way ANOVA with post-hoc Tukey test (* p<0.05, **p<0.01, ***p<0.001, ****p<0.0001). N=36.
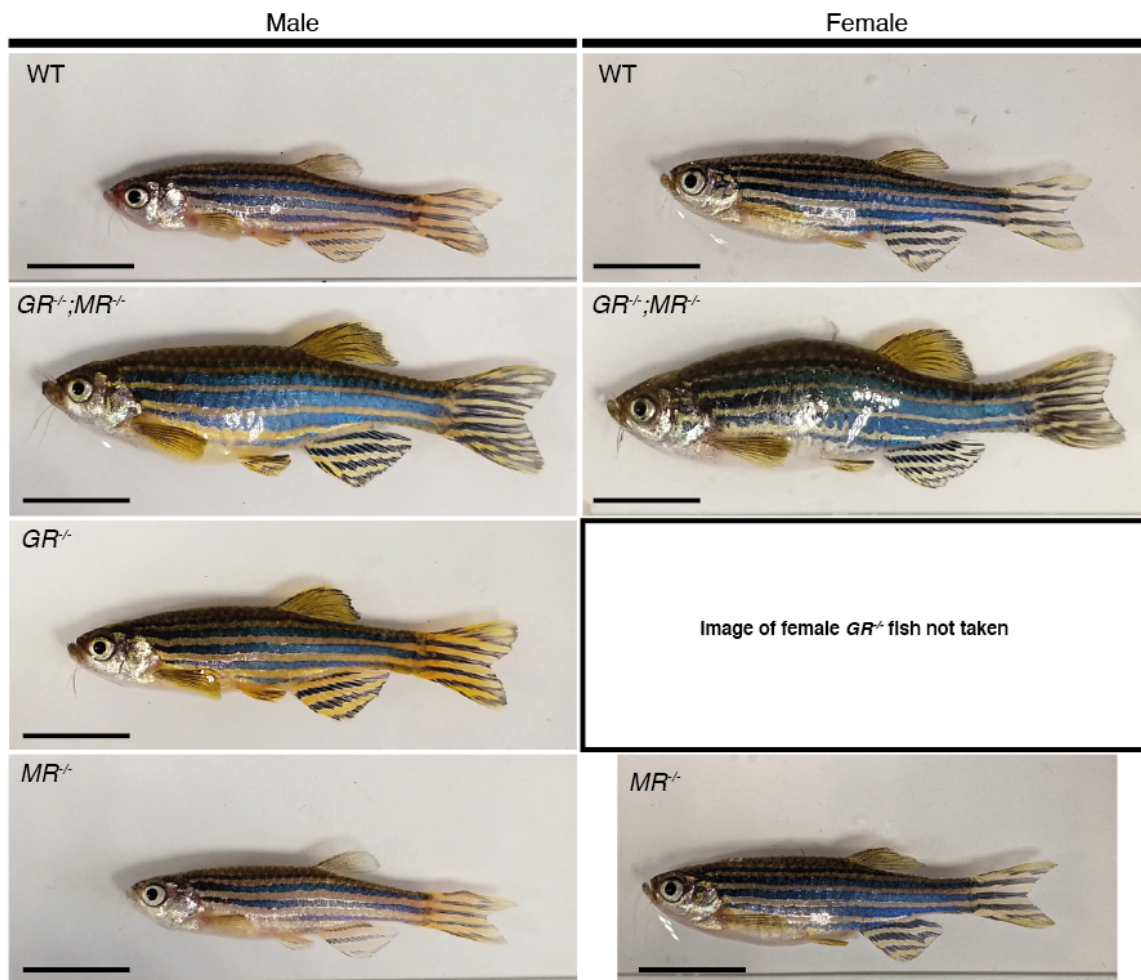
Figure 7.5. Representative images of WT, *GR*^{-/-}, *MR*^{-/-} and *GR*^{-/-}*;MR*^{-/-} 18-month old adult zebrafish shows size and secondary sex characteristic differences. Male and female MR^{-/-} mutants display similar size and typical secondary sex characteristics compared to WT fish. GR^{-/-} and GR^{-/-};MR^{-/-} mutants are significantly larger and males display a feminisation of secondary sex characteristics, i.e. males display strong blue and golden stripes on skin, blue and yellow striped anal fin colouration, and yellow-green pigmentated doral fin, characteristic of wildtype females.
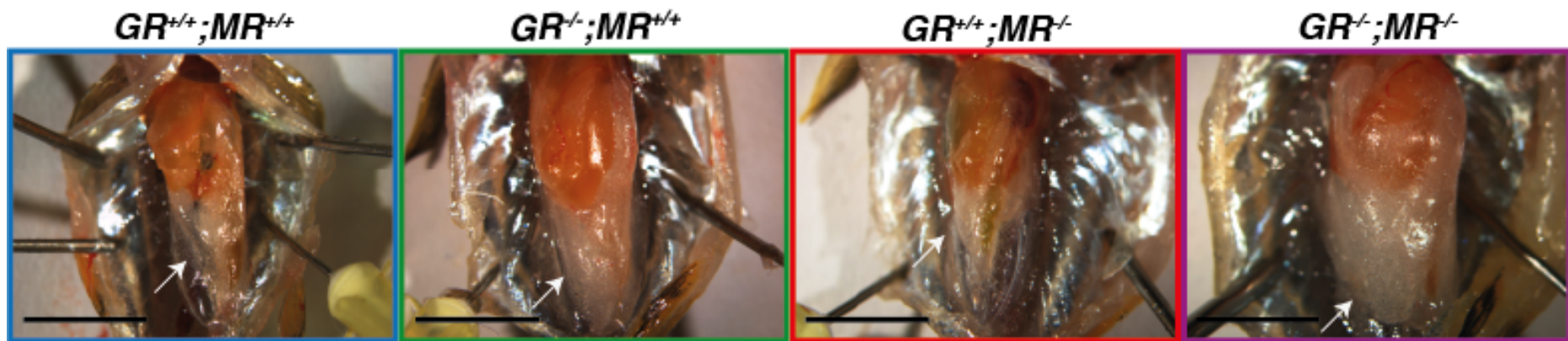
Figure 7.6. Representative macroscopic images of the abdominal cavity of WT, $GR^{-/-}$, $MR^{-/-}$ and $GR^{-/-};MR^{-/-}$ 18-month old adult zebrafish that show differences in visceral fat quantities. $MR^{-/-}$ mutants have similar quantities of visceral fat to WT fish. $GR^{-/-}$ mutants displayed higher quantities of visceral fat than WT or $MR^{-/-}$ mutant fish. $MR^{-/-}$; $GR^{-/-}$ double mutants exhibit the highest quantity of visceral fat, more than all other genotypes. White arrows indicated fat deposits. Scale bar = 5mm.

7.3 Discussion

To investigate the extent to which the functions of GR and MR might overlap or be distinct, I created double mutants homozygous for a loss-of-function MR mutation and a loss-of-function GR mutation. Surprisingly, $MR^{-/-};GR^{-/-}$ mutants were homozygous viable, however they were infertile when intercrossed, with females not spawning throughout their life. Initial characterisation of morphological biostatistics revealed a profound increase in body weight and body length of double mutants in comparison to wild-type, and to single mutant siblings, despite all lines being maintained at similar stock densities, with similar feeding quantities and sex ratios. $GR^{-/-}$ single mutants were significantly heavier and longer than wild-type and $MR^{-/-}$ single mutant fish. In correlation with our zebrafish body weight data, examination or organs by dissection revealed qualitative observations of extremely large deposits of visceral fat surrounding the internal organs of the of double mutants. In addition, $GR^{-/-}$ fish possessed noticeably greater visceral fat deposits than wild-type or $MR^{-/-}$ fish. Not only was the bodyweight and visceral fat greatest in double mutants, body length was greater also, with a markedly less significant increase in body length in $GR^{-/-}$ single mutant fish in comparison to wildtype and $MR^{-/-}$ single mutant fish. These observations demonstrate that in terms of not only bodyweight and fat accumulation, but also general zebrafish size, GR function can fully compensate for loss of MR function, whereas MR function can only partially compensate for loss of GR function.

Whilst these are preliminary results, the GR and the MR have been associated with metabolic processes and growth in mammals and in zebrafish (Faught and Vijayan, 2020; John et al., 2016; Rose et al., 2010; Sargis et al., 2010). In humans, clinical findings have correlated glucocorticoid levels to obesity and insulin resistance (Andrew et al., 2002). Moreover, it has been suggested in humans that obesity reflects a state of glucocorticoid resistance, resulting in adipocyte hypertrophy, lipogenesis and free fatty acid uptake (John et al., 2016). However, the impact of cortisol-bound GR on lipid homeostasis is dependent on whether cortisol exposure is acute or chronic. Acute glucocorticoid treatment is known to stimulate lipolysis, whereas chronic glucocorticoid exposure leads to glucocorticoid resistance and promotes weight gain and adipocyte expansion (Berthon et al., 2014). In humans, the MR is highly expressed in white and brown adipose tissues; loss of MR expression has been shown to inhibit adipogenesis, whereas MR activation by aldosterone promotes adipocyte expansion (Caprio et al., 2007). It is important to note that these MR experiments modelled acute MR regulation of adipocyte regulation, and the effects of chronic mineralocorticoid-resistance requires further study.

In a recent study of MR-KO mice, there were no significant differences in white or brown adipose levels in comparison to wild-type mice when assessed at postnatal day 5 (P5) (Ferguson et al., 2020). The authors generated an adipocyte-specific deletion of MR, which showed no significant changes in body weight. When these animals were treated with high-dose corticosterone for four weeks, they showed a similar increase in bodyweight as wild-type mice. This suggests GR signaling facilitates the observed corticosterone-mediated metabolic dysfunction (Ferguson et al., 2020).

In zebrafish, there is little evidence of adult zebrafish growth regulation by MR or GR as primarily larval studies have been reported. However, in our lab, glucocorticoid- and androgen deficient lines *fdx1b-/-* and *cyp11c1-/-* male fish exhibited significantly increased body weight and body length more than their respective wild-type siblings, as did *cyp11a2*$^{-/-}$ mutant fish, lacking all steroid hormone synthesis. Recently, a GR-KO zebrafish line was shown to increase zebrafish growth, including whole-body protein and lipid weight (Faught and Vijayan, 2019a). Together, my results, with support from another GR-KO mutant zebrafish line, mouse models and human conditions emphasise the importance of glucocorticoid-GR signaling on growth, bodyweight and adipose regulation. These double mutant studies provide novel insight into the relationship between the MR and GR in regulating body growth and adipocyte deposition, indicating that GR function can fully compensate for loss of MR function, whereas MR can only partially compensate for loss of GR function. However, the increased body weight in *GR*$^{-/-}$ and double mutants correlates with reduced locomotor activity of the fish. Whilst exercise is a key influencer in obesity, it remains unclear whether the increased body weight phenotype is the result of an energy expenditure imbalance due to decreased locomotor activity, or whether there are multiple, parallel impacts of loss of glucocorticoid signaling on a range of molecular mechanisms regulating growth, protein and lipid metabolism, and locomotor behaviour. Future experiments to understand the root cause of the surprising phenotypes of double mutants may provide further insights into the complex relationship between the functions of the MR and the GR.

Of note, double mutants were infertile, and females did not spawn eggs over multiple mating trials. Recently, the loss of GR function in zebrafish has been correlated with accelerated ovarian ageing (Faught et al., 2020). GRKO mutant zebrafish were shown to have a reduced reproductive lifespan, with premature ovarian ageing reducing fecundity rates and embryo survival. Whilst we did not record the number of eggs from each clutch, our double mutant may provide a novel tool to investigate the role of both the GR and MR in reproduction.

This thesis so far has focused on investigating the roles of the corticosteroid receptors in zebrafish. However, in parallel, I have also investigated a current knowledge gap in our understanding of the corticosteroid biosynthetic pathway in zebrafish.

Chapter 8. The loss of Cyp17a2 function results in glucocorticoid deficiency, mineralocorticoid excess, androgen-deficiency and female infertility.

8.1 Introduction

The P450 enzyme 17 hydroxylase (Cyp17a1) catalyses two critical reactions of steroid biosynthesis: first, 17α-hydroxylation, important for cortisol and sex steroid synthesis, followed by 17,20-lyase activity, which is specifically required for sex steroid production (Auchus et al., 2017). 17α-hydroxylation converts both pregnenolone and progesterone to 17α-hydroxypregnenolone (17OH-Preg) and 17α-hydroxyprogesterone (17OH-Prog), respectively. These are early precursors for 11-deoxycortisol and the canonical glucocorticoid, cortisol, as well as sex steroids including testosterone, and the principal androgen in fish, 11-ketotestosterone (Turcu and Auchus, 2017).

Cyp17a1 activity is required for sexual dimorphism and reproduction in vertebrates, initially to synthesize 19-carbon androgens and 18-carbon oestrogens from 17α-hydroxy-precursors, and thus acts at the gateway to the pathway leading to sex steroid production (Auchus et al., 2017). Cyp17a1 converts 17OH-preg to dehydroepiandrosterone (DHEA), and also converts 17OH-prog to androstenedione (A4) in the brain, gonads and the adrenal gland (Prough et al., 2016). A4 is a precursor for both androgen and oestrogen steroid hormone production and is known as a very weak androgen.

Rats and mice express Cyp17a1 in the gonads but not in the adrenal glands (Auchus et al., 2017). Therefore, rodents do not produce the glucocorticoid cortisol in adrenal tissue, and instead their dominant glucocorticoid is corticosterone, a mineralocorticoid precursor of aldosterone that is known to bind both the glucocorticoid and mineralocorticoid receptor. As Cyp17a1 is expressed in rodent gonads, this ensures that they produce the conventional mammalian sex steroids.

By contrast, in humans the 17α-hydroxylase activity of CYP17A1 allows for cortisol in the adrenal gland, and the 17,20 lyase activity produces androgens and oestrogens. A loss of 17-hydroxylase activity (17-OH Deficiency; 17OHD) floods the mineralocorticoid pathway with steroid precursors, resulting in steroidogenesis from pregnenolone to progesterone, then to 11-deoxycorticosterone (DOC) and corticosterone. In humans, corticosterone is a minor adrenal steroid, but in 17OH-deficiency (17OHD), it is known to rise from the ~10nM basal concentration

observed in unaffected individuals, to approximately ~1μM in the circulating blood of individuals homozygous for loss-of-function mutant alleles (Auchus et al., 2017). This rise in corticosterone is thought to provide sufficient compensatory glucocorticoid activity to mitigate the phenotypic consequences of cortisol-deficiency. An additional consequence of 17OHD is elevated concentrations of DOC, a mineralocorticoid agonist, from ~0.6nM to ~10nM. This results in near saturation of the MR, resulting in hypertension (Auchus et al., 2017). Further along the corticosteroid pathway, 17OHD leads to gonadal hormone deficiency that results in sexual infantilism and pubertal failure (Auchus et al., 2017). Thus, human CYP17A1 deficiency results in cortisol deficiency, which is alleviated through increased corticosterone concentrations. In addition, mineralocorticoid excess, and androgen and oestrogen deficiencies are typical in CYP17A1-deficienct patients.

In many vertebrates, including teleost fish, *cyp17a1* is expressed in the gonads as the 17α,20-lyase activity is required for sexual dimorphism. However, multiple species of teleost, including zebrafish (Pallan et al., 2015), tilapia and medaka (Zhou et al., 2007) have been discovered to contain a second gene coding a cytochrome P450c17: *cyp17a2*. These two genes are differentially expressed in certain tissues of tilapia, with *cyp17a2* being solely expressed in the head kidney, the location of the steroidogenic interrenal tissue (Zhou et al., 2007). Both *cyp17a1* and *cyp17a2* are expressed in the ovary (granulosa and theca cells) and testis (interstitial cells) (Zhou et al., 2007). However, a biochemically distinct difference was discovered between the two cytochrome P450c17s in tilapia; both Cyp17a1 and Cyp17a2 were shown by enzymatic assays to perform the 17α-hydroxylase activity, but only cyp17a1 possessed the ability to perform the 17,20 lyase activity (Zhou et al., 2007). These two genes were subcloned and recombinant constructs were transfected into HEK293 cells. Thin-layer chromatography assessed the activities (both 17α-hydroxylation and 17,20 lyase activities) of the tilapia Cyp17a1 and Cyp17a2 enzymes (Zhou et al., 2007). Cyp17a1 exhibited the ability to convert progesterone and pregnenolone to 17α-hydroxyprogesterone and 17α-hydroxypregnenolone, and then to catalyse their subsequent conversion to DHEA and androstenedione. By contrast, Cyp17a2 converted progesterone and pregnenolone to 17α-hydroxyprogesterone and 17α-hydroxypregnenolone, but did not have the ability to perform the 17,20 lyase reaction (Zhou et al., 2007).

Recent studies using thin layer chromatography have revealed that the zebrafish Cyp17a2 enzyme has the same limitation as the previously described *Tilapia* counterpart, which is a lack of 17,20 lyase activity even in the presence of b_5 and for an extended incubation time (Pallan et al., 2015). Interestingly, zebrafish Cyp17a2 was also discovered to be more active than Cyp17a1 in catalysing 17α-hydroxylation of both pregnenolone and progesterone. Further investigation of

the zebrafish Cyp17a1 and Cyp17a2 crystal structures revealed that they have similar active sites, which are remarkably similar to the human Cyp17a1 active site, despite only ~50% protein homology (Pallan et al., 2015). Pallan *et al.* (2015) determined that the difference between the 17,20 lyase activities of Cyp17a1 and Cyp17a2 were not attributable to structural changes limiting the binding of Cyp17a2 to 17α-hydroxyprogesterone and 17α-hydroxypregnenolone. Instead, they proposed two alternative hypotheses: i) structural residue alterations near the periphery of the heme prothestic group, requiring ferric peroxide for the 17,20 lyase reaction, and ii) in the presence of b5, Cyp17a1 may adopt multiple conformations, one of which facilitates the catalysis of the 17,20 lyase reaction.

Previously it has been shown that *cyp17a1*-deficiency in a TALEN-generated mutant zebrafish line produced an all-male phenotype (Zhai et al., 2017). More recently, a novel CRISPR-generated *cyp17a1*-deficient zebrafish line was developed (Zhai et al., 2018). These *cyp17a1*-deficient fish were oestrogen- and androgen-deficient, but not cortisol-deficient. As previously described, *cyp17a1*-deficiency leads to an all-male phenotype with normal testis, spermatogenesis and normal male sexual secondary sex characteristics and sexual behaviour, implying that male development does not require testosterone or oestrogen (Zhai et al., 2018). Interestingly, the development of a juvenile ovary to a mature ovary was arrested. Here, the authors found that either testosterone or estradiol treatment from 18dpf resulted in ovarian differentiation to produce mature oocytes. As testosterone is the precursor to estradiol, it was suggested that estradiol is essential in ovarian differentiation, and that estrogen-deficiency is the defining cause of the all-male cyp17a1-deficient fish (Zhai et al., 2018).

If Cyp17a1 is required for the correct synthesis of sex steroids, yet has no significant effect on the concentration of cortisol, then does this imply that the paralog *cyp17a2* is responsible for the 17α-hydroxylase activity that produces glucocorticoids; and what are the biochemical differences responsible for the differential enzymatic activity between the Cyp17a1 and Cyp17a2 paralogs?

With the multi-species evidence of Cyp17a1 performing both the 17α-hydroxylase and 17,20 lyase reaction and the *cyp17a1*-deficient zebrafish mutant exhibiting androgen and oestrogen deficiency, but not cortisol deficiency, we aimed to characterise the role of the P450-cytochrome enzyme Cyp17a2, by creating a loss-of-function mutant in the *cyp17a2* gene. I hypothesised that the loss of Cyp17a2 activity would result in the loss of 17α-hydroxylase activity in the interrenal tissue of the head kidney, causing a reduction in glucocorticoid precursors and the primary glucocorticoid, cortisol. In consequence, the early corticosteroid precursors would be predicted to flood the mineralocorticoid pathway, producing a mineralocorticoid excess, with a significant

increase in concentrations of 11-deoxycorticosterone (DOC) and corticosterone (Figure 8.1). However, we also hypothesise that there would be no change to sex steroids or sexually dimorphic phenotypes, as the gonadal function of *cyp17a1* would not be affected. Accordingly, CRISPR-Cas9 technology was utilised to create a *cyp17a2* loss-of-function mutant, and steroid biosynthesis and fertility were then investigated.
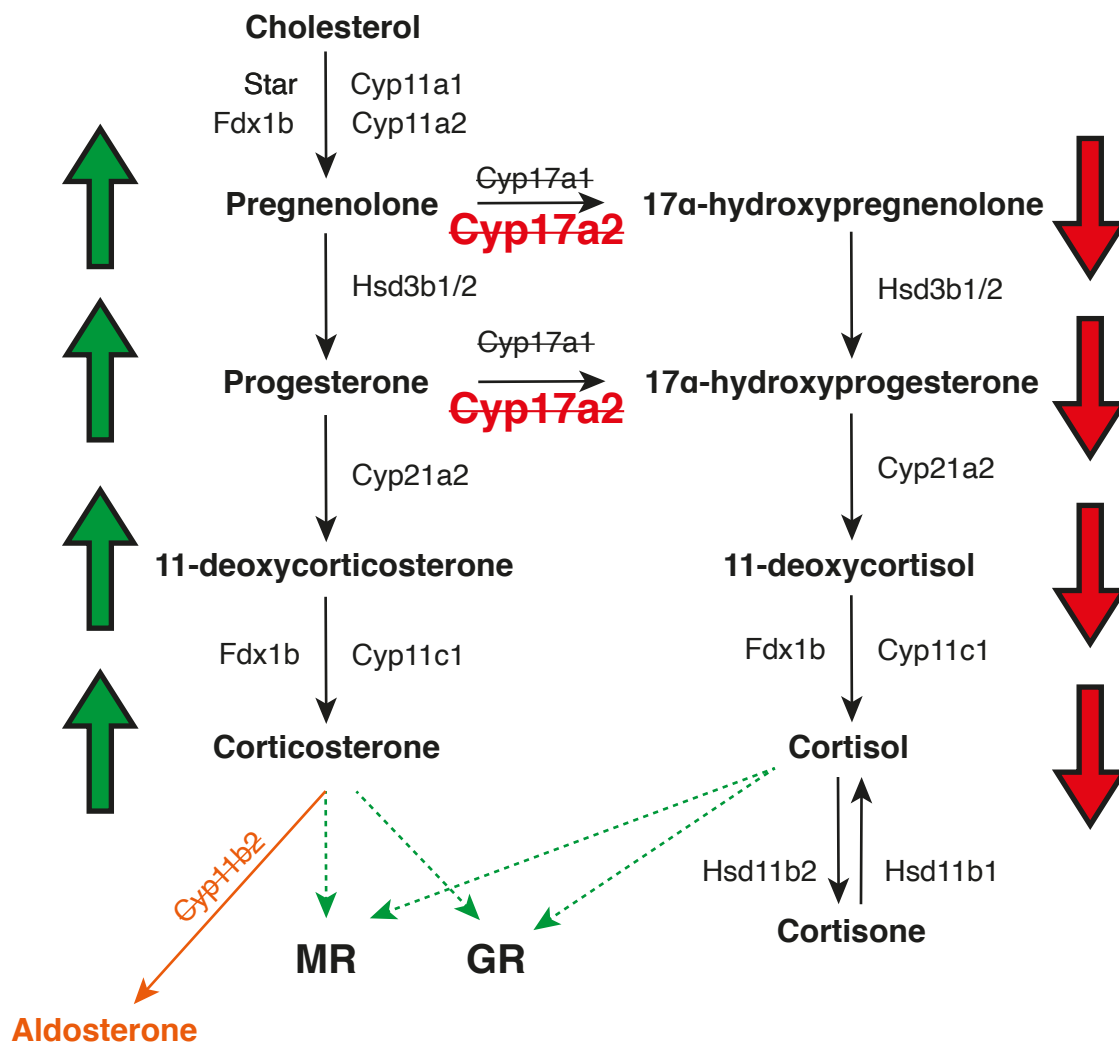
Figure 8.1. The glucocorticoid and mineralocorticoid steroid biosynthesis pathway in the interrenal tissue, annotated to visualize the Cyp17a2 loss-of-function hypothesis. In the mineralocorticoid pathway (left arm), a homolog of *CYP11B2* (aldosterone synthase) and subsequent steroid hormone, aldosterone, has not been discovered in zebrafish (orange text and arrows). Additionally, cyp17a1 is striked-through as it is not expressed in the interrenal tissue. I predict that the loss of Cyp17a2 activity (red and strikedthrough) caused by null mutations in *cyp17a2* would reduce the production of the principal glucocorticoid, cortisol, and its precursors. Steroids upstream of disruption would flood the mineralocorticoid pathway resulting in an increase in corticosterone and its precursors.

8.2 Results

8.2.1 Human CYP17A1, zebrafish cyp17a1 and cyp17a2 DNA and protein sequence alignments.

As the zebrafish has two paralog P450 genes, *cyp17a1* and *cyp17a2*, which are both homologs to the human *CYP17A1*, it is important to see what similarities there are between DNA and amino acid sequences. This provides an insight into conserved domains and potential homologous function. A DNA sequence alignment comparison of these three genes shows that there are approximately 50% similarity between all three genes (see Table 8.1). It was surprising to see that the zebrafish paralog genes, *cyp17a1* and *cyp17a2*, displayed a comparable degree of nucleotide sequence similarity to each other (54.97%) as they both do to the human *CYP17A1* gene (52.08% and 52.85% respectively). When translated, the amino acid sequence comparison (Thompson et al., 1994) reveals comparable levels of similarity, with overall ~50% conservation between the open reading frames encoded by these three genes (Table 8.2). However, visualization of the alignment shows higher levels of amino acid sequence conservation towards the C-terminus (Figure 8.3). Throughout the translated protein sequences of all three genes, P450 and EP450I fingerprint signatures have been identified (Yates et al., 2020). PRINTs domain analysis identifies 4 P450 fingerprints in *CYP17A1* between amino acid 302-454, toward the C-terminus of the protein sequence. This is similar in *cyp17a1* and *cyp17a2*, where four P450 domains are identified between amino acid 313-464 and 302-451 respectively (Figure 8.2).

Table 8.1. Percentage identity matrix of CLUSTAL-W DNA alignment for the Human *CYP17A1*, zebrafish *cyp17a1* and zebrafish *cyp17a2* genes

	hCYP17A1	zCyp17a1	zCyp17a2
hCYP17A1	100	52.08	52.85
zCyp17a1	52.08	100	54.97
zCyp17a2	52.85	54.97	100

Table 8.2. Percentage identity matrix of the Human CYP17A1, and zebrafish Cyp17a1 and Cyp17a2 protein sequences reported by ClustalW alignment.

%	hCYP17A1	zCyp17a1	zCyp17a2
hCYP17A1	100	48.62	41.89
zCyp17a1	48.62	100	51.31
zCyp17a2	41.89	51.31	100

```
hCYP17A1     1 MWELVA------L---LLLTLAYLFWPKRR----CPGAKYPKSLLSLPLVGSLPFLPRHG
zCyp17a1     1 MAEALILPWLLCLSLFSAVTLAALYLKQKMNGFVPAGNRSPPSLPSLPIIGSLMSLVSDS
zCyp17a2     1 MCSVSV------CVCFSALLLLLILVRRLLEGVGSSSVSFPCLPRLPLIGSLLHLRSNL


hCYP17A1    48 HMHNNFFKLQKKYGPIYSVRMGTKTTVIVGHHQLAKEVLIKKGKDFSGRPQMATLDIASN
zCyp17a1    61 PPHIFFQDLQKKYGDLYSLMMGSHKLLIVNNHHHAKEILIKKGKIFAGRPRTVTTDLLTR
zCyp17a2    55 PPHLLFTQLSSQYGPLFGLYAGPHLTLVVSEIGLVREVLLQRGREFAGRPKMVTTDLLTQ


hCYP17A1   108 NRKGIAFADSGAHWQLHRRLAMATFALFKDGDQKLEKIICQEISTLCDMLATHNGQSIDI
zCyp17a1   121 DGKDIAFADYSSTWKFHRKMVHGALCMFGEGSVSIEKIICREASSMCEVLTESQNSAVDL
zCyp17a2   115 GGKDIAFADYSPLWKNHRRLVHSSFTLFGEGSNKLQTIVQEAADSLCEELQACRGQSSDL


hCYP17A1   168 SFPVFVAVTNVISLLCFNTSYKNGDPELNVIQNYNEGIIDNLSKDSLVDLVPWLKIFPNK
zCyp17a1   181 GPELTRAVTNVVCALCFNSSYKRGDAEFESMLQYSQGIVDTVAKDSLVDIFPWLQIFPNK
zCyp17a2   175 SVVLMRAVTNVICRLVFSSSYQPSDPELQTVIQYNDGIVQTIARGGLVDIFPWLRIFPNK


hCYP17A1   228 TLEKLKSHVKIRNDLLNKILENYKEKFRSDSITNMLDTLMQAKMNSDNGNAGPDQDSELL
zCyp17a1   241 DLRILRQCISIRDKLLQKKYEEHKVTYSDNVQRDLLDALIRAKRSSENNNSSTRD--VGL
zCyp17a2   235 DLKRLKECVSIRDQLLYKKLLEHKKSLTPGEPRDLLDALLIGQQR---GSCGA----DDI


hCYP17A1   288 SDNHILTTIGDIFGAGVETTTSVVKWTLAFLLHNPQVKKKLYEEIDQNVGFSRTPTISDR
zCyp17a1   299 TEDHVLMTVGDIFGAGVETTTTVLKWSIAYLVHNPQVQRKIQEELDSKIGKERHPQLSDR
zCyp17a2   288 TEDHVLMTAAEAFGAGVETTSTTLLWTIAFLLHHPQLQERVQAELDECVGVDRPPCLSDR


hCYP17A1   348 NRLLLLEATIREVLRLRPVAPMLIPHKANVDSSIGEFAVDKGTEVIINLWALHHNEKEWH
zCyp17a1   359 GNLPYLEATIREVLRIRPVSPLLIPHVALQDSSVGEYTVQKGTRVVINLSLHHDEKEWK
zCyp17a2   348 PHLPLLDAVLCEVMRIRPVSPLIPHVAMQDTSLGGHSVPKGTRVLVNMWAIHHDPKHWD


hCYP17A1   408 QPDQFMPERFLNPAGTQLISPSVSYLPFGAGPRSCIGEILARQELFLIMAWLLQRFDLEV
zCyp17a1   419 NPELFDPGRFLNEEGDGLCCPSGSYLPFGAGVRVCLGEALAKMELFLFLAWILQRFTLEM
zCyp17a2   408 QPEQFNPERFLEPSCKKK--TQSSFLPFGAGPRVCVGESLARIELFLFVSRLLQRFSFSC


hCYP17A1   468 PDDGQLPSLEGIPKVVFLIDSFKVKIKVRQAWREAQAEGST
zCyp17a1   479 PTGQPLPDLQGKFGVVLQPKKFKVVAKVRADWEKSPLMQHC
zCyp17a2   466 PSEASLPDLQGRFGVVLQPERYTVTVTPRH-----------
```

Figure 8.2. Alignment of human CYP17A1, zebrafish cyp17a1 and cyp17a2 amino acid sequences. The alignment was generated with ClustalW and visualised using BOXSHADE. The pairwise identities between sequences are in Table 2. Greyscale indicates residue similarity. A grey-box highlights similar residues and a black box highlights identical residues. Red lines indicate PRINTs P450 fingerprint domains.
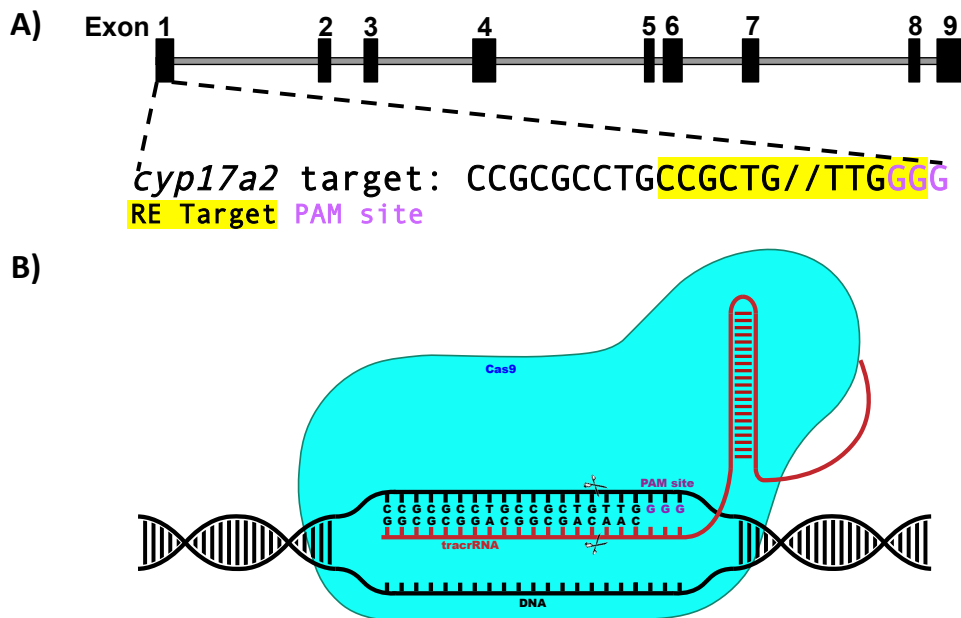
Figure 8.3. CRISPR-cas9 technology was utilised to generate a targeted mutation in *cyp17a2*. A) Exon 1 was targeted with a custom-designed guideRNA that would induce a DNA double-stranded break (//) that overlapped the restriction enzyme BsiYI's target sequence (yellow). B) Schematic of guideRNA (red) and Cas9 enzyme (blue) activity generating a DNA double-stranded break (scissors) 3 nucleotides from PAM site.

8.2.2 Targeted mutation of exon 1 of the zebrafish *cyp17a2* gene

To understand the function of *cyp17a2* in zebrafish, a genetic knock-out approach was taken. *cyp17a2* encodes one transcript that is 1488bp in length and comprised of 9 exons, encoding a 495aa long protein (Yates et al., 2020). A guide RNA (gRNA) of 18 nucleotides was designed to target nucleotides 115-132bp in exon 1. The gRNA consisted of a target specific CRISPR RNA (crRNA) that overlaps with a PAM site and a restriction enzyme (RE) target sequence. The tracrRNA scaffold (Figure 8.3) sequence was included in this gRNA.

The *cyp17a2*-specific gRNA was injected along with Cas9 protein into the yolks of 50 1-cell stage zebrafish embryos. After incubation of injected embryos for 24hrs at 28.5°C, 1dpf embryos were culled, genomic DNA was extracted, and the targeted genomic DNA sequence was amplified by PCR. A restriction digest assay revealed that genomic DNA PCR fragments generated from non-injected embryos were completely digested to two discrete products (Figure 8.4). By contrast, the PCR fragments produced from 5 of the 6 embryos injected with *cyp17a2* gRNA and Cas9 protein resulted in partial digestion, indicating that mutations had been induced which resulted in the disruption of the RE target site in an unknown number of embryonic cells (Figure 8.4). The remaining population of injected zebrafish embryos (F0) were raised to adulthood and at 3 months of age they were screened for germline mutations. CRISPR-injected females were outcrossed with wildtype males and vice versa; progeny were collected. The F_1 progeny were screened by PCR, restriction enzyme digestion and agarose gel electrophoresis for the presence of distinct alleles (Figure 8.5A). A germline mutation identified in this way was sequenced and a 29bp deletion was identified at 109-138bp (c.109_138del), which gave rise to a frameshift at codon 37 leading to a premature stop at codon 75 (p.C37FfsX75) (Figure 8.B). These F_1 progeny were raised to sexual maturity, sequenced, and heterozygous fish carrying this mutation were in-crossed. The resulting F_2 population were genotyped and genotype ratios indicated that the new allele exhibited Mendelian inheritance (Figure 8.6).
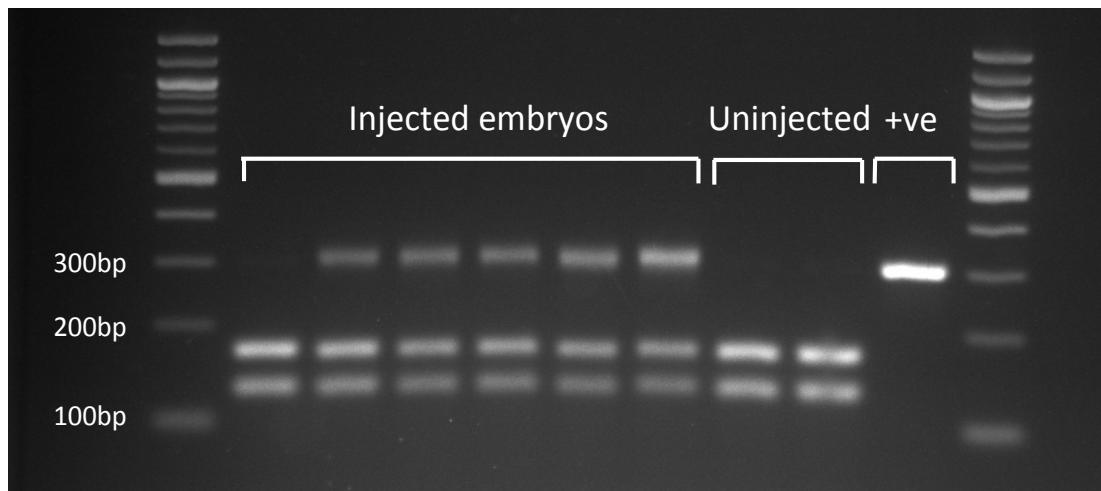
Figure 8.4. *Cyp17a2* CRISPR target validation assay. Restriction enzyme assay to screen for novel mutations in *cyp17a2*. DNA was extracted from six injected and three uninjected zebrafish embryos and the targeted genomic region was subsequently amplified by PCR. The *cyp17a2* guideRNA target sequence overlapped a restriction enzyme target site for BsiYI. All injected and two uninjected PCR products were digested with the restriction enzyme BsiYI. One uninjected sampled was used as a undigested positive control (+ve). The undigested PCR product is ~300bp. This ~300bp PCR product when digested, produces two discrete products: ~120bp and ~180bp, seen as two discrete bands in the uninjected samples. In 5/6 injected samples, there is a partial digestion and there are three discrete bands at ~300bp, ~180bp and ~120bp. This indicates that in 5/6 injected samples, the gRNA target has induced a mutation that has altered the DNA sequence and disrupted the restriction enzyme target site, preventing cleavage.

A) WT X F0

B)

```
>Cyp17a2WT     ATGTGTTCAGTGAGTGTGTGTGTGTGTTTCTCTGCTCTTCTTCTTCTCCTCCTGCTGTTA
>Cyp17a2Mutant ATGTGTTCAGTGAGTGTGTGTGTGTGTTTCTCTGCTCTTCTTCTTCTCCTCCTGCTGTTA
               ************************************************************
>Cyp17a2WT     GTCAGGCGTCTGCTGGAGGGTGTGGGCTCCTCCAGTGTGTCGTTCCCGTGTCTGCCGCGC
>Cyp17a2Mutant GTCAGGCGTCTGCTGGAGGGTGTGGGCTCCTCCAGTGTGTCGTTCCCGT-----------
               *************************************************
>Cyp17a2WT     CTGCCGCTGTTGGGGAGTTTACTGCATCTGCGCTCGAACCTCCCGCCACACCTGCTCTTC
>Cyp17a2Mutant -----------------TTACTGCATCTGCGCTCGAACCTCCCGCCACACCTGCTCTTC
                                *******************************************
>Cyp17a2WT     ACTCAG
>Cyp17a2Mutant ACTCAG
               *****
```

C)

```
>Cyp17a2WT     MCSVSVCVCFSALLLLLLLLVRRLLEGVGSSSVSFPCLPRLPLLGSLLHLRSNLPPHLLFTQLSSQYGPL
>Cyp17a2Mutant MCSVSVCVCFSALLLLLLLLVRRLLEGVGSSSVSFPFTASALQSPATPALHSAVVSVRAAVWALCRAAPH
               ***********************************                                 *
>Cyp17a2WT     FGLYAGPHLTLVVSEIGLVREVLLQRGREFAGRPKMVTTDLLTQGGKDIAFADYSPLWKNHRRLVHSSFT
>Cyp17a2Mutant AGGQ
               *
>Cyp17a2WT     LFGEGSNKLQTIVQEAADSLCEELQACRGQSSDLSVVLMRAVTNVICRLVFSSSYQPSDPELQTVIQYND
>Cyp17a2Mutant
>Cyp17a2WT     GIVQTIARGGLVDIFPWLRIFPNKDLKRLKECVSIRDQLLYKKLLEHKKSLTPGEPRDLLDALLIGQQRG
>Cyp17a2Mutant
>Cyp17a2WT     SGGADDITEDHVLMTAAEAFGAGVETTSTTLLWTIAFLLHHPQLQERVQAELDECVGVDRPPCLSDRPHL
>Cyp17a2Mutant
>Cyp17a2WT     PLLDAVLCEVMRIRPVSPILIPHVAMQDTSLGGHSVPKGTRVLVNMWAIHHDPKHWDQPEQFNPERFLEP
>Cyp17a2Mutant
>Cyp17a2WT     SGKKKTQSSFLPFGAGPRVCVGESLARIELFLFVSRLLQRFSFSCPSEASLPDLQGRFGVVLQPERYTVT
>Cyp17a2Mutant
>Cyp17a2WT     VTPRH
>Cyp17a2Mutant
```

Figure 8.5. *cyp17a2* mutant founder screening. A) The CRISPR/Cas9-injected F0 generation was outcrossed with wildtype fish; progeny from four different outcrosses are represented here (rows 1-4). DNA was extracted from 8 progeny from each outcross and the targeted genomic region was amplified by PCR. In Outcross 1, 25% (2/8) of progeny have a second allele slightly smaller in size than the wild-type allele. B) *cyp17a2* DNA sequencing identified a 29 base pair deletion in exon 1 of the progeny carrying this second allele C) This deletion created a frameshift that, when translated, results in a premature stop codon at amino acid 75 (p.C37FfsX75). The Outcross 1 progeny clutch was raised as the F1 generation carrying this deletion mutation.
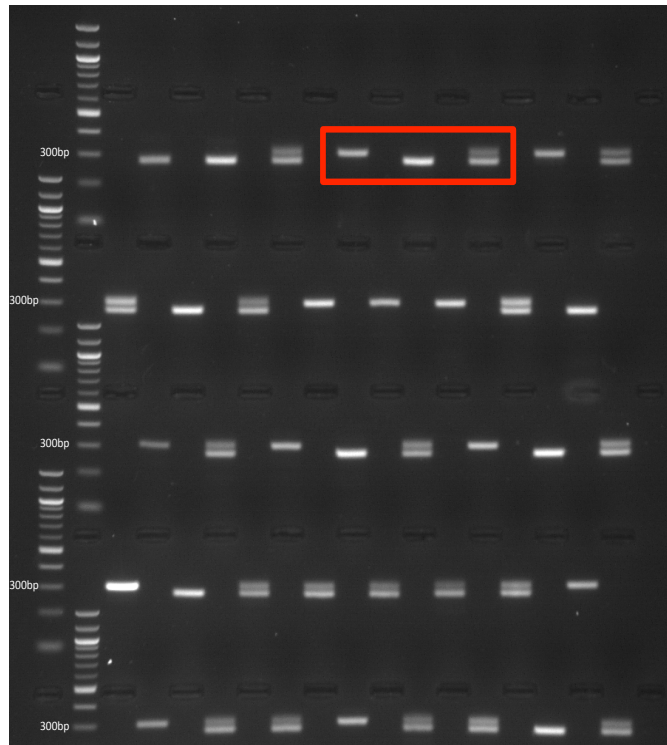
Figure 8.6. *cyp17a2* F$_2$ genotyping. A single pair of male and female F$_1$ *cyp17a2* zebrafish, heterozygous for the 29bp deletion, were in-crossed. The F$_2$ progeny were genotyped at 3months old by PCR. Genotype ratios did not deviate from Mendelian inheritance. Three F$_2$ individuals highlighted in the red rectangle are homozygous wildtype (left) homozygous mutant (middle) and heterozygous (right) F$_2$ progeny.

8.2.3 Visual background adaption assay indicates *cyp17a2*^{-/-} mutants are glucocorticoid-deficient

Glucocorticoid-resistant and glucocorticoid-deficient zebrafish models are well documented to display impaired visual background adaptation in zebrafish larvae i.e. gr[s357] mutants (Griffin et al., 2016; Ziv et al., 2013). These models exhibit a delay in the glucocorticoid-dependent neuroendocrine response of skin pigment contraction when exposed to bright light. Thus, mutants in which glucocorticoid signaling is defective display a darker skin pigment phenotype than wild-type siblings.

As *cyp17a2* is hypothesised to be responsible for the 17α-hydroxylase step during glucocorticoid synthesis, a VBA assay was performed to determine the impact of *cyp17a2* deficiency on glucocorticoid production. After a 1-hour dark period and subsequent 20-minute light period, approximately 20-25% of the progeny derived from a *cyp17a2*^{+/-} incross presented darker than the rest of the population, similar to Mendelian inheritance principles. Darker larvae are classed as VBA-negative (VBA-) as their VBA is defective, whilst lighter larvae are classed as VBA positive (VBA+) (Figure 8.7A). The mean skin pigment cell size on the dorsal head of VBA- larvae was significantly larger by approximately 300% than VBA+ larvae (p<0.0001, median area of VBA+ cells = $437\mu m^2$; median area of VBA- cells = $1296\mu m^2$) (Figure 8.7B). Retrospective genotyping confirmed that VBA- larvae were homozygous *cyp17a2* [-/-] mutants, whilst VBA+ were heterozygotes or homozygous wild-type individuals (Figure 8.7C). This impairment of the glucocorticoid-responsive VBA assay in *cyp17a2*^{-/-} larvae suggests that cyp17a2 is at least responsible for glucocorticoid synthesis.
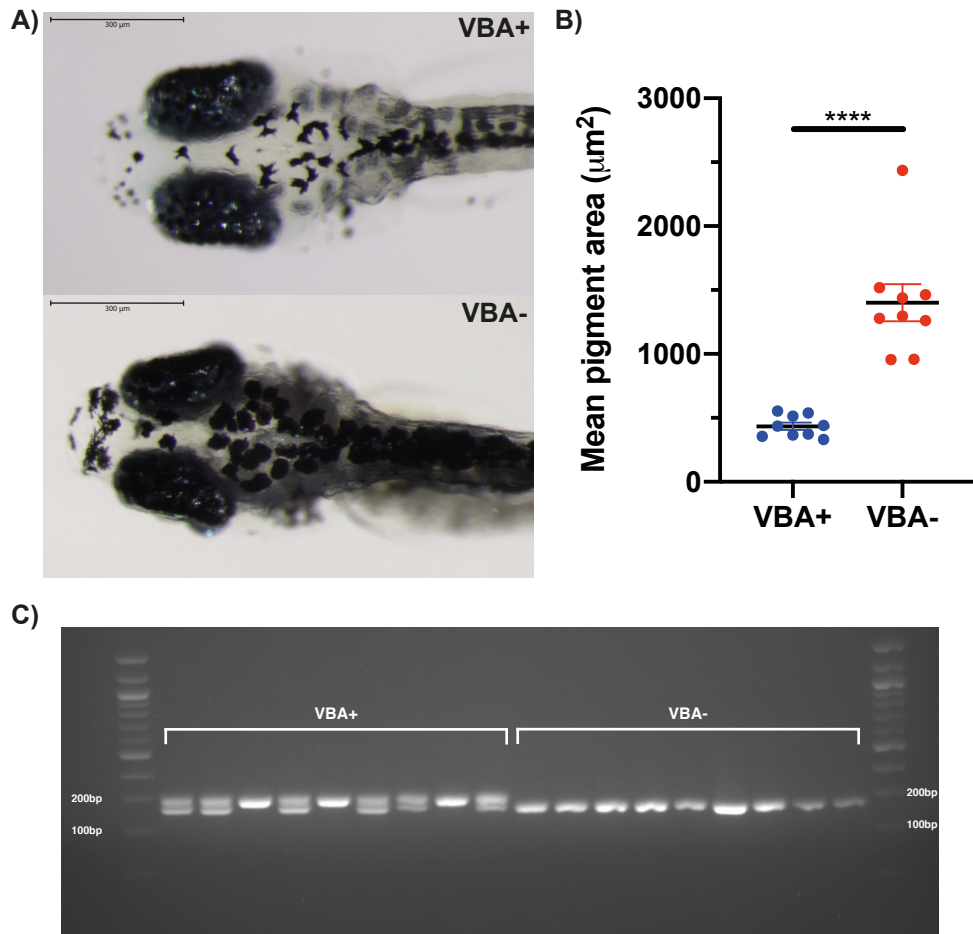
Figure 8.7. *cyp17a2^{-/-}* mutant 5dpf larvae exhibit an impaired visual background adaptation phenotype after exposure to the VBA stimulus. A) Representative images of VBA+ (left) and VBA- (right) sibling larva. B) Quantification of average melanophore size on each dorsal larva head. C) *cyp17a2* genotyping of VBA+ and VBA- larvae suggests reproducible homozygous mutant identification as VBA- phenotype. Plot represents mean ± SEM; results analysed using unpaired t-test, ****p<0.0001 (n=18).

8.2.4 Putative *cyp17a2*^{-/-} larvae are cortisol-deficient and exhibit a decrease in glucocorticoid-responsive gene expression

The concentrations of the steroid hormones cortisol and corticosterone were measured to test the hypothesis: cyp17a2 is responsible for cortisol synthesis, and a blockage at the 17-hydroxylation step would result in a flood of steroid hormones precursors into the mineralocorticoid pathway and cortisol-deficiency. A heterozygous (*cyp17a2*^{+/-}) incross was VBA-typed at 5dpf and separated into VBA+ (putative *cyp17a2*^{+/+} and *cyp17a2*^{+/-}) and VBA- (putative *cyp17a2*^{-/-}) larvae. 150 larvae were pooled and processed for steroid extraction. Concentrations of cortisol were significantly decreased to undectable levels in VBA- larvae in comparison to VBA+ controls (p=0.0012). Whereas for first time in zebrafish, corticosterone were detectable, and showed significantly increased concentrations in VBA- larvae (p=0.0277) (Figure 8.8).

Next, I measured the expression of well-established glucocorticoid-responsive genes *fkbp5* and *pck1* (Eachus et al., 2017a; Griffin et al., 2016). In my transcriptomic analysis of a loss-of-function GR mutant, I observed that *fkbp5* was the most significant differentially expressed gene (DEG) in both whole 5dpf larvae and dissected adult brain tissue. In addition to *fkbp5*, *pck1* is also a top DEG in 5dpf larvae, with both genes being severely downregulated (Chapters 5&6). Quantitative qRT-PCR indicated that the expression of both *fkbp5* (p<0.0001), and *pck1* (p=0.0121) was significantly decreased in VBA- (putative *cyp17a2*^{-/-} mutants) larvae compared to VBA+ controls (putative wildtype and heterozygous siblings), with *fkbp5* exhibiting almost complete extinction of gene expression in VBA- larvae (Figure 8.9).

Taken together, the results of my functional analysis of the effect of loss of *cyp17a2* function in larvae, strongly supports my hypothesis that loss of *cyp17a2* function causes glucocorticoid-deficiency.
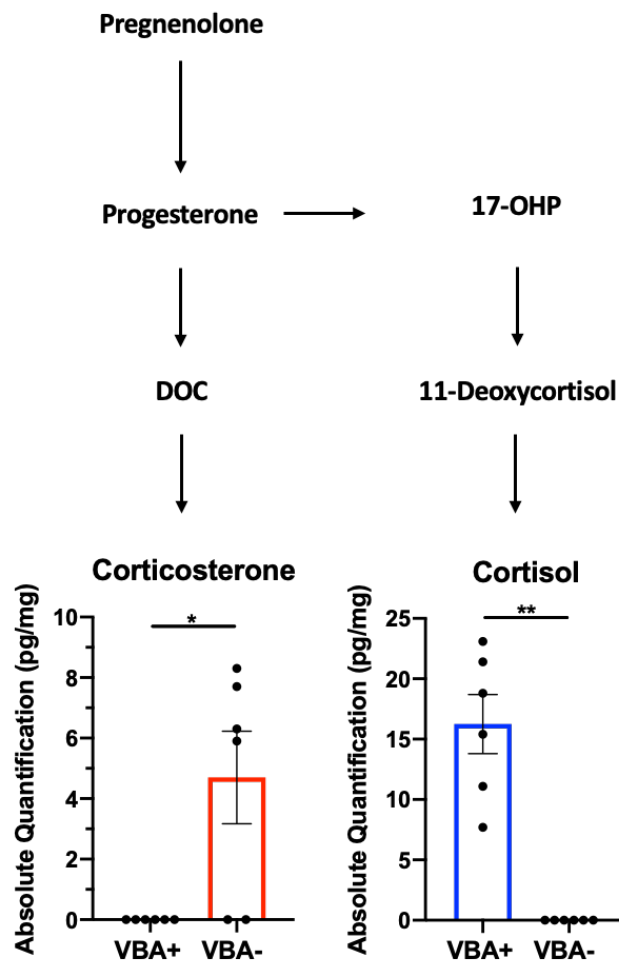
Figure 8.8. Putative c*yp17a2*$^{-/-}$ mutant 5dpf larvae exhibit elevated corticosterone and decreased cortisol steroid hormone profiles. Progeny of a *cyp17a2*$^{-/+}$ incross were VBA-typed at 4dpf. The concentration of each steroid was measured in samples prepared from 150 pooled VBA+ (putative *cyp17a2*$^{+/+}$ and *cyp17a2*$^{-/+}$) and 150 pooled VBA- (putative *cyp17a2*$^{-/-}$) 5dpf larvae. The concentration of the mineralocorticoid precursor corticosterone was significantly increased in VBA- larvae (p=0.0277). The concentration of the glucocorticoid cortisol was undetectable in VBA- larvae (p=0.0012). All bars represent mean ± SEM. All results were analysed using unpaired *t*-test with Welch's correction. * p<0.05; ** p<0.01 (n=12).
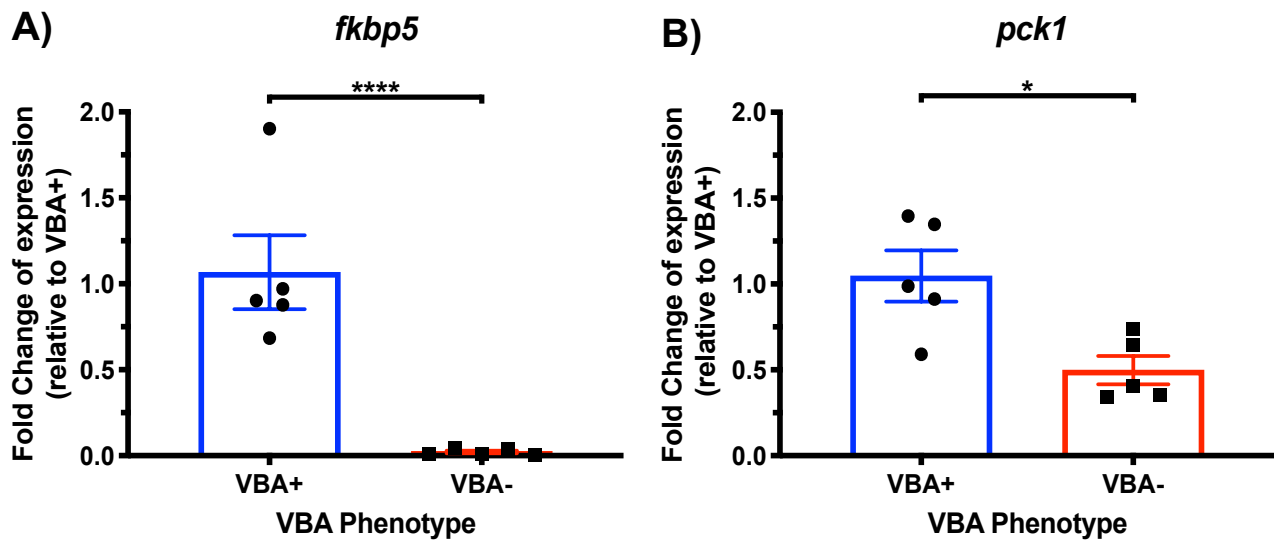
Figure 8.9. Altered expression of glucocorticoid-responsive genes in 5dpf VBA-, putative *cyp17a*2$^{-/-}$ mutant larvae. The expression of glucocorticoid-responsive genes: A) *fkbp5* ($p < 0.0001$) and B) *pck1* ($p = 0.0121$), were significantly decreased in VBA- putative *cyp17a*2$^{-/-}$ mutant larvae. All results were analysed using unpaired *t*-tests. **** $p < 0.0001$, * $p < 0.05$, n=10.

8.2.5 *cyp17a2*$^{-/-}$ 5dpf larvae exhibit reduced locomotion in different light conditions

Steroid hormones are known to exert strong effects on the vertebrate brain and influence a variety of behaviours. To investigate whether zebrafish larvae locomotor activity was affected by the loss of cyp17a2 function, the progeny of a heterozygous in-cross were raised to 4dpf and sorted into VBA+ and VBA- groups using the VBA assay. At 5dpf, locomotion of larvae during 5-minute alternating light/dark conditions was tracked, and distance travelled quantified during a 1-hour period. Data collection was recorded every 30 seconds. Retrospective genotyping was performed and matched with corresponding locomotor activity data for each larva.

Throughout the 1-hour period, it is apparent that for all genotypes, exposure to the dark condition elicited an increase in locomotor activity compared to light conditions (Figure 8.10A). In addition, homozygous *cyp17a2*$^{-/-}$ mutant larvae exhibited a reduced swimming behaviour (red), compared to wildtype (blue) and heterozygotes (green), with the mean distance travelled per genotype plotted every 30 seconds (Figure 8.10A). All three genotypes demonstrated significantly increased locomotion in the transition from light to dark conditions (wildtype, heterozygote, homozygotes, p<0.0001) (Figure 8.10B). When the mean distance travelled every 30 seconds by a larva is irrespective of light condition, *cyp17a2*$^{-/-}$ exhibit a significantly reduced locomotion activity when compared to wildtype (p=0.0025) and heterozygous (p=0.022) siblings (Figure 8.10C). As both light and dark conditions provide a significant change in locomotor activity, it is important to evaluate whether the reduced locomotion seen in *cyp17a2*$^{-/-}$ is evident in one, or both conditions. In both light (p=0.0111) and dark (p=0.0371) conditions, homozygous *cyp17a2*$^{-/-}$ mutant larvae consistently swam slower than wildtype siblings (Figure 8.10D&E).

8.2.6 The reduced locomotor activity in *cyp17a2*$^{-/-}$ mutant 5dpf larvae can be rescued with exogenous cortisol treatment

To investigate whether these results were rescuable, the progeny of a heterozygous incross were raised to 4dpf and sorted into VBA+ and VBA- using the VBA assay. This time, both VBA+ and VBA- larvae were divided into control groups (EtOH) and treated groups (10uM hydrocortisone in EtOH) and incubated overnight. The next morning, 5dpf larvae went through the same behaviour protocol and locomotion was tracked and measured. To increase numbers of larvae, three plates were tracked and measured consecutively. Each plate has VBA+ larvae in both control and treated groups, and VBA- larvae in control and treated groups. The data from the three consecutive plates was integrated and analysed (Figure 8.11).

As before, the transition from a light to dark condition stimulated a significant increase in locomotion for all three genotypes in both treatment groups: control (+/+, +/- and -/-, p<0.0001) and 10uM hydrocortisone (+/+, +/- and -/-, p<0.0001) not annotated in Figure 8.11. In control groups, a significant reduction in locomotor activity was evident in light conditions (+/+ and +/-, p<0.0001) compared to the level of locomotor activity in dark conditions (+/+ and +/-, p<0.0001). This was also the case for homozygous *cyp17a2⁻ᐟ⁻* mutant larvae, but in addition, homozygous *cyp17a2⁻ᐟ⁻* mutant larvae exhibited a significant reduction in locomotor movement in light and dark, indicative of a consistent behavioural phenotype caused by the loss of *cyp17a2* function (Figure 8.11). Unseen previously, in the control group there was, in addition, a significant decrease in locomotion activity between wildtype and heterozygotes in both light (p=0.0119) and dark (p=0.0006) conditions.

To understand if this behavioural phenotype is due to predicted endogenous glucocorticoid-deficiency, 4dpf larvae were treated with exogenous cortisol at a concentration (10μm) that has previously been shown in our lab, to induce a similar fold change in the glucocorticoid-responsive gene *fkbp5* expression as acute osmotic stress. Previous studies have shown that exogenous cortisol treatment significantly increases zebrafish larvae locomotion activity in light conditions and shows a non-significant trend to increased locomotion in dark conditions (Faught and Vijayan, 2018). My study confirmed that in the majority of genotypes/conditions, exogenous cortisol treatment caused a significant increase in locomotion activity (Figure 8.11). In both heterozygous and *cyp17a2⁻ᐟ⁻* genotypes, cortisol treatment resulted in a significant increase in distance travelled in both light (+/- p<0.0001; -/- p<0.0001) and dark (+/- p=0.0105; -/- p<0.0001) conditions. Whereas in wildtype siblings, there was a significant increase in locomotion in the dark conditions (p<0.0001), but a more variable, yet significant decrease in locomotion in the light (p<0.0001). Interestingly, treatment with exogenous hydrocortisone rescued the *cyp17a2⁻ᐟ⁻* phenotype by increasing locomotion activity to wildtype control and heterozygote control levels in both light (+/+ p=0.939; +/- p=0.5456) and dark conditions (+/+ p=0.4017; +/- p=0.6709), as seen by a loss of significance between their means (Figure 8.11). This data suggests that glucocorticoid deficiency is responsible for a reduction in locomotion in the *cyp17a2⁻ᐟ⁻* mutants and can be rescued back to wildtype levels with exogenous hydrocortisone treatment. Next, I was interested in the effect *cyp17a2*-deficiency had on adult zebrafish.

When both wildtype and *cyp17a2⁻ᐟ⁻* adult zebrafish were dissected for organ harvest, an additional phenotype was apparent in *cyp17a2⁻ᐟ⁻* mutants: *cyp17a2⁻ᐟ⁻* males had distinctly more visceral adipose tissue surrounding the gastrointestinal tract, liver and brain, than wild-type males. This observation is consistent with the phenotypes of zebrafish mutants known to exhibit

defective glucocorticoid signaling, such as *GR-/-* mutants and within our lab, both *cyp11a2-/-* and *cyp11c1-/-* were observed to have larger amounts of fat when dissected (Facchinello et al., 2017; Li et al., 2020; Oakes et al., 2020).
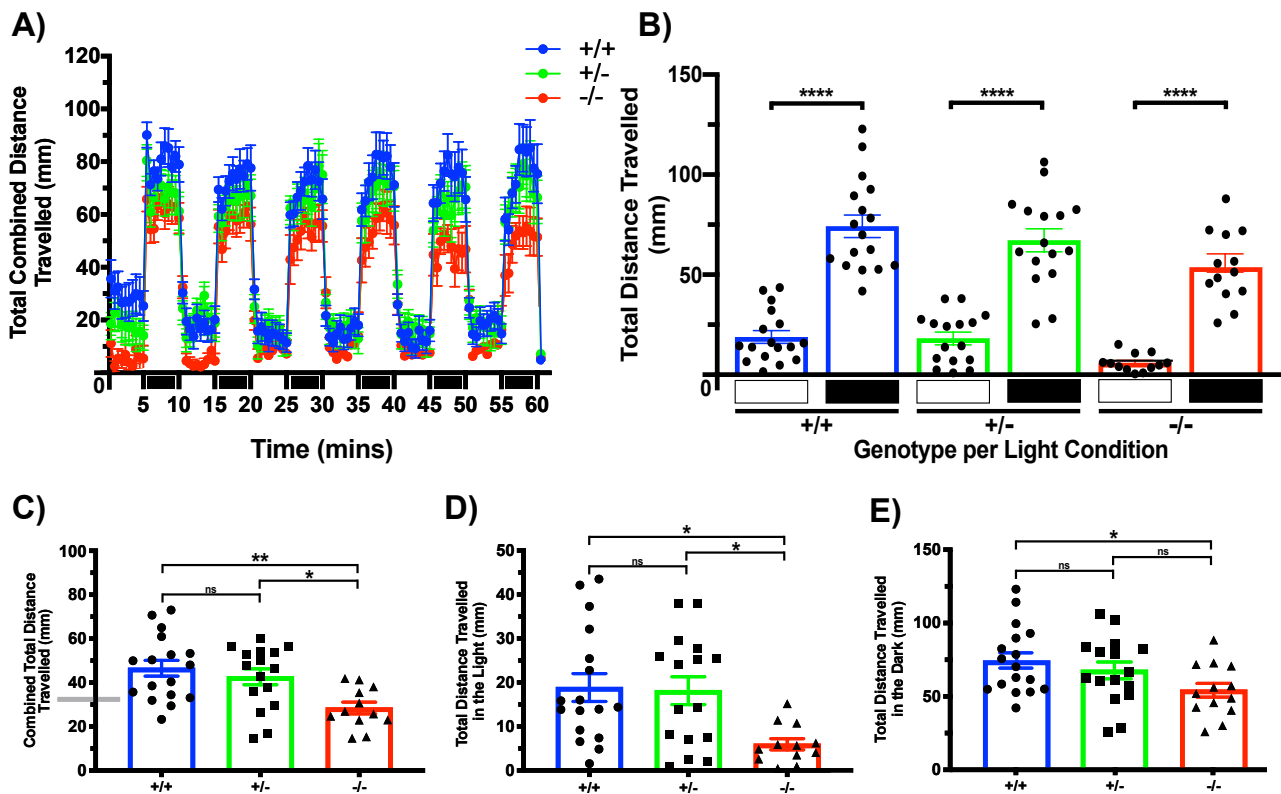
Figure 8.10. *cyp17a2-/-* mutant larvae have a reduced locomotion behavioural phenotype. A) The behavioural phenotype of a 5dpf F_2 clutch of zebrafish larvae that were genotyped retrospectively as wildtype, heterozygote or homozygote. Mean activity is plotted for each 30second recording bin for alternating light and dark conditions that is represented on the x-axis as white and black blocks, respectively. Activity was measured as total distance moved (mm) during 1 hour with alternating light/dark cycles of 5 minutes each. B) Total distance travelled during 1 hour for either light (white box) or dark (black box) periods. C) Total distance travelled of combined light and dark periods over 1 hour. D) Total distance travelled during the light periods over 1 hour. E) total distance travelled during the dark periods over 1 hour. All bars represent mean ± SEM. All results were analysed using post-hoc Tukey multiple comparison test. * p<0.05; **p<0.01 (n=17(+/+), 16(+/-) and 13(-/-)).
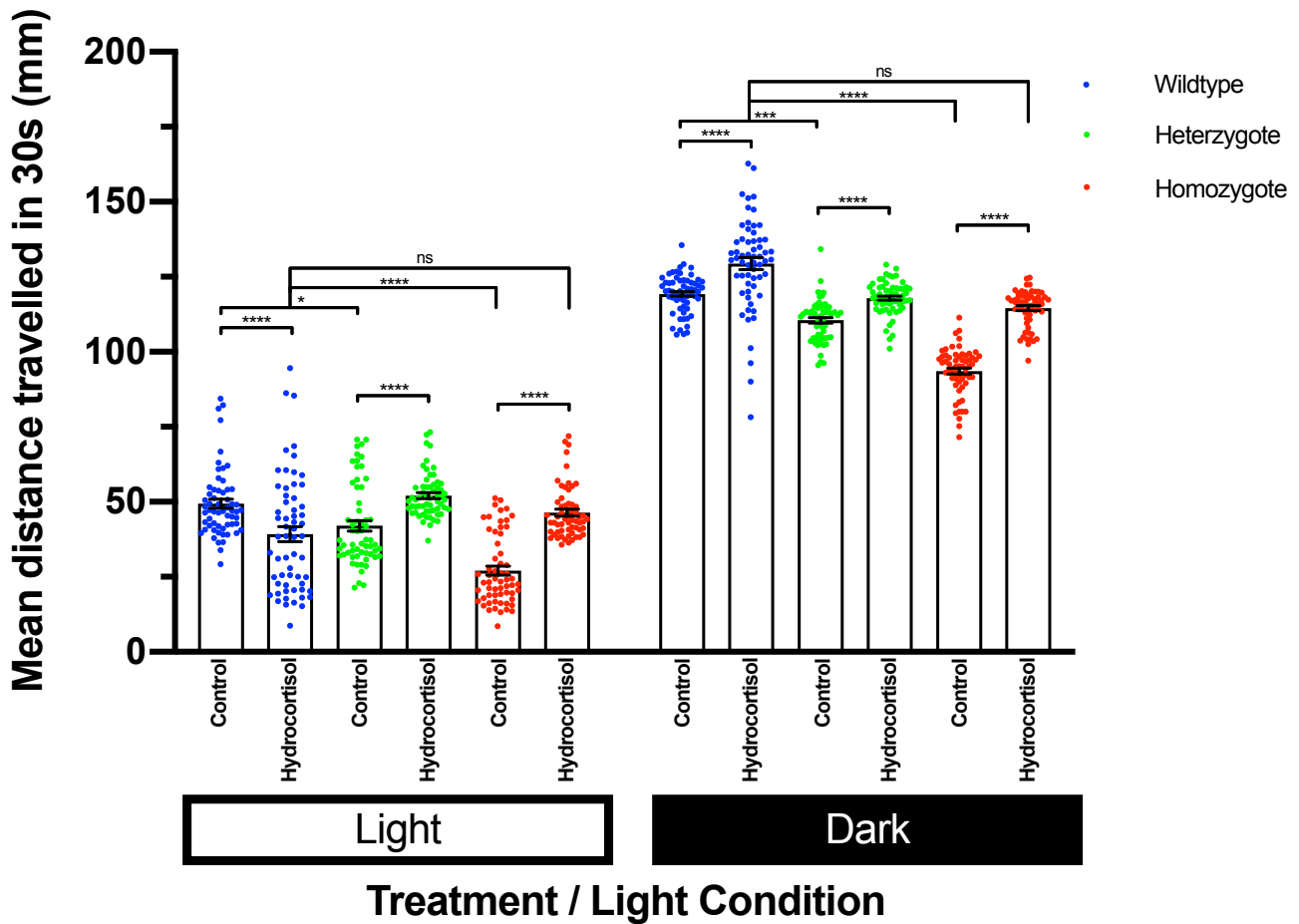
Figure 8.11. *cyp17a*2$^{-/-}$ **mutant larvae have a reduced locomotion behavioural phenotype that can be rescued with overnight 10μm hydrocortisone treatment.** The behavioural phenotype of a 5dpf F$_2$ clutch of zebrafish larvae, which were VBA-sorted on 4dpf, split into control (EtOH) and 10μm hydrocortisone treated groups and incubated at 28°C overnight. The next day, larvae were exposed to a behavioural protocol of alternating light/dark cycles of 5 minutes each over a period of 1 hour, with behavioural activity (distance travelled in mm) recorded every 30 seconds and retrospective genotyping performed as described previously. Graph displays mean distance travelled every 30seconds for each genotype (wildtype, blue; heterozygote, green; homozygote, red). All bars represent mean ± SEM. All results were analysed using post-hoc Tukey multiple comparison test. * p<0.05; ***p<0.001; ****p<0.0001 (n=144).

8.2.7 Morphological characterisation and biometrics of adult *cyp17a2*-/- mutant zebrafish.

Zebrafish that have defective glucocorticoid signaling, through either deficiency or resistance, have been shown to be significantly larger in weight and size than wildtype siblings (Faught and Vijayan, 2019; Li et al., 2020; Oakes et al., 2020; Chapter 7, this thesis). Consistent with this, *cyp17a2*-/- adult males were significantly heavier than male wildtype siblings at both 12months old (clutch 1) (p=0.0005) and 17months (clutch 2) (p<0.0001) (Figures 8.12&8.13). In addition, *cyp17a2*-/- adult males were significantly longer than male wildtype siblings at both 12months old (clutch 1) (p=0.0001) and 17months old (clutch 2) (p<0.0001) (Figure 8.12&8.13). In the first clutch, no females were found in either WT or *cyp17a2*-/- mutant lines. In the second clutch, only 6/24 WT fish were females and 3/17 *cyp17a2*-/-. A trend across the multiple lines grown at this time was seen in the aquarium. Possible reasons may be due reduced feeding or changes in variations in tank water temperature. Typical morphological secondary sex characteristics of wild-type AB zebrafish were identified in *cyp17a2*-/- mutants and *cyp17a2*+/+ wild-type controls (Figure 8.14).
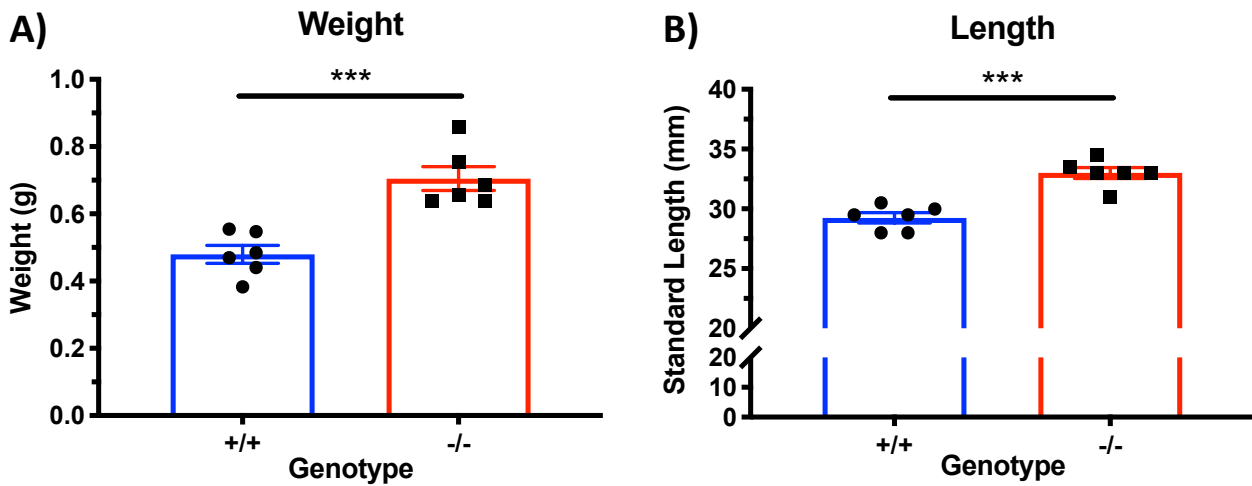
Figure 8.12. Increased body length and weight in 1-year old adult *cyp17a2^-/-* mutant male zebrafish. A) *Cyp17a2^-/-* mutant male zebrafish were heavier than wildtype siblings despite identical feeding regimes and maintenance at similar stocking densities. B) Male *cyp17a2^-/-* mutant zebrafish were also longer than wildtype siblings (Unpaired t-test, *** = <0.001; n=12).
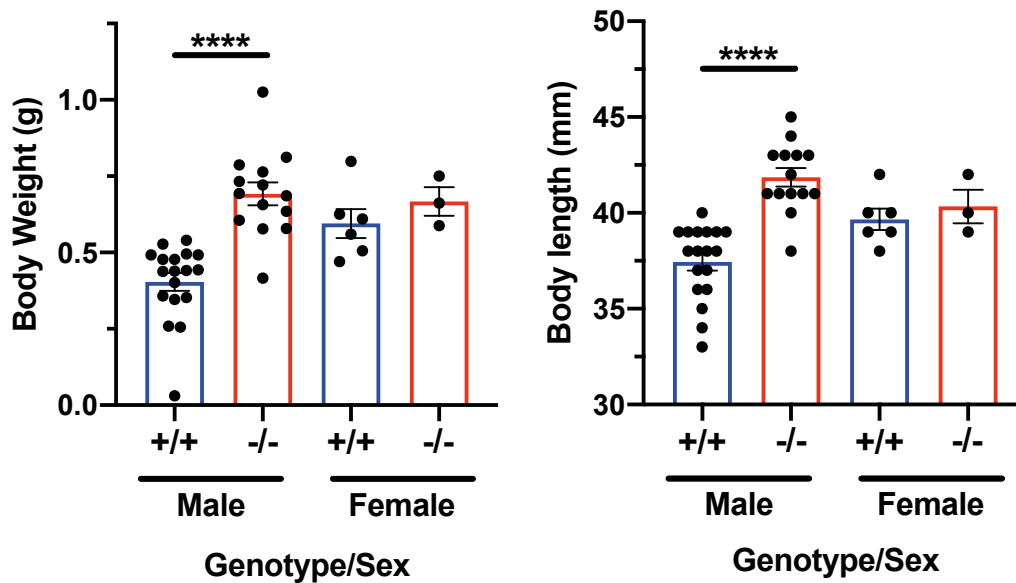
Figure 8.13. Increased body length and weight in 17-month-old adult *cyp17a2^-/-* mutant male zebrafish. Left) c*yp17a2^-/-* mutant male zebrafish were significantly heavier than wildtype siblings despite identical feeding regimes and maintenance at similar stocking densities. Right) Male *cyp17a2^-/-* mutant zebrafish were also significantly longer than wildtype siblings. No significant difference was seen in females, however numbers were low in both WT and *cyp17a2^-/-* mutants. (Mann Whitney test, **** = p<0.0001; n=32).
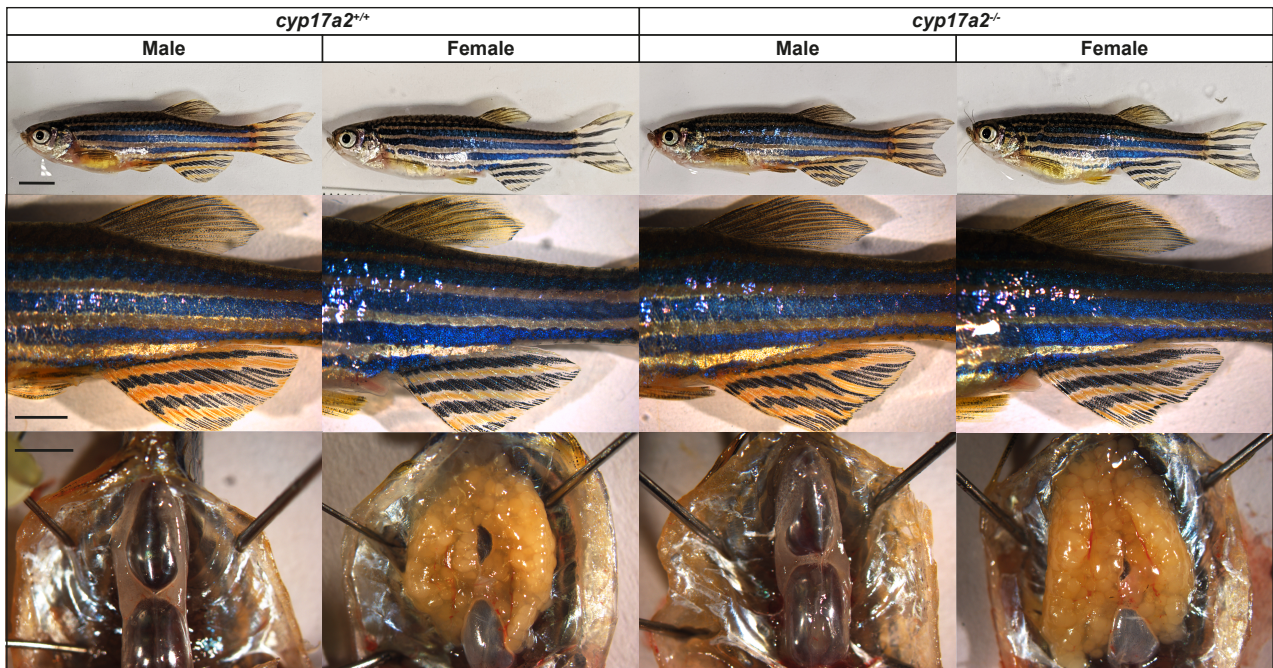
Figure 8.14. Loss of *cyp17a2* function results in normal phenotypic secondary sex characteristics in both male and female adult zebrafish. *Cyp17a2-/-* mutant males exhibited similar fin pigmentation patterns, such strongly orange striped anal fins, as wildtype siblings. Additionally, *cyp17a2-/-* mutant females exhibited similar fin pigmentation patterns, such as yellow striped anal fins, as wildtype siblings.

8.2.8 *cyp17a2⁻/⁻* homozygous mutant adult male zebrafish exhibit an excess of mineralocorticoid precursors and a decrease in glucocorticoid concentrations

The second part of my hypothesis is that after the block of glucocorticoid synthesis caused by loss of *cyp17a2* function, glucocorticoid precursors would accumulate and enter into the mineralocorticoid pathway, resulting in an excess production of mineralocorticoids and their precursors (Figure 8.1).

Aldosterone is the primary mineralocorticoid in mammals and essential for osmoregulation. In zebrafish, however, negligible concentrations of aldosterone have been detected. Consistent with this observation, a *CYP11B2* homolog has not yet been identified in any fish species, so it seems that aldosterone may not be synthesized in zebrafish. In humans, *CYP11B2* encodes a steroidogenic enzyme called aldosterone synthase, responsible for the aldosterone 3-step conversion: 11-deoxycorticosterone to corticosterone, then to 18-hydroxycorticosterone, and finally to aldosterone (Figure 8.15) (Reddish and Guengerich, 2019; Xing et al., 2011).
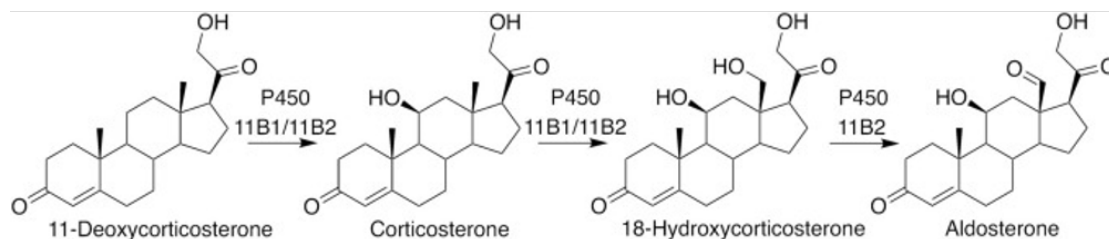
Figure 8.15. Physiological reactions performed by human P450 CYP11B2. CYP11B1 and CYP11B2 catalyse oxidations at 11- and 18- positions to 11-decycorticosterone to 18-hydroxycorticosterone, the final step to produce an aldehyde at position 18- (aldosterone) is solely performed by CYP11B2. Adapted from Reddish and Guengerich, 2019.

In order to determine the overall impact of *cyp17a2*-deficiency on steroid hormone production in zebrafish adults, LC-LS/MS was used to quantify whole body steroid hormone concentrations (Figure8.15&8.16). In the glucocorticoid pathway, there was no significant difference in concentration of the glucocorticoid precursor, 17α-hydroxyprogesterone, however this may be because concentrations were close to the limit of detection (Figure 8.16). A significantly decreased concentration of the glucocorticoid, 11-deoxycortisol, a cortisol precursor, was measured in *cyp17a2*$^{-/-}$ mutant males (p=0.03409). However, a non-significant decreased in cortisol concentrations was measured in my *cyp17a2*$^{-/-}$ mutant males compared to wildtype sibling males (p=0.1277) (Figure 8.16). I believe this is due to four wildtype samples expressing unusually low concentrations of cortisol in comparison to multiple experiments performed in our lab previously. Steroid measurements were repeated in replicate samples, which showed a significant decrease in cortisol concentrations in *cyp17a2*$^{-/-}$ mutant and *cyp17a2*$^{+/+}$ wild-type male siblings (p=0.0283) (Figure 8.17).

Preceding the 17-hydroxylase reaction, the concentration of the steroid hormone precursor progesterone was significantly increased in *cyp17a2*$^{-/-}$ mutant males compared to wildtype sibling males (p=0.001) (Figure 8.17). No significant differences were seen in the mineralocorticoid precursor 11-deoxycorticosterone; however, measurements were at the limit of detection (Figure 8.16). Interestingly, the concentration of the aldosterone-precursor, corticosterone, was profoundly higher in *cyp17a2*$^{-/-}$ mutant males than wildtype sibling males (mean: +/+=0, -/-=139.3; p=0.0057), which was confirmed in the repeated samples (mean: +/+=0, -/-=128.5; p=0.0033).
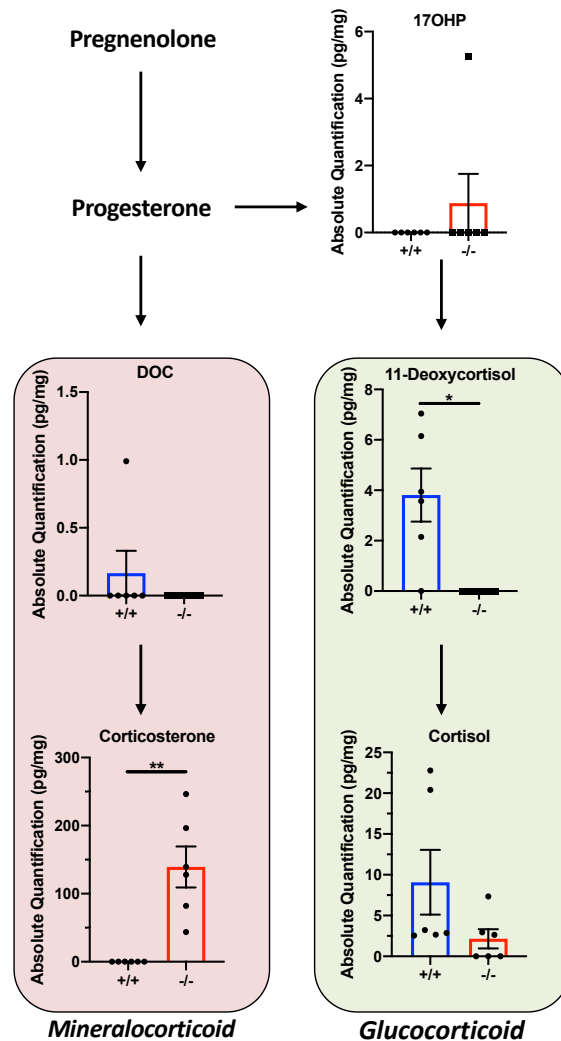
Figure 8.16 *Cyp17a2^{-/-}* mutant adult male zebrafish exhibit elevated mineralocorticoid and decreased glucocorticoid steroid hormone profiles. The concentration of each steroid was measured in samples prepared from whole zebrafish bodies. The mineralocorticoid and glucocorticoid pathways are highlighted in pink and green respectively. The concentration of mineralocorticoid precursor 11-deoxycorticosterone (DOC) was at the limit of detection. The concentration of the mineralocorticoid corticosterone was significantly increased in *cyp17a2^{-/-}* mutant male zebrafish (p=0.0057). The concentration of the glucocorticoid and sex steroid precursor 17α-hydroxyprogesterone was not significantly changed (p=3409). The glucocorticoid precursor 11-deoxycorticosterone was significantly decreased in *cyp17a2^{-/-}* mutants (p=0.0153); however, cortisol concentrations were not significantly decreased (p=0.1277). All results were analysed using unpaired t-tests or nonparametric Mann-Whitney test. * p<0.05, ** p<0.01 (n=12).
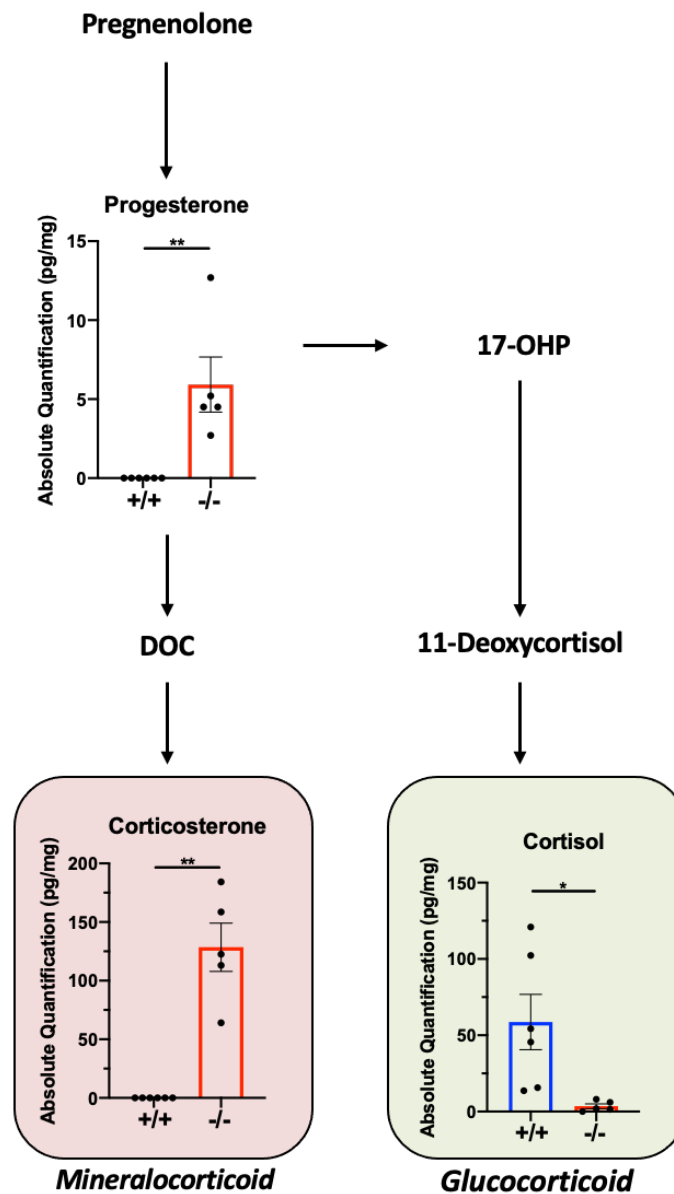
Figure 8.17. Decreased cortisol and increased corticosterone concentrations in *cyp17a2*-/- mutant male zebrafish are reproducible. Steroid measurements were repeated in replicate samples of *cyp17a2*-/- mutant and *cyp17a2*+/+ wild-type male siblings. The mineralocorticoid and glucocorticoid pathways are highlighted in pink and green respectively. The concentration of steroid hormone precursor progesterone was significantly increased in *cyp17a2*-/- mutants (p=0.001). The concentration of the mineralocorticoid precursor corticosterone was significantly increased in *cyp17a2*-/- mutant male zebrafish (p=0.0033). Whereas the concentration of the glucocorticoid cortisol was significantly decreased in *cyp17a2*-/- compared to wild-type siblings (p=0.0283). All results were analysed using unpaired t-tests with Welch's correction Mann-Whitney test. * p<0.05, ** p<0.01 (n=11).

8.2.9 *cyp17a2*$^{-/-}$ homozygous mutant adult male zebrafish exhibit variation in sex steroid synthesis.

As it was hypothesised that *cyp17a2*-deficiency would cause an increase in glucocorticoid precursors that could flood the mineralocorticoid pathway, there is also the possibility that a decrease in precursors such as 17-OHP may also affect the sex steroid pathway. To determine this, sex steroid concentrations were measured in *cyp17a2*$^{-/-}$ and wildtype adult sibling males in two independent experiments (Figure 8.18).

No significant differences were seen in concentrations of androstenedione (A4) (p=0.1389), 11β-hydroxyandrostenedione (11-OHA4) (p=0.5294) or testosterone (T) (p=0.3563). However, in fish, 11-ketotestosterone (11-KT) is the principal androgen as cyp11b1 is highly expressed in fish testes. In the first experiment, c*yp17a2*$^{-/-}$ mutant adult males exhibited a significant decrease in both the precursor 11-ketoandrostenedione (11-KA4) (p=0.0043) and the principal androgen 11-KT (p=0.01) (Figure 8.18A). However, this was not repeatable; in repeat samples showed no significant differences for A4, testosterone or 11-KT between wild-type and *cyp17a2*$^{-/-}$ adult male siblings.

As *cyp17a1*$^{-/-}$ zebrafish exhibited a significant reduction in whole body androgen concentrations in adult males (Zhai et al., 2018), the gene *cyp17a1* was sequenced from the genomic DNA of the six *cyp17a2*$^{-/-}$ mutant males that were used for steroid analysis, to investigate whether there may have been an off-target effect of the CRISPR gRNA on the *cyp17a1* gene. DNA alignment of *cyp17a1* and *cyp17a2* exon 1 showed 27.56% similarity, and the 18bp crRNA that targets *cyp17a2* exon 1, has an 8/18 nucleotide overlap (<50%) with the same region of the *cyp17a1* gene after alignment. This suggests that the gRNA was unlikely to target cyp17a1. To confirm, *cyp17a1* exon 1 was amplified by PCR and sequenced, which correctly aligned with ENSEMBL's zebrafish reference genome sequence of *cyp17a1* exon 1. An alignment between the crRNA sequence and the complete *cyp17a1* gene provided a maximum of 66.7% alignment in the non-coding region of intron 4, where no PAM site was aligned. Together, this indicates that it is very unlikely that my mutagenesis strategy will create off-target mutations in the *cyp17a1* gene.
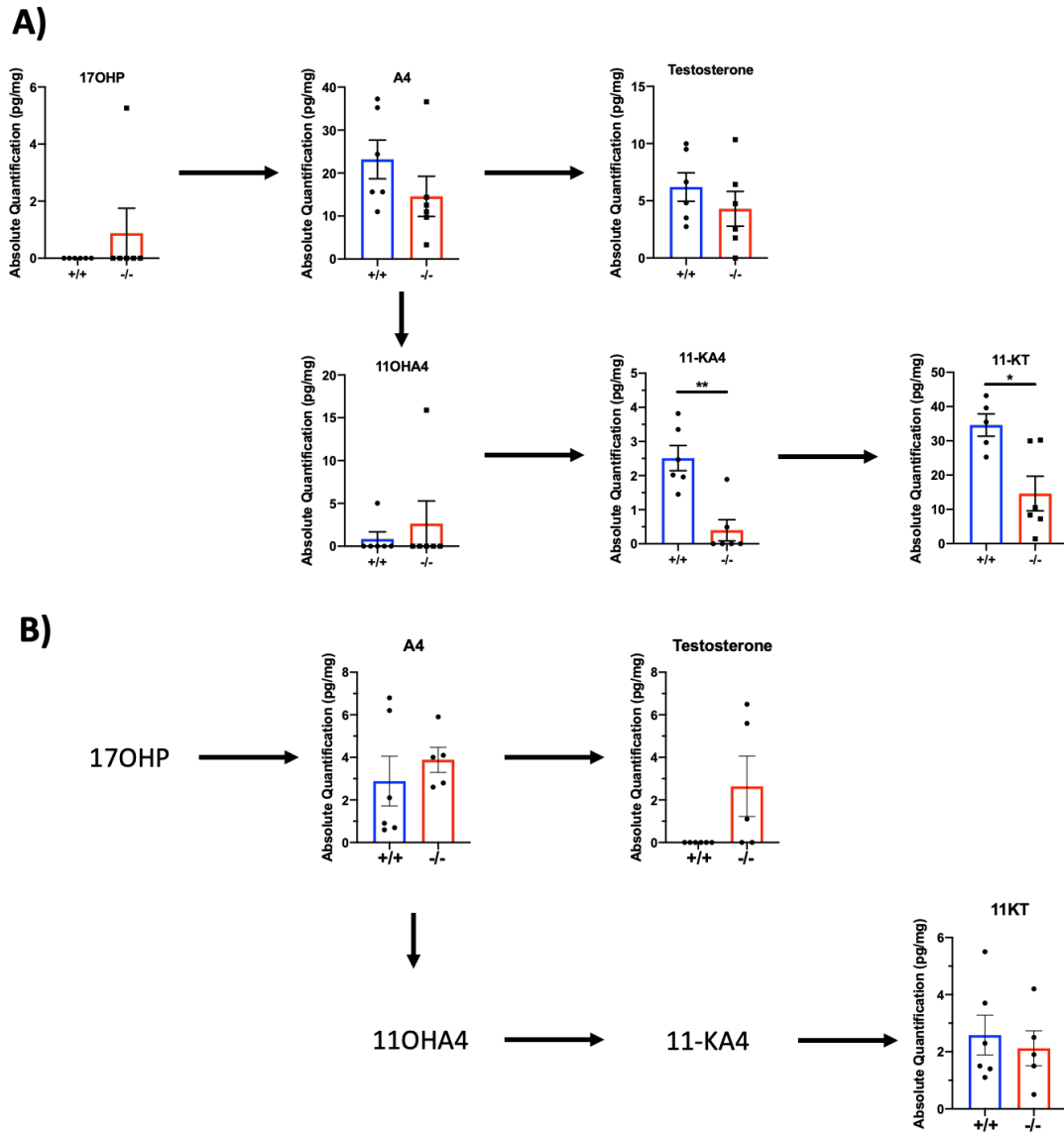
Figure 8.18. *Cyp17a2$^{-/-}$* **mutant male zebrafish exhibit high variation in androgen steroid profiles**. The concentration of each steroid was measured in samples prepared from whole zebrafish bodies in two independent experiments A&B. A) The concentration of the glucocorticoid and sex steroid precursor 17α-hydroxyprogesterone was not significantly different between *cyp17a2$^{-/-}$* mutants and wildtype siblings (p=0.3409). The concentration of androstenedione (A4) was not significantly decreased in *cyp17a2$^{-/-}$* mutants (p=0.1389), nor was there a significant difference in testosterone concentration (p=0.3563) or 11β-hydroxyandrostenedione (p=0.5294). However, the concentration of 11β-ketoandrostenedione (11-KA4) was significantly decreased (p=0.0043), as was the primary androgen in fish, 11β-ketotestosterone (11-KT) (p=0.01) in *cyp17a2$^{-/-}$* mutants. n=12.

B) Repeat samples showed no significant differences for A4, testosterone or 11-KT between wild-type and *cyp17a2$^{-/-}$* adult male siblings. n=11. All results were analysed using unpaired t-tests or nonparametric Mann-Whitney tests. * p<0.05, ** p<0.01.

8.2.10 *Cyp17a2*-/- mutant females are infertile using conventional breeding techniques

The the loss of *cyp17a2* function affected fertility in response to the conventional marbling technique (Westerfield, 2000). Tanks of wildtype or *cyp17a2*-/- mutant zebrafish containing both males and females were marbled weekly for three weeks. Fertilised embryos were successfully collected from the wildtype tank each week, however no eggs were collected from the tank of *cyp17a2*-/- mutants during any of the three trials. To investigate whether this apparent infertility was due to a defect in *cyp17a2*-/- male or female physiology, or both, *cyp17a2*-/- mutants and wildtype siblings were outcross pair-mated with unrelated wildtype fish. Outcrossing was repeated for three weeks to ensure technique habituation. In three weekly trials, *cyp17a2* wildtype sibling males (n=8) and females (n=7) successfully produced fertilized embryos from 71% and 76% of trials respectively. *Cyp17a2*-/- mutant males (n=7) were subfertile, successfully fertilising eggs in 48% of the trials, whereas *cyp17a2*-/- mutant females were infertile and unsuccessful in discharging any eggs in all trials (Table 8.3).

Table 8.3. Outcross breeding of *cyp17a2*-/- mutant zebrafish and wild-type siblings

Genotype & sex	No. of fish	Total no. of trials*	Trials that produced fertilised eggs
cyp17a2+/+ male	8	24	17 (71%)
cyp17a2+/+ female	7	21	16 (76%)
cyp17a2-/- male	7	21	10 (48%)
cyp17a2-/- female	6	18	0

*Trials were conducted weekly for three weeks. Fish were housed in their tanks, segregated by genotype.

Females are sometimes known as 'egg bound' and manual 'squeezing' is required to retrieve the eggs. Aquarium staff attempted manual 'squeezing' on two occasions and no eggs were released. When *cyp17a2*-/- female adult fish were sacrificed, they were put under anesthetic and manually 'squeezed' towards their genital papilla. Wildtype adult fish discharged eggs freely, whereas *cyp17a2*-/- mutants discharged 0 eggs despite persistent and substantial squeezing. When adult females were culled for organ harvesting and ovaries and eggs were collected, there was an observable increase in ovary tissue in *cyp17a2*-/- mutant females (Figure 8.14). This suggests a potential anatomical abnormality of the female reproductive system, potentially in the oviduct. Whole bodies of both wildtype and *cyp17a2*-/- female adults were fixed in 4% PFA and decalcified for sectioning, to investigate the microscopic anatomy and organization of the female

reproductive system. Unfortunately, due to time constraints, sectioning and H&E staining was not completed in time for this thesis.

8.3 Discussion

The specific roles of mineralocorticoids, glucocorticoids and the function of the *cyp17a1* paralog, *cyp17a2*, in zebrafish development and physiology, are poorly understood. Herein, I demonstrate that *cyp17a2*^{-/-} mutant zebrafish exhibit glucocorticoid-deficiency, supported by glucocorticoid-deficient phenotypes and gene expression, despite a significant excess of corticosterone. This supports my hypothesis: cyp17a2-deficiency would cause a block in the glucocorticoid biosynthetic pathway and would consequentially result in a flood of steroid precursors into the mineralocorticoid biosynthetic pathway (Figure 8.1).

Cyp17a2 is important for the production glucocorticoids as it encodes the only Cyp17 protein that is expressed in steroidogenic interrenal tissue in fish (Zhou et al., 2007) and able to perform the 17α-hydroxylase reaction required for glucocorticoid synthesis (Pallan et al., 2015). Herein, I have demonstrated that *cyp17a2*-deficient zebrafish larvae exhibit profound glucocorticoid-deficiency resulting in a defective VBA response of larval skin pigment cells, reduced larval locomotor activity that can be partially rescued by exogenous glucocorticoid exposure, and near extinction of the glucocorticoid-responsive gene *fkbp5* expression. Similar phenotypic and molecular changes have also been demonstrated in established glucocorticoid-deficient or glucocorticoid-resistant zebrafish larvae, lending further support to the suggestion that our *cyp17a2*^{-/-} larvae are glucocorticoid-deficient. For example, glucocorticoid-deficient larvae such as *cyp21a2*^{-/-}mutants; glucocorticoid and androgen-deficient larvae such as *cyp11a2*^{-/-}, *fdx1b*^{-/-} and *cyp11c1*^{-/-}mutants, and glucocorticoid-resistant larvae such as homozygous *gr*^{s357} and *gr*^{-/-} mutants, all exhibit VBA-negative phenotypes in the larval VBA test (Eachus et al., 2017; Facchinello et al., 2017; Griffiths et al., 2012; Li et al., 2020; Marchi et al., 2020; Oakes et al., 2019, 2020). In addition, the expression of *fkbp5* mRNA was barely detectable in putative *cyp17a2*^{-/-} mutant larvae (VBA-). This glucocorticoid target gene was the most significant downregulated gene in both *gr*^{s357} larval and *gr*^{s357} adult brain transcriptomes (see Chapters 5&6) and has been used previously to confirm impairment of glucocorticoid signaling in *cyp21a2*^{-/-}, *cyp11a2*^{-/-}, *fdx1b*^{-/-}, *cyp11c1*^{-/-} and *gr*^{-/-} mutant zebrafish (Eachus et al., 2017; Li et al., 2020; Marchi et al., 2020; Oakes et al., 2019, 2020).

Glucocorticoid signaling has a significant impact on zebrafish larval behaviour, as seen in glucocorticoid-resistant mutant larvae (Griffiths et al., 2012; Sireeni et al., 2020) and in cortisol-treated larvae (Best and Vijayan, 2017; Best et al., 2017; Faught and Vijayan, 2018). As with other zebrafish lines carrying glucocorticoid signaling mutations that result in abnormal behaviour (Best and Vijayan, 2017; Sireeni et al., 2020), *cyp17a2$^{-/-}$* mutant zebrafish larvae exhibit reduced locomotor activity compared to wild-type siblings. These results suggest that glucocorticoid signaling impacts on behaviour such as locomotor activity, which has also been seen in higher vertebrates such as mice; reviewed in (Kolber et al., 2008). Interestingly, defective glucocorticoid signaling in zebrafish larvae has been associated with 'depression-like' phenotypic behaviour that was shown to be alleviated with antidepressant substances such as diazepam and fluoxetine (Ziv et al., 2013). This glucocorticoid-behaviour association is correlated with human psychological disorders such as major depression and psychosis, which strongly influence human behaviour. For instance, a key hallmark of major depression is hypercortisolemia, usually associated with glucocorticoid-resistance and a decreased sensitivity of the HPA axis (Holsboer, 2000; Menke, 2019). Moreover, GR antagonists have been used to treat psychotic depression and reduce symptoms (Schatzberg, 2015), mutations in *nr3c1* (GR) have been associated with increased susceptibility of psychotic depression (Schatzberg et al., 2014); and preclinical studies of the impacts of CRH antagonist treatment and CRH receptor knock-out models report a reduction in anxiety-like symptoms and stress-induced behaviours (Liebsch et al., 1995; Swiergiel et al., 1993). Through multiple levels evidence throughout different evolutionary stages of vertebrates, glucocorticoid signaling has been shown to affect behaviour.

To my knowledge, this is the first-time corticosterone has been measured in zebrafish at higher than negligible concentrations. Interestingly, corticosterone is also a known glucocorticoid in mammals. In humans, corticosterone circulates at a lower concentration than cortisol (Raubenheimer et al., 2006), but in rodents, corticosterone is the principal glucocorticoid due to the lack of a 17-α hydroxylase (CYP17) enzyme in the adrenal gland (Auchus et al., 2017). Due to this, there is also a lack of adrenal androgen production in rodents (Auchus et al., 2017). The significant increase of corticosterone implies that cyp17a2 is a catalyst for mineralocorticoid production in zebrafish, and in future studies may provide the answer to 'can zebrafish synthesise aldosterone?'.

Together, this data contributes to a clearer understanding of the corticosteroid biosynthesis pathway of zebrafish and provides a new insight into the relationship between zebrafish and human endocrinology. Humans have only one enzyme that performs both the 17α-hydroxylase and 17,20 lyase activity: CYP17A1. By contrast, due to a teleost genome duplication event,

zebrafish contain two orthologs of the human *CYP17A1* gene: *cyp17a1* and *cyp17a2*. Whilst the zebrafish *cyp17a1* enzyme performs enzymatic reactions similar to the human CYP17A1, this does not make *cyp17a2* research redundant. Importantly, *cyp17a2* is solely expressed in the adult head kidney (interrenal tissue), but no significant difference in cortisol concentrations were detected in *cyp17a1*-deficient zebrafish. Accordingly, I suggest that cyp17a2 plays a similar role to CYP17A1 in terms of glucocorticoid production. In support of this argument, it is important to note that humans deficient in CYP17 function (17-OHD), are cortisol deficient but have ~100-fold increase in circulating corticosterone concentrations due to excess glucocorticoid precursors flooding the mineralocorticoid pathway (Auchus et al., 2017).

Our *cyp17a2*-deficient fish have a similar (~130-fold) increase in whole body corticosterone concentrations and cortisol-deficient phenotypes. In cases of 17-OHD, the effects of cortisol-deficiency usually do not lead to glucocorticoid-deficiency due to the elevated corticosterone acting as a substitute (Auchus et al., 2017). In rodents, corticosterone is the primary glucocorticoid and only small amounts of cortisol are synthesized due to low expression of *cyp17a1* in the adrenal gland. This leads to the question: does elevated corticosterone concentrations in *cyp17a2*-deficient fish alleviate effects of glucocorticoid deficiency? This alleviation is not seen in larvae, as they *cyp17a2*-/- mutants exhibit glucocorticoid-deficient phenotypes and fkbp5 gene expression, despite elevated concentrations of corticosterone. However, it is unknown whether this alleviation occurs in adult fish. To investigate this, mRNA expression of glucocorticoid-responsive genes such as *fkbp5* and *pck1* should be measured in adult organs such as the liver to evaluate whether corticosterone rescues any effects of cortisol-deficiency. In addition, *pomca* expression should be measured in the adult brain to evaluate whether there is a change in the function of the HPI axis.

One consistent phenotype seen in zebrafish mutants with impaired glucocorticoid signalling or androgen deficiency is an increase in size and length. Our biometric analysis of *cyp17a2*^{-/-} mutants indicates that adult males are heavier and longer than wildtype siblings. This phenotype was previously seen in adult male *gr*^{-/-} mutants and adult male double *mr*^{-/-};*gr*^{-/-} mutants, as well as in adult male glucocorticoid and androgen-deficient mutants *cyp11a2*^{-/-} and *cyp11c1*^{-/-} (Faught and Vijayan, 2019; Li et al., 2020; Oakes et al., 2020; Chapter 7, this thesis). Interestingly, corticosteroids are known to be important for the regulation of growth hormone (GH) synthesis (Thakore and Dinan, 1994). Specifically, glucocorticoids suppress the GH axis in mammals, and consistent with this, rats treated with glucocorticoids exhibit reduced growth, as do children after chronic treatment with glucocorticoids (Baxter, 1978; EVANS et al., 1943; Thakore and Dinan, 1994). This glucocorticoid-mediated growth suppression is through glucocorticoid

regulated increased transcription of the GH-receptor gene (Miller and Mayo, 1997). The mechanism of glucocorticoid-mediated suppression of the GH axis may also be conserved in zebrafish, as they produce growth hormone and have two growth hormone receptors (Di Prinzio et al., 2010). To investigate whether there is a change in GH or GH-receptors, mRNA expression should be quantified in the brain (pituitary) and in the liver of adult zebrafish in the future.

The most surprising phenotype was the infertility of female *cyp17a2*$^{-/-}$ fish. In multiple, distinct tests, adult *cyp17a2*$^{-/-}$ mutant females did not lay eggs. Whilst previous research has documented the expression of both *cyp17a1* and *cyp17a2* genes during gonadal differentiation of another teleost fish, the tilapia, functional data was not available to support the hypothesis that *cyp17a2* is crucial for normal development, survival and fertility (Zhou et al., 2007). Cyp17a2 was suggested to be important for ovary development as there is initially high *cyp17a1* and low *cyp17a2* expression during early and midvitellogenesis, then a synchronous transition to low *cyp17a1* and high *cyp17a2* expression in granulosa cells during the maturation stage of the developing ovary, with a subsequent increase in the fish-specific maturation-inducing hormone (MIH), important for the transition of postvitellogenic oocytes to mature oocytes and spawning (Zhou et al., 2007). The synchronous transition is important in fish, as vertebrate gonads enter a steroidogenic shift from an oestrogen-important follicular phase to a progesterogen-important maturation phase (Goff and Henderson, 1979). Due to the lack of available data, it is unclear whether the *cyp17a2*$^{-/-}$ female ovaries are immature. H&E staining of histological sections of the ovary and reproductive tract will provide crucial insight into the organisation and function of the *cyp17a2*$^{-/-}$ female reproductive system and will hopefully explain why these mutant females do not spawn. Additionally, ovaries can be harvested, and *in vitro* fertilization performed to investigate whether mature eggs are able to be fertilised and develop appropriately. To understand if there is both 17α-hydroxylase and 17,20 lyase activity in the ovary with the loss of cyp17a2 function during ovary maturation, oestrogen steroid measurements and oestrogen-responsive gene expression should also be investigated.

The results from this study show that homozygous *cyp17a2*$^{-/-}$ mutant zebrafish develop into viable adults. *Cyp17a2*$^{-/-}$ mutant larvae and adult male fish exhibited an altered steroid profile. Although the loss of *cyp17a2* function did not prevent sexual dimorphism, as was observed for loss-of-function mutations in its paralog *cyp17a1*, adult female fish were infertile and unable to spawn, whilst adult males were subfertile. As Cyp17a1 is important for the 17,20 lyase activity in the gonads, and Cyp17a2 is important for 17α-hydroxylase activity in the head kidney, it would be very interesting to create a double knockout *cyp17a1*$^{-/-}$;*cyp17a2*$^{-/-}$ zebrafish mutant, which may be an appropriate model for human 17OHD.

Chapter 9. Summary, general discussion and future plans

9.1 Summary of Results

This thesis has described molecular, genetic and phenotypic analysis of several zebrafish lines that carry targeted mutations in genes encoding essential components of steroid hormone signalling. These mutations disrupt the function of the steroid hormone receptors MR (*nr3c2*) and GR (*nr3c1*) and the cyp17a2 gene encoding a 17-hydroxylase enzyme. I have analysed the phenotypic consequences of losing the functions of GR and MR, both singly and in combination, and the phenotypic consequence of losing *cyp17a2* function. MR and GR (Griffiths et al., 2012) loss-of-function mutations resulted in a hyperactivated or de-repressed HPI axis state, resulting in elevated cortisol concentrations. Transcriptomic analysis of MR and GR mutant zebrafish larvae was conducted, to determine the systemic molecular impacts caused by the loss of MR or GR function, including HPI axis hyperactivation and whole body larval hypercortisolaemia. The impact of homozygosity for the GR *s357* mutation on the transcriptome of adult zebrafish brain was also assessed, revealing an altered expression profile which strongly suggests a major role for GR in regulating mitochondrial functions in neurons. Additionally, *cyp17a2* was shown to be essential for glucocorticoid synthesis in zebrafish and I also identified a role for this enzyme in female spawning.

9.2 – Loss of MR function results in a de-repression of the HPI axis and consequential elevated downstream molecular signalling and endocrine changes in zebrafish.

Previous work has shown that the MR is important in the regulation of the HPI axis-associated gene expression in zebrafish (Faught and Vijayan, 2018). However, these transcriptional changes did not result in downstream endocrinological changes, as $MR^{-/-}$ mutant zebrafish larvae had baseline wildtype concentrations of cortisol.

To determine what systemic biological and molecular functions the MR regulates in zebrafish, I generated two novel MR mutant zebrafish lines, the first carrying a 46bp deletion with a 2bp substitution, and the second carrying a 25bp insertion, both of which lead to an out of frame, nonsense mutation and a premature stop codon in the DBD. In chapter 3, I have described the HPI-associated molecular and endocrine impact resulting from the loss of MR DNA and ligand binding function in zebrafish. My results show higher *pomca* mRNA expression in the anterior pituitary in both MR^{46Del} and MR^{25Ins} mutants compared to age-matched $MR^{+/+}$ larvae, similar to

Faught and Vijayan's findings. ACTH, a post-translational modification product of POMC, is known to stimulate cholesterol and glucocorticoid biosynthesis (Clark, 2016). Transcriptomic analysis of MR^{46Del} mutants revealed a significant increase in expression of genes important for multiple stages of the cholesterol biosynthesis, the precursor of all steroid hormone (Figure 4.10). The gene important for the rate limiting step of glucocorticoid biosynthesis, which transports cholesterol from the outer to inner mitochondrial membrane, *star*, was significantly upregulated in $MR^{-/-}$ mutants, as was expression of downstream glucocorticoid synthesis genes *fdx1b*, *cyp11a2*, *hsd3b1* and *cyp21a2*. Corresponding to this comprehensive increased expression in both biosynthetic pathways, concentrations of the glucocorticoids 11-deoxycortisol and cortisol were significantly increased in $MR^{-/-}$ mutants. Increased glucocorticoid-responsive gene expression verified our steroid data. However, qPCR but not RNAseq-based transcriptomic analysis identified *fkbp5* as a DEG, whereas neither qPCR or RNAseq identified *pck1* as differentially expressed. Interestingly, in the glucocorticoid-deficient *cyp17a2$^{-/-}$* mutant zebrafish created during this project, *pck1* was significantly downregulated, but expression was not completely extinguished, as was the case for *fkbp5*, suggesting that a cortisol-independent mechanism exists that regulates its expression. Together, genetic, molecular and transcriptomic analysis revealed that the MR plays an important role in regulating basal cortisol levels through negative regulation of HPI axis activity.

Previous findings in mammals, have shown that both GR and MR regulate feedback to the pituitary gland, with GR providing negative feedback by inhibiting ACTH release and subsequent cortisol production, and it is presumed that positive feedback is provided by the high affinity of MR for low cortisol concentrations, driving low level glucocorticoid signalling such as basal secretion in the circadian cycle (Dallman et al., 1989; de Kloet et al., 1998; Steenbergen et al., 2011). However, mammalian studies have also clearly shown that MR antagonist (spironolactone) treatment results in increased circulating cortisol concentrations (Deuschle et al., 1998; Young et al., 1998). There is also strong evidence that loss of MR activity through administration of antagonists results in hyperactivation the HPA axis, seen by increased ACTH and cortisol secretion after CRH and AVP stimulation (Arvat et al., 2001; Dodt et al., 1993; Heuser et al., 2000). On the other hand, MR activation through agonist treatment abolishes metyrapone-induced ACTH secretion (Otte et al., 2003, 2004). These mammalian studies support my findings, which suggest that in zebrafish, MR represses the HPI axis.

One aspect of the HPI axis that was not investigated in my experiments was the $MR^{-/-}$ mutant's ability to elicit a stress response. Previously, Faught and Vijayan's $MR^{-/-}$ mutant exhibited a delayed but sustained stress response after a stressful stimulus compared to wild-type siblings.

This suggests an initial delay in neuroendocrine signaling and partial loss of the negative feedback loop on the HPI axis in their $MR^{-/-}$ mutant larvae (Faught and Vijayan, 2018). Differences between the $MR^{-/-}$ mutants described in this thesis and the published mutant of Faught and Vijayan include the exon targeted during mutagenesis and resulting MR and GR mRNA expression. In the published $MR^{-/-}$ mutant, MR mRNA expression is significantly higher than wildtype mutants, whereas in the mutants described in this thesis, MR mRNA expression is significantly downregulated. If the published $MR^{-/-}$ mutant is partially functional , then the difference in expression may cause the differences in cortisol profiles between the two mutants, as the $MR^{-/-}$ mutant described in this thesis is hypercortisolaemic, whereas the cortisol levels in the published $MR^{-/-}$ mutant are close to wild-type concentrations (Faught and Vijayan, 2018). It is worth noting that in both $MR^{-/-}$ mutants, it is unlikely that there is genetic compensation, as there are no close paralogs of $nr3c2$ besides $nr3c1$, and no transcriptional activation of $nr3c1$ was identified at either 96hpf (Faught and Vijayan, 2018) or at 5dpf in the $MR^{-/-}$ mutant described in this thesis.

9.2 – Insights into the regulation of MR and GR on the lipid metabolic pathway, macroscopic adipose deposits and growth.

In mammals, the MR's primary function is salt and water homeostasis through binding of its ligand aldosterone. However, the MR has equivalent affinity for aldosterone and the physiological glucocorticoid cortisol in humans. Indeed, the MR's affinity for cortisol in humans is >10-fold higher than that of the GR for cortisol, suggesting an important function for MR in responsding to low cortisol concentrations (Arriza et al., 1987). In tissues where aldosterone-MR interactions are important, the cortisol inactivating enzyme HSD11B2 is expressed, removing cortisol and facilitating the binding of aldosterone to MR. However, in tissues which express MR at high levels and HSD11B2 at low levels, such as adipose tissue, it is very likely that the endogenous ligand for MR is cortisol (Funder, 2005). As zebrafish do not produce aldosterone, but do produce cortisol, the zebrafish provides an opportunity to elucidate the role of MR-cortisol interactions in the adipocyte landscape.

Transcriptomic analysis of $MR^{-/-}$ 5dpf larvae revealed a multitude of genes upregulated in the lipogenesis pathway compared to wildtype controls (Chapter 4; Figure 4.10); from genes that encode enzymes important in acetyl-CoA to fatty acid elongation, triglyceride production, lipolytic and lipid transport genes. However, these results contradict previous findings, where MR-KO zebrafish larvae with and without cortisol treatment resulted in no significant differences in $hmgcs1$, $dgat2$ or $elovl2$ mRNA expression compared to wildtype controls (Faught and Vijayan, 2019b). Despite the contradictory qPCR results, Faught and Vijayan performed RNAseq on their

MR-KO and GR-KO lines and identified that cholesterol and lipid metabolic pathways were dysregulated in both mutants. One distinct difference between the *MR^46Del* mutant I created and the MR-KO mutant of Faught and Vijayan, is that the latter did not exhibit elevated cortisol concentrations, only a de-repression of HPI axis genes such as *pomca* and *crh* (Faught and Vijayan, 2018). However, transcriptomic comparison of wildtype larvae and their MR-KO+cortisol treatment condition, which more closely mirror the phenotype of the *MR^46Del* mutant I created, displayed a clear upregulation of cholesterol synthesis, lipogenesis and lipid transport and lipolysis associated genes. Many of these genes, including *dgat2*, *apoea*, *apoeb*, *elovl2*, *msmo1*, *hmgcs1*, *hmgcra* and finally *sc5d* were also identified in my dataset (Faught and Vijayan, 2019b). These results raise the interesting possibilities that the general increase in gene expression of lipid metabolism may be due to the loss of an MR-repressive function on these genes, or more indirectly by the observed hypercortisolaemia activating these genes via the GR, or a combination of both.

In mammals, the impact of corticosteroid-receptor (CR) signalling on lipid homeostasis is dependent on whether exposure is acute or chronic. Acute glucocorticoid treatment is known to stimulate lipolysis, whereas chronic glucocorticoid exposure leads to glucocorticoid resistance that promotes weight gain and adipocyte proliferation (Berthon et al., 2014). Previously, a GR-KO zebrafish line was shown to increase adult zebrafish growth, including whole-body protein and lipid weight (Faught and Vijayan, 2020). In their larval studies, cortisol-induced MR activation, but not GR-activation resulted in triglyceride accumulation; cortisol-induced GR activation decreased triglyceride levels but also required MR to be present (Faught and Vijayan, 2019a). It was suggested that MR was a primary regulator of lipogenic gene transcription, whilst GR activation regulated lipid catabolism (Faught and Vijayan, 2019a). To understand the extent to which the functions of GR and MR might overlap or be distinct, I generated a double mutant, homozygous for both corticosteroid receptors, GR^-/-;MR^-/- and compared the phenotypes of this double mutant with GR^-/- and MR^-/- single mutants.

9.3. Insights into the roles of MR and GR in regulating zebrafish bodyweight, size and fat: GR function can fully compensate for loss of MR function whereas MR can only partially compensate for loss of GR function.

Whilst lipid metabolism was not identified as an overrepresented Gene Ontology (GO) term in our transcriptomic analysis of *gr^s357* mutants, this may be due to this mutant still having a functional LBD, thus facilitating the binding of its ligand cortisol, and potentially interacting with relevant target genes via protein-protein interactions with other transcription factors.

Previously, adult $GR^{-/-}$ mutant zebrafish have been reported to be larger and heavier than wild-type siblings (Faught and Vijayan, 2019a). Initial characterisation of morphological biostatistics revealed a profound increase in zebrafish body weight and body size of double mutants in comparison to wildtype and single mutant siblings, despite similar stock densities, feeding quantity and sex ratios. Moreover, $GR^{-/-}$ single mutant fish were significantly heavier and longer than wildtype and $MR^{-/-}$ mutant fish, although this increase in body size was not as great as was the case for $GR^{-/-};MR^{-/-}$ double mutants. Extremely large deposits of visceral fat were observed surrounding the internal organs in the abdominal cavity of the of double mutants. $GR^{-/-}$ single mutant fish exhibited much less adipose tissue than double mutants, but they nevertheless possessed noticeably greater amounts of visceral adipose tissue than did wild-type or $MR^{-/-}$ single mutant fish. Whilst these are preliminary results, they suggest that loss of MR function alone has no appreciable effect on body weight, whereas loss of GR function causes a slight but significant increase in body weight, indicating that GR activity limits weight gain. However, loss of both GR and MR markedly increases body weight to over twice that of wild-type fish, indicating that both GR and MR are required to limit body weight. Thus, whilst GR function can fully compensate for loss of MR function, MR can only partially compensate for loss of GR function. Taken together these results imply that GR and MR may share some common target genes that regulate body weight. However, GR is also likely to regulate additional body weight genes that MR cannot target.

It is widely established that glucocorticoids modulate the secretion of the growth hormone from the anterior pituitary (Mazziotti and Giustina, 2013). In the pituitary glands of rats, GR colocalises with cells that produce corticotropin and growth hormone (Kononen et al., 1993), and *in vitro* studies have shown that glucocorticoids stimulate growth hormone synthesis in pituitary cells in both animal and human cell lines (Giustina and Veldhuis, 1998; Porter and Dean, 2001; Vakili et al., 2011). *In vivo* studies of long-term glucocorticoid treatment of rats showed a decrease in body growth and weight, suggesting cortisol-mediated GR activation has a repressive effect on growth. Our double mutant model may shed some light on the role of the MR and GR on growth hormone regulation.

Restrictions to laboratory access during the COVID-19 pandemic prevented further molecular analysis of $GR^{-/-};MR^{-/-}$ double mutant fish. Further research is required to identify whether the exacerbated increase in weight, size and visceral adipose tissue seen in the double mutants was due to: i) increase in lipogenesis, ii) increase in protein synthesis, iii) decrease in lipolysis, iv) decrease in proteolysis, v) increase in growth hormone, vi) reduced exercise, or a combination of factors.

9.4. Corticosteroid Receptors play an important role in regulating the neuronal transcriptome in larvae

In both *MR$^{-/-}$* and *gr^{s357}* homozygous mutant larval transcriptomes, DEGs encoding components of neuronal signalling were identified as overrepresented in my GO analysis. However, the direction of differential expression was different between the two mutants. In *MR$^{-/-}$* mutants, genes involved in synaptic signalling were primarily down-regulated in 5dpf larvae, whereas in *gr^{s357}* 5dpf larvae, genes associated with cellular components located in neurons and axons were primarily up-regulated.

In the *MR$^{-/-}$* mutant larval transcriptome, the primary Biological Process down-regulated in the *MR^{46Del}* mutant 5dpf larval transcriptome was synaptic signalling. This included genes expressed in glutamatergic and GABAergic neurons, encoding pre- and post-synaptic components, as well as neuromuscular junction proteins. The majority of genes are associated with cell surface ionotropic receptors important for both exocytosis and endocytosis and action potential generation. MR expression has been discovered at nuclear locations in both glutamatergic and GABAergic neuronal subtypes. In addition, MR has also been found in human neurons in the vicinity of presynaptic terminals, dendritic spines and dendrites (Prager et al., 2010). Prager et al (2010) suggested that MR may be positioned at multiple subcellular locations to co-ordinate glutamate neurotransmission and post-synaptic responses. As the MR is associated with learning and memory (Gomez-Sanchez and Montgomery, 2014), MR-mediated regulation of synapse signalling may be a potential mechanism in which the adrenal steroid hormones influence behaviour during stress. Interestingly, in the *gr^{s357}* mutant larval transcriptome, a general up-regulation of neuronal genes was identified, including those associated with GABA and glutamate signalling in synapses, synapse scaffolds important for neurotransmitter release, neuronal development, and axon guidance, migration and growth. Comparative analysis between the *gr^{s357}* and *MR^{46Del}* transcriptomes identified common DEGs that were up-regulated in *gr^{s357}* and down-regulated in *MR^{46Del}* transcriptomes, and were predominantly associated with neuronal cell adhesion, axon guidance and neurotransmitter release.

Taken together, my results suggest that the MR is required for transcriptional activation of synapse-associated genes, and in the hypercortisolaemic *gr^{s357}* mutants, the high levels of cortisol may robustly up-regulate neuronal gene transcription by activating the MR. Early life stress is known to influence the development of the HPA axis, wider neural networks within the CNS, including those influencing cognitive function, and is strongly correlated with later life occurrence of major depressive disorder, anxiety disorders and PTSD (Heim et al., 2010; Kessler

et al., 1997, 2010). In addition, a role has been postulated for the GR in the development of psychiatric disorders and indeed, altered expression of GR in the brain has been linked to childhood trauma-linked mental ill-health (McGowan et al., 2009). Moreover, the genetic disorder Chrousos Syndrome, which is caused by loss-of-function mutations in *the* NR3C1 gene, is characterised by hypercortisolaemia, chronic fatigue, anxiety and depression (Charmandari et al., 2013). To obtain new insights into the impacts of GR function on the vertebrate brain, I investigated the impact of the gr^{s357} mutation on the transcriptome of eighteen-month-old adult zebrafish brains.

9.5. MR and GR loss of function results in the dysregulation of genes associated with mitochondrial function

Mitochondrial function and the stress response are intrinsically connected. Physiological responses to an activated HPI axis include elevated blood glucose, metabolism changes and reallocation of cellular resources utilised by mitochondria to provide energy required for a stress response (Lapp et al., 2019).

In all three transcriptomic experiments, genes within the mitochondrial genome (mt-DNA) were identified as being differentially expressed. In the comparative analysis of the $MR^{-/-}$ and gr^{s357} larval transcriptomes, 14 mt-DNA genes were identified in both $MR^{-/-}$ and gr^{s357} mutant data sets as upregulated by ~2-fold . This most likely is due to the hypercortisolaemic steroid profile these larvae exhibit acting via the unmutated corticosteroid receptor, as dexamethasone treatment is known to stimulate transcription of genes such as *mt-COX1*, *mt-COX3* and *mt-ND1* in vitro in mammalian cells (Psarra and Sekeris, 2011). In the comparative analysis of the gr^{s357} larval and brain transcriptomes, 12 mt-DNA genes were identified as overlapping, but their expression change was in opposing directions. These mt-DNA genes were significantly up-regulated in the gr^{s357} 5dpf larval transcriptome, but significantly down-regulated in gr^{s357} adult brains. This reciprocal change may be due to acute and chronic effects of hypercortisolaemia, respectively, as previously it has been suggested that according to the type of stress studied and the duration, the direction of mtDNA transcriptional change appears to vary for a wide range of mitochondrial genes (Lapp et al., 2019).

These results suggest that the GR influences the transcription of a wide network of genes, some of which are specific to developmental stage or tissue, and others that are expressed in both 5dpf larvae and adult zebrafish brains. The major challenge will be to understand when during development and where (which tissues) the switch occurs. Further functional analysis into mt-

DNA copy number, epigenetic regulation of mt-DNA expression and mitochondrial function in gr^{s357} mutant zebrafish will provide greater understanding of the impact of stress hormones on mitochondrial function.

9.6. Corticosteroid biosynthesis is directed by Cyp17a2 in zebrafish

In mammals, The P450 enzyme 17 hydroxylase (Cyp17a1) catalyses two critical reactions of steroid biosynthesis: first, 17α-hydroxylation, important for cortisol and sex steroid synthesis, followed by 17,20-lyase activity, which is specifically required for sex steroid production (Auchus et al., 2017). However, zebrafish also contain a second gene coding a cytochrome P450c17: *cyp17a2*. In zebrafish and other teleosts, a biochemically distinct difference was discovered between the two cytochrome P450c17s; both Cyp17a1 and Cyp17a2 were shown by enzymatic assays to perform the 17α-hydroxylase activity, but only Cyp17a1 possessed the ability to perform the 17,20 lyase activity (Zhou et al., 2007). Recently, a *cyp17a1*-deficient mutant zebrafish line was shown to be androgen-deficient, but not cortisol-deficient, leading to my hypothesis that Cyp17a2 is responsible for cortisol synthesis in zebrafish and the loss of its function would flood steroid hormone precursors into the mineralocorticoid pathway.

To determine the role of Cyp17a2 in zebrafish, I generated a novel *cyp17a2*$^{-/-}$ mutant zebrafish line carrying a 29bp deletion in exon 1, which caused a frameshift mutation leading to premature translation termination. *Cyp17a2*$^{-/-}$ mutants exhibited severe cortisol deficiency, but a profound increase in corticosterone concentrations. Typical glucocorticoid-deficient phenotypes were observed, e.g. impaired pigment adaptation in the visual background adaptation assay, reduced locomotor behaviour that could be partially rescued by hydrocortisone treatment and increased weight and length. Surprisingly, adult females were infertile, as no eggs were spawned over multiple trials. Whether this infertility this is due to immature oocytes, disorganisation of the ovaries and/or impaired breeding behaviours is unknown, but provides an interesting line of enquiry to improve further understanding of zebrafish and teleost reproductive biology.

The steroid profile of the *cyp17a2*$^{-/-}$ mutants reflects a similar profile found in rodents. Rats and mice express Cyp17a1 in the gonads but not in the adrenal glands (Auchus et al., 2017). Therefore, rodents do not produce the glucocorticoid cortisol in adrenal tissue, and instead their dominant glucocorticoid is corticosterone, a mineralocorticoid precursor of aldosterone that is known to bind both the glucocorticoid and mineralocorticoid receptor. In humans, A loss of 17-hydroxylase activity (17-OH Deficiency; 17OHD) floods the mineralocorticoid pathway with steroid precursors (Auchus et al., 2017). However, patients with CYP17A1 deficiency are cortisol

deficient, but survive on corticosterone acting as the principal glucocorticoid. By contrast, in zebrafish, despite profound increases of corticosterone concentration, glucocorticoid-deficient phenotypes and the loss of *fkbp5* expression were not rescued. This is surprising as *in vitro* studies have demonstrated that 11-deoxycorticosterone can stimulate transcriptional activation of the MR, however the effect on the GR was not investigated (Pippal et al., 2011). A potential caveat of this *in vitro* study is that it was performed in a mammalian cell line, at 37°C, whereas the physiological temperature of zebrafish is 28°C. In terms of function, the effects of this environment of elevated temperature on transcriptional coregulators (coactivators or corepressors) of MR transactivation are unknown (Viengchareun et al., 2007).

As Cyp17a1 is important for the 17,20 lyase activity in the gonads, and Cyp17a2 is important for 17α-hydroxylase activity in the head kidney, it would be very interesting to create a double knockout *cyp17a1*$^{-/-}$;*cyp17a2*$^{-/-}$ zebrafish mutant, which may be an appropriate model for human 17OHD.

In conclusion, this thesis has described molecular, genetic and phenotypic analysis of several zebrafish lines that carry targeted mutations in genes encoding essential components of steroid hormone signalling. My study stresses the important role the MR play in regulating the HPA axis and steroid hormone pathways. Through multiple transcriptomic experiments, I have revealed novel systemic molecular impacts caused by the loss of MR or GR function, including an altered expression profile which strongly suggests a major role for GR in regulating mitochondrial functions in neurons, and a role for MR in regulating synaptic signalling. Additionally, *cyp17a2* was shown to be essential for glucocorticoid synthesis in zebrafish and I also identified a role for this enzyme in female spawning.

10. Appendices

All Appendices are located in the attached Supplementary Information Folder.

10.0 Supplementary Information Contents

10.1 Appendix I. Thesis supplementary figures

10.2 Appendix II. Chapter 4: *MR^{46Del}* larval transcriptomic analysis: list of significantly differentially expressed genes

10.3 Appendix III. Chapter 5: *gr^{s357}* larval transcriptomic analysis: list of significantly differentially expressed genes

10.4 Appendix IV. Chapter 6: *gr^{s357}* adult male brain transcriptomic analysis: list of significantly differentially expressed genes

10.5 Appendix V. Code for RNA sequencing analysis

11. References

Aase, K., Ernkvist, M., Ebarasi, L., Jakobsson, L., Majumdar, A., Yi, C., Birot, O., Ming, Y., Kvanta, A., Edholm, D., et al. (2007). Angiomotin regulates endothelial cell migration during embryonic angiogenesis. Genes Dev. *21*, 2055–2068.

Alexander, W.S. (2002). Suppressors of cytokine signalling (SOCS) in the immune system. Nat. Rev. Immunol. *2*, 410–416.

Alsop, D., and Vijayan, M.M. (2008). Development of the corticosteroid stress axis and receptor expression in zebrafish. Am. J. Physiol. Regul. Integr. Comp. Physiol. *294*, R711-9.

Alsop, D., and Vijayan, M.M. (2009a). Molecular programming of the corticosteroid stress axis during zebrafish development. Comp. Biochem. Physiol. Part A Mol. Integr. Physiol. *153*, 49–54.

Alsop, D., and Vijayan, M.M. (2009b). Molecular programming of the corticosteroid stress axis during zebrafish development. Comp. Biochem. Physiol. - A Mol. Integr. Physiol. *153*, 49–54.

Andrew, R., Gale, C.R., Walker, B.R., Seckl, J.R., and Martyn, C.N. (2002). Glucocorticoid metabolism and the metabolic syndrome: Associations in an elderly cohort. Exp. Clin.

Endocrinol. Diabetes.

Andrews, S. (2010). FastQC. Babraham Bioinforma.

Arriza, J., Weinberger, C., Cerelli, G., Glaser, T., Handelin, B., Housman, D., and Evans, R. (1987). Cloning of human mineralocorticoid receptor complementary DNA: structural and functional kinship with the glucocorticoid receptor. Science (80-.). *237*.

Arterbery, A.S., Deitcher, D.L., and Bass, A.H. (2010). Corticosteroid receptor expression in a teleost fish that displays alternative male reproductive tactics. Gen. Comp. Endocrinol. *165*, 83–90.

Arvat, E., Maccagno, B., Giordano, R., Pellegrino, M., Broglio, F., Gianotti, L., Maccario, M., Camanni, F., and Ghigo, E. (2001). Mineralocorticoid Receptor Blockade by Canrenoate Increases Both Spontaneous and Stimulated Adrenal Function in Humans*.

Auchus, R.J., Steroid, J., Mol, B., and Author, B. (2017). Steroid 17-Hydroxylase and 17,20-Lyase Deficiencies, Genetic and Pharmacologic HHS Public Access Author manuscript. J Steroid Biochem Mol Biol *165*, 71–78.

Azetsu, Y., Chatani, M., Dodo, Y., Karakawa, A., Sakai, N., Negishi-Koga, T., and Takami, M. (2019). Treatment with synthetic glucocorticoid impairs bone metabolism, as revealed by in vivo imaging of osteoblasts and osteoclasts in medaka fish. Biomed. Pharmacother.

Bailey, T.L., Boden, M., Buske, F.A., Frith, M., Grant, C.E., Clementi, L., Ren, J., Li, W.W., and Noble, W.S. (2009). MEME Suite: Tools for motif discovery and searching. Nucleic Acids Res.

Baker, M.E., and Katsu, Y. (2017). Evolution of the mineralocorticoid receptor: Sequence, structure and function. J. Endocrinol. *234*, T1–T16.

Baker, M.E., Funder, J.W., and Kattoula, S.R. (2013). Evolution of hormone selectivity in glucocorticoid and mineralocorticoid receptors. J. Steroid Biochem. Mol. Biol. *137*, 57–70.

Barclay, J.L., Petersons, C.J., Keshvari, S., Sorbello, J., Mangelsdorf, B.L., Thompson, C.H., Prins, J.B., Burt, M.G., Whitehead, J.P., and Inder, W.J. (2016). Thrombospondin-1 is a glucocorticoid responsive protein in humans. Eur. J. Endocrinol.

Baxter, J.D. (1978). Mechanisms of glucocorticoid inhibition of growth.

Beinke, S., and Ley, S.C. (2004). Functions of NF-κB1 and NF-κB2 in immune cell biology. Biochem. J.

Bereshchenko, O., Coppo, M., Bruscoli, S., Biagioli, M., Cimino, M., Frammartino, T., Sorcini, D., Venanzi, A., DiSante, M., and Riccardi, C. (2014). GILZ Promotes Production of Peripherally Induced Treg Cells and Mediates the Crosstalk between Glucocorticoids and TGF-β Signaling. Cell Rep. *7*, 464–475.

Berger, S., Bleich, M., Schmid, W., Cole, T.J., Peters, J., Watanabe, H., Kriz, W., Warth, R., Greger, R., and Schütz, G. (1998). Mineralocorticoid receptor knockout mice: pathophysiology of Na+ metabolism. Proc. Natl. Acad. Sci. U. S. A. *95*, 9424–9429.

Berger, S., Wolfer, D.P., Selbach, O., Alter, H., Erdmann, G., Reichardt, H.M., Chepkova, A.N., Welzl, H., Haas, H.L., Lipp, H.-P., et al. (2006). Loss of the limbic mineralocorticoid receptor impairs behavioral plasticity. Proc. Natl. Acad. Sci. U. S. A. *103*, 195–200.

Bern, H.A. (1967). Hormones and endocrine glands of fishes. Studies of fish endocrinology reveal major physiologic and evolutionary problems. Science *158*, 455–462.

Bersani, F.S., Morley, C., Lindqvist, D., Epel, E.S., Picard, M., Yehuda, R., Flory, J., Bierer, L.M., Makotkine, I., Abu-Amara, D., et al. (2016). Mitochondrial DNA copy number is reduced in male combat veterans with PTSD. Prog. Neuro-Psychopharmacology Biol. Psychiatry *64*, 10–17.

Berthon, B.S., MacDonald-Wicks, L.K., and Wood, L.G. (2014). A systematic review of the effect of oral glucocorticoids on energy intake, appetite, and body weight in humans. Nutr. Res.

Best, C., and Vijayan, M.M. (2017). Cortisol elevation post-hatch affects behavioural performance in zebrafish larvae. Gen. Comp. Endocrinol.

Best, C., Kurrasch, D.M., and Vijayan, M.M. (2017). Maternal cortisol stimulates neurogenesis and affects larval behaviour in zebrafish. Sci. Rep. *7*, 1–10.

Binart, N., Lombès, M., and Baulieu, E.E. (1995). Distinct functions of the 90 kDa heat-shock protein (hsp90) in oestrogen and mineralocorticosteroid receptor activity: effects of hsp90 deletion mutants. Biochem. J. 797–804.

Binder, E.B. (2009). The role of FKBP5, a co-chaperone of the glucocorticoid receptor in the pathogenesis and therapy of affective and anxiety disorders. Psychoneuroendocrinology *34*.

Blackburn, P.R., Campbell, J.M., Clark, K.J., and Ekker, S.C. (2013). The CRISPR system--keeping zebrafish gene targeting fresh. Zebrafish *10*, 116–118.

Blanchette-Mackie, E.J., and Scow, R.O. (1985). Lipid filling and lipolysis in adipose tissue and cells. Int. J. Obes. *9*, 7–14.

Bokström, H., and Norström, A. (1995). Effects of mifepristone and progesterone on collagen synthesis in the human uterine cervix. Contraception *51*, 249–254.

Bolger, A.M., Lohse, M., and Usadel, B. (2014). Trimmomatic: a flexible trimmer for Illumina sequence data. Bioinformatics *30*, 2114–2120.

Bonett, R.M., Hu, F., Bagamasbad, P., and Denver, R.J. (2009). Stressor and glucocorticoid-dependent induction of the immediate early gene krüppel-like factor 9: implications for neural development and plasticity. Endocrinology.

Bormann, J. (2000). The "ABC" of GABA receptors. Trends Pharmacol. Sci.

Van Den Bos, R., Mes, W., Galligani, P., Heil, A., Zethof, J., Flik, G., and Gorissen, M. (2017). Further characterisation of differences between TL and AB Zebrafish (Danio rerio): Gene expression, physiology and behaviour at day 5 of the larval stage. PLoS One.

Bose, H.S., Lingappat, V.R., and Miller, W.L. (2002). Rapid regulation of steroidogenesis by mitochondrial protein import. Nature *417*, 87–91.

De Bosscher, K., Haegeman, G., and Elewaut, D. (2010). Targeting inflammation using selective glucocorticoid receptor modulators. Curr. Opin. Pharmacol. *10*, 497–504.

Bridgham, J.T., Carroll, S.M., and Thornton, J.W. (2006). Evolution of Hormone-Receptor Complexity by Molecular Exploitation. Science (80-.). *312*.

Britto, F.A., Begue, G., Rossano, B., Docquier, A., Vernus, B., Sar, C., Ferry, A., Bonnieu, A., Ollendorff, V., and Favier, F.B. (2014). REDD1 deletion prevents dexamethasone-induced skeletal muscle atrophy. Am. J. Physiol. - Endocrinol. Metab. *307*, E983–E993.

Brun, N.R., van Hage, P., Hunting, E.R., Haramis, A.P.G., Vink, S.C., Vijver, M.G., Schaaf, M.J.M., and Tudorache, C. (2019). Polystyrene nanoplastics disrupt glucose metabolism and cortisol levels with a possible link to behavioural changes in larval zebrafish. Commun. Biol.

Bruner, K.L., Derfoul, A., Robertson, N.M., Guerriero, G., Fernandes-Alnemri, T., Alnemri, E.S., and Litwack, G. (1997). The unliganded mineralocorticoid receptor is associated with heat shock proteins 70 and 90 and the immunophilin FKBP-52. Recept. Signal Transduct. *7*, 85–98.

Bury, N.R., and Sturm, A. (2007). Evolution of the corticosteroid receptor signalling pathway in fish. Gen. Comp. Endocrinol. *153*, 47–56.

Bury, N.R., Sturm, A., Le Rouzic, P., Lethimonier, C., Ducouret, B., Guiguen, Y., Robinson-Rechavi, M., Laudet, V., Rafestin-Oblin, M.E., and Prunet, P. (2003). Evidence for two distinct functional glucocorticoid receptors in teleost fish. J. Mol. Endocrinol. *31*, 141–156.

Burzynski, L.C., Humphry, M., Pyrillou, K., Wiggins, K.A., Chan, J.N.E., Figg, N., Kitt, L.L., Summers, C., Tatham, K.C., Martin, P.B., et al. (2019). The Coagulation and Immune Systems Are Directly Linked through the Activation of Interleukin-1α by Thrombin. Immunity *50*, 1033-1042.e6.

Cain, D.W., and Cidlowski, J.A. (2017). Immune regulation by glucocorticoids. Nat. Rev. Immunol. *17*, 233–247.

Caprio, M., Fève, B., Claës, A., Viengchareun, S., Lombès, M., and Zennaro, M.-C. (2007). Pivotal role of the mineralocorticoid receptor in corticosteroid-induced adipogenesis. FASEB J.

Carr, B.R., and Simpson, E.R. (1981). Lipoprotein utilization and cholesterol synthesis by the human fetal adrenal gland. Endocr. Rev.

Cassuto, H., Kochan, K., Chakravarty, K., Cohen, H., Blum, B., Olswang, Y., Hakimi, P., Xu, C., Massillon, D., Hanson, R.W., et al. (2005). Glucocorticoids regulate transcription of the gene for phosphoenolpyruvate carboxykinase in the liver via an extended glucocorticoid regulatory unit. J. Biol. Chem. *280*, 33873–33884.

Chai, C., Liu, Y., and Chan, W.-K. (2003). Ff1b is required for the development of steroidogenic component of the zebrafish interrenal organ. Dev. Biol. *260*, 226–244.

Challet, E. (2019). The circadian regulation of food intake. Nat. Rev. Endocrinol.

Charmandari, E., Tsigos, C., and Chrousos, G. (2005). Endocrinology of the stress response [1]. Annu. Rev. Physiol. *67*, 259–284.

Charmandari, E., Kino, T., and Chrousos, G.P. (2013). Primary generalized familial and sporadic glucocorticoid resistance (chrousos syndrome) and hypersensitivity. Endocr. Dev.

Chatzopoulou, A., Heijmans, J.P.M., Burgerhout, E., Oskam, N., Spaink, H.P., Meijer, A.H., and Schaaf, M.J.M. (2016). Glucocorticoid-Induced Attenuation of the Inflammatory Response in Zebrafish. Endocrinology *157*, 2772–2784.

Chen, Y.F., Li, Y.F., Chen, X., and Sun, Q.F. (2013). Neuropsychiatric disorders and cognitive dysfunction in patients with Cushing's disease. Chin. Med. J. (Engl). *126*, 3156–3160.

Chinenov, Y., Coppo, M., Gupte, R., Sacta, M.A., and Rogatsky, I. (2014). Glucocorticoid receptor coordinates transcription factor-dominated regulatory network in macrophages.

Chrousos, G.P. (2009). Stress and disorders of the stress system. Nat. Rev. Endocrinol. *5*, 374–381.

Clark, B.J. (2016). ACTH action on StAR biology. Front. Neurosci. *10*, 547.

Cohen-Cory, S., Kidane, A.H., Shirkey, N.J., and Marshak, S. (2010). Brain-derived neurotrophic factor and the development of structural neuronal connectivity. Dev. Neurobiol.

Cole, T.J., and Young, M.J. (2017). Mineralocorticoid receptor null mice: Informing cell-type-specific roles. J. Endocrinol. *234*, T83–T92.

Cole, T.J., Blendy, J.A., Monaghan, A.P., Krieglstein, K., Schmid, W., Aguzzi, A., Fantuzzi, G., Hummler, E., Unsicker, K., and Schütz, G. (1995). Targeted disruption of the glucocorticoid receptor gene blocks adrenergic chromaffin cell development and severely retards lung maturation. Genes Dev.

Colombo, L., Dalla Valle, L., Fiore, C., Armanini, D., and Belvedere, P. (2006). Aldosterone and the conquest of land. J. Endocrinol. Invest. *29*, 373–379.

Combaret, L., Taillandier, D., Dardevet, D., Echet, D.B.´, Ralli`ere, C., Ralli`ere, R., Claustre, A., Grizard, J., and Attaix, D. (2004). Glucocorticoids regulate mRNA levels for subunits of the 19 S regulatory complex of the 26 S proteasome in fast-twitch skeletal muscles.

Cotelli, F., Andronico, F., Brivio, M., and Lamia, C.L. (1988). Structure and composition of the fish egg chorion (Carassius auratus). J. Ultrastruct. Res. Mol. Struct. Res. *99*, 70–78.

Cruz-Topete, D., and Cidlowski, J.A. (2014). One hormone, two actions: Anti- And pro-inflammatory effects of glucocorticoids. Neuroimmunomodulation *22*, 20–32.

Cruz, S.A., Lin, C.-H., Chao, P.-L., and Hwang, P.-P. (2013). Glucocorticoid receptor, but not mineralocorticoid receptor, mediates cortisol regulation of epidermal ionocyte development and ion transport in zebrafish (danio rerio). PLoS One *8*, e77997.

Dallman, M.F., Levin, N., Cascio, C.S., Akana, S.F., Jacobson, L., and Kuhn, R.W. (1989). Pharmacological Evidence that the Inhibition of Diurnal Adrenocorticotropin Secretion by Corticosteroids Is Mediated via Type I Corticosterone-Preferring Receptors*. Endocrinology *124*, 2844–2850.

David Sweatt, J. (2001). The neuronal MAP kinase cascade: A biochemical signal integration system subserving synaptic plasticity and memory. J. Neurochem.

Dembic, Z. (2015). Cytokines Important for Growth and/or Development of Cells of the Immune System. In The Cytokines of the Immune System, (Elsevier), pp. 263–281.

Deuschle, M., Weber, B., Colla, M., Müller, M., Kniest, A., and Heuser, I. (1998). Mineralocorticoid receptor also modulates basal activity of hypothalamus-pituitary-adrenocortical system in humans. Neuroendocrinology.

Dinarello, A., Licciardello, G., Fontana, C.M., Tiso, N., Argenton, F., and Valle, L.D. (2020). Glucocorticoid receptor activities in the zebrafish model: A review. J. Endocrinol.

Dobin, A., Davis, C.A., Schlesinger, F., Drenkow, J., Zaleski, C., Jha, S., Batut, P., Chaisson, M., and Gingeras, T.R. (2013). STAR: Ultrafast universal RNA-seq aligner. Bioinformatics *29*, 15–21.

Dodt, C., Kern, W., Fehm, H.L., and Born, J. (1993). Antimineralocorticoid canrenoate enhances secretory activity of the hypothalamus-pituitary-adrenocortical (HPA) axis in humans. Neuroendocrinology *58*, 570–574.

Dschietzig, T., Bartsch, C., Stangl, V., Baumann, G., and Stangl, K. (2004). Identification of the pregnancy hormone relaxin as glucocorticoid receptor agonist. FASEB J. *18*, 1536–1538.

Dschietzig, T., Bartsch, C., Baumann, G., and Stangl, K. (2009a). RXFP1-inactive relaxin activates human glucocorticoid receptor: Further investigations into the relaxin-GR pathway. Regul. Pept. *154*, 77–84.

Dschietzig, T., Bartsch, C., Wessler, S., Baumann, G., and Stangl, K. (2009b). Autoregulation of human relaxin-2 gene expression critically involves relaxin and glucocorticoid receptor binding to glucocorticoid response half-sites in the relaxin-2 promoter. Regul. Pept. *155*, 163–173.

Du, J., Wang, Y., Hunter, R., Wei, Y., Blumenthal, R., Falke, C., Khairova, R., Zhou, R., Yuan, P., Machado-Vieira, R., et al. (2009). Dynamic regulation of mitochondrial function by glucocorticoids. Proc. Natl. Acad. Sci. U. S. A. *106*, 3543–3548.

Eachus, H., Zaucker, A., Oakes, J.A., Griffin, A., Weger, M., Güran, T., Taylor, A., Harris, A., Greenfield, A., Quanson, J.L., et al. (2017a). Genetic Disruption of 21-Hydroxylase in Zebrafish Causes Interrenal Hyperplasia. Endocrinology *158*, 4165–4173.

Eachus, H., Zaucker, A., Oakes, J.A., Griffin, A., Weger, M., Güran, T., Taylor, A., Harris, A., Greenfield, A., Quanson, J.L., et al. (2017b). Genetic Disruption of 21-Hydroxylase in Zebrafish Causes Interrenal Hyperplasia. Endocrinology *158*, 4165–4173.

Edwards, C.R., Stewart, P.M., Burt, D., Brett, L., McIntyre, M.A., Sutanto, W.S., de Kloet, E.R., and Monder, C. (1988). Localisation of 11 beta-hydroxysteroid dehydrogenase--tissue specific protector of the mineralocorticoid receptor. Lancet (London, England) *2*, 986–989.

Ensembl (2016). GRCz10 - Zebrafish - nr3c2 - Mineralocorticoid Receptor.

Evans, H.M., Simpson, M.E., and Hao Li, C. (1943). Inhibiting effect of adrenocorticotropic

hormone on the growth of male rats. Endocrinology *33*, 237–238.

Ewels, P., Magnusson, M., Lundin, S., and Käller, M. (2016). MultiQC: summarize analysis results for multiple tools and samples in a single report. Bioinformatics *32*, 3047–3048.

Facchinello, N., Skobo, T., Meneghetti, G., Colletti, E., Dinarello, A., Tiso, N., Costa, R., Gioacchini, G., Carnevali, O., Argenton, F., et al. (2017). Nr3c1 null mutant zebrafish are viable and reveal DNA-binding-independent activities of the glucocorticoid receptor. Sci. Rep. *7*.

Fan, C. chung, and Ho, R. jye (1981). Response of white adipocyte of mouse and rabbit to catecholamines and ACTH - 1. Correlation of cyclic AMP levels and initial rates of lipolysis. Mol. Cell. Biochem. *34*, 35–41.

Faught, E., and Vijayan, M.M. (2016). Mechanisms of cortisol action in fish hepatocytes. Comp. Biochem. Physiol. Part - B Biochem. Mol. Biol. *199*, 136–145.

Faught, E., and Vijayan, M.M. (2018). The mineralocorticoid receptor is essential for stress axis regulation in zebrafish larvae. Sci. Rep. *8*.

Faught, E., and Vijayan, M.M. (2019a). Loss of the glucocorticoid receptor in zebrafish improves muscle glucose availability and increases growth. Am. J. Physiol. Metab. *316*, E1093–E1104.

Faught, E., and Vijayan, M.M. (2019b). Postnatal triglyceride accumulation is regulated by mineralocorticoid receptor activation under basal and stress conditions. J. Physiol. *597*, 4927–4941.

Faught, E., and Vijayan, M.M. (2020). Glucocorticoid and mineralocorticoid receptor activation modulates postnatal growth. J. Endocrinol.

Faught, E., Santos, H.B., and Vijayan, M.M. (2020). Loss of the glucocorticoid receptor causes accelerated ovarian ageing in zebrafish. Proc. R. Soc. B Biol. Sci.

Feelders, R.A., Pulgar, S.J., Kempel, A., and Pereira, A.M. (2012). The burden of Cushing's disease: Clinical and health-related quality of life aspects. Eur. J. Endocrinol. *167*, 311–326.

Ferguson, D., Hutson, I., Tycksen, E., Pietka, T.A., Bauerle, K., and Harris, C.A. (2020). Role of Mineralocorticoid Receptor in Adipogenesis and Obesity in Male Mice. Endocrinol. (United States).

Fernandes, D., Bebianno, M.J., and Porte, C. (2007). Mitochondrial metabolism of 17α-hydroxyprogesterone in male sea bass (Dicentrarchus labrax): A potential target for endocrine disruptors. Aquat. Toxicol.

Ferraù, F., and Korbonits, M. (2015). Metabolic comorbidities in Cushing's syndrome. In European Journal of Endocrinology, (BioScientifica Ltd.), pp. M133–M157.

Fietta, P., and Fietta, P. (2007). Glucocorticoids and brain functions. Riv. Di Biol. - Biol. Forum.

Fietta, P., Fietta, P., and Delsante, G. (2009). Central nervous system effects of natural and synthetic glucocorticoids: Psychiatry Clin. Neurosci.

Flik, G., Klaren, P.H.M., Van den Burg, E.H., Metz, J.R., and Huising, M.O. (2006). CRF and stress in

fish. Gen. Comp. Endocrinol. *146*, 36–44.

Franz, I.W., Lohmann, F.W., Koch, G., and Quabbe, H.J. (1983). Aspects of hormonal regulation of lipolysis during exercise: Effects of chronia β-receptor blockade. Int. J. Sports Med. *4*, 14–20.

Funder, J.W. (2005). Mineralocorticoid receptors: Distribution and activation. Heart Fail. Rev. *10*, 15–22.

Funder, J.W. (2017). Aldosterone and mineralocorticoid receptors—physiology and pathophysiology. Int. J. Mol. Sci. *18*.

Gaali, S., Kirschner, A., Cuboni, S., Hartmann, J., Kozany, C., Balsevich, G., Namendorf, C., Fernandez-Vizarra, P., Sippel, C., Zannas, A.S., et al. (2015). Selective inhibitors of the FK506-binding protein 51 by induced fit. Nat. Chem. Biol.

Gans, I., Hartig, E.I., Zhu, S., Tilden, A.R., Hutchins, L.N., Maki, N.J., Graber, J.H., and Coffman, J.A. (2020). Klf9 is a key feedforward regulator of the transcriptomic response to glucocorticoid receptor activity. *10*, 11415.

Gazzerro, E., Gangji, V., and Canalis, E. (1998). Bone morphogenetic proteins induce the expression of noggin, which limits their activity in cultured rat osteoblasts. J. Clin. Invest.

Gilmour, K.M. (2005). Mineralocorticoid Receptors and Hormones: Fishing for Answers. Endocrinology *146*, 44–46.

Giustina, A., and Veldhuis, J.D. (1998). Pathophysiology of the Neuroregulation of Growth Hormone Secretion in Experimental Animals and the Human*. Endocr. Rev.

Goff, A.K., and Henderson, K.M. (1979). Changes in Follicular Fluid and Serum Concentrations of Steroids in PMS Treated Immature Rats following LH Administration. Biol. Reprod. *20*, 1153–1157.

Gomez-Sanchez, E., and Montgomery, S. (2014). Brain mineralocorticoid receptors in cognition and cardiovascular homeostasis. Steroids *91*, 20–31.

Gonzalez-Nunez, V., Gonzalez-Sarmiento, R., and Rodríguez, R.E. (2003). Identification of two proopiomelanocortin genes in zebrafish (Danio rerio). Mol. Brain Res.

Goody, M.F., Sullivan, C., and Kim, C.H. (2014). Studying the immune response to human viral infections using zebrafish. Dev. Comp. Immunol.

Gorissen, M., Manuel, R., Pelgrim, T.N.M., Mes, W., de Wolf, M.J.S., Zethof, J., Flik, G., and van den Bos, R. (2015). Differences in inhibitory avoidance, cortisol and brain gene expression in TL and AB zebrafish. Genes, Brain Behav.

Green, M., and Sambrook, J. (2012). Molecular Cloning: A Laboratory Manual. (New York.: Cold Spring Harbor Laboratory Press,).

Greenwood, A.K., Butler, P.C., White, R.B., DeMarco, U., Pearce, D., and Fernald, R.D. (2003). Multiple Corticosteroid Receptors in a Teleost Fish: Distinct Sequences, Expression Patterns, and Transcriptional Activities. Endocrinology *144*, 4226–4236.

Griffin, A., Parajes, S., Weger, M., Zaucker, A., Taylor, A.E., O'Neil, D.M., Müller, F., and Krone, N. (2016). Ferredoxin 1b (Fdx1b) Is the Essential Mitochondrial Redox Partner for Cortisol Biosynthesis in Zebrafish. Endocrinology *157*, 1122–1134.

Griffiths, B.B., Schoonheim, P.J., Ziv, L., Voelker, L., Baier, H., Gahtan, E., Haller, J., and Anacker, C. (2012). A zebrafish model of glucocorticoid resistance shows serotonergic modulation of the stress response.

Groot, E.P., and Alderdice, D.F. (1985). Fine structure of the external egg membrane of five species of Pacific salmon and steelhead trout. Can. J. Zool. *63*, 552–566.

Halls, M.L., Bathgate, R.A.D., and Summers, R.J. (2007). Comparison of signaling pathways activated by the relaxin family peptide receptors, RXFP1 and RXFP2, using reporter genes. J. Pharmacol. Exp. Ther. *320*, 281–290.

Hansen, I.A., To, T.T., Wortmann, S., Burmester, T., Winkler, C., Meyer, S.R., Neuner, C., Fassnacht, M., and Allolio, B. (2003). The pro-opiomelanocortin gene of the zebrafish (Danio rerio). Biochem. Biophys. Res. Commun.

Hayward, T., Young, A., Jiang, A., Crespi, E.J., and Coffin, A.B. (2019). Glucococorticoid receptor activation exacerbates aminoglycoside-induced damage to the zebrafish lateral line. Hear. Res.

He, X.Y., Isaacs, C., and Yang, S.Y. (2018). Roles of Mitochondrial 17β-Hydroxysteroid Dehydrogenase Type 10 in Alzheimer's Disease. J. Alzheimer's Dis. *62*, 665–673.

ter Heegde, F., De Rijk, R.H., and Vinkers, C.H. (2015). The brain mineralocorticoid receptor and stress resilience. Psychoneuroendocrinology *52*, 92–110.

Heim, C., Shugart, M., Craighead, W.E., and Nemeroff, C.B. (2010). Neurobiological and psychiatric consequences of child abuse and neglect. Dev. Psychobiol.

Heuser, I., Deuschle, M., Weber, A., Kniest, A., Ziegler, C., Weber, B., and Colla, M. (2000). The role of mineralocorticoid receptors in the circadian activity of the human hypothalamus–pituitary–adrenal system: Effect of age. Neurobiol. Aging *21*, 585–589.

Holsboer, F. (2000). The corticosteroid receptor hypothesis of depression. Neuropsychopharmacology *23*, 477–501.

Houtepen, L.C., Schür, R.R., Wijnen, J.P., Boer, V.O., Boks, M.P.M., Kahn, R.S., Joëls, M., Klomp, D.W., and Vinkers, C.H. (2017). Acute stress effects on GABA and glutamate levels in the prefrontal cortex: A 7T 1H magnetic resonance spectroscopy study. NeuroImage Clin.

Hunter, R.G., Seligsohn, M., Rubin, T.G., Griffiths, B.B., Ozdemir, Y., Pfaff, D.W., Datson, N.A., and McEwen, B.S. (2016). Stress and corticosteroids regulate rat hippocampal mitochondrial DNA gene expression via the glucocorticoid receptor. Proc. Natl. Acad. Sci. U. S. A. *113*, 9099–9104.

Huttenlocher, A., and Horwitz, A.R. (2011). Integrins in cell migration. Cold Spring Harb. Perspect. Biol.

Hwang, W.Y., Fu, Y., Reyon, D., Maeder, M.L., Tsai, S.Q., Sander, J.D., Peterson, R.T., Yeh, J.R., and

Joung, J.K. (2013). Efficient genome editing in zebrafish using a CRISPR-Cas system. Nat Biotechnol *31*, 227–229.

Imai, E., Stromstedt, P.E., Quinn, P.G., Carlstedt-Duke, J., Gustafsson, J.A., and Granner, D.K. (1990). Characterization of a complex glucocorticoid response unit in the phosphoenolpyruvate carboxykinase gene. Mol. Cell. Biol. *10*, 4712–4719.

Jiang, J. qiao, Young, G., Kobayashi, T., and Nagahama, Y. (1998). Eel (Anguilla japonica) testis 11β-hydroxylase gene is expressed in interrenal tissue and its product lacks aldosterone synthesizing activity. Mol. Cell. Endocrinol.

John, K., Marino, J.S., Sanchez, E.R., and Hinds, T.D. (2016). The glucocorticoid receptor: Cause of or cure for obesity? Am. J. Physiol. - Endocrinol. Metab.

Jones, M.T., Hillhouse, E.W., and Burden, J.L. (1977). Dynamics and mechanics of corticosteroid feedback at the hypothalamus and anterior pituitary gland. J. Endocrinol.

Kadmiel, M., and Cidlowski, J.A. (2013). Glucocorticoid receptor signaling in health and disease. Trends Pharmacol. Sci. *34*, 518–530.

Kalueff, A. V., Stewart, A.M., and Gerlai, R. (2014). Zebrafish as an emerging model for studying complex brain disorders. Trends Pharmacol. Sci.

Kelly, S.P., and Chasiotis, H. (2011). Glucocorticoid and mineralocorticoid receptors regulate paracellular permeability in a primary cultured gill epithelium. J. Exp. Biol. *214*, 2308–2318.

Kessler, R.C., Davis, C.G., and Kendler, K.S. (1997). Childhood adversity and adult psychiatric disorder in the US National Comorbidity Survey. Psychol. Med.

Kessler, R.C., McLaughlin, K.A., Green, J.G., Gruber, M.J., Sampson, N.A., Zaslavsky, A.M., Aguilar-Gaxiola, S., Alhamzawi, A.O., Alonso, J., Angermeyer, M., et al. (2010). Childhood adversities and adult psychopathology in the WHO world mental health surveys. Br. J. Psychiatry.

Kiilerich, P., Milla, S., Sturm, A., Valotaire, C., Chevolleau, S., Giton, F., Terrien, X., Fiet, J., Fostier, A., Debrauwer, L., et al. (2011). Implication of the mineralocorticoid axis in rainbow trout osmoregulation during salinity acclimation. J. Endocrinol. *209*, 221–235.

Kimoto, T., Ishii, H., Higo, S., Hojo, Y., and Kawato, S. (2010). Semicomprehensive Analysis of the Postnatal Age-Related Changes in the mRNA Expression of Sex Steroidogenic Enzymes and Sex Steroid Receptors in the Male Rat Hippocampus. Endocrinology *151*, 5795–5806.

Kino, T. (2015). Stress, glucocorticoid hormones, and hippocampal neural progenitor cells: Implications to mood disorders. Front. Physiol.

de Kloet, E.R. (2003). Hormones, brain and stress. Endocr. Regul. *37*, 51–68.

de Kloet, E.R., Vreugdenhil, E., Oitzl, M.S., and Joëls, M. (1998). Brain Corticosteroid Receptor Balance in Health and Disease [1]. Endocr. Rev. *19*, 269–301.

Klok, M.D., Alt, S.R., Irurzun Lafitte, A.J.M., Turner, J.D., Lakke, E.A.J.F., Huitinga, I., Muller, C.P., Zitman, F.G., Ronald de Kloet, E., and DeRijk, R.H. (2011). Decreased expression of

mineralocorticoid receptor mRNA and its splice variants in postmortem brain regions of patients with major depressive disorder. J. Psychiatr. Res.

Kolber, B.J., Wieczorek, L., and Muglia, L.J. (2008). Hypothalamic–pituitary–adrenal axis dysregulation and behavioral analysis of mouse mutants with altered glucocorticoid or mineralocorticoid receptor function. Stress *11*, 321–338.

Kononen, J., Honkaniemi, J., Gustafsson, J. å, and Pelto-huikko, M. (1993). Glucocorticoid receptor colocalization with pituitary hormones in the rat pituitary gland. Mol. Cell. Endocrinol.

Kopylova, E., Noé, L., and Touzet, H. (2012). SortMeRNA: Fast and accurate filtering of ribosomal RNAs in metatranscriptomic data. Bioinformatics *28*, 3211–3217.

Kramer, B.M.R., Kolk, S.M., Berghs, C.A.F.M., Tuinhof, R., Ubink, R., Jenks, B.G., and Roubos, E.W. (2001). Dynamics and plasticity of peptidergic control centres in the retino-brain-pituitary system ofXenopus laevis. Microsc. Res. Tech. *54*, 188–199.

Kumai, Y., Nesan, D., Vijayan, M.M., and Perry, S.F. (2012). Cortisol regulates Na+ uptake in zebrafish, Danio rerio, larvae via the glucocorticoid receptor. Mol. Cell. Endocrinol. *364*, 113–125.

Kuo, T., McQueen, A., Chen, T.C., and Wang, J.C. (2015). Regulation of glucose homeostasis by glucocorticoids. Adv. Exp. Med. Biol. *872*, 99–126.

Kwak, S.P., Patel, P.D., Thompson, R.C., Akil, H., and Watson, S.J. (1993). 5'-Heterogeneity of the mineralocorticoid receptor messenger ribonucleic acid: differential expression and regulation of splice variants within the rat hippocampus. Endocrinology *133*, 2344–2350.

Kwan, W., Cortes, M., Frost, I., Esain, V., Theodore, L.N., Liu, S.Y., Budrow, N., Goessling, W., and North, T.E. (2016). The Central Nervous System Regulates Embryonic HSPC Production via Stress-Responsive Glucocorticoid Receptor Signaling. Cell Stem Cell.

Lapp, H.E., Bartlett, A.A., and Hunter, R.G. (2019). Stress and glucocorticoid receptor regulation of mitochondrial gene expression. J. Mol. Endocrinol. *62*, R121–R128.

Lee, H.B., Schwab, T.L., Sigafoos, A.N., Gauerke, J.L., Krug, R.G., Serres, M.K.R., Jacobs, D.C., Cotter, R.P., Das, B., Petersen, M.O., et al. (2019). Novel zebrafish behavioral assay to identify modifiers of the rapid, nongenomic stress response. Genes, Brain Behav.

Lee, M.J., Pramyothin, P., Karastergiou, K., and Fried, S.K. (2014). Deconstructing the roles of glucocorticoids in adipose tissue biology and the development of central obesity. Biochim. Biophys. Acta - Mol. Basis Dis. *1842*, 473–481.

Leitman, D.C., Benson, S.C., and Johnson, L.K. (1984). Glucocorticoids stimulate collagen and noncollagen protein synthesis in cultured vascular smooth muscle cells. J. Cell Biol.

Li, N., Oakes, J.A., Storbeck, K.-H., Cunliffe, V.T., and Krone, N.P. (2020a). The P450 side-chain cleavage enzyme Cyp11a2 facilitates steroidogenesis in zebrafish.

Li, N., Oakes, J.A., Storbeck, K.H., Cunliffe, V.T., and Krone, N.P. (2020b). The P450 side-chain

cleavage enzyme Cyp11a2 facilitates steroidogenesis in zebrafish. J. Endocrinol. *244*, 309–321.

Liebsch, G., Landgraf, R., Gerstberger, R., Probst, J.C., Wotjak, C.T., Engelmann, M., Holsboer, F., and Montkowski, A. (1995). Chronic infusion of a CRH1 receptor antisense oligodeoxynucleotide into the central nucleus of the amygdala reduced anxiety-related behavior in socially defeated rats. Regul. Pept. *59*, 229–239.

Lieschke, G.J., and Currie, P.D. (2007). Animal models of human disease: zebrafish swim into view. Nat. Rev. Genet. *8*, 353–367.

Lin, J.C., Hu, S., Ho, P.H., Hsu, H.J., Postlethwait, J.H., and Chung, B.C. (2015). Two zebrafish hsd3b genes are distinct in function, expression, and evolution. Endocrinology.

Liston, C., and Gan, W.B. (2011). Glucocorticoids are critical regulators of dendritic spine development and plasticity in vivo. Proc. Natl. Acad. Sci. U. S. A.

Löhr, H., and Hammerschmidt, M. (2011a). Zebrafish in endocrine systems: Recent advances and implications for human disease. Annu. Rev. Physiol.

Löhr, H., and Hammerschmidt, M. (2011b). Zebrafish in Endocrine Systems: Recent Advances and Implications for Human Disease. Annu. Rev. Physiol. *73*, 183–211.

Lösel, R., and Wehling, M. (2003). Nongenomic actions of steroid hormones. Nat. Rev. Mol. Cell Biol. *4*, 46–55.

Lösel, R.M., and Wehling, M. (2008). Classic versus non-classic receptors for nongenomic mineralocorticoid responses: Emerging evidence. Front. Neuroendocrinol. *29*, 258–267.

Love, M.I., Huber, W., and Anders, S. (2014a). Moderated estimation of fold change and dispersion for RNA-seq data with DESeq2. Genome Biol. *15*, 550.

Love, M.I., Huber, W., and Anders, S. (2014b). Moderated estimation of fold change and dispersion for RNA-seq data with DESeq2. Genome Biol. *15*.

Lowin, T., Straub, R.H., Neumann, E., Bosserhoff, A., Vogel, C., Moissl, C., Anders, S., Müller-Ladner, U., and Schedel, J. (2009). Glucocorticoids increase α5 integrin expression and adhesion of synovial fibroblasts but inhibit ERK signaling, migration, and cartilage invasion. Arthritis Rheum.

Magariños, A.M., McEwen, B.S., Flügge, G., and Fuchs, E. (1996). Chronic psychosocial stress causes apical dendritic atrophy of hippocampal CA3 pyramidal neurons in subordinate tree shrews. J. Neurosci.

Marchi, D., Santhakumar, K., Markham, E., Li, N., Storbeck, K.H., Krone, N., Cunliffe, V.T., and Van Eeden, F.J.M. (2020). Bidirectional crosstalk between hypoxia-inducible factor and glucocorticoid signalling in zebrafish larvae. PLoS Genet. *16*.

Massagué, J., Seoane, J., and Wotton, D. (2005). Smad transcription factors. Genes Dev. *19*, 2783–2810.

Mayanagi, T., Morita, T., Hayashi, ichiro, Fukumoto, K., and Sobue, K. (2008). Glucocorticoid

Receptor-mediated Expression of Caldesmon Regulates Cell Migration via the Reorganization of the Actin Cytoskeleton.

Mazziotti, G., and Giustina, A. (2013). Glucocorticoids and the regulation of growth hormone secretion. Nat. Rev. Endocrinol.

McCann, K.E., Lustberg, D.J., Shaughnessy, E.K., Carstens, K.E., Farris, S., Alexander, G.M., Radzicki, D., Zhao, M., and Dudek, S.M. (2021). Novel role for mineralocorticoid receptors in control of a neuronal phenotype. Mol. Psychiatry.

McCormick, S.D. (2001). Endocrine Control of Osmoregulation in Teleost Fish. Am. Zool. *41*.

McCormick, S.D., and Bradshaw, D. (2006). Hormonal control of salt and water balance in vertebrates. Gen. Comp. Endocrinol. *147*, 3–8.

McCormick, S.D., Regish, A., O'Dea, M.F., and Shrimpton, J.M. (2008). Are we missing a mineralocorticoid in teleost fish? Effects of cortisol, deoxycorticosterone and aldosterone on osmoregulation, gill Na+,K+-ATPase activity and isoform mRNA levels in Atlantic salmon. Gen. Comp. Endocrinol. *157*, 35–40.

McEwen, B.S. (2012). Brain on stress: How the social environment gets under the skin. Proc. Natl. Acad. Sci. U. S. A. *109*, 17180–17185.

McEwen, B.S., and Wingfield, J.C. (2010). What is in a name? Integrating homeostasis, allostasis and stress. Horm. Behav. *57*, 105–111.

McGonnell, I.M., and Fowkes, R.C. (2006a). Fishing for gene function--endocrine modelling in the zebrafish. J. Endocrinol. *189*, 425–439.

McGonnell, I.M., and Fowkes, R.C. (2006b). Fishing for gene function--endocrine modelling in the zebrafish. J. Endocrinol. *189*, 425–439.

McGowan, P.O., Sasaki, A., D'Alessio, A.C., Dymov, S., Labonté, B., Szyf, M., Turecki, G., and Meaney, M.J. (2009). Epigenetic regulation of the glucocorticoid receptor in human brain associates with childhood abuse. Nat. Neurosci.

Medina, A., Seasholtz, A.F., Sharma, V., Burke, S., Bunney, W., Myers, R.M., Schatzberg, A., Akil, H., and Watson, S.J. (2013). Glucocorticoid and mineralocorticoid receptor expression in the human hippocampus in major depressive disorder. J. Psychiatr. Res.

Meijer, O.C., Buurstede, J.C., and Schaaf, M.J.M. (2019). Corticosteroid Receptors in the Brain: Transcriptional Mechanisms for Specificity and Context-Dependent Effects. Cell. Mol. Neurobiol. *39*, 539–549.

Menke, A. (2019). Is the HPA axis as target for depression outdated, or is there a new hope? Front. Psychiatry *10*.

Miller, W.L. (2013). Steroid hormone synthesis in mitochondria. Mol. Cell. Endocrinol. *379*, 62–73.

Miller, T.L., and Mayo, K.E. (1997). Glucocorticoids Regulate Pituitary Growth Hormone-

Releasing Hormone Receptor Messenger Ribonucleic Acid Expression*. Endocrinology *138*, 2458–2465.

Mindnich, R., Deluca, D., and Adamski, J. (2004). Identification and characterization of 17β-hydroxysteroid dehydrogenases in the zebrafish, Danio rerio. In Molecular and Cellular Endocrinology, p.

Mitra, R., and Sapolsky, R.M. (2008). Acute corticosterone treatment is sufficient to induce anxiety and amygdaloid dendritic hypertrophy. Proc. Natl. Acad. Sci. U. S. A.

Moghadam-Kia, S., and Werth, V.P. (2010). Prevention and treatment of systemic glucocorticoid side effects. Int. J. Dermatol. *49*, 239–248.

Morbiato, E., Frigato, E., Dinarello, A., Maradonna, F., Facchinello, N., Argenton, F., Carnevali, O., Dalla Valle, L., and Bertolucci, C. (2019). Feeding Entrainment of the Zebrafish Circadian Clock Is Regulated by the Glucocorticoid Receptor. Cells.

Morrison, N., Harrap, S.B., Arriza, J.L., Boyd, E., and Connor, J.M. (1990). Regional chromosomal assignment of the human mineralocorticoid receptor gene to 4q31.1. Hum. Genet. *85*, 130–132.

Moustakas, A., Souchelnytskyi, S., and Heldin, C.-H. (2001). Smad regulation in TGF-β signal transduction.

Muto, A., Orger, M.B., Wehman, A.M., Smear, M.C., Kay, J.N., Page-McCaw, P.S., Gahtan, E., Xiao, T., Nevin, L.M., Gosse, N.J., et al. (2005). Forward Genetic Analysis of Visual Behavior in Zebrafish. PLoS Genet. *1*, e66.

Muto, A., Taylor, M.R., Suzawa, M., Korenbrot, J.I., and Baier, H. (2013). Glucocorticoid receptor activity regulates light adaptation in the zebrafish retina. Front. Neural Circuits.

Nelson, D.W., Gao, Y., Spencer, N.M., Banh, T., and Yen, C.L.E. (2011). Deficiency of MGAT2 increases energy expenditure without high-fat feeding and protects genetically obese mice from excessive weight gain. J. Lipid Res. *52*, 1723–1732.

Nelson, G., Wilde, G.J.C., Spiller, D.G., Kennedy, S.M., Ray, D.W., Sullivan, E., Unitt, J.F., and White, M.R.H. (2003). NF-κB signalling is inhibited by glucocorticoid receptor and STAT6 via distinct mechanisms. J. Cell Sci. *116*, 2495–2503.

Nematollahi, M.A., van Pelt-Heerschap, H., Atsma, W., and Komen, J. (2012). High levels of corticosterone, and gene expression of star, cyp17a2, hsd3b, cyp21, hsd11b2 during acute stress in common carp with interrenal hyperplasia. Gen. Comp. Endocrinol. *176*, 252–258.

Nesan, D., Kamkar, M., Burrows, J., Scott, I.C., Marsden, M., and Vijayan, M.M. (2012). Glucocorticoid Receptor Signaling Is Essential for Mesoderm Formation and Muscle Development in Zebrafish. Endocrinology *153*, 1288–1300.

Nistor, M., Schmidt, M., and Schiffner, R. (2018). The relaxin peptide family-potential future hope for neuroprotective therapy? A short review. Neural Regen. Res. *13*, 402–405.

Oakes, J.A., Li, N., Wistow, B.R.C., Griffin, A., Barnard, L., Storbeck, K.-H., Cunliffe, V.T., and Krone,

N.P. (2019). Ferredoxin 1b Deficiency Leads to Testis Disorganization, Impaired Spermatogenesis, and Feminization in Zebrafish. Endocrinology *160*, 2401–2416.

Oakes, J.A., Barnard, L., Storbeck, K.-H., Cunliffe, V.T., and Krone, N.P. (2020a). 11β-Hydroxylase loss disrupts steroidogenesis and reproductive function in zebrafish. J. Endocrinol. *247*, 197–212.

Oakes, J.A., Barnard, L., Storbeck, K.-H., Cunliffe, V.T., and Krone, N.P. (2020b). 11β-Hydroxylase loss disrupts steroidogenesis and reproductive function in zebrafish. J. Endocrinol. *247*, 197–212.

Oakley, R.H., and Cidlowski, J.A. (2013). The biology of the glucocorticoid receptor: New signaling mechanisms in health and disease. J. Allergy Clin. Immunol. *132*, 1033–1044.

Ohr, H., and Hammerschmidt, M. (2011). PH73CH09-Hammerschmidt Zebrafish in Endocrine Systems: Recent Advances and Implications for Human Disease Introduction: the zebrafish model. Annu. Rev. Physiol *73*, 183–211.

Oikarinen, A., Haapasaari, K.M., Sutinen, M., and Tasanen, K. (1998). The molecular basis of glucocorticoid-induced skin atrophy: Topical glucocorticoid apparently decreases both collagen synthesis and the corresponding collagen mrna level in human skin in vivo. Br. J. Dermatol. *139*, 1106–1110.

Oishi, Y., Fu, Z.W., Ohnuki, Y., Kato, H., and Noguchi, T. (2002). Molecular basis of the alteration in skin collagen metabolism in response to in vivo dexamethasone treatment: Effects on the synthesis of collagen type I and III, collagenase, and tissue inhibitors of metalloproteinases. Br. J. Dermatol. *147*, 859–868.

Oliver, N., Newby, R.F., Furcht, L.T., and Bourgeois, S. (1983). Regulation of fibronectin biosynthesis by glucocorticoids in human fibrosarcoma cells and normal fibroblasts. Cell.

Ota, S., and Kawahara, A. (2014). Zebrafish: A model vertebrate suitable for the analysis of human genetic disorders. Congenit. Anom. (Kyoto).

Otte, C., Jahn, H., Yassouridis, A., Arlt, J., Stober, N., Maass, P., Wiedemann, K., and Kellner, M. (2003). The mineralocorticoid receptor agonist, fludrocortisone, inhibits pituitary-adrenal activity in humans after pre-treatment with metyrapone. Life Sci. *73*, 1835–1845.

Otte, C., Jahn, H., Kiefer, F., Yassouridis, A., Maass, P., Stober, N., Wiedemann, K., and Kellner, M. (2004). Mineralocorticoid receptor-mediated inhibition of the hypothalamic-pituitary-adrenal axis in aged humans. Exp. Clin. Endocrinol. Diabetes *112*, P20.

Oyarbide, U., Rainieri, S., and Pardo, M.A. (2012). Zebrafish (Danio rerio) larvae as a system to test the efficacy of polysaccharides as immunostimulants. Zebrafish *9*, 74–84.

Pallan, P.S., Nagy, L.D., Lei, L., Gonzalez, E., Kramlinger, V.M., Azumaya, C.M., Wawrzak, Z., Waterman, M.R., Guengerich, F.P., and Egli, M. (2014). Structural and Kinetic Basis of Steroid 17,20-Lyase Activity in Teleost Fish Cytochrome P450 17A1 and Its Absence in Cytochrome

P450 17A2.

Pallan, P.S., Nagy, L.D., Lei, L., Gonzalez, E., Kramlinger, V.M., Azumaya, C.M., Wawrzak, Z., Waterman, M.R., Guengerich, F.P., and Egli, M. (2015). Structural and kinetic basis of steroid 17α,20-lyase activity in teleost fish cytochrome P450 17A1 and its absence in cytochrome P450 17A2. J. Biol. Chem. *290*, 3248–3268.

Palstra, A.P., Mendez, S., Dirks, R.P., and Schaaf, M.J.M. (2019). Cortisol acting through the glucocorticoid receptor is not involved in exercise-enhanced growth, but does affect the white skeletal muscle transcriptome in zebrafish (danio rerio). Front. Physiol.

Pannasch, U., Färber, K., Nolte, C., Blonski, M., Yan Chiu, S., Messing, A., and Kettenmann, H. (2006). The potassium channels Kv1.5 and Kv1.3 modulate distinct functions of microglia. Mol. Cell. Neurosci.

Parajes, S., Griffin, A., Taylor, A.E., Rose, I.T., Miguel-Escalada, I., Hadzhiev, Y., Arlt, W., Shackleton, C., Müller, F., and Krone, N. (2013). Redefining the Initiation and Maintenance of Zebrafish Interrenal Steroidogenesis by Characterizing the Key Enzyme Cyp11a2. Endocrinology *154*, 2702–2711.

Parichy, D.M., Elizondo, M.R., Mills, M.G., Gordon, T.N., and Engeszer, R.E. (2009). Normal table of postembryonic zebrafish development: Staging by externally visible anatomy of the living fish. Dev. Dyn.

Patel, A., Malik, M., Britten, J., Cox, J., and Catherino, W.H. (2016). Mifepristone inhibits extracellular matrix formation in uterine leiomyoma. Fertil. Steril. *105*, 1102–1110.

Pavlidis, M., Theodoridi, A., and Tsalafouta, A. (2015). Neuroendocrine regulation of the stress response in adult zebrafish, Danio rerio. Prog. Neuro-Psychopharmacology Biol. Psychiatry *60*, 121–131.

Pearce, D., Bhargava, A., and Cole, T.J. (2003). Aldosterone: its receptor, target genes, and actions. Vitam. Horm. *66*, 29–76.

Perry, S.F., Goss, G.G., and Laurent, P. (1992). The interrelationships between gill chloride cell morphology and ionic uptake in four freshwater teleosts. Can. J. Zool. *70*, 1775–1786.

Philip, A.M., and Vijayan, M.M. (2015). Stress-immune-growth interactions: Cortisol modulates suppressors of cytokine signaling and JAK/STAT pathway in rainbow trout liver. PLoS One *10*.

Picard, M., Prather, A.A., Puterman, E., Cuillerier, A., Coccia, M., Aschbacher, K., Burelle, Y., and Epel, E.S. (2018). A Mitochondrial Health Index Sensitive to Mood and Caregiving Stress. Biol. Psychiatry *84*, 9–17.

Pickrell, A.M., and Youle, R.J. (2015). The roles of PINK1, Parkin, and mitochondrial fidelity in parkinson's disease. Neuron *85*, 257–273.

Pikulkaew, S., De Nadai, A., Belvedere, P., Colombo, L., and Dalla Valle, L. (2010). Expression analysis of steroid hormone receptor mRNAs during zebrafish embryogenesis. Gen. Comp.

Endocrinol. *165*, 215–220.

Pikulkaew, S., Benato, F., Celeghin, A., Zucal, C., Skobo, T., Colombo, L., and Dalla Valle, L. (2011). The knockdown of maternal glucocorticoid receptor mRNA alters embryo development in zebrafish. Dev. Dyn. *240*, 874–889.

Pilgram, G.S.K., Potikanond, S., Baines, R.A., Fradkin, L.G., and Noordermeer, J.N. (2010). The roles of the dystrophin-associated glycoprotein complex at the synapse. Mol. Neurobiol.

Pinto-Ribeiro, F., Moreira, V., Pêgo, J.M., Leão, P., Almeida, A., and Sousa, N. (2009). Antinociception induced by chronic glucocorticoid treatment is correlated to local modulation of spinal neurotransmitter content. Mol. Pain *5*, 41.

Pippal, J.B., and Fuller, P.J. (2008). Structure-function relationships in the mineralocorticoid receptor. J. Mol. Endocrinol. *41*, 405–413.

Pippal, J.B., Yao, Y., Rogerson, F.M., and Fuller, P.J. (2009). Structural and Functional Characterization of the Interdomain Interaction in the Mineralocorticoid Receptor. Mol. Endocrinol. *23*, 1360–1370.

Pippal, J.B., Cheung, C.M.I., Yao, Y.-Z., Brennan, F.E., and Fuller, P.J. (2011). Characterization of the zebrafish (Danio rerio) mineralocorticoid receptor. Mol. Cell. Endocrinol. *332*, 58–66.

Popoli, M., Yan, Z., McEwen, B.S., and Sanacora, G. (2012). The stressed synapse: The impact of stress and glucocorticoids on glutamate transmission. Nat. Rev. Neurosci.

Porter, T.E., and Dean, K.J. (2001). Regulation of chicken embryonic growth hormone secretion by corticosterone and triiodothyronine: Evidence for a negative synergistic response. Endocrine.

Prager, E.M., Brielmaier, J., Bergstrom, H.C., McGuire, J., and Johnson, L.R. (2010). Localization of mineralocorticoid receptors at mammalian synapses. PLoS One.

Di Prinzio, C.M., Botta, P.E., Barriga, E.H., Ríos, E.A., Reyes, A.E., and Arranz, S.E. (2010). Growth hormone receptors in zebrafish (Danio rerio): Adult and embryonic expression patterns. Gene Expr. Patterns *10*, 214–225.

Prough, R.A., Clark, B.J., and Klinge, C.M. (2016). Novel mechanisms for DHEA action. J. Mol. Endocrinol. *56*, R139–R155.

Psarra, A.M.G., and Sekeris, C.E. (2011). Glucocorticoids induce mitochondrial gene transcription in HepG2 cells. Role of the mitochondrial glucocorticoid receptor. Biochim. Biophys. Acta - Mol. Cell Res. *1813*, 1814–1821.

Quinn, P.M.J., Moreira, P.I., Ambrósio, A.F., and Alves, C.H. (2020). PINK1/PARKIN signalling in neurodegeneration and neuroinflammation. Acta Neuropathol. Commun. *8*, 189.

Radley, J.J., Rocher, A.B., Miller, M., Janssen, W.G.M., Liston, C., Hof, P.R., McEwen, B.S., and Morrison, J.H. (2006). Repeated stress induces dendritic spine loss in the rat medial prefrontal cortex. Cereb. Cortex.

Rajakumar, A., and Senthilkumaran, B. (2020). Steroidogenesis and its regulation in teleost-a review. Fish Physiol. Biochem.

Raubenheimer, P.J., Young, E.A., Andrew, R., and Seckl, J.R. (2006). The role of corticosterone in human hypothalamic- pituitary-adrenal axis feedback. Clin. Endocrinol. (Oxf). *65*, 22–26.

Reddish, M.J., and Guengerich, F.P. (2019). Human cytochrome P450 11B2 produces aldosterone by a processive mechanism due to the lactol form of the intermediate 18-hydroxycorticosterone. J. Biol. Chem.

Reul, J.M.H.M., and De Kloet, E.R. (1985). Two receptor systems for corticosterone in rat brain: Microdistribution and differential occupation. Endocrinology *117*, 2505–2511.

Riccardi, C. (2015). GILZ as a mediator of the anti-inflammatory effects of glucocorticoids. Front. Endocrinol. (Lausanne). *6*.

Rogerson, F.M., and Fuller, P.J. (2000). Mineralocorticoid action. Steroids *65*, 61–73.

Rogerson, F.M., and Fuller, P.J. (2003). Interdomain interactions in the mineralocorticoid receptor. Mol. Cell. Endocrinol. *200*, 45–55.

Rogerson, F.M., Brennan, F.E., and Fuller, P.J. (2004). Mineralocorticoid receptor binding, structure and function. In Molecular and Cellular Endocrinology, (Elsevier), pp. 203–212.

Rose, A.J., Vegiopoulos, A., and Herzig, S. (2010). Role of glucocorticoids and the glucocorticoid receptor in metabolism: Insights from genetic manipulations. J. Steroid Biochem. Mol. Biol.

Rozeboom, A.M., Akil, H., and Seasholtz, A.F. (2007). Mineralocorticoid receptor overexpression in forebrain decreases anxiety-like behavior and alters the stress response in mice. Proc. Natl. Acad. Sci. U. S. A. *104*, 4688–4693.

Sakamoto, T., Yoshiki, M., Takahashi, H., Yoshida, M., Ogino, Y., Ikeuchi, T., Nakamachi, T., Konno, N., Matsuda, K., Sakamoto, H., et al. (2016). Principal function of mineralocorticoid signaling suggested by constitutive knockout of the mineralocorticoid receptor in medaka fish. Sci. Rep. *6*, 37991.

Sander, J.D., and Joung, J.K. (2014). CRISPR-Cas systems for editing, regulating and targeting genomes. Nat. Biotechnol. *32*, 347–355.

Sans, N., Prybylowski, K., Petralia, R.S., Chang, K., Wang, Y.X., Racca, C., Vicini, S., and Wenthold, R.J. (2003). NMDA receptor trafficking through an interaction between PDZ proteins and the exocyst complex. Nat. Cell Biol.

Sargis, R.M., Johnson, D.N., Choudhury, R.A., and Brady, M.J. (2010). Environmental endocrine disruptors promote adipogenesis in the 3T3-L1 cell line through glucocorticoid receptor activation. Obesity.

Sawamoto, A., Okuyama, S., Yamamoto, K., Amakura, Y., Yoshimura, M., Nakajima, M., and Furukawa, Y. (2016). 3,5,6,7,8,31,41 -Heptamethoxyflavone, a citrus flavonoid, Ameliorates corticosterone-induced depression-like behavior and restores brain-derived neurotrophic

factor expression, neurogenesis, and neuroplasticity in the hippocampus. Molecules *21*.

Schaaf, M.J.M., Champagne, D., Van Laanen, I.H.C., Van Wijk, D.C.W.A., Meijer, A.H., Meijer, O.C., Spaink, H.P., and Richardson, M.K. (2008). Discovery of a functional glucocorticoid receptor β-isoform in zebrafish. Endocrinology *149*, 1591–1598.

Schaaf, M.J.M., Chatzopoulou, A., and Spaink, H.P. (2009a). The zebrafish as a model system for glucocorticoid receptor research. Comp. Biochem. Physiol. - A Mol. Integr. Physiol.

Schatzberg, A.F. (2015). Anna-Monika Award Lecture, DGPPN kongress, 2013: The role of the hypothalamic-pituitary-adrenal (HPA) axis in the pathogenesis of psychotic major depression. World J. Biol. Psychiatry *16*, 2–11.

Schatzberg, A.F., Keller, J., Tennakoon, L., Lembke, A., Williams, G., Kraemer, F.B., Sarginson, J.E., Lazzeroni, L.C., and Murphy, G.M. (2014). HPA axis genetic variation, cortisol and psychosis in major depression. Mol. Psychiatry *19*, 220–227.

Schmid, W., Cole, T.J., Blendy, J.A., and Schütz, G. (1995). Molecular genetic analysis of glucocorticoid signalling in development. J. Steroid Biochem. Mol. Biol.

Schoonheim, P.J., Chatzopoulou, A., and Schaaf, M.J.M. (2010a). The zebrafish as an in vivo model system for glucocorticoid resistance. Steroids.

Schoonheim, P.J., Chatzopoulou, A., and Schaaf, M.J.M. (2010b). The zebrafish as an in vivo model system for glucocorticoid resistance. Steroids *75*, 918–925.

Scobie, K.N., Hall, B.J., Wilke, S.A., Klemenhagen, K.C., Fujii-Kuriyama, Y., Ghosh, A., Hen, R., and Sahay, A. (2009). Krüppel-like factor 9 is necessary for late-phase neuronal maturation in the developing dentate gyrus and during adult hippocampal neurogenesis. J. Neurosci.

Sekeris, C.E. (1990). The mitochondrial genome: A possible primary site of actin of steroid hormones. In Vivo (Brooklyn). *4*, 317–320.

Semenov, M. V., Habas, R., MacDonald, B.T., and He, X. (2007). SnapShot: Noncanonical Wnt Signaling Pathways. Cell *131*, 1378.e1-1378.e2.

Sharpe, L.J., and Brown, A.J. (2013). Controlling cholesterol synthesis beyond 3-hydroxy-3-methylglutaryl-CoA reductase (HMGCR). J. Biol. Chem. *288*, 18707–18715.

Shen, W.-J., Azhar, S., and Kraemer, F.B. (2018). SR-B1: A Unique Multifunctional Receptor for Cholesterol Influx and Efflux. Annu. Rev. Physiol. *80*, 95–116.

Shewade, L.H., Schneider, K.A., Brown, A.C., and Buchholz, D.R. (2017). In-vivo regulation of Krüppel-like factor 9 by corticosteroids and their receptors across tissues in tadpoles of Xenopus tropicalis. Gen. Comp. Endocrinol.

Shi, C., Lu, Y., Zhai, G., Huang, J., Shang, G., Lou, Q., Li, D., Jin, X., He, J., Du, Z., et al. (2020). Hyperandrogenism in POMCa-deficient zebrafish enhances somatic growth without increasing adiposity. J. Mol. Cell Biol.

Shin, J.T., and Fishman, M.C. (2002). From zebrafish to human: Modular medical models. Annu.

Rev. Genomics Hum. Genet.

Sireeni, J., Bakker, N., Jaikumar, G., Obdam, D., Slabbekoorn, H., Tudorache, C., and Schaaf, M. (2020). Profound effects of glucocorticoid resistance on anxiety-related behavior in zebrafish adults but not in larvae. Gen. Comp. Endocrinol. *292*, 113461.

Skoglund, P., and Keller, R. (2010). Integration of planar cell polarity and ECM signaling in elongation of the vertebrate body plan. Curr. Opin. Cell Biol.

Smith, S.J., Cases, S., Jensen, D.R., Chen, H.C., Sande, E., Tow, B., Sanan, D.A., Raber, J., Eckel, R.H., and Farese, R. V. (2000). Obesity resistance and multiple mechanisms of triglyceride synthesis in mice lacking Dgat. Nat. Genet.

Son, G.H., Geum, D., Jung, H., and Kim, K. (2001). Glucocorticoid inhibits growth factor-induced differentiation of hippocampal progenitor HiB5 cells. J. Neurochem. *79*, 1013–1021.

Spiga, F., Walker, J.J., Terry, J.R., and Lightman, S.L. (2014). HPA axis-rhythms. Compr. Physiol.

Spirovski, M.Z., Kovacev, V.P., Spasovska, M., and Chernick, S.S. (1975). Effect of ACTH on lipolysis in adipose tissue of normal and adrenalectomized rats in vivo. Am. J. Physiol. *228*, 382–385.

Spörl, F., Korge, S., Jürchott, K., Wunderskirchner, M., Schellenberg, K., Heins, S., Specht, A., Stoll, C., Klemz, R., Maier, B., et al. (2012). Krüppel-like factor 9 is a circadian transcription factor in human epidermis that controls proliferation of keratinocytes. Proc. Natl. Acad. Sci. U. S. A.

Spulber, S., Raciti, M., Dulko-Smith, B., Lupu, D., Rüegg, J., Nam, K., and Ceccatelli, S. (2018). Methylmercury interferes with glucocorticoid receptor: Potential role in the mediation of developmental neurotoxicity. Toxicol. Appl. Pharmacol.

Steenbergen, P.J., Richardson, M.K., and Champagne, D.L. (2011). The use of the zebrafish model in stress research. Prog. Neuro-Psychopharmacology Biol. Psychiatry *35*, 1432–1451.

Stocco, D.M. (2001). StAR protein and the regulation of steroid hormone biosynthesis. Annu. Rev. Physiol. *63*, 193–213.

Stolte, E.H., van Kemenade, B.M.L.V., Savelkoul, H.F.J., and Flik, G. (2006). Evolution of glucocorticoid receptors with different glucocorticoid sensitivity. J. Endocrinol. *190*, 17–28.

Stolte, E.H., de Mazon, A.F., Leon-Koosterziel, K.M., Jesiak, M., Bury, N.R., Sturm, A., Savelkoul, H.F.J., van Kemenade, B.M.L. V., and Flik, G. (2008). Corticosteroid receptors involved in stress regulation in common carp, Cyprinus carpio. J. Endocrinol. *198*, 403–417.

Stone, S.J., Myers, H.M., Watkins, S.M., Brown, B.E., Feingold, K.R., Elias, P.M., and Farese, R. V. (2004). Lipopenia and Skin Barrier Abnormalities in DGAT2-deficient Mice. J. Biol. Chem.

Sturm, A., Bury, N., Dengreville, L., Fagart, J., Flouriot, G., Rafestin-Oblin, M.E., and Prunet, P. (2005). 11-Deoxycorticosterone Is a Potent Agonist of the Rainbow Trout (*Oncorhynchus mykiss*) Mineralocorticoid Receptor. Endocrinology *146*, 47–55.

Südhof, T.C. (2018). Towards an Understanding of Synapse Formation. Neuron.

Swiergiel, A.H., Takahashi, L.K., and Kalin, N.H. (1993). Attenuation of stress-induced behavior by antagonism of corticotropin-releasing factor receptors in the central amygdala in the rat.

Takahashi, H., and Sakamoto, T. (2013). The role of 'mineralocorticoids' in teleost fish: Relative importance of glucocorticoid signaling in the osmoregulation and 'central' actions of mineralocorticoid receptor. Gen. Comp. Endocrinol. *181*, 223–228.

Tan, E.M.L., Qin, H., Kennedy, S.H., Rouda, S., Fox IV, J.W., and Moore, J.H. (1995). Platelet-derived growth factors-AA and -BB regulate collagen and collagenase gene expression differentially in human fibroblasts. Biochem. J. *310*, 585–588.

Taylor, J.S., Van de Peer, Y., Braasch, I., and Meyer, A. (2001). Comparative genomics provides evidence for an ancient genome duplication event in fish. Philos. Trans. R. Soc. B Biol. Sci.

Tecalco-Cruz, A.C., Ríos-López, D.G., Vázquez-Victorio, G., Rosales-Alvarez, R.E., and Macías-Silva, M. (2018). Transcriptional cofactors Ski and SnoN are major regulators of the TGF-β/Smad signaling pathway in health and disease. Signal Transduct. Target. Ther. *3*.

Thakore, J.H., and Dinan, T.G. (1994). Growth hormone secretion: The role of glucocorticoids. Life Sci. *55*, 1083–1099.

Thompson, J.D., Higgins, D.G., and Gibson, T.J. (1994). CLUSTAL W: Improving the sensitivity of progressive multiple sequence alignment through sequence weighting, position-specific gap penalties and weight matrix choice. Nucleic Acids Res. *22*, 4673–4680.

Timmermans, S., Souffriau, J., and Libert, C. (2019). A general introduction to glucocorticoid biology. Front. Immunol. *10*, 1545.

Tokarz, J., Möller, G., Hrabě De Angelis, M., and Adamski, J. (2013a). Zebrafish and steroids: What do we know and what do we need to know? J. Steroid Biochem. Mol. Biol. *137*, 165–173.

Tokarz, J., Norton, W., Möller, G., Hrabé de Angelis, M., and Adamski, J. (2013b). Zebrafish 20β-Hydroxysteroid Dehydrogenase Type 2 Is Important for Glucocorticoid Catabolism in Stress Response. PLoS One *8*, e54851.

Tokarz, J., Möller, G., Hrabě De Angelis, M., and Adamski, J. (2015). Steroids in teleost fishes: A functional point of view. Steroids *103*, 123–144.

Tronche, F., Kellendonk, C., Kretz, O., Gass, P., Anlag, K., Orban, P.C., Bock, R., Klein, R., and Schütz, G. (1999). Disruption of the glucocorticoid receptor gene in the nervous system results in reduced anxiety. Nat. Genet.

Turcu, A.F., and Auchus, R.J. (2017). Clinical significance of 11-oxygenated androgens. Curr. Opin. Endocrinol. Diabetes Obes. *24*, 252–259.

U, M., Shen, L., Oshida, T., Miyauchi, J., Yamada, M., and Miyashita, T. (2004). Identification of novel direct transcriptional targets of glucocorticoid receptor. Leukemia *18*, 1850–1856.

Ulrich-Lai, Y.M., and Herman, J.P. (2009). Neural regulation of endocrine and autonomic stress responses. Nat. Rev. Neurosci.

Usher, M.G., Duan, S.Z., Ivaschenko, C.Y., Frieler, R.A., Berger, S., Schütz, G., Lumeng, C.N., and Mortensen, R.M. (2010). Myeloid mineralocorticoid receptor controls macrophage polarization and cardiovascular hypertrophy and remodeling in mice. J. Clin. Invest. *120*, 3350–3364.

Vakili, H., Jin, Y., Nagy, J.I., and Cattini, P.A. (2011). Transgenic mice expressing the human growth hormone gene provide a model system to study human growth hormone synthesis and secretion in non-tumor-derived pituitary cells: Differential effects of dexamethasone and thyroid hormone. Mol. Cell. Endocrinol.

Vegiopoulos, A., and Herzig, S. (2007). Glucocorticoids, metabolism and metabolic diseases. Mol. Cell. Endocrinol. *275*, 43–61.

Veillette, P.A., Sundell, K., and Specker, J.L. (1995). Cortisol Mediates the Increase in Intestinal Fluid Absorption in Atlantic Salmon during Parr-Smolt Transformation. Gen. Comp. Endocrinol. *97*, 250–258.

Vicente-Manzanares, M., Choi, C.K., and Horwitz, A.R. (2009). Integrins in cell migration - The actin connection. J. Cell Sci.

Viengchareun, S., Le Menuet, D., Martinerie, L., Munier, M., Pascual-Le Tallec, L., and Lombès, M. (2007). The mineralocorticoid receptor: insights into its molecular and (patho)physiological biology. Nucl. Recept. Signal. *5*, e012.

Viho, E.M.G., Buurstede, J.C., Mahfouz, A., Koorneef, L.L., van Weert, L.T.C.M., Houtman, R., Hunt, H.J., Kroon, J., and Meijer, O.C. (2019). Corticosteroid Action in the Brain: The Potential of Selective Receptor Modulation. Neuroendocrinology.

Vreugdenhil, E., and Berezikov, E. (2010). Fine-tuning the brain: MicroRNAs. Front. Neuroendocrinol.

de Waal, P.P., Wang, D.S., Nijenhuis, W.A., Schulz, R.W., and Bogerd, J. (2008). Functional characterization and expression analysis of the androgen receptor in zebrafish (Danio rerio) testis. Reproduction.

Wagle, M., Mathur, P., and Guo, S. (2011). Corticotropin-releasing factor critical for zebrafish camouflage behavior is regulated by light and sensitive to ethanol. J. Neurosci.

Wang, L., Liang, Y., Lin, R., Xiong, Q., Yu, P., Ma, J., Cheng, M., Han, H., Wang, X., Wang, G., et al. (2020). Mettl5 mediated 18S rRNA N6-methyladenosine (m6A) modification controls stem cell fate determination and neural function. Genes Dis.

Weaver, I.C.G., Meaney, M.J., and Szyf, M. (2006). Maternal care effects on the hippocampal transcriptome and anxiety-mediated behaviors in the offspring that are reversible in adulthood. Proc. Natl. Acad. Sci. U. S. A.

Weger, M., Diotel, N., Weger, B.D., Beil, T., Zaucker, A., Eachus, H.L., Oakes, J.A., do Rego, J.L., Storbeck, K.H., Gut, P., et al. (2018). Expression and activity profiling of the steroidogenic enzymes of glucocorticoid biosynthesis and the fdx1 co-factors in zebrafish. J. Neuroendocrinol.

Wehling, M., Käsmayr, J., and Theisen, K. (1991). Rapid effects of mineralocorticoids on sodium-proton exchanger: genomic or nongenomic pathway? Am. J. Physiol. *260*, E719-26.

Weiner, I.D. (2016). Untangling the complex relationship between dietary acid load and glucocorticoid metabolism. Kidney Int.

Weiss, A., and Attisano, L. (2013). The TGFbeta superfamily signaling pathway. Wiley Interdiscip. Rev. Dev. Biol.

Wellman, C.L. (2001). Dendritic reorganization in pyramidal neurons in medial prefrontal cortex after chronic corticosterone administration. J. Neurobiol.

Wendelaar Bonga, S.E. (1997a). The stress response in fish. Physiol. Rev. *77*, 591–625.

Westerfield, M. (2000). The Zebrafish Book: A Guide for the Laboratory Use of Zebrafish (Danio Rerio) (University of Oregon Press).

Wilson, K.S., Matrone, G., Livingstone, D.E.W., Al-Dujaili, E.A.S., Mullins, J.J., Tucker, C.S., Hadoke, P.W.F., Kenyon, C.J., and Denvir, M.A. (2013). Physiological roles of glucocorticoids during early embryonic development of the zebrafish (*Danio rerio)*. J. Physiol. *591*, 6209–6220.

Winklhofer, K.F., and Haass, C. (2010). Mitochondrial dysfunction in Parkinson's disease. Biochim. Biophys. Acta - Mol. Basis Dis. *1802*, 29–44.

Wu, H., Xiong, W.C., and Mei, L. (2010). To build a synapse: Signaling pathways in neuromuscular junction assembly. Development.

Xing, G.Q., Russell, S., Webster, M.J., and Post, R.M. (2004). Decreased expression of mineralocorticoid receptor mRNA in the prefrontal cortex in schizophrenia and bipolar disorder. Int. J. Neuropsychopharmacol.

Xing, Y., Cohen, A., Rothblat, G., Sankaranarayanan, S., Weibel, G., Royer, L., Francone, O.L., and Rainey, W.E. (2011). Aldosterone Production in Human Adrenocortical Cells Is Stimulated by High-Density Lipoprotein 2 (HDL2) through Increased Expression of Aldosterone Synthase (CYP11B2).

Yang, N., Li, Y.C., Xiong, T.Q., Chen, L.M., Zhai, Y., Liang, J.M., Hao, Y.P., Ma, D.H., and Zhang, Y.F. (2019). Dexamethasone ameliorates the damage of hippocampal filamentous actin cytoskeleton but is not sufficient to cease epileptogenesis in pilocarpine induced epileptic mice. Epilepsy Res. *154*, 26–33.

Yang, N., Zhang, Y., Wang, J.T., Chen, C., Song, Y., Liang, J.M., Ma, D.H., and Zhang, Y.F. (2020). Effects of dexamethasone on remodeling of the hippocampal synaptic filamentous actin cytoskeleton in a model of pilocarpine-induced status epilepticus. Int. J. Med. Sci. *17*, 1683–1691.

Yates, A.D., Achuthan, P., Akanni, W., Allen, J., Allen, J., Alvarez-Jarreta, J., Amode, M.R., Armean, I.M., Azov, A.G., Bennett, R., et al. (2020). Ensembl 2020. Nucleic Acids Res. *48*, D682–D688.

Young, E.A., Lopez, J.F., Murphy-Weinberg, V., Watson, S.J., and Akil, H. (1998). The Role of

Mineralocorticoid Receptors in Hypothalamic-Pituitary-Adrenal Axis Regulation in Humans*.

Yuen, E.Y., Liu, W., Karatsoreos, I.N., Feng, J., McEwen, B.S., and Yan, Z. (2009). Acute stress enhances glutamatergic transmission in prefrontal cortex and facilitates working memory. Proc. Natl. Acad. Sci. U. S. A.

Zhai, G., Shu, T., Xia, Y., Jin, X., He, J., and Yin, Z. (2017). Androgen signaling regulates the transcription of anti-Müllerian hormone via synergy with SRY-related protein SOX9A. Sci. Bull. *62*, 197–203.

Zhai, G., Shu, T., Xia, Y., Lu, Y., Shang, G., Jin, X., He, J., Nie, P., and Yin, Z. (2018). Characterization of Sexual Trait Development in cyp17a1-Deficient Zebrafish. Endocrinology *159*, 3549–3562.

Zhang, Q., Ye, D., Wang, H., Wang, Y., Hu, W., and Sun, Y. (2020). Zebrafish cyp11c1 Knockout Reveals the Roles of 11-ketotestosterone and Cortisol in Sexual Development and Reproduction. Endocrinology.

Zhang, X., Saarinen, A.M., Campbell, L.E., De Filippis, E.A., and Liu, J. (2018). Regulation of lipolytic response and energy balance by melanocortin 2 receptor accessory protein (MRAP) in adipocytes. In Diabetes, (American Diabetes Association Inc.), pp. 222–234.

Zheng, Q., Xiao, H., Shi, H., Wang, T., Sun, L., Tao, W., Kocher, T.D., Li, M., and Wang, D. (2020). Loss of Cyp11c1 causes delayed spermatogenesis due to the absence of 11-ketotestosterone. J. Endocrinol.

Zhou, H., Mak, W., Kalak, R., Street, J., Fong-Yee, C., Zheng, Y., Dunstan, C.R., and Seibel, M.J. (2009). Glucocorticoid-dependent Wnt signaling by mature osteoblasts is a key regulator of cranial skeletal development in mice. Development *136*, 427–436.

Zhou, H., Sivasankar, M., Kraus, D.H., Sandulache, V.C., Amin, M., and Branski, R.C. (2011). Glucocorticoids regulate extracellular matrix metabolism in human vocal fold fibroblasts. Laryngoscope *121*, 1915–1919.

Zhou, H., Mehta, S., Srivastava, S.P., Grabinska, K., Zhang, X., Wong, C., Hedayat, A., Perrotta, P., Fernández-Hernando, C., Sessa, W.C., et al. (2020). Endothelial cell–glucocorticoid receptor interactions and regulation of Wnt signaling. JCI Insight *5*.

Zhou, L., Li, Y., and Yue, B.Y. (1998). Glucocorticoid effects on extracellular matrix proteins and integrins in bovine trabecular meshwork cells in relation to glaucoma. Int. J. Mol. Med. *1*, 339–346.

Zhou, L.Y., Wang, D.S., Kobayashi, T., Yano, A., Paul-Prasanth, B., Suzuki, A., Sakai, F., and Nagahama, Y. (2007). A novel type of P450c17 lacking the lyase activity is responsible for C21-steroid biosynthesis in the fish ovary and head kidney. Endocrinology *148*, 4282–4291.

Ziv, L., Muto, A., Schoonheim, P.J., Meijsing, S.H., Strasser, D., Ingraham, H.A., Schaaf, M.J.M., Yamamoto, K.R., and Baier, H. (2013a). An affective disorder in zebrafish with mutation of the glucocorticoid receptor. Mol. Psychiatry *18*, 681–691.